Technical Report CHL-97-23
September 1997

US Army Corps of Engineers
Waterways Experiment Station

Physical Model Studies of Ponce DeLeon Inlet, Florida

by Gordon S. Harkins, Paul Puckette, Cecil Dorrell

Prepared for U.S. Army Engineer District, Jacksonville

The contents of this report are not to be used for advertising, publication, or promotional purposes. Citation of trade names does not constitute an official endorsement or approval of the use of such commercial products.

The findings of this report are not to be construed as an official Department of the Army position, unless so designated by other authorized documents.

Technical Report CHL-97-23
September 1997

Physical Model Studies of Ponce DeLeon Inlet, Florida

by Gordon S. Harkins, Paul Puckette, Cecil Dorrell

U.S. Army Corps of Engineers
Waterways Experiment Station
3909 Halls Ferry Road
Vicksburg, MS 39180-6199

Final report

Approved for public release; distribution is unlimited

Prepared for U.S. Army Engineer District, Jacksonville
Jacksonville, FL 32232-0019

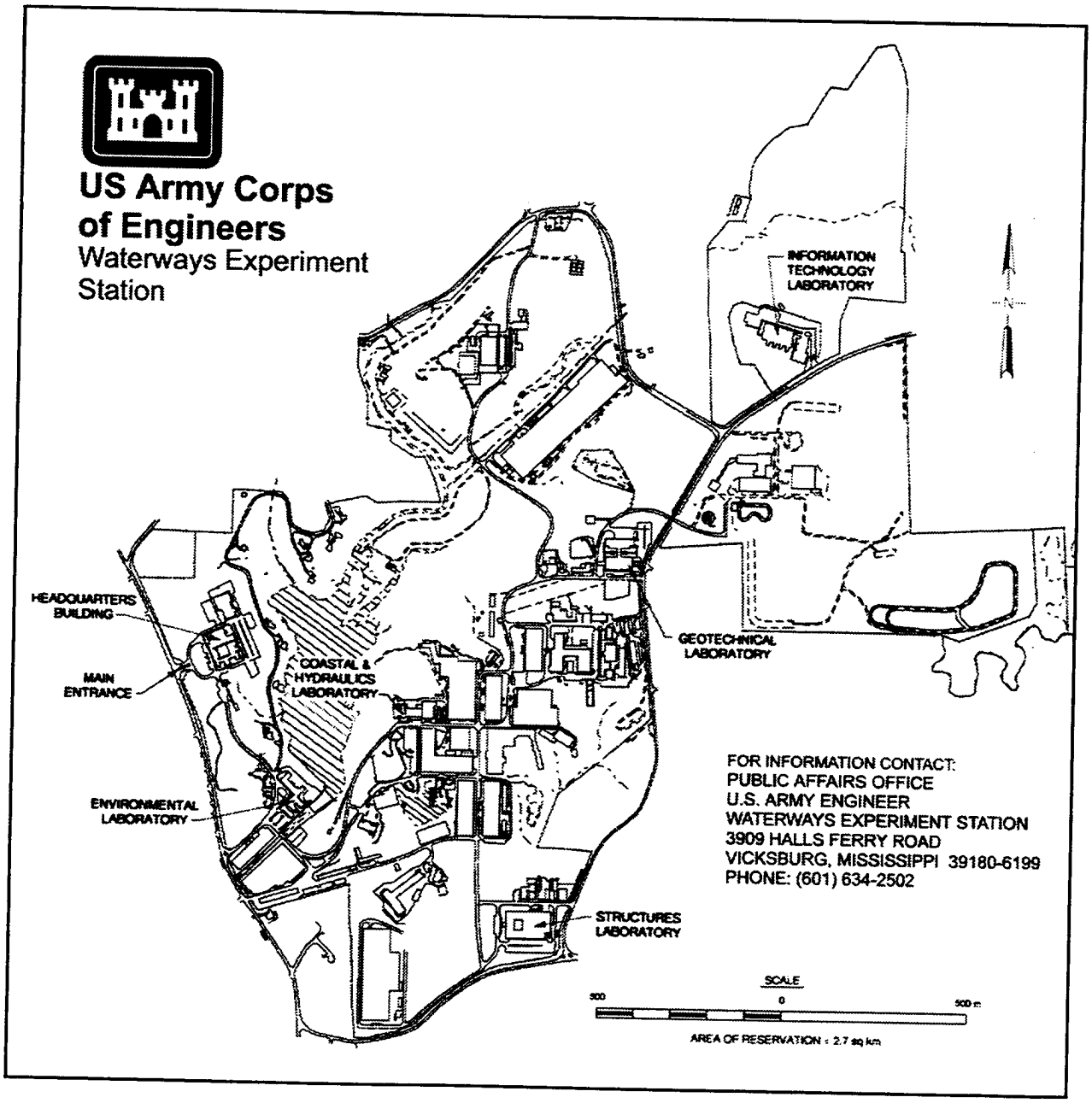

Waterways Experiment Station Cataloging-in-Publication Data

Harkins, Gordon S.

Physical model studies of Ponce DeLeon Inlet, Florida / by Gordon S. Harkins, Paul Puckett, Cecil Dorrell ; prepared for U.S. Army Engineer District, Jacksonville.

230 p. : ill. ; 28 cm. -- (Technical report ; CHL-97-23)

Includes bibliographic references.

1. Inlets -- Florida. 2. Sediment transport -- Florida -- Models. 3. Ocean waves -- Models. I. Puckett, Paul. II. Dorrell, Cecil C. III. United States. Army. Corps of Engineers. Jacksonville District. IV. U.S. Army Engineer Waterways Experiment Station. V. Coastal and Hydraulics Laboratory (U.S. Army Engineer Waterways Experiment Station) VI. Title. VII. Series: Technical report (U.S. Army Engineer Waterways Experiment Station) ; CHL-97-23.

TA7 W34 no.CHL-97-23

Contents

Preface vii

1—Introduction 1

Study Location 1
Background 1
Impetus for the Federal Project 2
Initial Inlet Response and Project Modifications 3
Study Objectives 4

2—Field Measurements 6

Introduction 6
Water Level Measurements 6
Water Velocity Measurements 9
Current Measurements with the BBADCP 10
Current Measurements with the Endeco Current Meters 13

3—Physical Model 17

Model Design 17
Model Bathymetry 21
Jetty Construction 22
Model Appurtenance 22

4—Selection of Experimental Conditions 28

Introduction 28
Prototype Wave Conditions 28
Conditions for Safe Navigation 29
Selection of Wave Conditions for South Jetty Extension Experiments 29
Selection of Wave Conditions for North Jetty Weir Experiments 32
Water Levels Modeled 35
Process for Defining Boundary Flow Conditions 36
Flow Conditions Simulated 37

5—South Jetty Experimental Results 42

Overview of the Experimental Plan 42
Assessment of Sedimentation Reduction Using Dye and Tracer Experiments 43

Impacts of Preferred South Jetty Extension on Waves and Velocities 46
Velocity Results 52

6—North Jetty Experimental Results 55

Overview of the Testing Plan 55
Impacts of Weir Openings on Sedimentation 57
Impact of Reopening the Weir on Navigation 63

7— Conclusions and Recommendations 74

References 76

Appendix A: Water Level Data A1

Appendix B: BBADCP - Data Range A - H B1

Appendix C: Endeco Current Meter Data C1

Appendix D: South Jetty Photos D1

Appendix E: North Jetty Photos E1

Appendix F: Notation F1

SF 298

List of Figures

Figure 1. Study location 2

Figure 2. Location of water level gauges, current survey range lines, and in situ current meters at Ponce DeLeon Inlet 7

Figure 3. Example of velocity vector plots at various depths 11

Figure 4. Example of contour plot of velocity magnitude 13

Figure 5. Example of depth-averaged magnitude and direction 14

Figure 6. Magnitude and direction time series for Range C 15

Figure 7. Discharge rates for Range C 16

Figure 8. General physical model layout 19

Figure 9. Physical model 20

Figure 10. Range line and station number positions 38

Figure 11. The south jetty extension lengths and orientations 43

Figure 12. South jetty gauge layout 47

Figure 13. Wave averaged, normalized wave heights for all the flow condition experiments conducted for the south jetty dogleg extension 48

Figure 14. Existing and 305-m (1,000-ft) dogleg extension for wave gauges located in the inlet channel 50

Figure 15. Bathymetry between wave gauges 8 and 13 51

Figure 16. Mean velocity measurements for the existing south jetty and the 305-m (1,000-ft) dogleg extension. Spring peak ebb flow 53

Figure 17. Mean velocity measurements for the existing south jetty and the 305-m (1,000-ft) dogleg extension. Spring peak flood flow 54

Figure 18. North jetty weir lengths 56

Figure 19. Gauge layout for north jetty weir experiments using the plunger wave generator 60

Figure 20. Wave height measurements at gauge 4 for spring peak flood water level and flow 65

Figure 21. Wave height measurements at gauge 6 for spring peak flood water level and flow 66

Figure 22. Wave height measurements at gauge 5 for spring peak flood water level and flow 67

Figure 23. Wave height measurements at gauge 7 for spring peak flood water level and flow 68

Figure 24. Wave heights normalized by the existing conditions and then averaged over the four navigation waves 69

Figure 25. Wave attenuation with wave propagation down inlet channel for spring peak ebb water level for the weir closed and the 457-m (1,500-ft) weir opening 70

Figure 26. Wave attenuation with wave propagation down inlet channel for spring peak flood water level for the weir closed and the 457-m (1,500-ft) weir opening 71

Figure 27. Velocity measurements for the four weir conditions for a spring peak ebb flow and water level for wave cases N1 and N2 72

Figure 28. Velocity measurements for the four weir conditions for a spring peak flood flow and water level for wave cases N1 and N2 73

List of Tables

Table 1. Gauge Descriptions and Data Collected 8

Table 2. Description of Endeco 174 Locations and Data Collection 10

Table 3. Physical Model Scale Relations 18

Table 4. Location and Water Depth of WIS Stations Near Ponce DeLeon Inlet 29

Table 5. Maximum Wave Heights Considered for Safe Transit 30
Table 6. WIS Mean Peak Wave Period at Stations 21 and 22 31
Table 7. South Jetty Extension Deepwater Wave Conditions Simulated to Study Navigation Concerns 31
Table 8. Target Storm Wave Conditions 32
Table 9. Experimental Wave Conditions for Studying South Jetty Modifications 33
Table 10. North Jetty Alternative Experimental Wave Conditions 34
Table 11. Steady-State Static Water Levels Simulated in Physical Model 35
Table 12. Spring Peak Flood Velocity 39
Table 13. Spring Peak Ebb Velocity 39
Table 14. Comparison Between Measured Prototype Discharge and Simulated Model Discharge Values for Spring Peak Ebb and Flood Flows 40
Table 15. Imposed Storm Boundary Forcing Conditions on a Peak Spring Storm Flow Across the Three Range Lines which Correspond with the Three Stilling Basins 40
Table 16. Summary of Inlet Velocity Observations 41
Table 17. South Jetty Experiment Series 44
Table 18. Summary of H_{m0} Wave Heights at Gauge 13 52
Table 19. North Jetty Weir, Plunger (North of Shore Normal) Wave Generator Experimental Matrix 58
Table 20. North Jetty Weir, DSWG (South of Shore Normal) Wave Generator Experimental Matrix 59

Preface

This study was authorized by the U.S. Army Engineer District, Jacksonville (CESAJ) and was conducted during the period July 1995 through December 1995 by personnel of the U.S. Army Engineer Waterways Experiment Station's (WES), Coastal Engineering Research Center (CERC), Wave Processes Branch (WPB), Prototype Measurement and Analysis Branch (PMAB), and Coastal Processes Branch.

The following individuals from CESAJ were closely involved in technical review of results and recommendations from the physical model studies: Messrs. Joe Gurule, Tom Martin, Ian Mathis, Tim Murphy, Mitch Granat, and Dick Powell. The point of contact and modeling technical study manager for CESAJ was Mr. Mitch Granat. Mr. Dick Powell was overall planning technical study manager for CESAJ.

The authors would like to thank Messrs. Bruce Taylor and Terry Hull from Taylor Engineering, and Dan O'Brien, Port Authority Ponce DeLeon Inlet, for their cooperation in this study.

This report was prepared by Messrs. Gordon S. Harkins, Hydraulic Engineer, and Cecil C. Dorrell, Civil Engineering Technician, WPB. Mr. Paul Puckette of PMAB wrote Chapter 2. The work was performed under the direct supervision of Mr. Bruce A. Ebersole, Chief, Coastal Processes Branch; Mr. H. Lee Butler, Chief, Research Division; Mr. Dennis G. Markle, Chief, WPB; and Mr. C.E. Chatham, Chief, Wave Dynamics Division and under the general supervision of Mr. Charles C. Calhoun, Jr., Assistant Director, CERC, and Dr. James R. Houston, Director, CERC.

This report is being published by the WES Coastal and Hydraulics Laboratory (CHL). The CHL was formed in October 1996 with the merger of the WES Coastal Engineering Research Center and Hydraulics Laboratory. Dr. James R. Houston is the Director of the CHL and Messrs. Richard A. Sager and Charles C. Calhoun, Jr., are Assistant Directors.

At the time of publication of this report, Director of WES was Dr. Robert W. Whalin. Commander was COL Bruce K. Howard, EN.

1 Introduction

Study Location

Ponce DeLeon Inlet is located along the Atlantic Coast of the state of Florida approximately 12.4 km (10 miles) south of Daytona Beach. Ponce DeLeon Inlet is in Volusia County, approximately 81 km (65 miles) south of St. Augustine Harbor and 71 km (57 miles) north of Canaveral Harbor (Figure 1). The inlet connects the Atlantic Ocean with the Halifax and Indian Rivers, both of which join the Intracoastal Waterway.

Background

Ponce DeLeon Inlet has been a natural inlet for over five centuries and a man-made confined inlet for approximately a quarter of a century. Prior to construction in 1968 to stabilize the inlet, Ponce DeLeon Inlet had been used as a natural passage through the barrier islands separating the Atlantic Ocean from Halifax River and Indian River North. The inlet has remained open and basically in its present location for over 130 years.

Most barrier beach inlet systems are dynamic and strive to reach an equilibrium between alongshore sediment transport and tidal flushing. Before man confined Ponce DeLeon Inlet, it was a shallow and dynamic inlet. From the first documented survey of the inlet in 1765 through 1925, the controlling depth across the sandbar ranged between 1.2 m (4.2 ft) and 1.8 m (6.0 ft). Since construction of north and south jetties, a channel through the inlet throat has remained deep while the majority of the inlet remains shallow due to an influx of sand into the inlet system (much of which presently moves around the south jetty).

The inlet has always been difficult to navigate. The following is a description of Ponce DeLeon Inlet from Taylor (1989): "Throughout its history, Ponce DeLeon Inlet has been recognized as a difficult and capricious inlet through which to navigate. Under adverse conditions, when wind, wave and tide conspire, the inlet has often presented a clear threat to life and property." Although Ponce DeLeon was a famous explorer who traveled with some experienced sailors, not all who travel

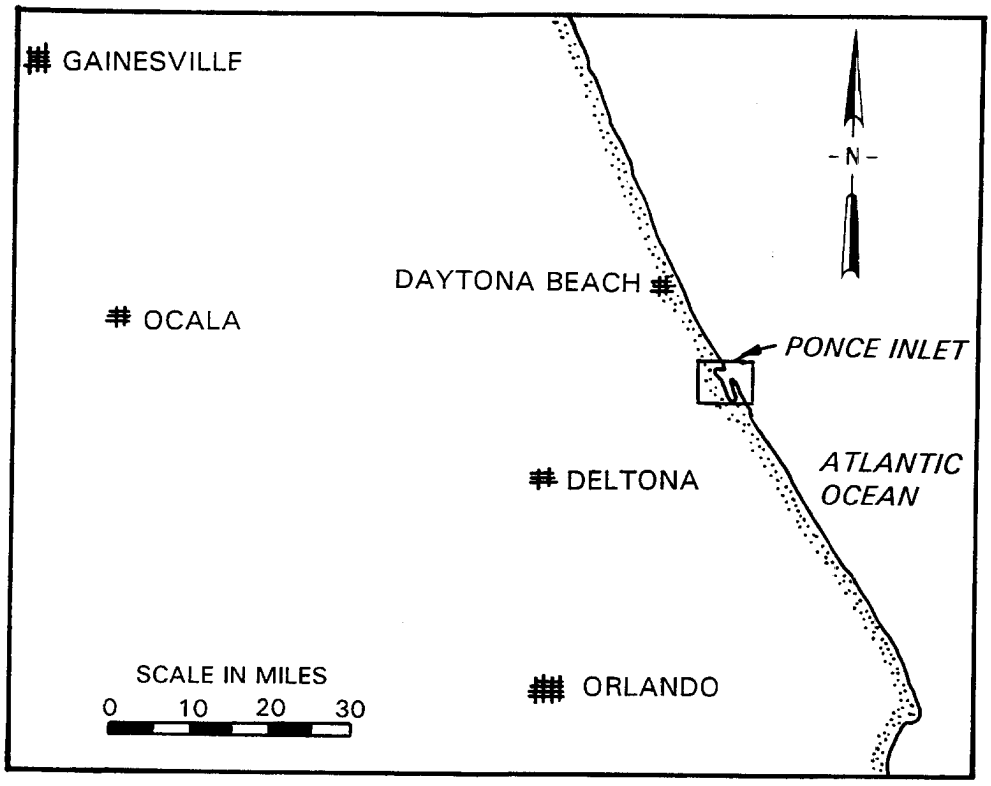

Figure 1. Study location

through the inlet have as much boating experience as the inlet's namesake's crew. Ponce DeLeon Inlet has been regarded as the seventh-worst inlet for navigation in the United States. The U.S. Department of Commerce has posted the following warning to mariners in the *United States Coast Pilot: Atlantic Coast: Cape Henry to Key West*: "Mariners are advised that due to constant shifting of the channel, passage through the inlet is not recommended; buoys marking the channel may not be marking the best water...Local knowledge and extreme caution is advised." Conditions have improved since the project was constructed, a deep gorge in the throat is self-maintaining. However, the narrow and meandering channel and its proximity to the north jetty, strong wave-current interactions, along with very shallow water adjacent to the marked channel make navigation difficult. Scour due to the proximity of the deep channel to the rubble jetty has also been a problem along the north jetty since it was constructed.

Impetus for the Federal Project

Numerous attempts were made in the early 1900's to dredge and stabilize the channel with minimal success. This prompted a request in June 1941, from the City of New Smyrna, located just south of Ponce DeLeon Inlet, representing a variety of local interests, that the Federal Government provide a channel 3.7m (12 ft) minimum depth at mean low water (mlw), stabilized by rock jetties.

In 1952 "Survey-Review Report on Ponce DeLeon Inlet, Florida" (U.S. Army Corps of Engineers (USACE), 1952) was prepared by the U. S. Army Engineer District, Jacksonville (CESAJ) recommending a navigational project at Ponce DeLeon Inlet. After further studies, "Survey-Review Ponce DeLeon Inlet, Florida" (USACE 1963) was compiled by CESAJ. The second report concluded by recommending a jetty weir system. Funding for the original project was authorized under the River and Harbor Act adopted October 27, 1965.

Design of the Ponce DeLeon Inlet project was defined in the "General and Detail Design Memorandum for Ponce DeLeon Inlet" (USACE 1967) prepared by CESAJ dated November 29, 1967. The proposed project consisted of a 549-m (1,800-ft) mean low water (mlw) weir section within a 1,295-m (4,250-ft) north jetty , an impoundment basin in the inlet to trap sand passing over the weir and into the inlet, and a 1,355-m (4,444-ft) south jetty.

The federal navigation project at Ponce DeLeon Inlet began in July 1968 with the construction of the south jetty, followed by the construction of the north jetty later that year. The project was officially completed in July 1972 although revisions to the original design and maintenance concerns began immediately after project construction was completed.

The as-built project differs slightly from the proposed project. Construction difficulties and cost overruns reduced the length of the north jetty by 61 m (200 ft) to an overall length of 1,234 m (4,050 ft) and the south jetty by 112 m (366 ft) to an overall length of 1,243 m (4,078 ft). Original design alignment of the entrance channel was chosen to take advantage of deeper waters of the natural channels as they exited the inlet, at the time of the last preconstruction survey performed in 1967.

Initial Inlet Response and Project Modifications

A historical analysis of inlet behavior was described in "Engineering Evaluation of Ponce DeLeon Inlet, Final Phase II Report" (Taylor et al. 1990). In the report, shoreline changes due to project construction and subsequent modifications were addressed. Pre- and post-project surveys of the shoreline locations as well as changes in bathymetry are described.

Following construction, the project did not perform exactly as anticipated. According to Taylor (1990), the orientation of the main inlet channel migrated northward towards the south side of the north jetty between 1967 and 1978. The areas south of the south jetty and along the south side of the inner channel were accretional areas, while the north interior shoal and the shoreline north of the north jetty were erosional areas. The shoal on the south side of the inner channel accreted approximately 460 m (1,500 ft) northward. The ebb shoal also continued to grow.

In August 1972, a year after the north jetty construction was complete, riprap was placed along the south side of the area adjacent to the weir section to provide

scour protection. The area which was supposed to be an impoundment basin had actually become an erosional area.

Obviously, the weir was not working as planned and sand was not accreting as was hoped. The weir allowed additional wave energy and cross currents into the inlet. To minimize the difficult navigational problems, first the shoreward 91 m (300 ft) of the weir was closed in April 1979. The north jetty continued to experience scour problems while the shoreline just south of and adjacent to the north jetty continued to erode westward. Finally the entire weir was closed in 1984. Between 1981 and 1984, the shoal on the south side of the entrance channel (immediately north of the south jetty) continued to grow.

Following weir closure in 1984, the inlet began to adjust to the new system of constraints and hydrodynamic forces imposed upon it and has been evolving in a fairly consistent manner ever since. The main inlet channel on the bay side has tended to rotate to a more northwest/southeast orientation. As it has evolved, the distribution of flow moving to the north and south interior bays has changed, and the erosional pressure on the north interior spit inside the north jetty has increased. Areal loss of the interior north spit has been dramatic in recent years.

Reopening the weir was first addressed in the "General and Detailed Design Memorandum, Addendum 1" (USACE 1983), which discussed the performance of the Ponce DeLeon Inlet project and addressed the planned closure of the weir section. The weir was supposed to be reopened after subsequent dredging, and realignment of the interior channels and adjacent shorelines, with a reduced length and increased crest elevation after sand was deposited on the north side of the north jetty. The primary purpose for closing the weir, according to this report, was to enhance the southerly migration of the navigation channel away from the north jetty and to eliminate the navigation problems associated with the open weir. At the outset of the present study, weir reopening was considered as a possible means for preventing the high erosion rate of the north spit, preserving its integrity, and as a means for reducing erosional pressure on the north jetty.

Study Objectives

Work completed by the U. S. Army Engineer Waterways Experiment Station's (WES) Coastal and Hydraulics Laboratory represents several elements of the larger study of Ponce DeLeon Inlet aimed at improving navigation conditions within the inlet and preventing damage to the north jetty. A numerical model study conducted by Taylor Engineering, Inc., in Jacksonville, FL, for the local cost-sharing partner, the Ponce DeLeon Port Authority, addressed changes in the tidally generated flow characteristics over the complete tidal cycle in the absence of waves (for existing and proposed inlet modifications). Work performed at WES included field measurements and physical modeling of wave- and current-driven sediment transport and analysis of wave and current patterns for alternative inlet configurations. The work of WES and Taylor Engineering, Inc., involved continuous exchange of data and information and was closely coordinated.

To accurately develop, calibrate, and evaluate the accuracy of the physical and numerical models, field data were utilized. These data included water level measurements for approximately 2 months at locations both inside the inlet and in the ocean, velocity measurements made with a vessel-mounted current profiler along eight transects crossing the inlet and interior channels, and in situ current measurements made with an instrument moored to the bottom at three locations. Current measurements made with the vessel-mounted current profiler were recorded in the inlet throat, and the northern and southern channels for 1 day each.

A steady-state three-dimensional (3-D) physical model was designed and constructed to study spring peak ebb and flood velocity characteristics for various water level, flow, and wave conditions for the existing inlet and proposed inlet modifications. Objectives of the physical model study were as follows:

a. Assess proposed alternatives for improving navigation and inlet stabilization at Ponce DeLeon Inlet. It is assumed that sediment is being transported past the end of the south jetty and is being deposited in the inlet. A preferred south jetty length and orientation were to be found, built, and studied in the physical model. The preferred south jetty extension would not adversely impact navigation or surfing characteristics just south of the inlet.

b. Investigate the impact of reopening the north jetty weir with present-day bathymetry. The weir was originally closed because the impoundment basin was ineffective and navigation into the inlet was difficult because of the increased wave energy and cross currents in the inlet. Various weir lengths, waves, and flow conditions were tested in the physical model. A preferred north jetty configuration was identified.

2 Field Measurements

Introduction

As part of the Ponce DeLeon Inlet Feasibility Project, a field data collection study was undertaken during the summer of 1994 to measure the hydrodynamic conditions at Ponce DeLeon Inlet. The field data collected were used as input to the physical and numerical models of the inlet and interior channels and also to validate and calibrate these models. Water level data were collected for approximately 2-1/2 months at five locations in and near the inlet. Water velocity data were collected over two different tidal cycles at several ranges and at a few discrete points in the inlet and in the interior channels.

Water Level Measurements

Water level data were collected from approximately 21 July 1994 through 28 September 1994. Table 1 contains information about data collection coordinates, water depths, and duration of data collection. Gauge locations are shown in Figure 2. Water level data were collected with a Sea Data internal-recording Temperature/Depth Recorder 2 (TDR-2). This sensor uses a strain gauge to measure the pressure due to the water over the gauge. The sensor averages the pressure over 6 min and then stores the averaged value in the memory on the gauge. At the completion of the deployment, the gauges are retrieved and downloaded, and the pressure values are converted to feet of seawater after subtracting a standard barometric pressure of 101.3 kP (14.7 lb/in.^{2}). Differences between daily pressure fluctuations and the standard barometric pressure were not accounted for because of the following reasons; (a) constituent analysis of the sea surface elevation to find the tidal components inherently eliminates random processes like daily pressure fluctuations, and (b) daily pressure fluctuations affect all gauges equally.

At each of the interior water level sites, two TDR's were mounted on steel pipes. Two TDRs were used at all sites to improve the probability that quality data would be collected. The distance from each sensor to the top of its pipe was measured. The pipes were then jetted in next to Coast Guard channel markers and secured to the markers using chain bindings. Distance from the top of the pipe to the surface

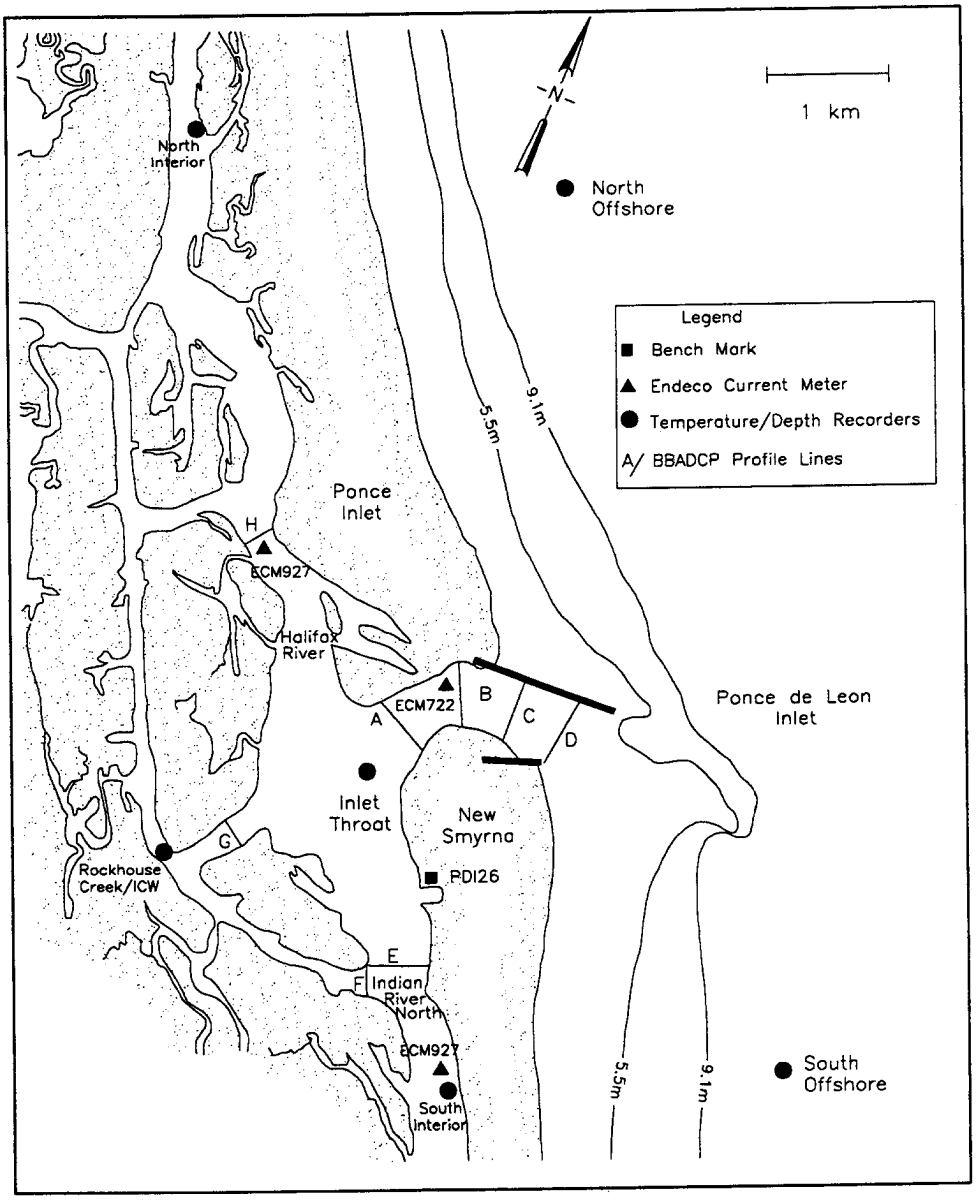

Figure 2. Location of water level gauges, current survey range lines, and in situ current meters at Ponce DeLeon Inlet

of the water at the time of deployment was also measured. After the gauges had been installed, a survey team from CESAJ surveyed in the tops of the pipes using standard survey equipment and existing benchmarks.

At the two offshore sites, TDR's were mounted on trawler-resistant pods. After the pods were deployed, steel poles were jetted into the seafloor and the pods were secured to these poles. This was done to reduce the possibility of the pods being dragged off and also to prevent the pod from sinking due to scour.

Table 1
Gauge Descriptions and Data Collected

Site	File	Location State Plane NAD-27 (m)	Water Depth (m)	First Record GMT	Last Record GMT
Interior South	TDR156.TMS	161262 E 522960 N	2.9	7-21-94 11.617	9-28-94 12.20
Interior North[1]	TDR408.TMS	157073 E 528535 N	1.8	7-21-94 19.617	9-28-94 13.817
Inlet Throat	TDR88.TMS	160060 E 524732 N	10.0	7-21-94 10.933	9-28-94 15.233
Rockhouse Creek/ICW	TDR154.TMS	158779 E 523660 N	3.0	7-21-94 19.033	9-28-94 14.433
Offshore North	TDR328.TMS	159700 E 528925 N	13.7	7-21-94 14.233	9-29-94 20.433
Offshore South[2]	TDR85.TMS	163436 E 523885 N	13.1	7-21-94 17.217	9-12-94 19.617

[1] Drift adjustment applied: -0.0592 mm/hr.
[2] Drift adjustment applied: 0.488 mm/hr.

For three of the interior sites, at least one of the TDR's provided a complete time series. At the inlet throat site, there is a period of approximately 4 days for which there is no data. At the interior south site, the data appear to exhibit a slight drift when compared with data from other sites. Data from this site have been adjusted using a simple linear detrending function. The function subtracted 0.0592 mm from the measured value for each hour from the start of data collection. At the northern offshore site there is a complete time series. At the southern offshore site, there are approximately 53 days of data. Data from the southern offshore site also appeared to have a slow drift. Data from this site have been adjusted by the addition of 0.488 mm to the measured value for each hour from the start of data collection.

For the interior gauges, the water levels have been referenced to mean low water taken from the bench mark PDI-26 at the Ponce DeLeon Inlet Coast Guard Station. When the gauges were installed, the distance from the top of the pipe to the surface of the water was measured for each site. Since the elevation of the tops of the pipes relative to mlw was known, a water level referenced to mean low water could be calculated. After the gauges were retrieved and the data downloaded, the water level that was measured when each gauge was installed was compared to the water level that was measured by the gauge. From this comparison, an offset value was determined to adjust the gauge results to values referenced to mlw. For the offshore locations, it was not possible to determine gauge elevations relative to a standard vertical datum. The water levels have been referenced to the average of the measured water levels. Plots of the water levels are provided in Appendix A.

Tidal constituent analysis was performed on the time series for the M2, S2, N2, K1, O1, P1, and K2 constituents. These constituents were chosen because they are the constituents with the largest diurnal and semidiurnal amplitudes. Other relatively large amplitude constituents, SA and SSA, cannot be resolved because the

length of the available records is insufficient. Results of the analysis for the different sites are provided in Appendix A.

Measured water levels were compared to values computed using these constituents. For all sites, the phases are in good agreement. The amplitudes vary greatly in some instances, however. The difference is due in part to short-term, nonastronomical water level variations that are included in the measured water levels. Some of the difference occurs because the calculated water levels do not contain the SA and SSA constituents. Overall, the comparisons indicate that the computed constituents may be used to make reasonable estimates of the water level due to the diurnal and semidiurnal tidal components.

Water Velocity Measurements

Two sets of water velocity measurements were taken as part of the field measurement study. The first set of data was collected on 22 July 1994 under spring tidal conditions. The second set was collected on 27 September 1994 under near neap tidal conditions. Data were collected for two different tidal and flow conditions so that a range of conditions were available for calibrating the models. Both sets of data were processed in the same manner and the results are reported in Appendix B.

For the first set of measurements, data were collected along four ranges in Ponce DeLeon Inlet and at four ranges across the interior channels over a 13-hr period that covered peak ebb and flood conditions. Locations of these ranges are shown in Figure 2 (labeled A, B, C, D, E, F, G, H). Data in the inlet were collected using a vessel-mounted 1,200-kHz Broadband Acoustic Doppler Current Profiler (BBADCP), and the data in the interior channels were collected using a vessel-mounted 600-kHz BBADCP. Ideally, 1,200-kHz BBADCP would have been used in the interior channels, but only one 1,200-kHz unit was available, and it was decided to use it in the inlet since it would provide better measurements in a dynamic environment. An Endeco 174 single-point current meter was also deployed in the inlet at the location marked ECM722 in Figure 2. For the second data collection effort, measurements were taken with a 1,200-kHz BBADCP along the four ranges in the inlet. Ranges A and D were identical to those run in July. Ranges B and C had the same starting positions, but their ending points were adjusted slightly so that they were oriented perpendicular to the current. Two Endeco 174 current meters were deployed in the interior channels leading into the inlet, one in the north channel and one in the south. Their locations are labeled ECM927 in Figure 2. Information regarding the July and September deployments of the Endeco current meters is provided in Table 2.

Table 2
Description of Endeco 174 Locations and Data Collection

Site	Location State Plane NAD-27 (m)	Water Depth (m)	Gauge Depth (m off bottom)	Start Time (GMT)	Stop Time (GMT)
ECM729 Inlet Throat	160142 E 525493 N	~5	1.8	7-22-94 12:00	7-23-94 02:40
ECM927 North Chan	158706 E 525804 N	~4	1.8	9-24-94 22:00	9-28-94 13:20
ECM927 South Chan	161248 E 522970 N	~3	1.8	9-26-94 21:20	9-28-94 12:25

Current Measurements with the BBADCP

During data collection, the vessel proceeds across the channel from one side to the other along predetermined ranges. Approximately every 4 sec the BBADCP measures the water velocity in a series of depth cells that cover almost the entire water column from near the surface to near the bottom. For the 1,200-kHz BBADCP, the depth cells were 25 cm (10 in.) deep and for the 600-kHz system, they were 50 cm (20 in.). These depth cells are referred to as bins, and the water velocity measured represents the average water velocity in that bin. The entire set of data points collected every 4 sec is referred to as an ensemble. The first bin in an ensemble starts approximately 50-60 cm (20-24 in.) below the head of the BBADCP, and the last bin ends at a distance above the bottom approximately equal to 8 percent of the water depth. For the 600-kHz system, the last bin ends at a distance above the bottom approximately equal to 15 percent of the water depth. Since the head of the BBADCP is mounted 40 cm (16 in.) below the water surface, the first velocity measurement is at an approximate depth of 1.0 m (3.3 ft). Due to these limitations, there is a layer of water near the surface and near the bottom for which no velocity measurements are made.

The BBADCPs collect an enormous amount of data that must be processed and checked for errors. The BBADCPs constantly monitor the data as they are collected and exclude any that do not pass certain predefined levels of quality. Ship track plots of the data are generated to visually assess the quality of the data and identify any inconsistencies. An example of a ship track plot from Range C is given in Figure 3. The thick curved line represents the track of the vessel as it crossed the channel along the range line. The short straight lines extending from the ship track lines are the instantaneous velocity vectors of the current at the noted depths of 1.0 (3.3), 2.5 (8.2), 4.0 (13.1), and 5.5 m (18.0 ft). The lines point in the direction the currents are going and have a length proportional to the magnitude of the current. The legend bar points in the direction of north, and the legend is equivalent to a velocity of 100 cm/sec. The current speeds shown in Figure 3 are about 1 m/sec. Locations where there is not a velocity vector along the vessel track line indicate that the water at that location was shallower than the water depth indicated in the

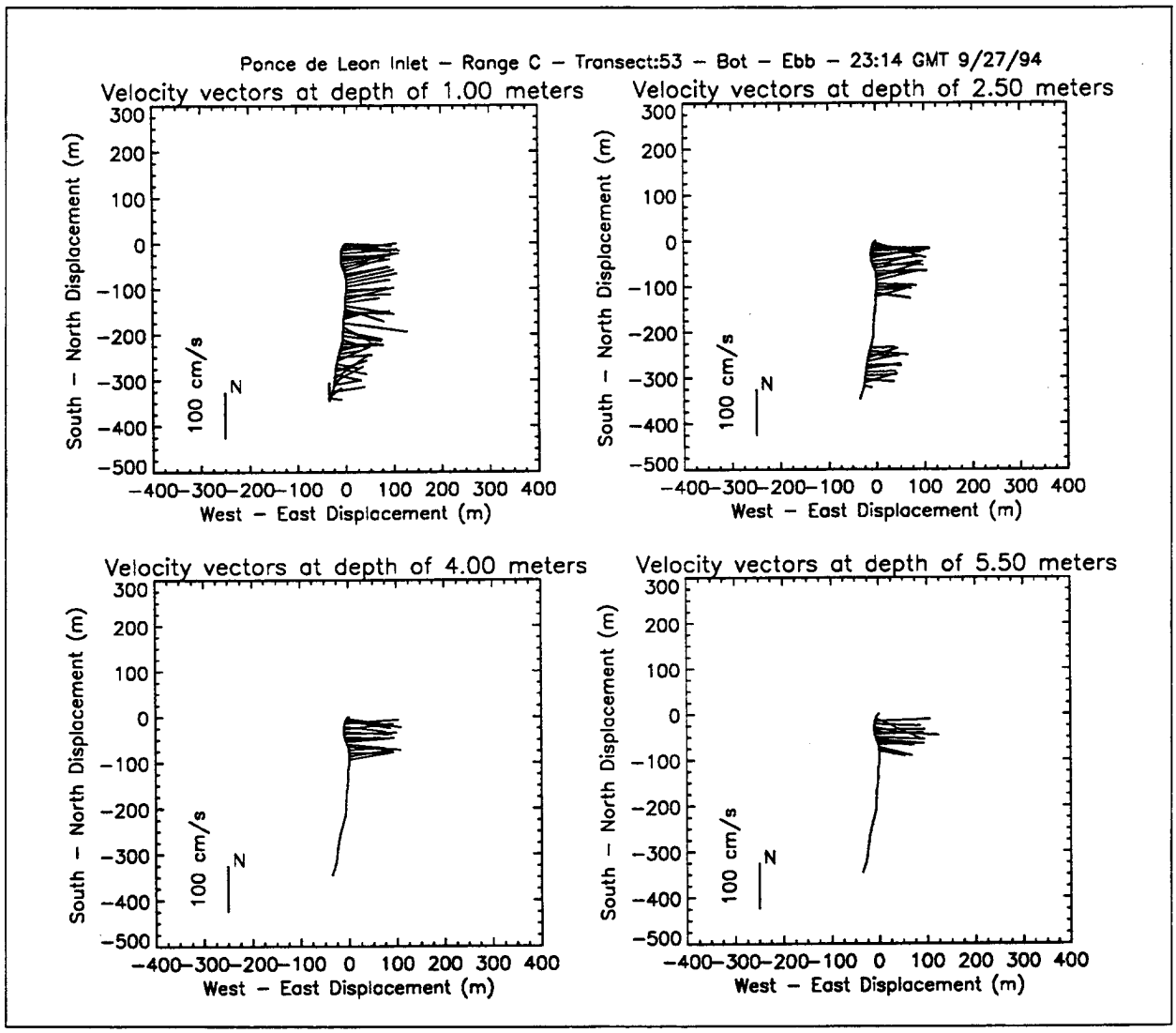

Figure 3. Example of velocity vector plots at various depths

graph title or, in a few cases, the data did not pass the BBADCP's internal quality control checks.

The BBADCP sampling is time controlled; therefore, the spatial positioning of the ensembles is dependent on the vessel's velocity. Ideally, the boat would run the same course at the same speed every time it made a transect on a range line. The interaction of wind, currents, and waves with the dynamics of a small boat make this impossible. This results in sampling positions that vary slightly from one transect to the next along the same range, and it is necessary to account for this in the postprocessing.

The approach used with these data to account for the variable spacing of the ensembles is to define an "ideal" line for each of the ranges. The ideal lines, as

shown in Figure 2, are straight lines between the start and stop positions for each range. Assuming that the water velocities in the channel are nearly constant over short distances parallel to the channel axis, the position of each ensemble can be projected onto the ideal line. The position of the sample on the ideal line is that point where a line that is perpendicular to the ideal line intersects the ensemble sample location. Assuming that the ideal line is perpendicular to the channel axis, the location of the samples across the inlet will remain the same. In this manner, the ensembles from the various transects can be referenced to a common spatial frame.

Data collected for this study are presented in a series of plots in which the ensemble locations are positioned along the ideal line. Start and stop positions of the ideal line are provided on the plots. The coordinates given are northings and eastings in Florida State Plane 0901, NAD 27, in meters.

Contour plots of the data are provided in the appendices. These plots represent a vertical cross section of the velocity magnitude across the inlet. An example of a contour plot is provided in Figure 4. The data were also depth-averaged and examples of these data are shown in Figure 5. The plots for the peak ebb and flood conditions for each range from both deployments are provided in Appendix B.

Time series of the depth-averaged velocity were generated by taking each range and dividing it into several segments of equal lengths with the midpoint of the segment defined as a station. The depth-averaged values that were in each of these segments were averaged horizontally over the segment length and tagged with the averaged time and position of the ensembles included in the average. The average values for each section for each transect were assembled to create a time series of the velocity in that segment. Figure 6 is an example of the time series for Range C. Plots of the time series for the other ranges are provided in Appendix B.

Using data collected for velocity and water depth, the BBADCP calculates an estimate of the discharge at each range for each transect. The discharge estimate calculated is based on the component of the water velocity that is perpendicular to the theoretical transect line across the channel and is independent of the path that the vessel takes in getting from one side of the channel to the other. As mentioned above, the BBADCP cannot collect velocity information at the top of the water column or near the bottom. To calculate a value for the total discharge, it is necessary to make estimates of the velocity for these regions where no data are collected. Estimated velocities are then integrated over the area to come up with an estimate of discharge. For the region between the top of the first bin and the water surface, the BBADCP assumes a constant velocity value based on the water velocity in the top bin. For the bottom estimate, the BBADCP takes the velocity measured in the last bin and applies an exponential decay function which gives zero velocity at the bottom. It is also possible to include estimates for discharge through the region between the banks and the start and stop positions of the range lines. During this field deployment, considerable effort was made to start and stop the lines as close to the banks as possible. In most cases, the start and stop of the line were within 4.6 m (15 ft) of the bank. Estimates made of the discharge in these side regions indicated that it was typically less than 1 percent of the total discharge; therefore, it was decided not to include it in the reported discharge measurements. Figure 7 is an

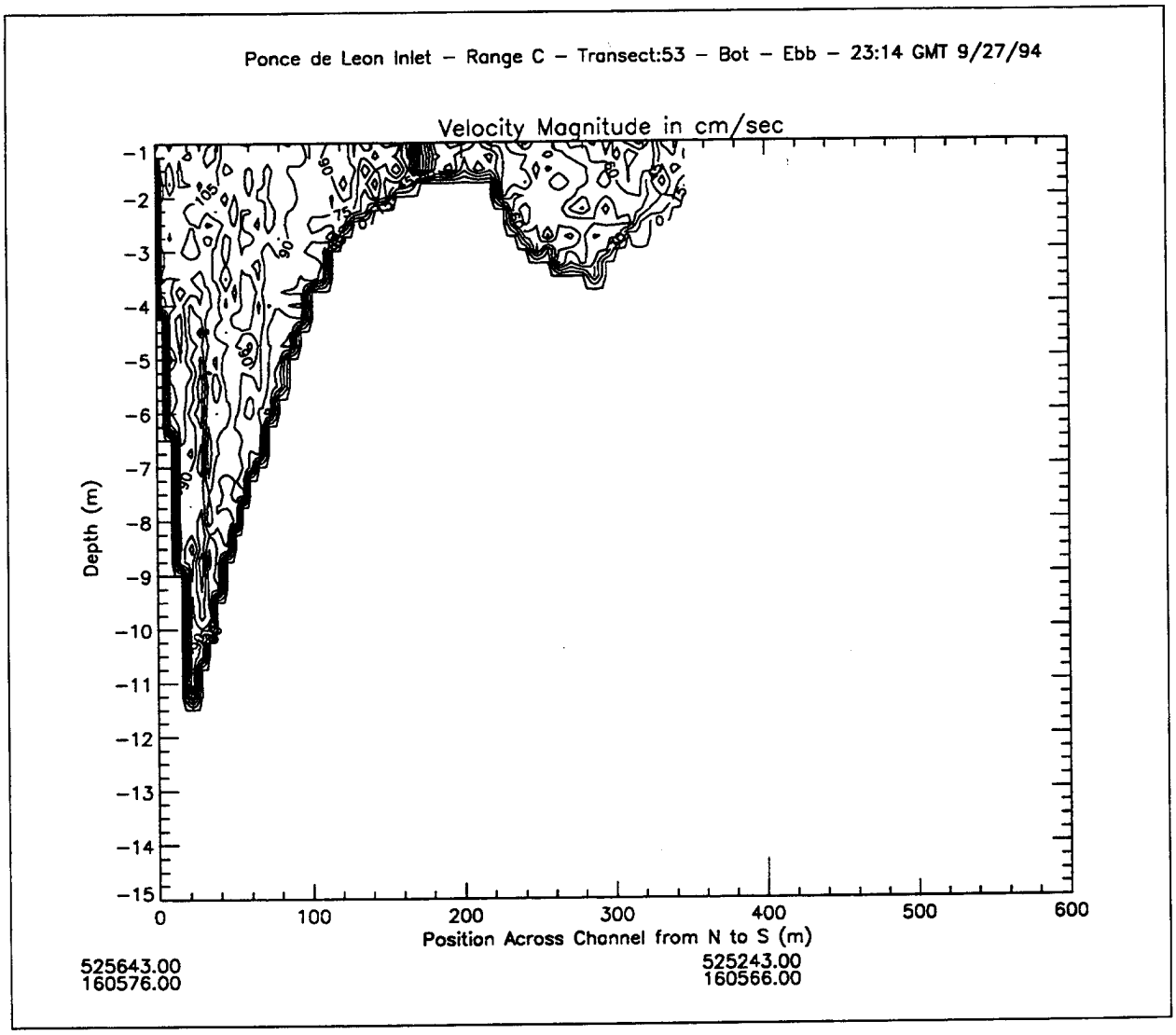

Figure 4. Example of contour plot of velocity magnitude

example of a discharge data plot. Plots of the discharge rates for each range are provided in Appendix B.

Current Measurements with the Endeco Current Meters

The Endeco 174 current meters are neutrally buoyant, torpedo-shaped instruments that are suspended in the water column on a mooring. They determine water velocity magnitude by measuring how fast a propeller mounted on the back of the instrument turns as the water flows over it. The instrument orients itself in the direction the current is going, and this direction is measured by an internal compass. The instrument averages the magnitude and direction of the current over 5-min

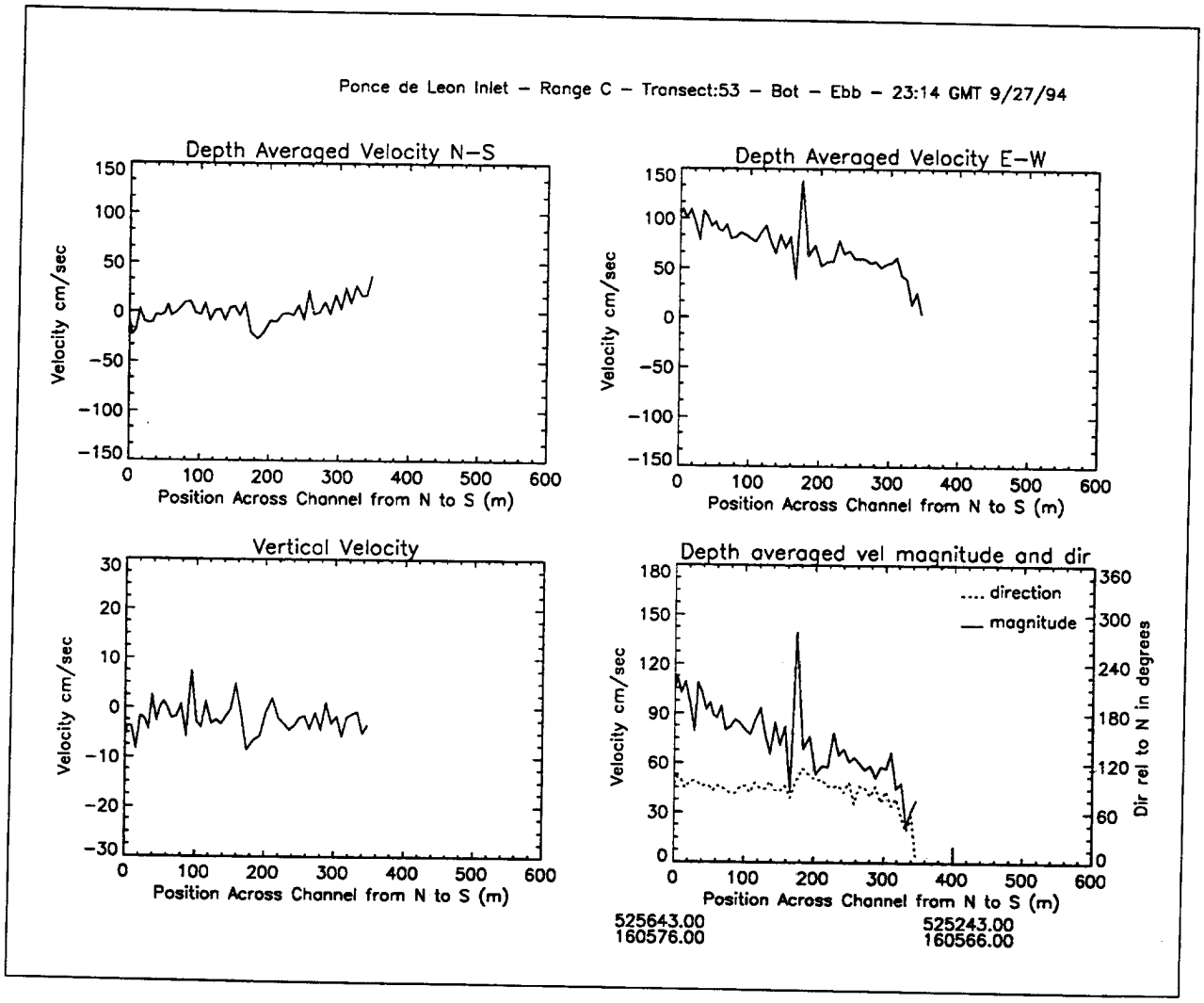

Figure 5. Example of depth-averaged magnitude and direction

intervals and records the data internally. The gauges are moored on a taut mooring that is supported at the top of the buoy. The vertical location of the gauge in the water column is determined by where the gauge is attached to the mooring line.

During the first deployment, an Endeco 174 was placed in the throat of the inlet near the northern end of Range B. Data were collected over the same time period that the BBADCP data were collected. The velocities measured by the BBADCP were in good agreement with the velocities measured with the Endeco.

During the second deployment, one Endeco was placed in the southern interior channel leading into the inlet and a second Endeco was placed in the northern interior channel leading into the inlet. Data plots from the Endecos are provided in Appendix C.

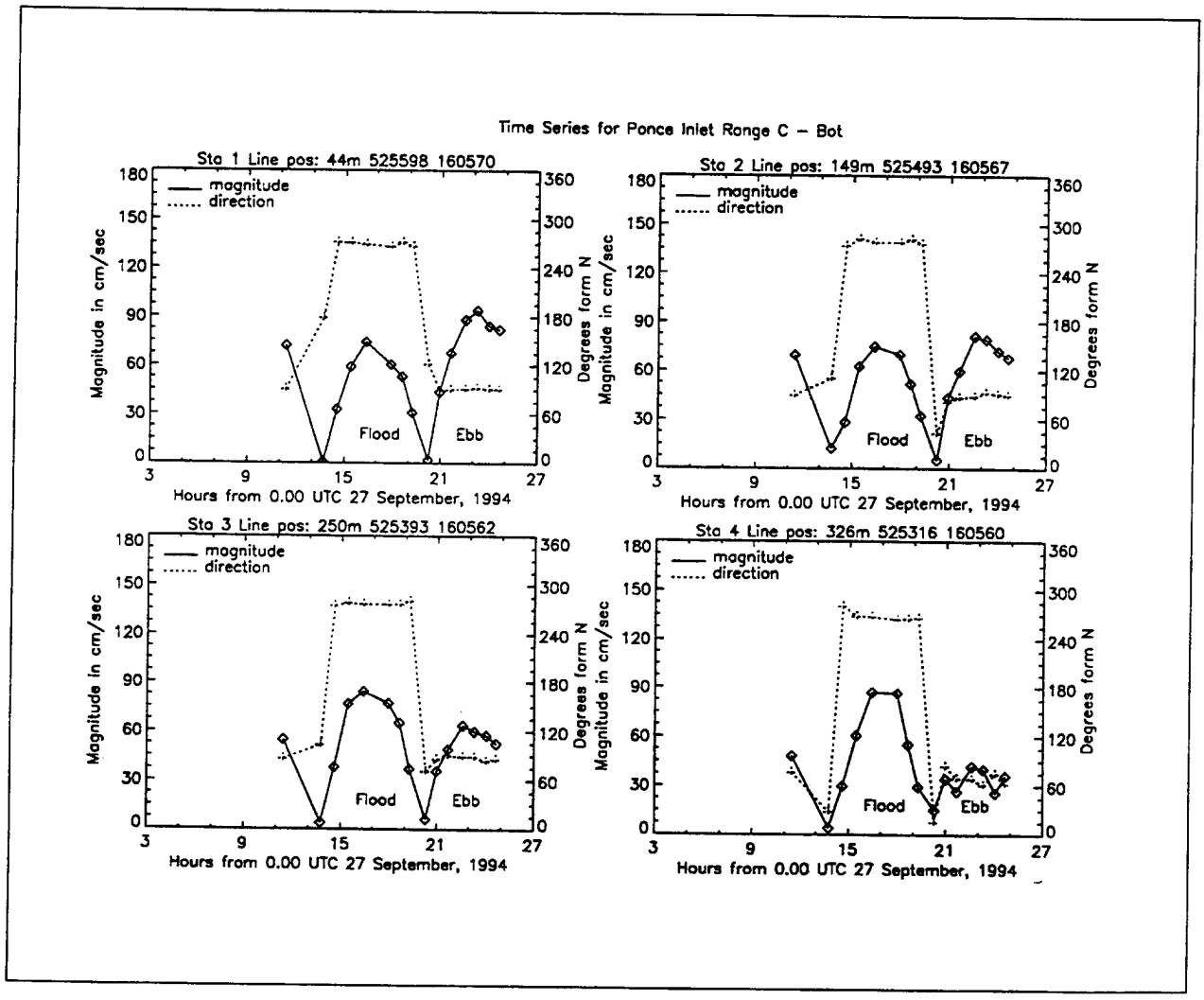

Figure 6. Magnitude and direction time series for Range C

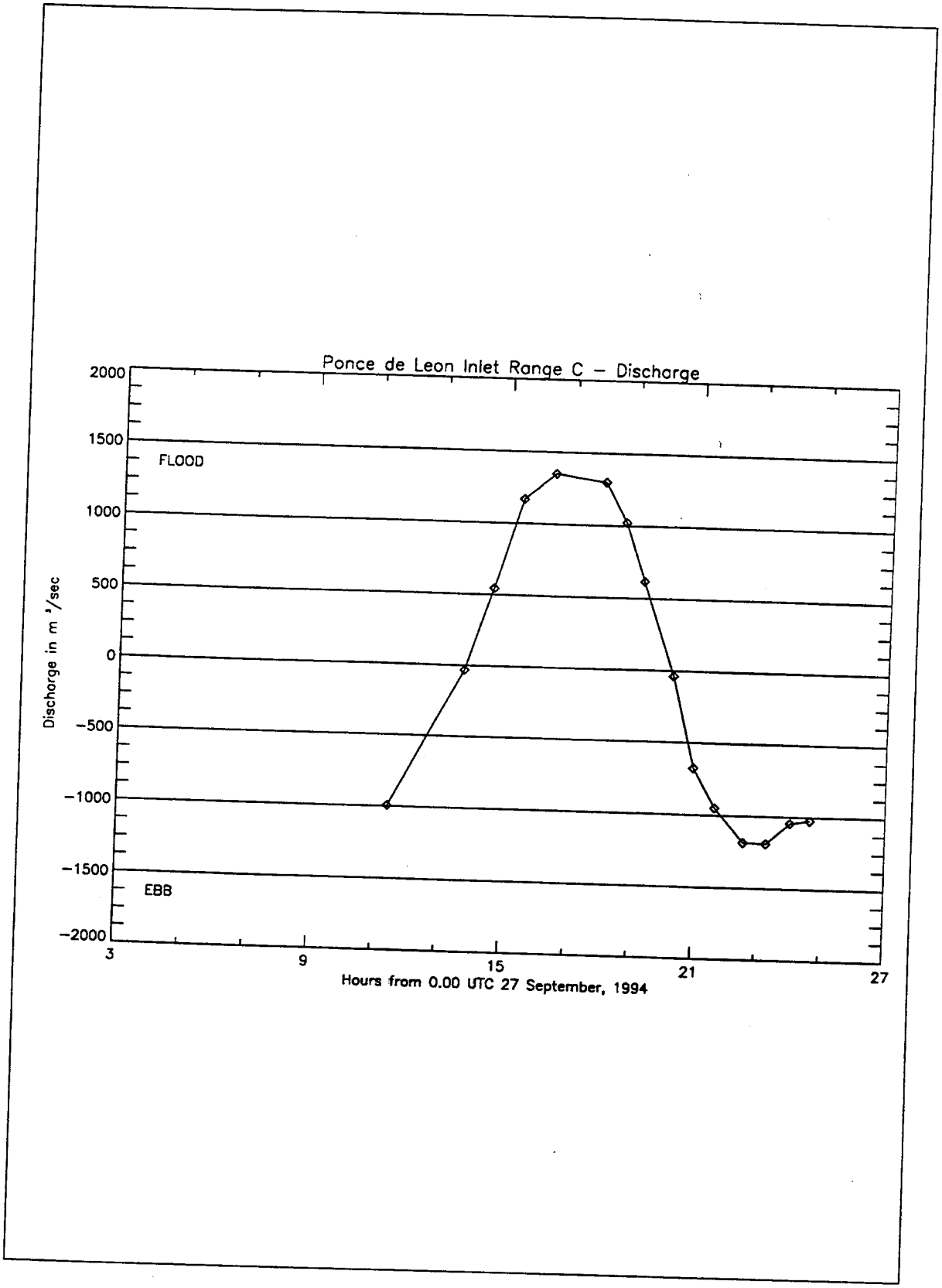

Figure 7. Discharge rates for Range C

3 Physical Model

Model Design

Ponce DeLeon Inlet physical model was constructed at an undistorted linear scale of 1:100, model to prototype. This scale was chosen based upon the following factors:

a. Size of the physical model which can accurately reproduce the necessary wave and flow patterns within physical limitations imposed by basin size and hardware constraints. For example, reproducing both the entire ebb shoal and the inland waterways was required.

b. Depth of water necessary to generate realistic waves without excessive scale effects.

c. Available shelter size and building limitations.

d. Model construction costs.

Following selection of the linear scale, the model was designed and operated in accordance with Froude's model law (Stevens et al. 1942). Scale relations used for design and operation of the model are given in Table 3.

The model reproduced Ponce DeLeon Inlet and the Atlantic Ocean in the vicinity of the inlet out to the -10.7-m (-35-ft) mlw contour. The landward extent of the model included a portion of the Halifax River, Rockhouse Creek, and Indian River, as shown in Figures 8 and 9. The total area reproduced in the model corresponded to approximately 900,000 sq m (21 acres) in the prototype.

The model was built in a shelter which has support beams located every 12 m (40 ft) running down the center of the building. Model placement within the building was determined by other ongoing projects and the location of the support beams. To minimize the impact of the beams on model studies, the model was placed such that one beam fell at the seaward end of the north jetty. The next beam fell on the south shore and the beam on the other side of the one located at the tip of the north jetty fell outside of the model limits, as can be seen in Figure 8.

Table 3
Physical Model Scale Relations[1]

Characteristics	Model-Prototype Dimension	Scale Relations
Length	L	L_r= 1:100
Area	L^2	A_r=1:10,000
Volume	L^3	$V_r=L_r^3$=1,000,000
Time	T	$T_r=L_r^{1/2}$=1:10
Velocity	L/T	$V_r=L_r^2$=10
Discharge	L^3/T	$Q_r=L_r^{5/2}$

[1] Dimensions are in terms of length (L) and time (T).

Heights of waves generated from a wavemaker are a function of the water depth at the wavemaker. To generate required wave heights and to minimize unwanted spurious wave components, the wave machines were located in the prototype depth of 30.5 m (100 ft). A 1:5 (vertical : horizontal) slope was used to transition between the basin floor and the beginning of the model contours at a depth of - 10.7 m (-35 ft) mlw. This steep transition slope was chosen because of limitations on the basin size.

Ideally, a quantitative, three-dimensional, tidal, moveable-bed model investigation would best determine the impacts of jetty modifications with regards to sediment accretion and erosion in the inlet. However, this type of model investigation is difficult and expensive to conduct. Fixed-bed models are a cost-effective alternative to moveable bed models. A fixed-bed, nontidal model is one in which the local bathymetry is molded in concrete. A nontidal model considers representative static, nonvarying water level and velocity conditions. To qualitatively study sediment transport, tracer material is placed on top of the concrete model. Location of the material after experimental runs gives an indication of sediment pathways and deposition and scour areas in the prototype. Comparing tracer motion between plans helps to identify preferred configurations.

Design of tracer material

As discussed previously, a fixed-bed model was constructed and a properly scaled tracer material was used to examine accretion and erosion in the inlet. Tracer was chosen in accordance with the scaling relations of Noda (1972), which indicate a relation among the four basic scaling ratios, i.e., the horizontal scale N_x; the vertical scale N_z; the sediment size ratio N_D; and the relative specific weight ratio N_ρ.[1] These relations were determined experimentally using a wide range of conditions and bottom materials. Froude scaling laws are not used for tracer material since the

[1] For convenience, symbols and abbreviations are listed in the notation (Appendix F).

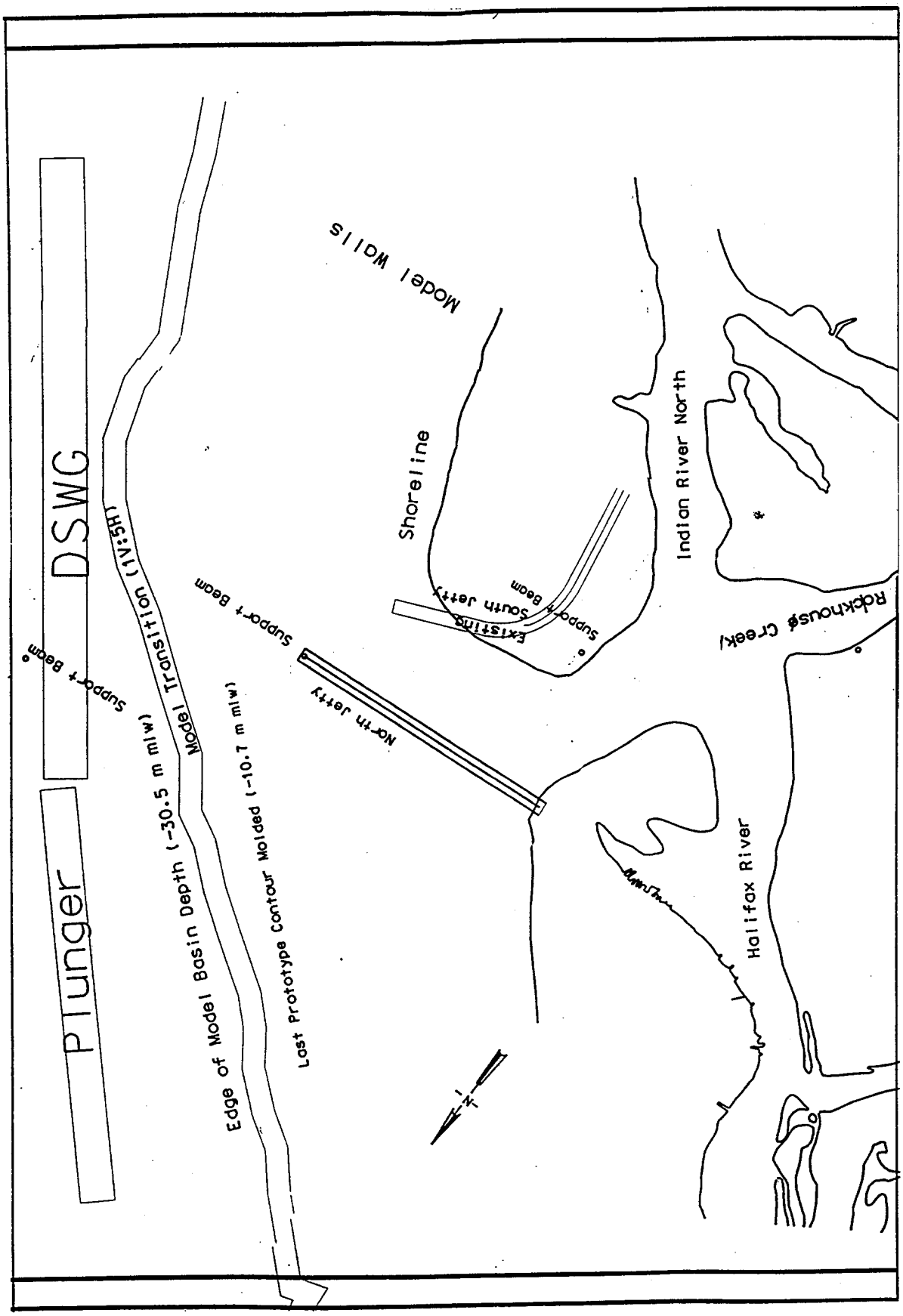

Figure 8. General physical model layout

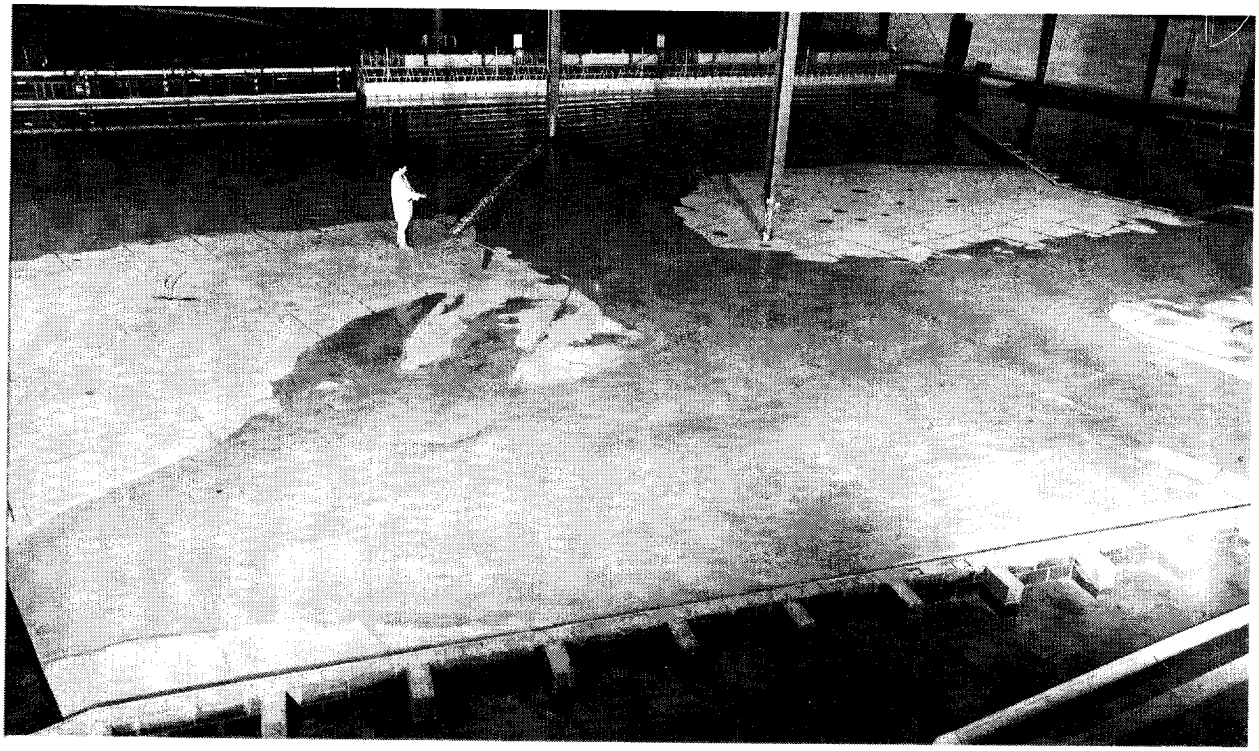

Figure 9. Physical model

physical properties of sand cannot be replicated with a material with a grain size that is 100 times smaller.

Noda's scaling relations indicate that movable-bed models with scales in the vicinity of 1:100 (model:prototype) should use a distorted model in which the horizontal and vertical scales are not equal. Since the fixed-bed model was undistorted to allow accurate reproduction of short-period wave and current patterns, the following procedures (which have been successfully used and validated for undistorted models) were used to design a tracer material (Bottin and Briggs 1996). A representative median sand grain size for Ponce DeLeon inlet is D_{50}=0.25 mm, specific gravity = 2.65[1] to 2.68 (Jones and Mehta 1978). Noda's relationship is given as

$$N_D \, (N_\rho)^{1.85} = (N_z)^{0.55} \tag{1}$$

where

[1] Personal communication, 1995, Terry Hull, Civil Engineer, Taylor Engineering, Jacksonville, FL.

$$N_\rho = \frac{\left(\frac{\rho_{solid}}{\rho_{water}} - 1\right)_{prototype}}{\left(\frac{\rho_{solid}}{\rho_{water}} - 1\right)_{model}} \quad (2)$$

where

$(\rho_{solid})_{prototype}$ = 1,365 kg/m^3 (2.65 slugs/ft^3) is the density of the prototype sand

$(\rho_{solid})_{model}$ = 670 kg/m^3 (1.3 slugs/ft^3) is the density of the tracer material

$(\rho_{water})_{prototype}$ = 1,025 kg/m^3 (1.99 slugs/ft^3) is the density of the seawater

$(\rho_{water})_{model}$ = 999 kg/m^3 (1.94 slugs/ft^3) is the density of the fresh water

The physical model used fresh water to minimize hardware corrosion and minimize cost and N_z = 100 and

$$N_D = \frac{(D_{50})_{prototype}}{(D_{50})_{model}} \quad (3)$$

Solving for $(D_{50})_{model}$ assuming crushed coal tracer, the size used in the model is 0.46 mm. The median grain size is actually larger than the prototype grain size. Several types of tracer material were available at WES, but previous studies (Giles and Chatham 1974, Bottin and Chatham 1975) have indicated that crushed coal more nearly represents sand motion. The scaled proper tracer size was then sieved and used in the model.

The scaling characteristics described above assume the tracer is fully submerged so that the specific gravity of the substance (relative to water) is correct. The material was always wetted before it was used in the model to assure proper sinkage. Once the tracer material is transported to shore and enters the swash zone, the material is no longer scaled and will move slower than prototype material.

Model Bathymetry

Three hydrographic surveys were used for model construction. All data were received digitally in Microstation design file format from CESAJ. The first data set, the largest and most recent, is the Light Detection and Ranging (LIDAR)-based Scanning Hydrographic Operational Airborne LIDAR Survey (SHOALS). This survey was conducted July 31 and August 1, 1994. This technology uses a laser transmitter and receiver for water surface and sea bottom detection. The helicopter-based system covered the majority of the area of interest; however, in certain

shallow-water areas, the coverage was incomplete and no on-land data were available with this method. To supplement the SHOALS survey, data collected in July 1994, including beach profiles, were incorporated into the design of the physical model. A third data set, collected in April 1994 and including 30.5-m (100-ft) cross sections of the inlet interior and entrance channels, was also used. All surveys were referenced to mlw.

Jetty Construction

South and north jetties were constructed in the model as defined in the prototype as-built drawings. In addition, a survey down the center line of the north jetty was conducted (April 1995) to aid in accurately reproducing the north jetty. Experience has shown (Le Méhauté 1965, Dai and Jackson 1966, Brasfeild and Ball 1967), for a 1:100 scale model that the geometric scale of the rock size must be doubled (over-sized in model) to accurately reproduce wave transmission and reflection from rubble structures. Model armor stone was geometrically oversized by a factor of two from those used in the prototype. Jetty underlayer and core were modeled with concrete and the shape of the jetties was controlled by setting templates perpendicular to the structure every 1.5 m (5 ft) or whenever the breakwater side slopes changed. The north jetty weir was simulated by a thin plastic strip embedded in the concrete underlayer and surveyed in to its mlw elevation and then rock was placed over the weir to represent existing conditions. The prototype weir was made sand tight up to the 0.9-m (3-ft) mlw elevation in 1984. However, to expedite removal and construction of the weir section, necessary under the large number of experimental conditions run, an impermeable concrete core layer was used in the physical model.

Model Appurtenance

Wavemakers

The seaward boundary of the model extends over 43 m (160 ft) in length and two wave machines were used to cover the modeled areas of interest. The Directional Spectral Wave Generator (DSWG) is 27 m (90 ft) in length and was used to generate waves approaching from south of shore normal. This wave machine was used for the south jetty experiments and a few north jetty weir experiments. A unidirectional spectral wavemaker was used for the majority of the north jetty weir experiments. It was a plunger wave machine measuring 18 m (60 ft) in length.

The DSWG is a unique wavemaker that can make waves from different directions without having to reposition the machine. It is an electronically controlled, electromechanical system, designed and built by MTS Systems Corporation, Minneapolis, MN. It consists of four modules with 15 paddles in each module. Paddles are 0.5 m (1.5 ft) wide and 0.8 m (2.5 ft) high. Each wave paddle is

independently driven at its joints by electric motors operating in piston mode. This configuration, along with flexible plastic plate seals between the paddles, produces a smoother, cleaner wave form (Outlaw and Briggs 1986, Harkins 1991).

Typical peak wave periods generated with the DSWG are 0.8 to 3.0 sec, with longer and shorter periods possible. The range of strokes is ± 15.2 cm (6 in.), corresponding to ±10-V input signal. Offset angles between paddles can be continuously varied within the range of 0 to 180 deg using the "snake principle" to produce directional waves at any angle from the wave machine for most wave periods.

Waves in nature have varying wave height, period, and direction. Although the DSWG is capable of generating realistic sea conditions, the wave conditions simulated were unidirectional spectral waves. This means that the wave conditions simulated had varying wave height and period (spectral) but that all waves came from the same direction. This simplification was made to be consistent with the waves produced by the plunger wave machine which is not capable of generating directional waves (from multiple directions). This simplification produces long-crested waves, although typically short-crested seas are found along the Atlantic Coast of Florida.

The DSWG was aligned 86 deg south of shore normal, approximately parallel with the back wall of the model basin, which is almost parallel with the shoreline orientation.

The plunger wavemaker is a spectral, unidirectional wave machine. This wave machine was used to generate waves for the north jetty weir experiments. It is called a "plunger" wave machine because the wave board is in the shape of a trapezoid and it is plunged into the water column. Wave heights generated by wave machines are a function of wave period and wavemaker stroke. The stroke for the plunger wave machine is the distance between the plunger's highest and lowest position. As the period increases, the stroke must become longer to maintain a given wave height. The stroke for this machine is ±11.4 cm (9 in.), which limited the generation of large, long-period storm waves for this model study.

The finite length of each machine limited the model area which could be covered by either machine. The wave field produced by finite length wavemakers is a function of the distance to the model and diffraction that occurs at the end of the machines. A compromise between area covered by the DSWG and plunger wave machine for their respective experiments had to be made. The DSWG was positioned to generate sediment motion to the north and to cover the inlet mouth. Waves from the plunger wave machine covered the area of the weir but not the inlet mouth.

Simulating the appropriate wave conditions is a process consisting of the following steps. First, the proper wave parameters for the model wave climate are calculated and a control signal representing the wave paddle's displacement from its mean position as a function of time is written digitally to tape. For the plunger wave machine, this consists of a single time series since the entire wave paddle moves in unison. For the DSWG, 60 control signal time series are generated, one for each individual paddle. The waves are generated, analyzed, and the control signal time

series modified to increase or decrease the wave height. No correction is needed for the wave period or direction.

Wave conditions are typically reproducible to within ±2 percent. This includes experimental, instrument, and round-off error associated with analysis of wave conditions.

Velocity flow-generating system

The Ponce DeLeon Inlet physical model was a steady-state, nontidal model. Although the water surface elevation and flow conditions change during a tidal cycle in nature, it was decided to simulate steady, or near steady, water level and flow conditions. The decision to use a "steady-state" approach was based on cost to provide time-dependent flow capability, time constraints on performing the study, available basin facilities, project objectives and expectations of the dominant processes in the primary region of interest. The dominant processes for sediment transport are wave driven and tidally driven flow. Sediment transport is greatest during peak tidal flows assuming all other forces remain constant. By reproducing these flows over an extended period of time, the physical model results should be conservative.

A water circulation system, consisting of a 20.3-cm (8-in.) PVC pipe, 30-HP, 0.3-cms (3-cfs) pump was used to generate peak spring flood and ebb velocity conditions. Depending upon the flow direction, water was added or removed at three stilling basins and behind the wavemakers through perforated PVC pipe. The velocity flow system was a closed loop circulation system in that water removed at one point in the physical model was added back at another point in the model, thus keeping the water level constant. An ultrasonic flow meter was strapped on to each pipe adjacent to each of the stilling basins. These meters measured the volume of water flowing through the pipe for a given time, and provided a means for adjusting flows to desired rates. Further discussion of the circulation system and the flow/water level conditions simulated can be found in the following chapter on model calibration.

Wave gauges

Thirteen parallel wire capacitance gauges were used to measure model wave heights. A calibration curve for each wave gauge was recorded each morning by automatically stepping wave rods throughout the water column over eleven steps. Twenty-one voltages were obtained for the eleven different steps (one for the two end points and two for each point in between, except for the zero position, where three values are recorded) to minimize the effect of slack in the drivers and hysteresis in the sensors.

Wave gauges are mounted on individual tripod stands, which were initially leveled and positioned at an appropriate height above the water column. The tripod legs are 0.9 cm (0.375 in.) in diameter and were positioned to minimize any interference

with incident waves being measured at the capacitance wave rods. Gauges are kept in position throughout a testing period.

Velocity gauges

Five SonTek Acoustic Doppler Velocimeters (ADV) velocity gauges were used to measure the simulated flood and ebb flow. Data collected for these gauges are recorded on a personal computer running SonTek's ADV software. This software provides a real-time display of the velocity data collected.

Gauges are factory calibrated and do not change unless the gauge is physically damaged. Changes in the speed of sound associated with changes in water temperature are easily compensated for by entry of sampled water temperature. Temperature changes were entered on a daily basis. Velocity gauge sensors were located at mid-depth in the water column with the x-direction located parallel to the major flow direction and the y-direction located perpendicular from the major direction of flow. The positive x-direction points offshore. The orientation of the probes allowed the principal velocity direction to be along the x-axis in most cases. The velocity resolution of the gauge is 0.1 mm/sec and data were collected at a rate of 10 Hz.

The velocity gauges also were located on tripod stands with the electronic housing located above water and connected to the acoustic transmitter and receiver by a 0.9-cm-(0.36-in.-) diam. stem. Tripod legs were aligned so that they were not in line with the principal flow direction and the velocity gauges. The transducers are located 6.1 cm (2.4 in.) apart and were connected by a 0.46-cm-(0.18-in.-) wide stem.

ADV's operate on the Doppler principle. First, a short acoustic pulse of known frequency is transmitted into the water column by the transducer and the pulse is reflected off particles in the water column, and then sensed by the receiver. By calculating the frequency shift in the returned signal, the speed of particles in the water column is calculated. The velocity of the water is assumed to be equal to the velocity of the particles. Particles, or seeding material, were added to the water to increase the number of particles that will reflect the acoustic pulse transmitted by the ADV transducer. The seeding material is called hollow spheres and has the same density as water and a 10-μm diameter.

Computer support

A Digital VAX 11/750 minicomputer was used to control the DSWG and plunger wave machine, calibrate the wave gauges, and collect wave gauge data. During wave gauge calibration, the computer continuously samples a sensor that determines the position of the wave gauge with the water column. When all of the wave gauges reach the proper position, the wave gauge voltage is sampled.

Wave gauge data are recorded concurrently with wave generation on the VAX 11/750. Wave gauge data are converted from analog voltage to digital values at a rate of 10 Hz. These data are stored in a binary file and represent voltage values.

A Digital VAX 3600 minicomputer was used for preliminary analysis of the measured wave data and to calculate control signals for the wavemakers. On the VAX 3600, the raw binary voltage file is combined with the calibration curves to provide the wave height record which is then converted from model to prototype units.

A 100-MHz Intel pentium processor computer running Microsoft Disk Operating System was used to collect velocity data from the SonTek gauges. This computer also was used for postprocessing of these data to calculate the mean velocity for each gauge.

Water level controller and point gauge

Water depth was maintained within ±0.01 cm (0.002 ft) of the desired level by an automatic water level float and an on/off solenoid control valve. When the float fell below a predetermined position, a 1.27-cm (0.5- in.) water line was turned on until the water reached the appropriate level. The float and water level controller probe were placed in a PVC tube with a small hole in the tube, which filtered out high-frequency noise associated with waves. The water level controller was placed in the corner of the model closest to the DSWG wave machine because of proximity to the water source. Water from the water level controller was discharged into a head-bay which had a depth of 1.5 m (5 ft) below the basin floor and did not impact generated flow or waves.

Another water level indicator called a point gauge was positioned over the inlet throat depth recorder (see Figure 2) and was used to measure the water surface elevation after the flow was established for each different flow regime. The water surface was measured at this location since there was a tilting of the water surface caused by the velocity flow generation system. The water level was manually adjusted until the correct level was obtained. The float elevation of the automatic water level controller then was adjusted to the proper elevation.

Wave absorbing material

A 0.6-m- (2-ft-) wide solid layer of fiber wave absorber was placed horizontally at strategic locations along the inside perimeter of the ocean side of the model to dampen wave energy that might otherwise be reflected from the model walls. Although studies quantifying the effectiveness of the rubberized "horse hair" have not been published, this material has been used for over 25 years as a passive wave absorber since it is effective in decreasing side wall reflection. This material, in 1.2-m- (4-ft-) wide, 0.6-m- (2-ft-) wide rolls, also was positioned behind the wave generators to dampen reflection from the model backwall. A 3-cm- (1-in.-) wide by

30-cm- (1-ft-) long piece also was placed on the seaward side of the support pole located at the tip of the north jetty to decrease the reflectivity of the vertical pole.

4 Selection of Experimental Conditions

Introduction

To address both physical model study objectives, navigation and sediment transport considerations needed to be addressed in the series of physical model experiments. Navigability in the channel is influenced by wave characteristics that result from strong wave-current-bottom interactions. Navigability also is influenced by the hazardous shallow-water areas that result from shoaling in the inlet interior caused by large sediment fluxes around the south jetty. As part of the experimental test plan, a set of "navigation" wave conditions was chosen to represent the larger wave conditions under which boaters would still make use of the inlet. The experimental plan also included a set of storm wave conditions that were selected to represent the storm-driven longshore sand transport regime. In addition to wave conditions, a set of typical spring astronomical, maximum ebb and flood velocity, and storm hydrodynamic conditions (currents and water levels) also were defined for use in experiments. The process for selecting the different experimental conditions is described below.

Prototype Wave Conditions

Prototype wave conditions can be inferred from 40 years of hindcast wave data presented in the WES Wave Information Study (WIS) reports (Hubertz et al. 1993, Brooks and Brandon 1995). The revised Atlantic Hindcast was queried to extract a data set containing 3-hr estimates of the wave climate from January 1, 1956 to December 31, 1975 for two WIS stations (one north and one south of Ponce DeLeon Inlet). The two stations are WIS stations 21 and 22. Their locations and depths are shown in Table 4. A second data set contained hindcast wave information from 1976 through 1993, including wave fields produced by hurricanes. Data for the same two stations were extracted from the more recent hindcast.

Physical model natural contours begin at the -10.7-m (35-ft) mlw depth contour. Since the WIS stations were located at the -18-m (59-ft) and -22-m (66-ft) depths,

Table 4
Location and Water Depth of WIS Stations Near Ponce DeLeon Inlet

WIS Station Number	Latitude	Longitude	Water Depth (m)
21	29.00	80.50	18
22	29.25	80.75	22

all wave conditions were first transformed using the Shoreline Modeling System (SMS) software to the depth corresponding to the beginning of the physical model contours. Straight and parallel contours were assumed between the WIS locations and the -10.7-m (35-ft) mlw depth.

Conditions for Safe Navigation

Criteria were needed to establish typical wave conditions under which boaters thought they could safely transit the inlet. The wave height upper limit then would be simulated in the physical model experiments. In a personal communication with Mr. Mitch Granat, Table 5 was provided.[1] This table was compiled by Mr. Ian Mathis (CESAJ) and represents information from commercial and recreational boaters from Ponce DeLeon Inlet, Hillsboro Inlet, and St. Augustine Inlet, all located on the Atlantic Coast of Florida.

Selection of Wave Conditions for South Jetty Extension Experiments

The purpose of the proposed extension of the south jetty was to reduce northward sediment transport around the tip of the jetty without adversely impacting navigation in the inlet. Ten wave cases were selected for examination in the experimental test series. Four of the wave conditions are termed "navigation" waves (waves S1- S4). These four waves have periods and incident directions that typically occur under nonstorm conditions. The process for selecting periods and angles is discussed below. A single H_{m0} wave height, 1.5 m, was selected for all four navigational wave conditions. As can be seen in Table 5, a 1.9-m (6.2-ft) wave height is the largest wave condition for all boats and boats less than 7.6 m (25 ft) require waves less than 1.5 m for boaters to feel that they can safely transit the inlet. H_{m0} is an energy-based calculation and is approximately equal to $H_{1/3}$, which is calculated in the time domain. $H_{1/3}$, is the height of the highest 1/3 waves. One must be careful in comparing an offshore wave height of 1.5 m with the wave height listed in Table 5. Wave heights experienced inside the inlet are a function of

[1] Personal Communication, 11 October 1995, Mitch Granat, Civil Engineer, U.S. Army Engineer District, Jacksonville.

water depth, deepwater wave height, wave period and direction, and transformation over complex bathymetry and currents. For comparative purposes between experiments, a deeper water wave height was chosen as the target instead of a wave height at the inlet mouth, since each wave would have to be calibrated for each of the four water depths tested. The differences between deepwater wave heights and wave heights at the inlet will be discussed in detail in Chapter 5. The high-end wave height was chosen to try to minimize scale effects, thereby maximizing accuracy of the data collected in the physical model.

Table 5
Maximum Wave Heights Considered for Safe Transit[1]

Boat Length (m)	Inlet Wave Height (m)	
	Head-on to the Vessel	Broadside to the Vessel
<6 (20 ft)	1.1± 0.15 (3.5± 0.5 ft)	0.8-1.1 (2.5 - 3.5 ft)
6 - 7.6 (20-25 ft)	1.4 ± 0.15(4.5± 0.5 ft)	1.1 ± 0.15 (3.5± 0.5 ft)
> 7.6 (25 ft)	1.5 ± 0.15 (5.0±0.5 ft)	1.4 ± 0.15 (4.5± 0.5 ft)

[1]Any waves larger than 1.9 m (6.0 ft) would be considered to be a problematic condition for any user.

Mr. Dan O'Brien, Director, Ponce DeLeon Inlet Port Authority indicated that the worst wave conditions, from a navigational standpoint, occurred when waves propagated directly up the inlet.[1] The complex offshore bathymetry will sometimes cause this condition. Two wave directions were chosen. The first direction selected (60 deg true north, (TN), or 0 deg shore normal) was perpendicular to the local shoreline. This is the principal direction at which waves approach the shoreline, based on the results from an analysis of the 40-year WIS record. The second direction selected (80 deg TN or 20 deg shore normal) is approximately parallel with the north jetty and is 20 deg south of the local shoreline normal. This condition was chosen to produce waves that propagate straight up the channel.

The mean peak wave period at Ponce DeLeon Inlet for each of the 20-year hindcast is shown in Table 6. To represent typical wave conditions as well as slightly longer waves that would tend to produce more severe wave-current-bottom interactions, wave periods of 8 and 12 sec were selected for navigation wave conditions.

Table 7 provides the four target wave conditions selected for the navigation studies for south jetty modifications. In Table 7, H_{m0} is the wave height in a water depth of 9.1 m (30 ft) mlw, T_p is the peak spectral period, θ_p is the principal direction of wave propagation with angles measured clockwise relative to an orthogonal to the local shoreline (the shoreline is oriented along an azimuth of about 330 deg), compass direction is defined as the angle from which waves propagate (measured clockwise from TN), and gamma is the peakedness of the spectra in the frequency domain. The angle convention for θ_p was chosen to indicate the angle of wave

[1] Personal Communication, 1995, Dan O'Brien, Director, Ponce DeLeon Inlet Port Authority, FL.

Table 6
WIS Mean Peak Wave Period at Stations 21 and 22

Station Number	Data Range (years)	Mean, Peak Wave Period (sec)
21	1956 - 1975	7.2
	1976 - 1993	9.2
22	1956 - 1975	7.0
	1976 - 1993	9.0

Table 7
South Jetty Extension Deepwater Wave Conditions Simulated to Study Navigation Concerns

Wave Parameters	Nav. Wave S1	Nav. Wave S2	Nav. Wave S3	Nav. Wave S4
H_{mo} (m)	1.5	1.5	1.5	1.5
T_p (sec)	8	12	8	12
θ_p (deg)	0	0	20	20
Compass Dir. (deg)	60	60	80	80
γ	3.3	4.0	3.3	4.0

incidence to the shoreline. A shallow-water incident wave angle of 0 deg reflects waves approaching from deep water at about 60 deg east of north. The parameter gamma controls the wave "groupiness" and reflects the distance waves have traveled. As waves travel long distances, there is a natural switch toward long-period grouped swell waves. Values of gamma chosen correspond to appropriate values for the peak period. Values of 3.3 and 4.0 produce a broad spectrum in the frequency domain and are indicative of wind waves.

In addition to lower-energy navigation waves, six storm wave conditions were chosen to investigate the effectiveness of the South Jetty extension in reducing the amount of northbound alongshore sediment transport that moved around the jetty. Only two storm conditions were originally planned, but after generating them and assessing the response that they produced, additional conditions were added for reasons discussed below.

Extreme wave heights were identified by scanning the storm events in the WIS hindcast records. Maximum storm wave heights for each year of the hindcast were extracted, and 1-year and 5-year wave heights were selected based on a frequency-of-occurrence analysis of wave height for the two WIS stations. An average wave height value for each return period then was calculated, and a wave period was chosen by picking the modal (most frequently occurring) period of the storm height/period pairs.

The angle of wave incidence was determined based upon calculated sediment transport rates and the chosen wave periods and heights. SMS software was used to compute the maximum potential longshore sand transport rates for each year of the hindcast, maximum transport rates were ranked, and 1-year and 5-year rates were selected. The 1- and 5-year transport rates from the two WIS stations were averaged, and then the SMS software was used to iteratively solve for the angle of incidence which yielded the desired sediment transport rates (using the storm wave and height and periods defined above). Angles of 3 and 11.5 deg, relative to shore normal, were selected. Table 8 summarizes these wave conditions.

Table 8
Target Storm Wave Conditions

Wave Parameters	1-year	5-year
H_{mo} (m)	3.6	4.8
T_p (sec)	11.5	13.0
θ_p (deg)	3.0	11.5
γ	4.0	4.5

The SMS calculation procedure assumes straight and parallel contours from the 10.7-m (35-ft) mlw depth contour to shore. However, the contours of the ebb shoal are very complex, and not straight and parallel. The presence of the ebb shoal changes the incident wave angle seen at the breaker zone. Based on preliminary experimental results, the calculated angles did not cause northerly sediment transport. In fact, the 1-year storm caused southerly transport. To increase the sediment transport to the north, a review of incident wave conditions from the 40-year WIS data set were used in choosing wave angles of 20 and 30 deg south of shore normal (80 deg east of north and due east). The set of storm wave conditions was expanded to include additional cases with the larger angles of incidence producing the desired northward sediment transport in the model.

Table 9 lists the entire set of wave conditions adopted for use in experiments of the south jetty extension alternatives, as measured at two calibration wave gauges.

Selection of Wave Conditions for North Jetty Weir Experiments

The purpose of modeling different north jetty weir sections was to quantify changes in wave energy and current velocity within the inlet which might impact navigation and to examine the deposition of material after it is transported over the weir. To address the navigation and sediment transport questions, a scheme similar to that used for selecting waves for the south jetty extension experiments was used to select wave conditions for the north jetty weir experiments.

Table 9
Experimental Wave Conditions for Studying South Jetty Modifications

Experiment/ Wave Number	Wave Condition	H_{mo} Wave Height Defined in 9.1-m Water Depth		Peak Wave Period (sec)	Compass Direction Measured from TN
		Target Wave Heights, m	Simulated Wave Heights, m		
S1	Nav. Wave 1[1]	1.5	1.5	8	60
S2	Nav. Wave 2[1]	1.5	1.6	12	60
S3	Nav. Wave 3[1]	1.5	1.6	8	80
S4	Nav. Wave 4[1]	1.5	1.5	12	80
S5	1-year 3 deg SSN[2]	3.6	3.9	11.5	63
S6	5-year 11 deg SSN[2]	4.8	4.6	13	71
S7	1-year 20 deg SSN[2]	3.6	3.8	11.5	80
S8	5-year 20 deg SSN[2]	4.8	4.8	13	80
S9	1-year 30 deg SSN[2]	3.6	4.0	11.5	90
S10	5-year 30 deg SSN[2]	4.8	4.7	13	90

[1]Navigation conditions.
[2]Sediment transport conditions.

For navigation waves, the same wave height and periods that were used for the south jetty extension experiments also were used for the north jetty weir experiments. The primary purpose of running these waves was to address changes in wave conditions inside the inlet for different weir openings. The secondary purpose of navigation waves was to determine the amount of sediment transported over the weir under more typical wave conditions.

The angle chosen for the navigation waves should be a typical wave direction at Ponce DeLeon inlet but should still allow waves to propagate over the weir. Unlike the south jetty experiments, for the north jetty weir experiments, one angle was chosen for the navigation waves as well as the 1-year and 5-year storm events. The angle used was again calculated based upon sediment transport rates for storm events.

The largest wave heights for waves from north of shore normal were identified in the WIS hindcast record. The 1-year and 5-year wave heights of 3.6 m (12 ft) and 5.7 m (19 ft), respectively, were selected by averaging the results over the two WIS stations and the modal period associated with this wave height was chosen. Wave periods of 12 and 15.5 sec were selected for the two storm conditions.

The angle of incidence was determined by calculating the sediment transport rate for the chosen wave height/period combinations for the two storm conditions. A wave angle of 4 deg north of shore normal was initially calculated and generated with the plunger wave machine. This angle corresponded to the best compromise

between the 1-year and 5-year storm-induced sediment transport rates predicted by the SMS.

Hardware limitations associated with the plunger wavemaker limited the height of the 5-year storm wave. The 5.7-m (18.7-ft) wave height could not be generated for the chosen period. This wave also tended to break on the model transition to the natural contours. Since this wave was chosen to investigate sediment transport characteristics, the same alongshore transport rate could be modeled by a smaller wave generated at a more oblique angle. The SMS assumes straight and parallel contours and thus provides an underestimate for the chosen wave angle for the bathymetry north of the north jetty. To increase the sediment transport rate for a smaller incident wave height, the angle of incidence was increased to 8 deg. The chosen wave height for the 1-year storm conditions remained the same. This angle was chosen as a compromise between wave height, period, and wave direction and was chosen to simulate the proper alongshore sediment transport characteristics for one angle and two sediment transport rates associated with the 1-year and 5-year storms.

As was mentioned in Chapter 3, the wave field produced by the plunger wave machine covered the weir opening lengths but not the inlet mouth. To ascertain differences in waves propagating down the inlet to different flow regimes, the navigation waves (waves S1- S4) also were tested during the north jetty weir experiments. Table 10 summarizes conditions reproduced in the physical model during the north jetty experiments as measured by two calibration wave gauges located along the 9.1-m (30-ft) depth contour.

Table 10
North Jetty Alternative Experimental Wave Conditions

Wave Number	Wave Condition	H_{m0} Wave Height Defined in 9.1-m Water Depth		Peak Wave Period (sec)	Compass Direction Measured from TN
		Target Wave Heights, m	Simulated Wave Heights, m		
N1	Nav. Wave 1	1.5	1.5	8	52
N2	Nav. Wave 2	1.5	1.6	12	52
N3	1-year Storm 8 deg NSN	3.6	3.7	12	52
N4	Five Year Storm	5.7	4.2	15.5	52
S1	Nav. Wave 1	1.5	1.5	8	60
S2	Nav. Wave 2	1.5	1.6	12	60
S3	Nav. Wave 3	1.5	1.6	8	80
S4	Nav. Wave 4	1.5	1.5	12	80

Note: All waves were generated with an angle of 8 deg north of shore normal or 52 deg east of north.

Water Levels Modeled

Because a steady-state physical modeling approach was adopted, the water level in the model was held constant during each experiment. Four different static water levels were considered in the experimental series, two representing water levels typical of spring peak ebb and flood velocity conditions, and two representing water levels associated with spring peak ebb and flood velocity in combination with a hypothetical annual storm event. Water levels were defined using results from the numerical model investigation (Taylor et al. 1996).

The primary location of interest for the physical model experiments is the inlet channel. For this reason water levels were chosen to be those that correspond with peak flows through the inlet channel, specifically flows across the four-field range lines labeled A-D as shown in Figure 2. According to numerical model results provided by Taylor Engineering, water surface elevations of 0.4 m (1.5 ft) mlw and 1.28 m (4.2 ft) mlw correlate with maximum flow velocities for peak spring ebb and flood tidal flow, respectively, at the inlet mouth water level recorder location.

Two additional water levels associated with an annual storm and peak spring tidal conditions also were defined for use in the experimental series. It is assumed that the majority of alongshore sediment transport occurs under storm conditions. Typically under these conditions, the water surface would be elevated along the coastline due to wind setup and atmospheric pressure gradients. Taylor Engineering staff performed simulations of a hypothetical storm event at spring tide, and calculated water levels and flows at times of peak ebb and flood velocity. Water surface elevations of 1.1 m (3.5 ft) and 1.34 m (4.4 ft) mlw were computed for storm peak spring ebb and flood velocities, respectively. For a detailed explanation of how the water surface elevations were calculated see Taylor et al. (1996) documenting the numerical modeling work performed concurrently with the physical model study. Table 11 summarizes the modeled water levels as measured by a point gauge at the location of the inlet mouth water level recorder shown in Figure 2.

Table 11
Steady-State Static Water Levels Simulated in Physical Model

Naming Convention	Water Level Above mlw (m)
Spring Peak Ebb (SPE)	0.40
Spring Peak Flood (SPF)	1.28
Spring Peak Ebb Storm (SPES)	1.10
Spring Peak Flood Storm (SPFS)	1.34

Process for Defining Boundary Flow Conditions

As stated earlier, discharge values into the three stilling basins in the physical model were calculated by ultrasonic flow meters strapped onto the pipes adjacent to the basins. These meters induce an ultrasonic signal into the pipe and measure the velocity of particles in the water by calculating the Doppler shift in the returned signal. By knowing the interior diameter of the pipe, the meter can be used to calculate the discharge through the pipe.

An iterative process was used to establish correct flows into or out of the three stilling basins. The circulation system was a coupled system in that changes in the amount of water going in to one stilling basin affected the amount of water going into the other two stilling basins. For each flow condition, seven valves were set, four of which required adjusting. Four valves were set around the pump to control the flow direction, two of which were closed completely. The valve on the suction end of the pump was completely opened while the valve on the outflow end of the pump was "choked" down to only allow approximately the same quantity of water that was going into the three stilling basins through the pipe. First, the pump was started and the circulation line was bled of any air in the lines. The flow into one stilling basin was adjusted first by opening or closing the valve adjacent to the basin until the ultrasonic flow meter reading matched the target discharge value. The next two stilling basins were adjusted in the same way. This process was repeated until the proper discharge was reached on all stilling basins. The opposite flow condition was achieved by closing the two valves around the pump that were opened and opening the other two valves that were closed.

Every effort was made to consistently reproduce the desired flow condition each time it was generated. However, even small changes in any of the five non-closed valve settings can lead to changes in the discharge into a basin of up to 15 percent. The pump system could not be turned off and then immediately restarted without changes in the flow distribution between the three stilling basins. For this reason, the reproducibility in velocity measurements within the inlet is probably no better than ±10 percent. Changes in velocity measurements of less than 10 percent in the physical model could be attributable to experimental error. Consequently, for assessing very small changes in the velocity patterns associated with different project alternatives, the numerical model is a better tool, since model results are very reproducible.

An abundance of prototype flow data were available for use in calibrating and evaluating the physical model. Prototype data were available at several locations throughout the inlet system, as velocity measurements and discharge values across the transect lines, and at discrete points. Figure 7 shows the discharge values during peak spring flood and ebb tidal flow across the field range line C.

Peak velocities and peak discharge values did not occur at the same time in the prototype at all transect lines because of differences in tidal phase. Nevertheless, the peak discharge values in the inlet throat were used to drive the physical model, not the actual discharge values at the locations of the stilling basins at the time peak

flows occurred within the inlet throat. This is also a ramification of using a steady-state modeling approach. In nature, the water surface elevation and flows are changing as the tidal wave propagates into and out of the inlet. However, the physical model was a steady-state nontidal model with a closed-loop circulation system. Water was pumped through the model and then discharged back into the model at a different location. The water surface elevation was kept constant while the flows were running since water was not added to or lost from the system.

Comparison of velocities measured in the physical model with desired values based on field measurements was an integral part of the iterative model calibration/evaluation process. Discrete points along the field range lines, called station numbers, were identified as candidate locations for comparing prototype velocities with point velocity measurements made with the ADV velocity gauges in the physical model. Points along the range lines were identified, and are indicated by the small "x's" in Figure 10. Points for actual comparison of model and field data were selected based on the following set of criteria:

a. Located in the deepest portion along the transect since this is the location where the majority of water flows.

b. Located in a region of small horizontal gradients in the velocity. These areas were chosen so that small errors in the placement of the velocity gauge in the model did not correspond with large changes in the measured velocities.

c. The location satisfied criteria 1 and 2 for both peak flood and ebb velocity conditions.

Using the criteria outlined above, stations 8, 2, 1, and 2 were chosen for Ranges A through D, respectively, and are marked with velocity gauge symbols (Figure 10).

Velocities measured in the physical model were compared to the velocities measured at these points along the field measurement transects to facilitate the iterative boundary flow adjustment process.

Flow Conditions Simulated

The field-measured peak discharge values across range lines E, G, and H (Figure 2) were used initially as boundary conditions or input for the three stilling basins. The peak velocity for each range line for the ebb and flood spring conditions is shown in Tables 12 and 13. The velocities measured at the four chosen stations were compared against the field measurements and then the discharges into the three stilling basins were either increased or decreased until the average value between the velocity gauges located on the four station numbers and the field measurements was a minimum. The discharge values were increased or decreased by a constant value into the three stilling basins. These desired flows were established in the physical model using the iterative adjustment process discussed earlier.

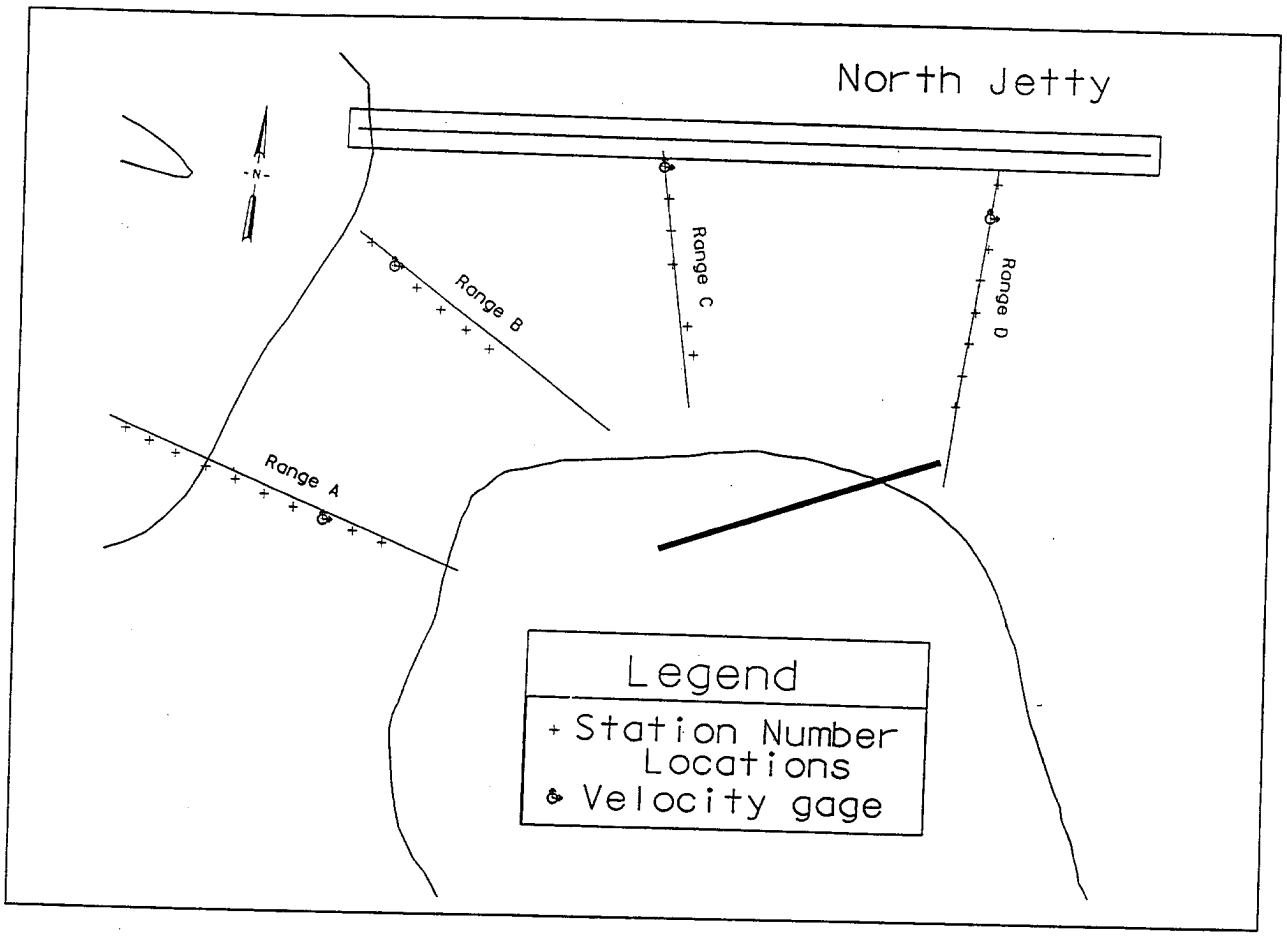

Figure 10. Range line and station number positions

For spring peak flood (SPF), the peak discharge values measured in the prototype provided good agreement between the peak velocities measured in the prototype and the physical model (Table 12). For this condition, measured velocities at the four station locations, or gauges, used to calibrate/evaluate the physical model were, on average, only off by 1 percent as can be seen from Table 12. One should note that this is the average over all gauges, with some gauges reading too low and others reading too high. The sign of the difference was retained in the calculation of the average to show the average magnitude of the differences found. The average, absolute value of the percent difference is off by 14 percent. In this case, the absolute values of the difference were averaged.

For spring peak ebb (SPE) flow, the field-measured, peak discharge values had to be increased by 30 percent to minimize the differences between the prototype and the physical model measured velocities at the four station numbers. For this flow, the results for the four station locations show an average difference of 7 percent while the absolute average difference was 13 percent as can be seen in Table 13. One can note from the percent differences that the model flows are too fast at range lines A and B and too slow at range lines C and D.

Table 12
Spring Peak Flood Velocity

Spring Peak Flood Flows					
		Current Speed in cm/sec			
			Model		Percent
Range	Station No.	Prototype	Theoretical	Average	Difference
A	8	91	9.1	6.7	27
B	2	105	10.5	12.3	-17
C	1	82	8.2	7.9	4
D	2	84	8.4	9.1	-8
Avg. =					1
Absolute Average Difference =					14

Table 13
Spring Peak Ebb Velocity

Spring Peak Ebb Flows					
		Current Speed in cm/sec			
			Model		Percent
Range	Station No.	Prototype	Theoretical	Average	Difference
A	8	94	9.4	10.3	-10
B	2	83	8.3	8.6	-4
C	1	120	12	9.7	19
D	2	109	10.9	8.7	20
Avg. =					7
Absolute Average Difference =					13

It is unclear why the ebb flow had to be increased by 30 percent over the measured prototype flow. One explanation could be that the physical model did not reproduce the bottom friction well for steady-state flow. Other explanations include difficulties in reproducing head differences between the inlet and the edge of the model because of the obstruction of the wave machines. Although the water surface is slightly elevated for the flood flow, the same problem was not seen. Actual discharge values used in the physical model in prototype units are shown in Table 14.

A storm condition was numerically modeled to ascertain the increase in water level and flow conditions caused by a typical annual storm event. See Taylor et al. (1996) for details on how the flows were calculated. Based on results from the calibration/validation of the numerical model, the model under-predicted discharge values when compared to field measurements. The optimal numerically produced discharge values along range lines E, G, and H (south channel, Rock House Creek, and north channel, respectively) for spring peak conditions plus storm-induced flows were less than the field-measured peak tidal flows alone. These three range lines correspond with the physical model stilling basins where water was added

Table 14
Comparison Between Measured Prototype Discharge and Simulated Model Discharge Values for Spring Peak Ebb and Flood Flows

Range Line	Measured Discharge Values, cu m/sec			
	Spring Peak Ebb (SPE) Flow		Spring Peak Flood (SPF) Flow	
	Prototype	Model	Prototype	Model
E	660	858	890	890
G	120	156	340	340
H	100	130	760	760

or removed. To remedy this problem and obtain more representative storm flows for use in the physical model, the numerical model storm flows were increased according to the following process.

Using results from the numerical model, the ratio of the storm-plus-tide discharge to the tide-only discharge was calculated for the three boundary range lines (E, G, and H) for both ebb and flood. This ratio represents the predicted, or simulated, increase in discharge associated with the storm condition. The ratios at each range line were within 6 percent of each other for both flood and ebb flow. Therefore, ratios were averaged and one value was found for flood flow, and one for ebb flow. The flow condition termed "spring peak ebb storm" (SPES) consisted of peak spring ebb plus storm-induced flow that was 129 percent of the calibrated tide-only discharge, i.e., the storm ebb discharge was increased an additional 29 percent. For the spring peak flood storm (SPFS) flow, consisting of peak spring flood plus storm-induced flow, the discharge was 137 percent of the calibrated tide-only discharge, i.e., the storm flood discharge was increased by 37 percent. These flow increases were applied to the stilling basin discharge rates for the tide-only conditions. The actual discharge values used are shown in Table 15.

Table 15
Imposed Storm Boundary Forcing Conditions on a Peak Spring Storm Flow Across the Three Range Lines which Correspond with the Three Stilling Basins

Range Line	Discharge Values, cu m/sec	
	Spring Peak Ebb Storm (SPES) Flow (Added)	Spring Peak Flood Storm (SPFS) Flow (Removed)
E	850	1,220
G	155	466
H	130	1,040

As stated earlier, an increased water level also was calculated by the numerical model for SPES and SPFS conditions. For SPES, the water level was increased to 1.1 m (3.5 ft) mlw. For SPFS flow, the water level was increased to 1.34 m (4.4 ft) mlw.

Increasing the discharge values for a constant water level causes increased velocity. However, when the water level was increased, the cross-sectional area of the channel over which the water flows increased. Table 16 compares numerical model-generated and physical model-generated velocities for two sets of conditions, tide-plus-storm and tide only. On ebb, the storm water level was increased by 0.6 m (2 ft). Some velocities increased and others decreased for the storm ebb condition. On flood, the water level was increased by 0.06 m (0.2 ft), while the discharge was increased by 37 percent. Flood velocity at all transects increased.

Table 16
Summary of Inlet Velocity Observations

Velocity Conditions in cm/sec (Model Units)							
Range	Station No.	SPES	SPE	Percent Change	SPFS	SPF	Percent Change
A	8	10.6	10.3	+3.0	9.0	6.7	+35
B	2	8.2	8.6	-5.0	13.5	12.3	+10
C	1	9.5	9.7	-2.0	8.2	7.9	+5
D	2	9.7	8.7	+11.0	10.1	9.1	+11

5 South Jetty Experimental Results

Overview of the Experimental Plan

Results from experiments of the existing south jetty and several proposed extensions were used to determine an optimal south jetty configuration for reducing the movement of sand around the jetty and into the inlet. First, wave and current measurements for combinations of the four water level /flow conditions and ten wave cases outlined earlier were made for the existing south jetty condition. The measurements served as a baseline data set to be used for comparative purposes. Dye experiments then were used to determine flow characteristics in the vicinity of the existing south jetty and several proposed extensions to determine the best jetty length for reducing sediment influx. A "worst-case" water level/flow condition, in the sense of having the greatest potential to move sand into the inlet, also was determined. The most promising alternatives were evaluated using moveable tracer experiments, which led to selection of a preferred plan. The preferred alterative was then subjected to the complete set of wave and water level/flow conditions to compare its performance to that of the present jetty configuration.

Based on input from CESAJ, two south jetty concepts were considered. One consisted of a straight extension of the south jetty in line with the longitudinal axis of the existing structure. The second alternative consisted of the extension oriented parallel with the north jetty and was termed the dogleg extension. South jetty extension lengths of 152 m (500 ft), 244 m (800 ft), and 305 m (1,000 ft) were evaluated as possible lengths with the chosen length to be determined by a combination of physical model wave, sediment transport and dye study results, along with a numerical model assessment. The alternative south jetty extensions that were considered are shown in Figure 11.

Dye patterns indicated that the full-length extension (305 m (1,000 ft)) would be needed. The dye experiments also indicated the "worst case" combination of water level, flow, and wave condition which caused the quickest dye movement into the inlet. Once the length of the south jetty was determined, tracer experiments were used to determine the preferred orientation. This "worst case" condition was the

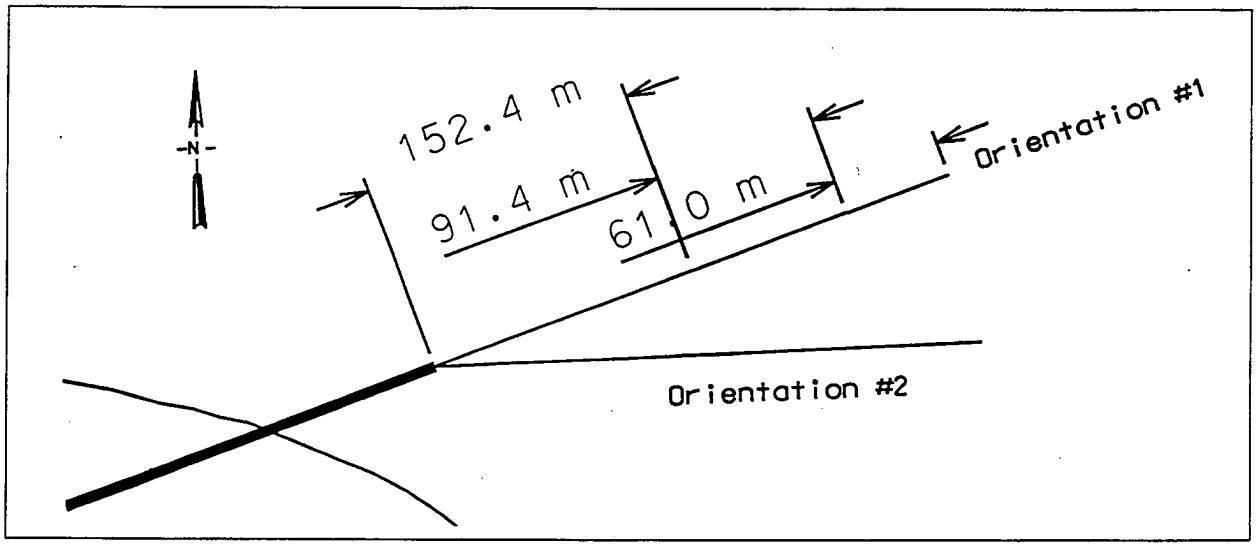

Figure 11. The south jetty extension lengths and orientations

only hydrodynamic case run during tracer experiments. Results from the physical model tracer experiments were somewhat inconclusive. However, the flow distribution results from the numerical model experiments indicated the dogleg extension provided a more uniform flow distribution across the width of the inlet.

Wave and velocity measurements then were made on the preferred dogleg jetty with combinations of the four water level/flow conditions and the ten wave conditions. Results were compared to the baseline data set for existing conditions. Table 17 summarizes the various experiments conducted. Wave conditions for the south jetty extension experiments are defined in Table 9.

Assessment of Sedimentation Reduction Using Dye and Tracer Experiments

Initially, dye was used to observe current patterns in the vicinity of the south jetty. A dye patch was added to the water just south of the south jetty and results were recorded on a 1.9-cm (3/4-in.) videotape. Copies of these video recordings are on file at CESAJ ("Ponce DeLeon Inlet Physical Model South Jetty Tests"). The dye experiments helped indicate the appropriate south jetty length that would be needed to stop sediment transport past the jetty tip. The dye experiments indicated that the 305-m (1,000-ft) extension would provide the best barrier for the observed flow patterns. Dye motion is clearly visible in the video but is difficult to capture in still photos.

Initially, ebb and flood storm discharge and water level conditions were simulated for varying storm wave conditions for the existing south jetty. For the ebb condition, there was little motion to the north in the vicinity of the south jetty except

Table 17
South Jetty Experiment Series

Water Levels (m)	Flows	Experiment and Measurements Conducted	Waves									
			1	2	3	4	5	6	7	8	9	10
0.5	SPE	Dye							a	a	a	a
		Tracer										
		Wave Height	a,c	a, c	a, c	a, c	a, c	a,c	a,c	a,c	a,c	a,c
		Velocity	a,c	a, c	a, c	a, c	a, c	a,c	a,c	a,c	a,c	a,c
1.1	SPES	Dye										
		Tracer										
		Wave Height						a,c	a,c	a,c	a,c	a,c
		Velocity						a,c	a,c	a,c	a,c	a,c
1.28	SPF	Dye							a,b, c	a,b,c	a,b, c	a,b,c
		Tracer										
		Wave Height	a,c	a, c	a, c	a, c	a, c	a,c	a,c	a,c	a,c	a,c
		Velocity	a,c	a, c	a, c	a, c	a, c	a,c	a,c	a,c	a,c	a,c
1.34	SPFS	Dye										
		Tracer										a,b,c
		Wave Height						a,c	a,c	a,c	a,c	a,c
		Velocity						a,c	a,c	a,c	a,c	a,c

Note: a = existing conditions
b= 305-m straight south jetty extension
c = 305-m dogleg south jetty extension

in the area from the south jetty east approximately 157 m (500 ft). For flood conditions, the dye moved at a constant rate across the proposed full length of the south jetty extension.

For the 305-m (1,000-ft) extensions only the spring peak flood condition and the 1-year and 5-year waves were simulated. For the straight and dogleg extensions, dye moved quickly to the north at the tip of the jetty and along the extent of the existing portion of the jetty (the shoreward 150 m (500 ft)).

The "worst case" motion of sediment transport was associated with spring peak flood storm water level and flow (SPFS) plus the 5-year storm wave condition (H_{m0} = 4.7 m, T_p = 13.0 sec, from 30 deg south of shore normal). This condition

caused the quickest dye movement into the inlet in the physical model. Northbound wave-driven longshore currents and tidal currents combined to produce the high rate of movement. The black crosses shown in the video, in line with the jetty axis, denote the 152-m (500-ft), 244-m (800-ft), and 305-m (1,000-ft) extensions.

Tracer experiments were first run on the existing conditions to provide a benchmark or base condition with which the alternatives could be compared. A 4-m (13-ft) strip of tracer was positioned south of the south jetty as can be seen in Photo D1, Appendix D. The flow and waves then were run for a prototype equivalent of 1 hr 15 min with results of the tracer motion shown in Photo D2. Tracer is moving past the tip of the jetty and crosses the marked 152-m (500-ft) and 244-m (800-ft) proposed jetty lengths. All tracer seems to cross landward of the 305-m (1,000-ft) length.

One should also note that tracer is passing the south jetty at its landward juncture. Wave upwash and return take the tracer past the jetty. The tracer moves slower at the air/water interface than the sand would, since the proper scaling assumes the tracer will be submerged. This indicates that the shoreward migration of sand is probably worse than the tracer studies indicate. However, the fixed bed model cannot simulate scour which would most likely occur under these storm events adjacent to the south jetty which might limit the landward flow of sediment past the jetty. The landward limit of the south jetty was terminated when the fixed bed model elevation was equal to the elevation of the south jetty. Near this point, the south jetty consists of a single stone. The structure near this point is most likely more porous than the prototype jetty. Additional attention, however, should be focused on the field condition of the south jetty in this location if additional improvements are warranted.

The 305-m (1,000-ft) straight and dogleg jetty extensions were tested under the same "worst-case" hydrodynamic conditions as the existing condition. Results are shown in Photos D3 - D6. The tracer initially was placed in the same location along the same line as was used in the existing condition experiments. Consequently, the tracer is closer to the dogleg jetty at the start of the experiment. There is some motion past both extension configurations, with slightly more occurring for the dogleg jetty extension. This may have been a result of the proximity of the tracer swatch to the structure itself. The general tracer motion appears to be very similar between the two plans.

The two 305-m (1,000-ft) south jetty extensions significantly decrease the transport of tracer past the south jetty and into the inlet. If these experiments were run for even longer lengths of time, the results would be even more noticeable.

Results of the numerical model study show some advantages associated with the dogleg section. This alternative seemed to "pull" flow slightly away from the north jetty. The numerical model indicated more uniform flow across the inlet mouth for the dogleg extension compared to the straight extension, generally providing better navigation conditions. The reader is referred to the report by Taylor Engineering (1996) for more detailed discussion of the results of those experiments.

Considering all factors, the dogleg extension was determined to be the preferred south jetty extension alternative.

Impacts of Preferred South Jetty Extension on Waves and Velocities

Experiments were conducted to assess the impacts of the south jetty extension on inlet navigability. The requirement was that any extension to the south jetty would not worsen already troublesome navigation conditions. Concerns also were expressed about the impact of the south jetty extension on the surfing climate in the area, which is a favorite spot for local surfers, as indicated by Mr. Tom Martin.[1] This impact assessment was performed by comparing wave and current conditions measured at discrete points for existing and altered south jetty conditions. Although only a portion of the results are presented herein, all wave and velocity measurements for all runs are on file at CESAJ.

Thirteen wave gauges were deployed throughout the model to record point measurements of wave energy. For the south jetty extension experiments, the gauge layout can be seen in Figure 12. Gauges 1-3 were located along the 9-m (30-ft) depth contour and were used to measure the incident wave conditions. Gauges 4-6 were located in the vicinity of the local surfing area to help quantify any differences in wave conditions caused by the south jetty extension. Gauge 7 was located at the tip of the 305-m (1,000-ft) south jetty extension. Gauges 8-10 were located across the inlet mouth and were used to quantify changes at the location where boaters are subjected to the open ocean wave climate as they traverse the inlet. Gauges 11 and 12 were located in the inlet in shallow-water areas that have been indicated as shoaling and wave breaking zones, where navigation has been particularly difficult at times. Gauge 13 was positioned adjacent to the interior north spit, and is in the most protected area within the inlet throat.

To assess the changes to the wave climate associated with an alternative, the ratios of the H_{m0} values for the alternative plans to the H_{m0} values for the existing plan were computed at each gauge location. If

$$\frac{H_{m0}\,(\text{alternative plans})}{H_{m0}\,(\text{existing plan})} > 1 \qquad (4)$$

then there is more energy for the alternative plan at that location. Normalized H_{m0} values greater than one indicate an increase in wave energy relative to the existing jetty condition. Likewise, values less than one indicate a decrease in wave energy. One would like to see values less than or equal to one for all gauge locations.

[1] Personal Communication, 1995, Tom Martin, Civil Engineer, U.S. Army Engineer District, Jacksonville.

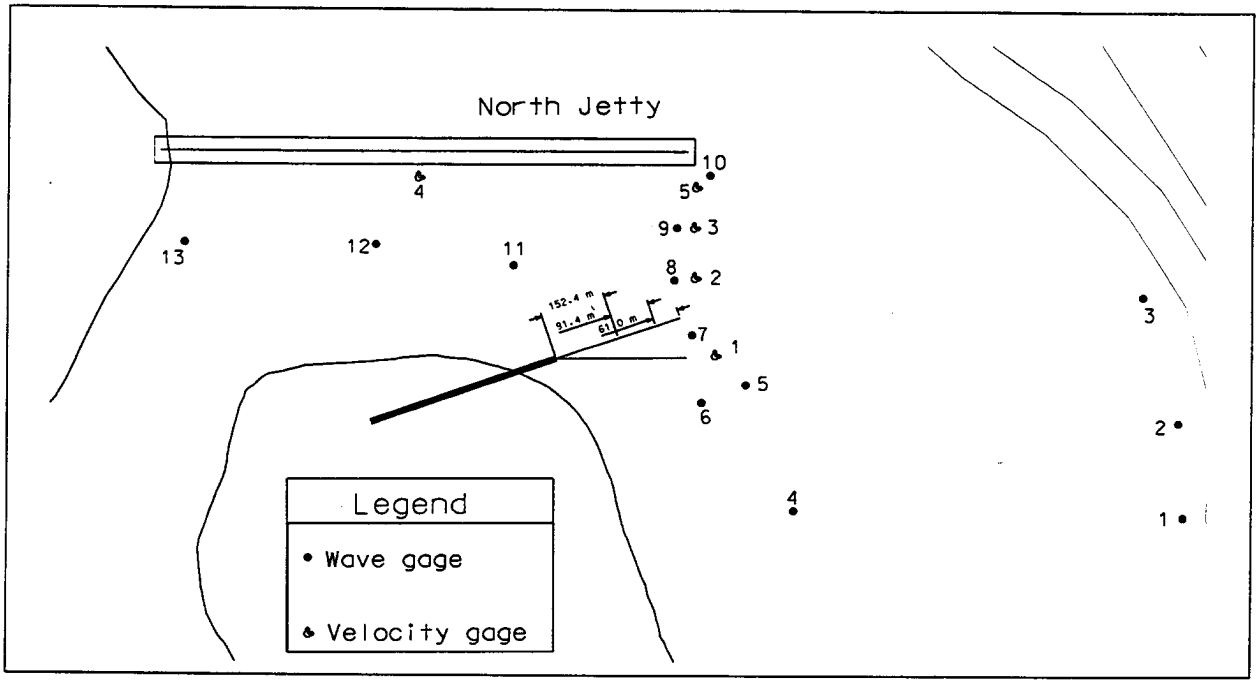

Figure 12. South jetty gauge layout

Normalized wave height results for all 13 measurement locations can be seen in Figure 13. Measurement locations also are referred to as "gauges" or "gauge numbers." Significant wave heights (H_{m0}) were first computed for all gauges; for various combinations of incident wave parameters, water level/flow condition, and for a particular jetty configuration. Wave heights were normalized in the following way: for a given water level/flow condition, wave heights for the 305-m dogleg alternative were divided by wave heights for the existing condition. Then, for each of the four water level/flow conditions, an average value was calculated for each gauge and this result is plotted in Figure 13. These normalized wave heights represent an average of a number of values for different incident wave conditions. For spring peak flows, results for the four "navigation" wave conditions were used in the averaging; for storm flows, six storm wave conditions were used in the averaging. The following discussion focuses on the lower wave energy and spring peak flow conditions, since these are the types of conditions under which recreational boaters are likely to use the inlet.

Surfing area

Gauges 4-6 were positioned south of the south jetty in the vicinity of the New Smyrna Beach surfing area. During spring peak ebb (SPE) flow, the dogleg alternative increases wave heights in the surfing area by about 10 percent on average, for the conditions tested. Increases at the three gauges ranged from 6 percent to 12 percent. This is probably desirable from a surfing perspective. During flood tide, there was no change in wave height, on average. One location experienced a slight

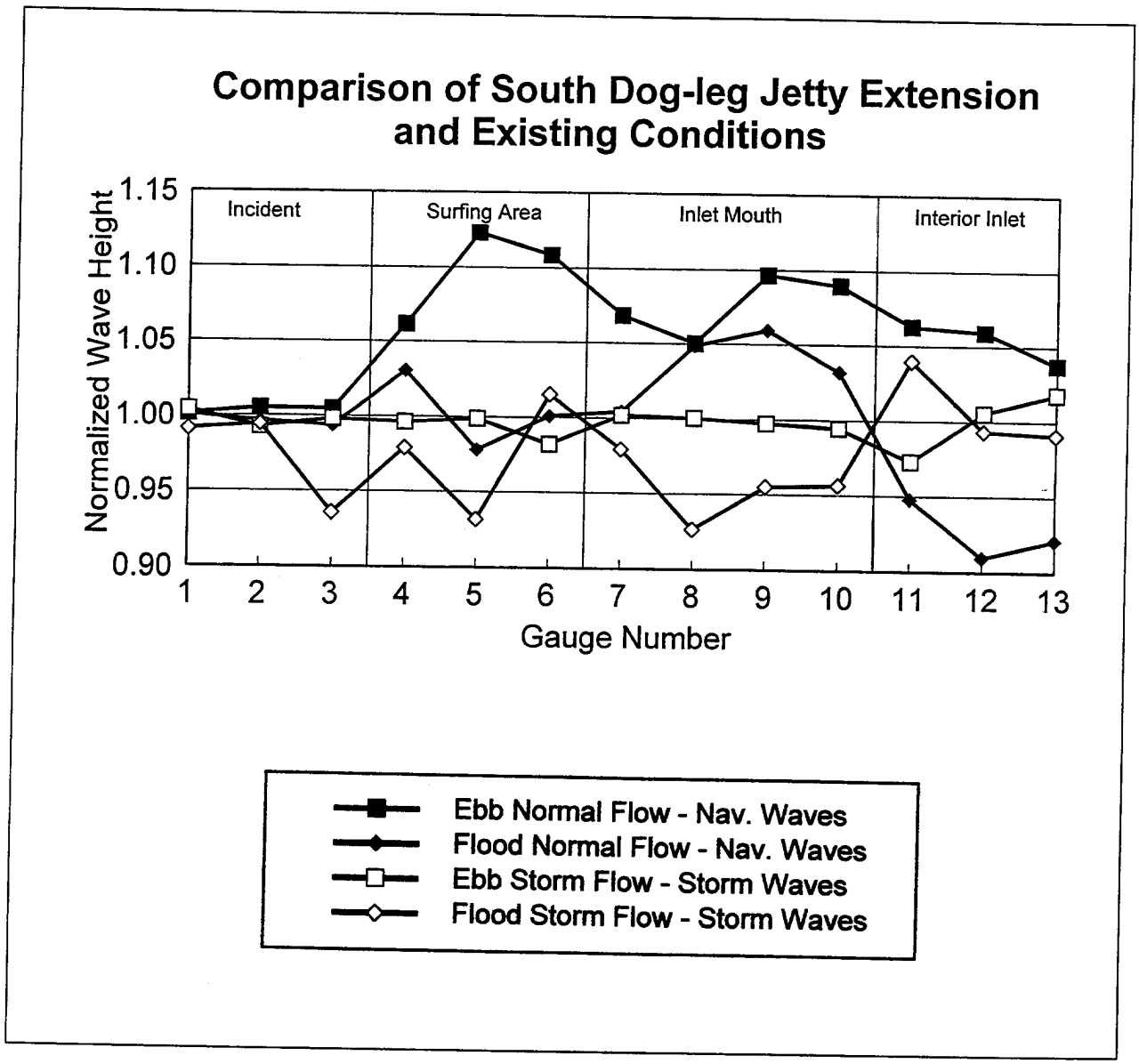

Figure 13. Wave averaged, normalized wave heights for all the flow condition experiments conducted for the south jetty dogleg extension

increase, one showed a slight decrease, and the third gauge showed no change. Overall, the average increase in wave height is fairly small, about 5 percent. If the south jetty is extended, there will probably be some changes in the offshore bathymetry due to sediment accretion caused by the extension. Changes to wave height and direction may result in response to these bottom changes, but these changes are not expected to adversely impact surfing in the area. If anything, the changes are expected to slightly improve surfing.

Inlet mouth

Gauges 7-10 were located in the inlet mouth. During spring peak ebb flow, average wave conditions across the mouth of the inlet increased by 3 - 7 percent, compared to the existing condition. The dogleg concentrated the flow slightly, increasing current speeds through the inlet which interacted with the opposing waves to create slightly higher waves. This small increase is not expected to adversely impact navigability through the mouth. For flood flow, the dogleg caused waves to increase by about 3 percent, on average. The reason for the increase is not clear. On flood flow, waves tended to "ride" on the currents moving in the same direction, increasing their speed. This process tended to reduce wave heights. The slight increase in wave heights during flood flow was not expected. Changes to wave direction created by changes to current patterns may have caused the increase. However, the small magnitude of the increase is not sufficient to adversely impact navigability.

Interior inlet

For spring peak ebb flow, wave heights in the inlet throat increased by about 5 percent on average for the dogleg extension. Waves on spring peak flood flow showed a persistent decrease (7 percent on average) which one would intuitively expect for the reasons cited above. Some increase in wave height during ebb is to be expected as a result of the jetty extension constraining and slightly concentrating the flow. However, the slight increases in wave height are not expected to adversely impact navigation through the channel.

Gauges 8, 11, 12, and 13 were arranged in an array through the inlet throat to assess the attenuation of wave height with distance west of the inlet mouth and how that attenuation changed for the various jetty extensions. Gauge 8 is at the inlet mouth, gauge 13 is adjacent to the interior north spit. Figure 14 shows the variation in significant wave height for spring peak ebb (SPE) flow, the "worst case," for each of the four "navigation" wave conditions, for existing conditions and the 305-m dogleg extension alternative. The wave height is reduced from about 1.2 m at the mouth to 0.2 m at the north spit. Much of the attenuation (more than 50 percent) occurs between gauges 8 and 11. A review of the bathymetry between these two gauges provides an explanation for the sharp drop in wave height as can be seen in Figure 15. Wave refraction will tend to align wave crests parallel to the bottom contours with the waves bending toward shallower water. The pattern of attenuation is nearly the same for the existing jetty and the dogleg extension, which is not surprising because of strong refraction occurring over the complex bathymetry. There is no significant improvement or degradation to navigation in the inlet, in terms of wave height associated with the dogleg extension. The average change in wave height for gauges 11, 12, and 13 is a 5-percent change between existing conditions and the dogleg extension over the four navigation wave cases tested. The maximum difference was 11 percent. Gauge 8 showed an average difference of a 5-percent increase, which could be attributed to reflection off the structure.

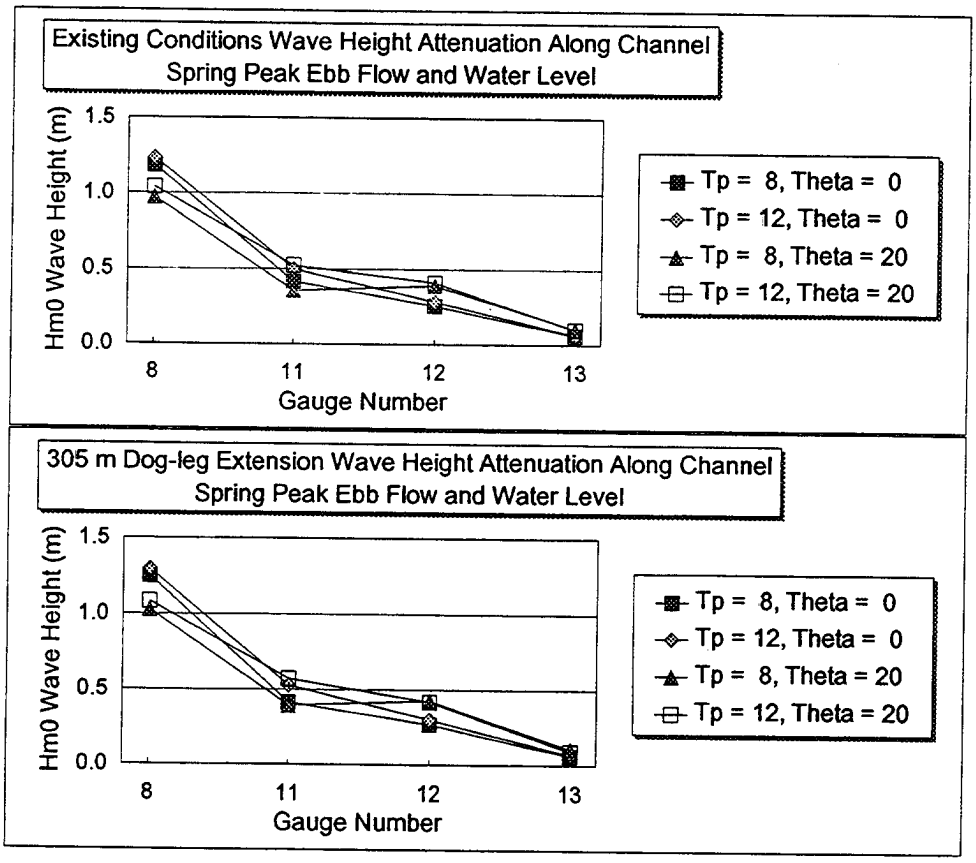

Figure 14. Existing and 305-m (1,000-ft) dogleg extension for wave gauges located in the inlet channel

Storm conditions were not of particular interest from the navigability standpoint, since recreational boaters are unlikely to be using the inlet. However, it is interesting to note in Figure 13 that on average, the dogleg extension reduced storm wave conditions throughout most of the inlet area, albeit by about 2-3 percent on average.

Wave impacts on north interior shoal

Gauge 13 was positioned adjacent to the north shoal, in an area of high erosional pressure. Table 18 summarizes the H_{m0} wave heights for the spring peak flood storm water level and flow conditions for the 1- and 5-year storm waves for varying angles south of shore normal. Wave heights were considerably higher at gauge 13 under the increased water depth associated with flood conditions. It can be seen that the 305-m (1,000-ft) dogleg extension does not change the wave-induced scour pressure along the interior north shoal.

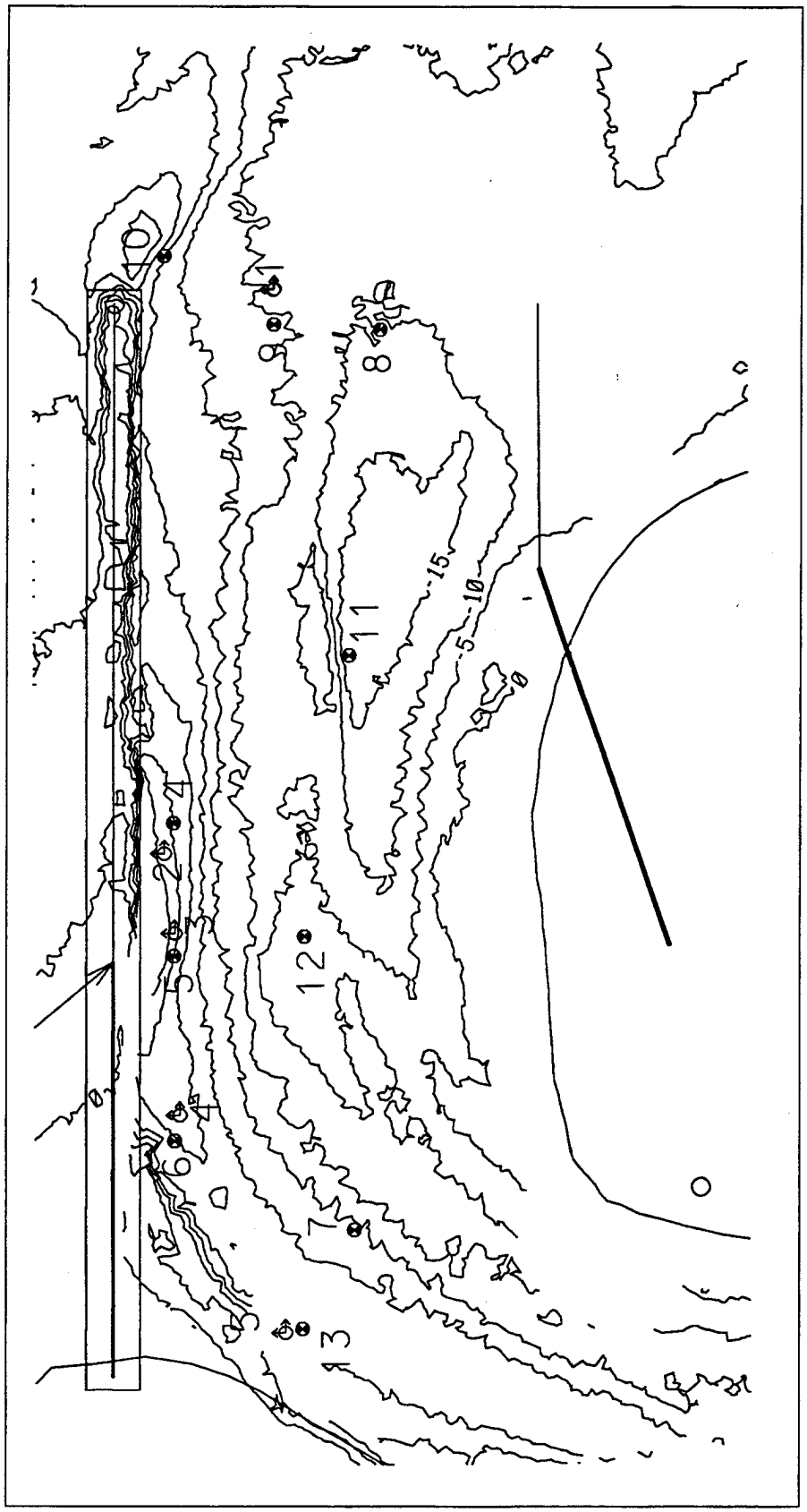

Figure 15. Bathymetry between wave gauges 8 and 13

Table 18
Summary of H_{m0} Wave Heights at Gauge 13

Flood Storm Conditions		
	H_{m0} Wave Height (m)	
Wave Condition	Existing Cond.	Dogleg Extension
1-year Storm Wave - 3 deg SSN	0.70	0.77
5-year Storm Wave - 11 deg SSN	0.63	0.67
1-year Storm Wave - 20 deg SSN	0.73	0.73
5-year Storm Wave - 20 deg SSN	0.66	0.66
1-year Storm Wave - 30 deg SSN	0.82	0.71
5-year Storm Wave - 30 deg SSN	0.77	0.73

Velocity Results

Velocity gauges were positioned throughout the physical model (Figure 12) to ascertain differences in velocity between existing conditions and the 305-m (1,000-ft) dogleg extension. Velocity gauge 1 was positioned just seaward of the tip of the 305-m (1,000-ft) dogleg extension to assess scour potential. Velocity gauges 2, 3, and 5 were positioned across the mouth of the inlet to measure changes at the entrance to the inlet and the impact on navigability. Velocity gauge 4 was positioned about midpoint along the north jetty, in the present position of the scour hole adjacent to the jetty.

Velocity measurements were made at each gauge to indicate if mean velocities change substantially when waves are included and to assess modifications to the flow field associated with the altered south jetty. Although the flows cannot be as easily controlled as in a numerical model, velocity measurements can supplement numerical model results, especially to investigate the role of wave/current interaction. Currents influence waves, but also waves influence currents. Neither process is addressed in the numerical model. The velocity measurements represent an average velocity computed for the entire duration of the "steady-state" experiment. The average or mean velocity was used to eliminate the induced orbital velocities associated with the passage of a wave.

Figure 16 shows velocity results for spring peak ebb (SPE) flow and water level conditions. The magnitude of the current velocity increases substantially from south to north across the inlet mouth, from about 20 cm/sec on the southern side to about 100 cm/sec along the north jetty. This observation is consistent with the BBADCP velocity data measured in the inlet throat at transect D (D is located east of the mouth). Current velocities at gauge 1 are small, suggesting that on ebb flow, scour around the tip of the jetty extension will not be a problem. The field data also show very small velocities at the tip of the existing south jetty under peak ebb flow. Velocities at all measurement locations seem to be dominated by the tidal component, with little wave influence (i.e., velocities for the no-wave conditions are quite

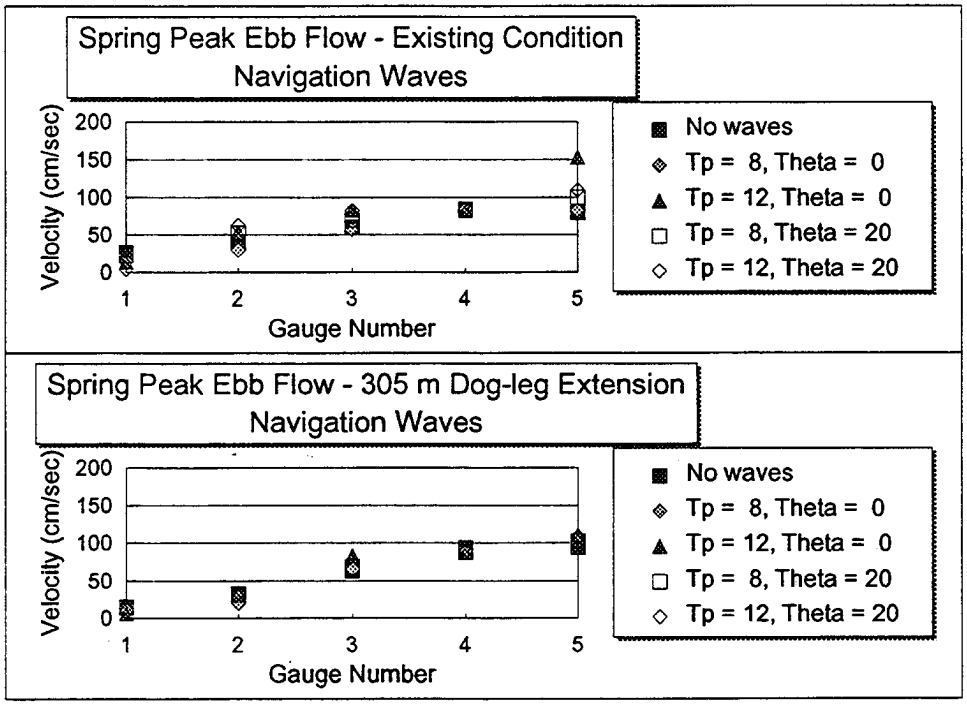

Figure 16. Mean velocity measurements for the existing south jetty and the 305-m (1,000-ft) dogleg extension. Spring peak ebb flow

similar to the examined wave conditions). Waves only influence current velocities, altering them by 10-20 percent on average, except at gauge 5 for existing conditions where velocities were increased up to 50 percent depending on the incident wave condition. This is probably not surprising for the low-energy navigation waves. One would expect that the role of wave-driven currents would be much more important for storm conditions. Velocity results were similar for existing conditions and the 305-m dogleg extension with differences in the range of experimental error. No major changes to navigation, from a current persective, are expected for this alternative.

Results for spring peak flood (SPF) flow and water level conditions are shown in Figure 17. The increase in current speed from south to north across the inlet mouth again is evident, although velocities increase from about 50 cm/sec to 90 cm/sec. The field data show a more uniform distribution of current speed across the inlet at transect D, ranging from 65 to 80 cm/sec. Scour around the jetty extension is more likely on flood flow, but the scour potential is less than for the north jetty tip. Velocity measurements at gauge 4, which is in the scour hole, show the greatest flood velocity of the locations sampled (120 cm/sec). The field data also show the greatest velocities on flood flow to be in the scour hole (about 140 to 150 cm/sec).

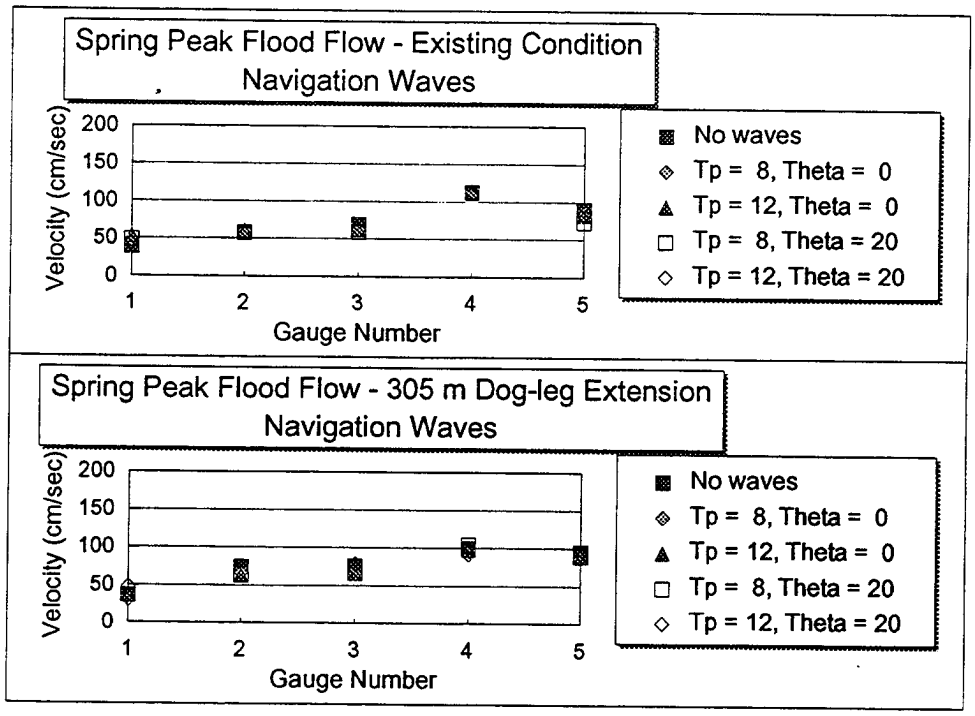

Figure 17. Mean velocity measurements for the existing south jetty and the 305-m (1,000-ft) dogleg extension. Spring peak flood flow

Results for spring peak flood flow are similar to spring peak ebb flow in the sense that tidal flows dominate. Again, waves alter measured velocities by an amount in the range of 10-20 percent. Results for existing and dogleg configurations also are similar, with differences in the range of experimental error. At gauge 4, results for the dogleg extension do show a slight persistent decrease in velocity compared to existing conditions. This is consistent with observations from the numerical model results that show the dogleg tends to slightly pull the region of higher current away from the north jetty. Again, no major changes to navigation, from a current persective, are expected for this alternative.

6 North Jetty Experimental Results

Overview of the Testing Plan

The length and orientation of the north jetty have strongly influenced hydraulic conditions at Ponce DeLeon Inlet. Initially, the north jetty was built with a 549-m-(1,800-ft-) long weir which was reduced in size by 91 m (300 ft) in 1979. In 1984, the remaining 457-m (1,500-ft) weir section was closed. The "General and Detailed Design Memorandum, Addendum 1" (USACE 1983), which was written to address the effectiveness of the north jetty, stated that the north jetty weir would be reopened after sand accreted north of the north jetty and after the channel had realigned itself away from the north jetty. Although neither of these two conditions has been met, physical model experiments were conducted to examine the optimal weir length.

Goals of and reasons for the weir experiments include the following:

a. Redistribute ebb and flood flows through the weir and inlet to reduce erosional hydraulic pressure on the south side of the north jetty.

b. Create depositional environment adjacent to the north jetty for effective use as a trap to bypass sediment.

c. Reorient flood flow away from north interior spit to reduce erosional pressures.

d. Provide sufficient sediment supply to maintain equilibrium of north interior spit.

Four north jetty weir configurations were tested in the physical model. Although the 457-m (1,500-ft) weir was closed in 1984 because it was ineffective in redistributing tidally induced flow and in developing an accretional area of sediment transported over the weir, the north jetty still was studied with this length weir opening to determine if changes in bathymetric conditions would increase its effectiveness. This weir length also provided a baseline condition. Two smaller weir openings of

305 m (1,000 ft) and 152 m (500 ft) also were analyzed. Each weir opening started at the same seaward point along the north jetty, as can be seen in Figure 18. A closed weir, called the existing condition, also was analyzed and provided another baseline condition for comparative purposes. The height of the weir reproduced in the physical model was 0.0 m mlw, which corresponded to initial prototype construction of the north jetty weir. The weir opening lengths, elevation, and heights were selected by CESAJ.

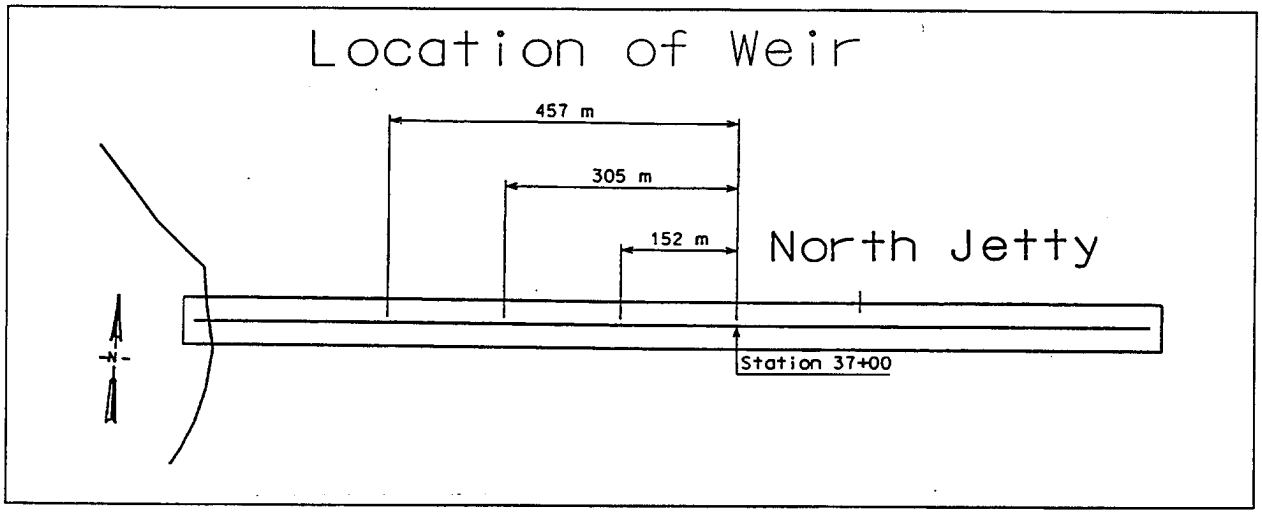

Figure 18. North jetty weir lengths

To address the goals of the physical model north jetty weir experiments, a program consisting of dye and tracer experiments and wave and current measurements was conducted. Numerous wave, water level, and flow conditions were simulated in the physical model. To understand the tidally driven hydraulic conditions, dye experiments were first performed in the absence of waves for the four weir conditions and the four water level and flow conditions. Tracer experiments then were run. Unlike the south jetty extension experiments, in which storm conditions were assumed to cause the majority of sediment transport around the jetty, sediment transport over and across the weir was assumed to occur under less energetic events, especially for the longer length weir openings, and thus storm and nonstorm conditions were analyzed. Initial experiments were conducted with waves and without flow, to simplify understanding of the sediment transport problem. No flow or low-flow conditions are more prevalent in the tidal cycle than are extreme flow conditions associated with the peak spring condition. After the wave-only runs were completed, tracer experiments were run on the wave-plus-spring-peak flow conditions. For the spring peak conditions, the smaller period navigation wave was simulated while for the spring peak storm flow, the 1-year storm event was simulated.

Wave height and velocity measurements also were collected after the dye and tracer experiments were completed. These experiments were run to analyze the impact upon navigation of opening the weir. Both the plunger wave machine and the DSWG were utilized because of the limited extent of the plunger machine. The plunger wave machine was used to generate waves coming from north of shore

normal and was used to examine waves coming through the weir and their related impacts on navigation and sedimentation conditions within the interior parts of the inlet. To study wave current interaction in the vicinity of the inlet mouth due to differing weir configurations, the DSWG was used to generate waves up the channel.

Table 19 summarizes the north jetty experimental series using the plunger wave machine. Table 20 describes the experiments conducted with the DSWG. Figure 19 illustrates the locations of the 13 wave gauges and 5 velocity gauges used during this portion of the north jetty testing program.

All north jetty weir experiments were conducted with the preferred 305-m (1,000-ft) south jetty extension in place in the physical model. The consensus from CESAJ was that construction of the south jetty extension was probable and that all weir conditions should be tested with the preferred south jetty extension present.

Impacts of Weir Openings on Sedimentation

Dye results

Dye was used to study flow patterns for the different north jetty weir openings for a range of hydrodynamic conditions (combinations of waves, currents, and water levels). During ebb flow, dye was added along a line across the inlet throat; while during flood flow, dye was added along a cross-shore line north of the north jetty and parallel to it. Experiments were conducted for spring peak ebb (SPE), spring peak ebb storm (SPES), spring peak flood (SPF), and spring peak flood storm (SPFS) flows/water levels, without waves. A small number of experiments were run using the same flows with waves. Results of these experiments are reported here. A 1.9-cm (3/4-in.) video was taken of the resulting dye patterns for different wave and current regimes. A VHS copy of the tape is on file at CESAJ.

In general, the following results were found:

a. On ebb flow, most of the water was entrained and flowed out of the inlet mouth through the existing deep channel along the north jetty. Very little dye and flow were transported over and across the weir.

b. On flood flow, the majority of the water flows into the inlet through the inlet mouth.

c. Waves from the north tended to push more water over the weir under flood conditions than just currents alone. When waves were present, water tended to flow more quickly past the north interior spit.

These results were similar to those found with the numerical model (Taylor et al. 1996). Use of dye provided a good visual tool for assessing current patterns. The numerical model provided a more consistent and quantitative assessment of the

Table 19
North Jetty Weir, Plunger (North of Shore Normal) Wave Generator Experimental Matrix

Water Levels (m)	Flow	Experiment/ Measurement Conducted	No Waves	Waves							
				No Flow				Flow			
				N1[1]	N2	N3	N4	N1	N2	N3	N4
0.5	SPE	Dye	a,b,c,d								
		Tracer		b	b	b	b	b,c,d			
		Wave Height		a,b,c,d	a,b,c,d	a,b,c,d	a,b,c,d	a,b,c,d	a,b,c,d	a,b,c,d	a,b,c,d
		Velocity						a,b,c,d	a,b,c,d	a,b,c,d	a,b,c,d
1.1	SPES	Dye	a,b,c,d								
		Tracer								b,c,d	
		Wave Height		a,b,c,d	a,b,c,d	a,b,c,d	a,b,c,d	a,b,c,d	a,b,c,d	a,b,c,d	a,b,c,d
		Velocity						a,b,c,d	a,b,c,d	a,b,c,d	a,b,c,d
1.28	SPF	Dye	a,b,c,d								
		Tracer		b	b	b	b	b,c,d			
		Wave Height		a,b,c,d	a,b,c,d	a,b,c,d	a,b,c,d	a,b,c,d	a,b,c,d	a,b,c,d	a,b,c,d
		Velocity						a,b,c,d	a,b,c,d	a,b,c,d	a,b,c,d
1.34	SPFS	Dye	a,b,c,d							c,d	
		Tracer								b,c,d	
		Wave Height						a,b,c,d	a,b,c,d	a,b,c,d	a,b,c,d
		Velocity						a,b,c,d	a,b,c,d	a,b,c,d	a,b,c,d

Note: a = existing conditions
b = 457-m weir opening
c = 305-m weir opening
d = 152-m weir opening
[1]Wave conditions are described in Table 10.

relative performance of one opening versus another. Experimental results indicate that the weir was ineffective in appreciably decreasing the ebb tidal flow past the north jetty, for any weir opening length. Ebb flow along the north jetty was not appreciably decreased even under the increased storm water level (an increase from 0.4 m (1.5 ft) mlw to 1.1 m (3.5 ft) mlw). This gives some indication that even decreasing the height of the weir would not change the ebb flow considerably. On flood flow, some water passed over the weir, but the majority flowed through the existing inlet channel. Compared to existing conditions, the dye experiment results do not show changes in the flow distribution under flood conditions which would change scour pressure along the north jetty. Very small changes to currents in the inlet channel suggest that the area behind the weir would not be effective for use as a deposition basin. One factor that was not considered in the experiments is the

Table 20
North Jetty Weir, DSWG (South of Shore Normal) Wave Generator Experimental Matrix

Water Levels (m)	Flow	Experiment/ Measurement Conducted	Waves			
			S1[1]	S2	S3	S4
0.5	SPE	Wave Height	a,b,c,d	a,b,c,d	a,b,c,d	a,b,c,d
		Velocity	a,b,c,d	a,b,c,d	a,b,c,d	a,b,c,d
1.28	SPF	Wave Height	a,b,c,d	a,b,c,d	a,b,c,d	a,b,c,d
		Velocity	a,b,c,d	a,b,c,d	a,b,c,d	a,b,c,d

Note: a = existing conditions
b = 457-m weir opening
c = 305-m weir opening
d = 152-m weir opening
[1]The wave conditions are described in Table 9.

long-term bathymetric change that might occur if the weir is opened, and how those bathymetric changes would alter current patterns. It is possible, and perhaps likely, that some sand entering through the weir could deposit in the scour hole and reduce its depth, but substantial accretion is unlikely.

Tracer results

To investigate the movement of sediment transport through the different lengths of north jetty weir openings, crushed coal tracer was added to the model. These tracer experiments were used to help determine if a particular weir length would be practical in terms of sedimentation in the scour hole adjacent to the north jetty and provide for a source of sand to the north interior spit. Initially, tracer was placed along a line north of and adjacent to the full length of the 457-m (1,500-ft) weir as can be seen in Photo E1, Appendix E. The tracer patch was approximately 5 m (16 ft) long. The black shorter line is the tracer material and to the right is the weir and jetty. The seaward tip of the weir ends at the seaward end of the tracer patch. The same initial tracer line was used for the complete set of north jetty weir opening tracer experiments.

For each tracer experiment, photos were taken at the mid-point of the experiment (corresponds to 1 hr 15 min in the prototype) and at the end of the run (equivalent to 2 hr 30 min). The large scale of the model and position of the ceiling lights degraded the contrast in the photos. However, the tracer is clearly visible.

457-m (1,500-ft) weir opening

Water level played an important role in determining the amount of tracer that is transported over the weir as a result of the limited water depth above the weir. To quantify the effect of water level, waves were run with different water levels, but without flows. The four water levels used are described in Table 11.

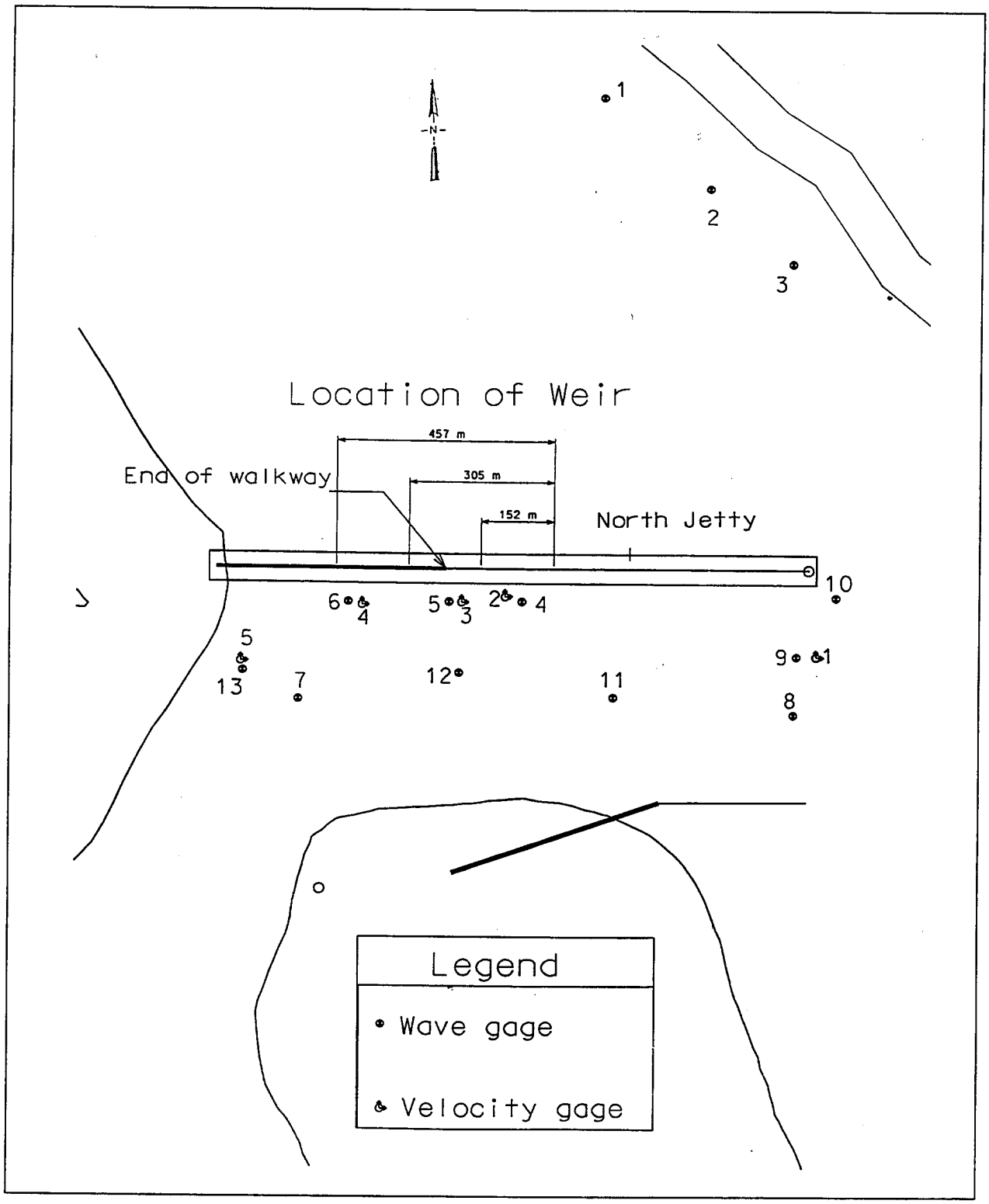

Figure 19. Gauge layout for north jetty weir experiments using the plunger wave generator

First results without flows, for the spring peak ebb water level, which is only 0.5 m (1.5 ft) above the weir crest elevation, will be presented. Under navigation wave N1 from the north (H_{m0} = 1.5 m, T_p = 8.0 sec - prototype scale), there is almost no motion across the weir at either the mid-point or end of the run (Photos E2-E3). A small amount of tracer was deposited in the deep scour hole adjacent to the weir. Under the larger-period waves (12 sec, H_{m0} = 1.5 m), more material was transported across the weir as can be seen in Photos E4-E5. In Photo E5, tracer deposited in the scour hole is clearly visible. Under the 1-year (N3) and 5-year (N4) storm waves, there is clearly more sediment movement toward and over the weir as can be seen in Photos E6-E9. During spring peak ebb water level, the tracer was deposited in the scour hole. Although clearly this is an advantage of opening the weir, under flood-flow water level, the tracer is not always just deposited in the scour hole, as will be described next.

Under spring peak-flood water level, no flow condition and the first two navigation waves (waves N1 and N2, Table 10), the results are similar to the spring peak ebb water level results, as can be seen in Photos E10-E13. However, there is clearly more tracer transported over the weir. When storm waves were simulated, the disadvantages of opening the full length 457-m (1,500-ft) weir can be seen in Photos E14-E17. All tracer passes over the weir and into the channel. For the spring peak-ebb water level, the tracer was deposited at the deepest point of the scour hole, but for the spring peak-flood water level, the tracer was deposited approximately 30 -120 m (100 - 400 ft) south of the north jetty up to the 305-m (1,000-ft) weir opening position. In the absence of flows, the tracer was deposited adjacent to the weir. Tracer was more widely dispersed at the seaward end of the weir opening and was not deposited in the scour hole.

Results for waves and flow under the spring peak ebb flow, nonstorm conditions indicate that results for the full 457-m (1,500-ft) weir opening are similar to those for experiments with no flow. Photos E18-E19 show the mid-point and final results for the navigation wave N1 under a spring peak ebb water level and flow. Very little tracer was transported across the weir, unlike Photos E20-E21, which show the results for the 1-year storm waves and spring peak ebb storm water level and flow in which there was 1.1 m (3.5 ft) of water above the top of the weir. Tracer was deposited approximately 30 - 75 m (100 - 250 ft) south of the north jetty for the seaward 230 m (750 ft) of the weir opening. For the landward 230 m (750 ft), the tracer was deposited just south of the scour hole, except for the landward 75 m (250 ft), where the tracer was deposited up to 50 m (160 ft) south of the jetty.

Under spring peak flood water level and flow, a larger percentage of the tracer material was transported over the weir even for navigation wave N1, as can be seen in Photos E22-E23 as compared to the no-flow condition shown in Photos E10-E11. Unlike the no-flow conditions, when the flood flow was present, tracer was deposited further to the west from the deepest portion of the scour hole. The flood flow pushed the tracer further landward and would provide a source of material for the north interior spit which is presently experiencing rapid erosion. This is consistent with the observed growth of the spit when the weir was originally open. Results for the 1-year storm wave conditions and spring peak flood storm water level and flow are shown in Photos E24 - E25. The tracer was deposited in the

navigation channel and also in the shallower areas of the channel east of the jetty. Again on flood flow, the tracer was not being deposited in the deepest part of the scour hole, but was being deposited in an area that would feed the north interior spit. It also would tend to accrete in the navigation channel and possibly make navigation more difficult.

Results from the 457-m (1,500-ft) weir opening show tracer being deposited into the inlet both adjacent to the north jetty and away from the weir. Conditions behind the weir did not seem to be conducive to establishment of an impoundment basin. For the more energetic wave conditions and deeper water associated with flood water levels, tracer was being deposited as far as 100+ m (400 ft) south of the jetty. Depth in this area was approximately 4.6 m (15 ft) below mlw. Sediment did not settle into the deepest part of the scour hole adjacent to the north jetty.

305-m (1,000-ft) weir opening

The second alternative considered was to open the outer 305-m (1,000-ft) weir section to address changes in the amount of tracer transported across a shorter weir. Tracer results for the 305-m weir opening were very similar to the full length weir opening. For the shorter weir openings, only wave and flow combinations were run. No experiments were conducted with waves alone.

For spring peak ebb flow and water level and navigation wave N1, very little tracer was transported over the weir, as can be seen in Photos E26 - E27. There was an accretion of sand adjacent to the weir on the north side. If this occurred in the prototype, over time, the sand level would probably build up to the weir elevation; whereas in the physical model the weir was slightly higher than the surrounding beach. A build-up of sand adjacent to the weir would aid in sand being transported into the inlet.

Under the elevated water level associated with the spring peak ebb storm conditions, additional tracer was transported by the 1-year storm waves and deposited in the inlet. The tracer was still being deposited away from the deepest portion of the scour hole as can be seen in Photos E28 - E29. The tracer was being deposited up to 60 m (200 ft) from the center line of the north jetty. Ebb flow increased the seaward transport of tracer with more tracer being deposited at the seaward end of the weir opening as compared to the no-flow condition.

For flood conditions, the deeper water over the weir and the direction of flow helped transport tracer into the inlet as can be seen in Photos E30-E33. Photo E31 shows some acceleration in the tracer motion at the shoreward end of the 305-m (1,000-ft) weir opening with little motion over the weir seaward of this area.

152-m (500-ft) weir opening

The final alternative examined was to open the outer 152-m (500-ft) weir section. Again the results were similar to the 457-m and 305-m weir opening results.

The results are shown in Photos E34 - E41, respectively (two photos for each condition), for navigation wave N1 and a spring peak ebb water level and flow, a 1-year storm wave and spring peak ebb storm water level and flow, navigation wave N1 and a spring peak flood water level and flow, and a 1-year storm wave and a flood storm water level and flow. For the spring peak ebb water level and flow, essentially no tracer was deposited through the 157-m (500-ft) weir opening. However, under spring peak ebb storm water level and flow conditions, tracer was transported through the weir opening and deposited 20 - 60 m (70 - 200 ft) south of the opening. Tracer was actually transported through the jetties between the rock and then deposited adjacent to the jetty. Transport through the structure was only noticed for the 152-m (500-ft) weir opening. This is probably due to the extent of the closed breakwater and reduced wave action on the south side of the north jetty.

Summary of weir opening tracer results

Reopening the weir was investigated with tracer material in the physical model to see if an impoundment basin could be established adjacent to the north jetty and if sand would accrete adjacent to the north spit. The impoundment basin also would help to eliminate the scour hole. Results indicate that material is transported away from the area behind the weir. Transport conditions were not favorable for establishment of an impoundment area adjacent to the north jetty. Tracer motion over the weir on flood flows pushed the material further into the interior of the inlet. This would be advantageous for the accretion of the north interior spit but at the expense of decreasing the depth of the inlet. More sediment was transported over and across the weir under larger waves, elevated water levels, and flood flows.

Impact of Reopening the Weir on Navigation

Wave considerations

Wave and velocity measurements were made to assess the impact of reopening the weir on navigation. The wave gauge arrangement used for the north jetty weir experiments is shown in Figure 19. Wave gauges 1-7 were located at new positions compared to south jetty experiments. Wave gauges 8-13 were not moved. Gauges 1-3 were relocated in front of the plunger wave machine along the 9-m (30-ft) depth contour to measure the incident wave condition. Gauges 4-6 were relocated adjacent to the north jetty weir, within the navigation channel, and were positioned to assess the wave climate in the inlet for the three different weir openings. Specifically, gauge 4 was located in the center of the 152-m (500-ft) weir opening, gauge 5 was located adjacent to the 305-m (1,000-ft) weir opening, and gauge 6 was located adjacent to the 457-m (1,500-ft) weir opening 380 m (1,250 ft) west of the offshore end of the weir. Gauge 7 was positioned approximately mid-channel at a distance from the north jetty weir openings, and was used to quantify the overall impacts of opening different length weirs. Gauges 8-10 again were used to analyze differences in wave heights across the inlet mouth. Gauges 11-12 were positioned in the shallow area of the inlet, while gauge 13, the most interior gauge, was located adjacent to the north spit.

Opening the weir will increase wave energy inside the inlet and possibly adversely impact navigation. Wave height measurements were taken for the following two primary reasons throughout the physical model:

a. To quantify the wave energy increase inside the inlet as a result of opening different lengths of the north jetty weir. This was examined by conducting experiments with waves but without flows. Waves were made with the plunger wave machine.

b. To quantify the wave energy increase in the inlet by changes in the flow redistribution associated with different lengths of the north jetty weir opening. For this case, experiments involved simulation of waves and flows. Waves were made with the DSWG wavemaker.

In general, as expected, experimental results indicated that the deeper the water over the weir, the more wave energy enters the inlet across the weir. The spring peak flood water level (1.28 m (4.2 ft mlw)) allows the most energy into the inlet and results for this water level are presented. Figures 20-22 compare wave heights for wave gauges 4-6 (see Figure 19 for gauge locations), located adjacent to the north jetty weir. Results are presented for each of four weir conditions (three openings and the existing condition in which the weir is closed), two navigation waves (cases N1 and N2 defined in Table 10), and two flow/water level conditions (spring peak flood water level with and without flood spring peak flow).

When the weir is open, measurements at these gauge locations for waves from the north reflect waves that either propagate through the north jetty itself, through the weir opening, or around the tip of the north jetty. When the weir is closed, the wave energy either propagates through the north jetty or down the channel. However, the plunger wave machine is limited in length and the wave height propagating around the tip of the north jetty is influenced by diffraction of waves as they leave the generator. The diffractive effect caused by the limited length of the plunger wave machine reduces the energy associated with waves propagating down the channel. Wave heights measured in the inlet are less than what might be observed in the field, but results are useful for relative comparisons of the influence of the different weir openings.

One can see that weir length is important in determining the amount of energy that is seen at gauges 5 and 6, the gauges sheltered by partial openings. For example, the wave height varies only slightly for these different weir openings for gauge 4. However, for gauge 5 located in the opening of the 305-m (1,000-ft) weir, wave heights for the two larger weir openings are within approximately 20 percent of each other, but much larger than the heights for the smallest opening. Waves measured at gauge position 5 are the largest of the three gauge locations. Gauge 6 is sheltered by the north jetty, except for the 457-m (1,500-ft) weir opening and waves for this case should show the largest wave height. This is true in all cases except for the spring peak flood water level and no flow for navigation wave N1 where the 305-m (1,000-ft) weir has a slightly larger H_{m0} wave height. With the weir closed, maximum wave heights decrease from about 0.3 m at gauge 4 , to 0.2-0.3 m at gauge 5, to 0.1-0.2 m at gauge 6. With the smallest weir opening,

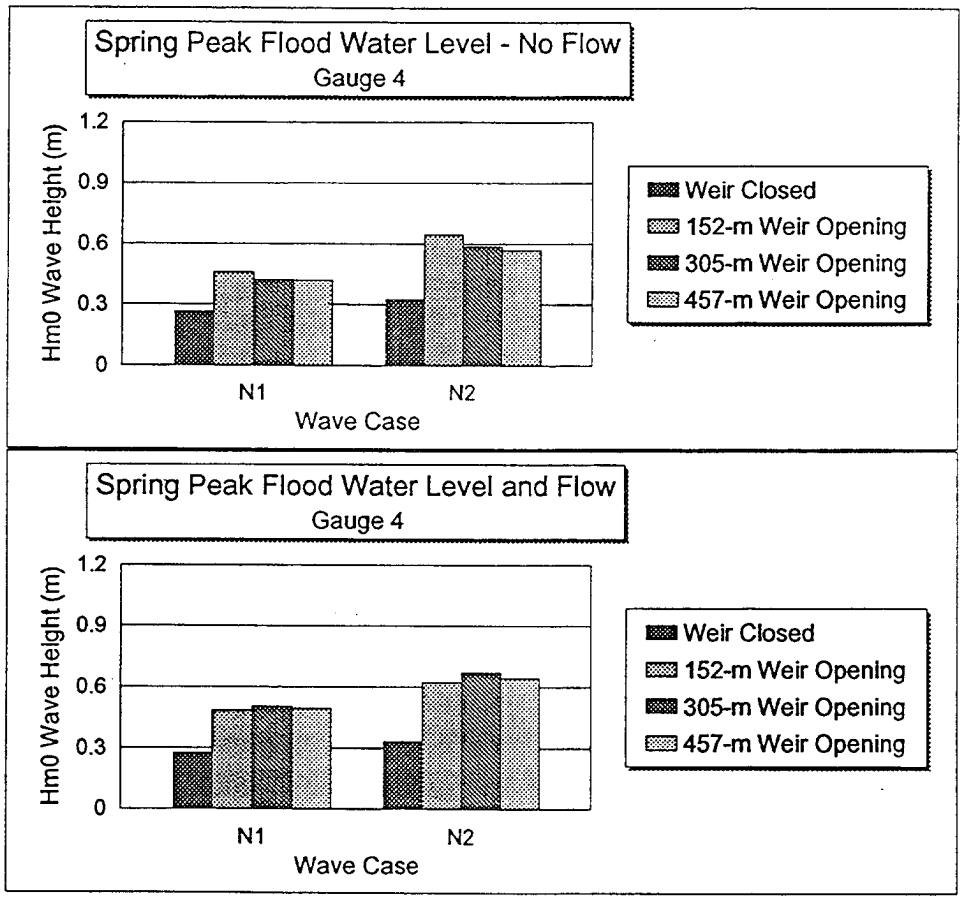

Figure 20. Wave height measurements at gauge 4 for spring peak flood water level and flow

those values increase to 0.4-0.6 m at gauge 4, 0.4-0.6 m at gauge 5, and 0.1 to 0.3 m at gauge 6. The presence of flood flow seems to increase wave heights by about 10-30 percent at gauges 4-6. Waves measured at gauges 4 through 6 for ebb water level/flow conditions were much smaller and limited greatly by the depth of water over the weir.

From a navigational standpoint, the wave height seen by boaters coming through the weir is smaller than the maximum wave heights considered for safe transit as shown earlier (Table 5). However, the waves coming through the weir would be propagating at an angle to the vessels, which perhaps can pose problems. Wave heights shown in Figures 20-22 are associated with waves propagating over the weir, and around and through the jetty. However, wave energy propagation down the channel is smaller than in the prototype because of the limited length of the plunger wave machine.

Gauge 7, located to the southeast of the weir opening in the navigation channel (see Figure 19 for gauge location), gives some indication of the increased wave energy associated with the different weir conditions (Figure 23). The wave height at this gauge location is up to five times greater for the 457-m (1,500-ft) weir opening

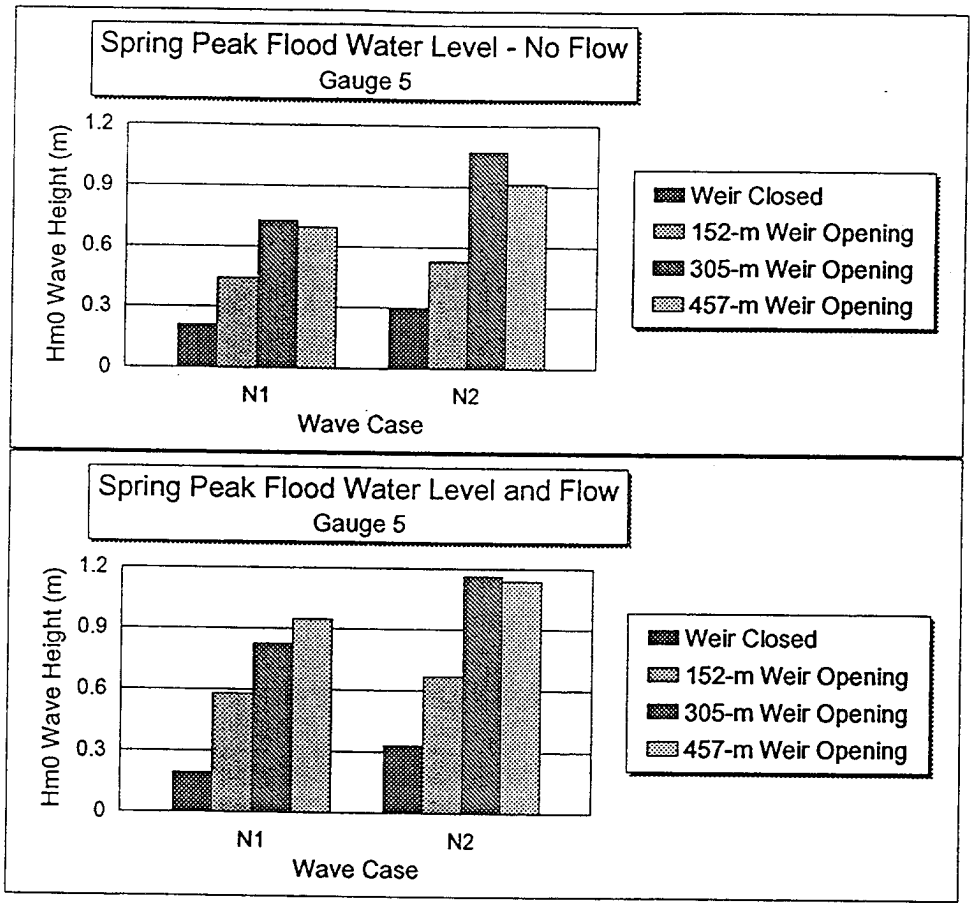

Figure 21. Wave height measurements at gauge 5 for spring peak flood water level and flow

than for the wave height when the weir is closed but it should be noted that the maximum wave height at gauge 7 is less than 0.4 m (1.3 ft) for spring peak flood water level and flow.

Gauges 8-10 are located across the inlet mouth and gauge 11 is located just seaward of the inlet shoal. Wave gauges were positioned in these locations to examine differences in wave heights related to flow redistribution through various weir openings. To evaluate impacts of weir openings on waves at the inlet mouth, waves were generated by the DSWG.

The four navigation waves used to study navigational concerns for the south jetty extension experiments, defined in Table 10, were run to quantify different wave heights within the inlet mouth due to different weir openings and water level/flow conditions. To simplify analysis of the results, wave heights for the existing conditions (weir closed) were used to normalize the results from the various weir opening experiments. Each data point in Figure 24 reflects an average of four normalized wave heights (one for each of the four navigation waves simulated). Results are shown for both spring peak ebb and spring peak flood water level/flow conditions. Results indicate there is no significant change in the measured wave height at the

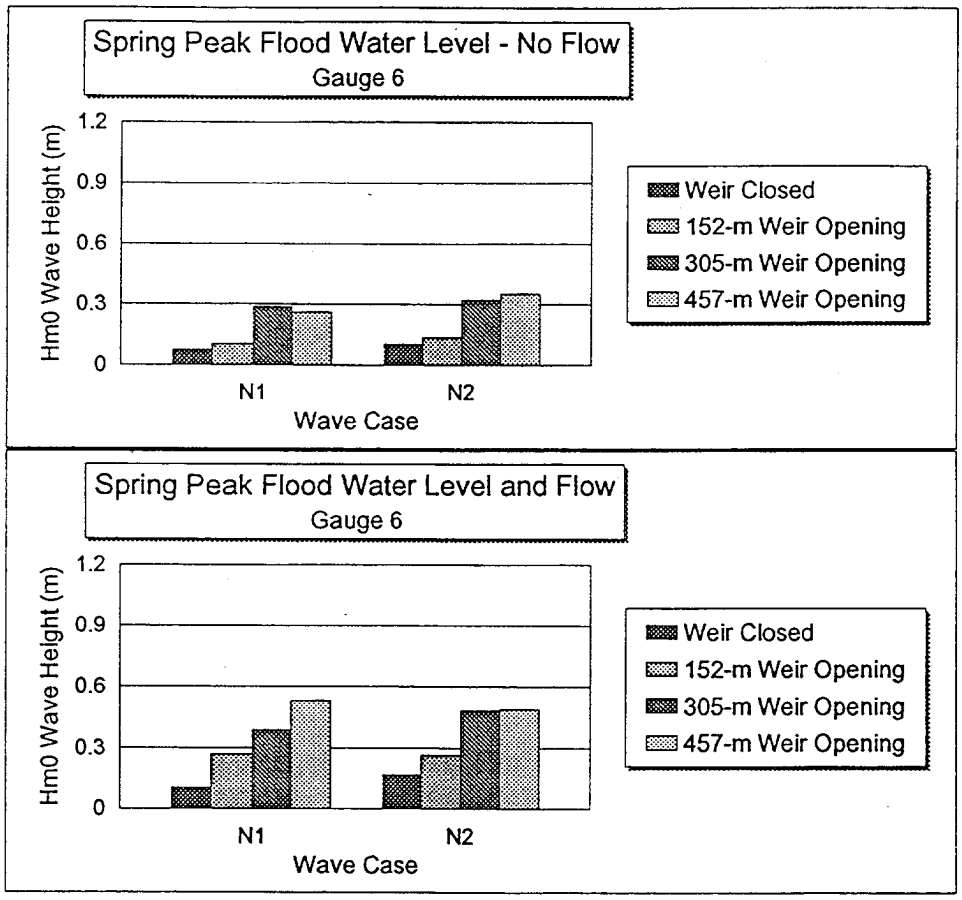

Figure 22. Wave height measurements at gauge 6 for spring peak flood water level and flow

inlet mouth caused by any of the weir openings. Changes are less than about 5 percent. The two larger weir open conditions illustrate a general trend of increased wave amplitude on flood condition. Caution should be used in comparing different weir openings since differences fall within the range of experimental error associated with wave and flow reproducibility. The important concept to glean from this figure is that wave conditions across the inlet mouth do not change measurably between existing conditions and the three different weir openings.

According to Dan O'Brien, Coordinator, Ponce DeLeon Inlet Port Authority, on an ebb flow with waves from the southeast, the waves shoal up considerably and break in the inlet. Wave gauges 8, 11, 12, 7, and 13 represent positions down the channel with gauge 8 located in the inlet mouth and gauge 13 furthest landward (see Figure 19). These gauges are not in the deepest portion of the channel but were positioned in shoaling areas. Figures 25 and 26 show results at these locations for the spring peak ebb and flood flows presented for the closed weir condition and the 457-m (1,500-ft) weir open condition. The full-length weir was chosen to bracket the conditions found. There do not appear to be significant differences between the existing condition and the 457-m (1,500-ft) weir condition for the south-of-shore-normal wave conditions examined.

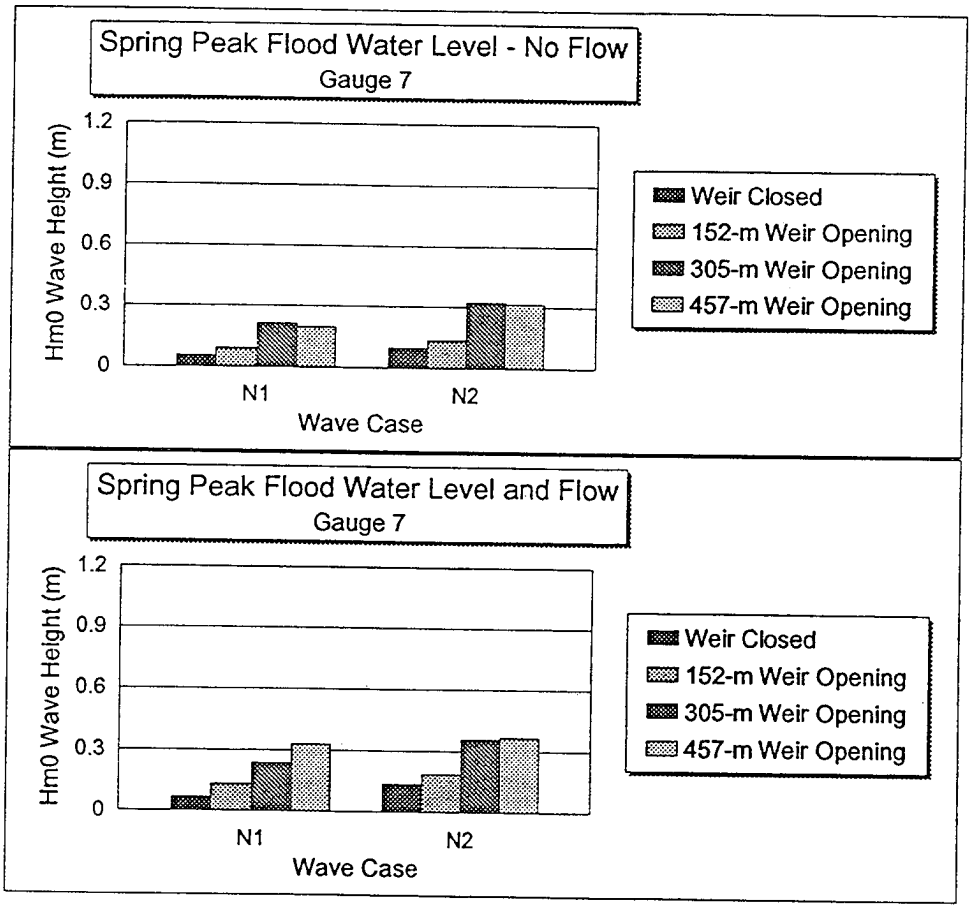

Figure 23. Wave height measurements at gauge 7 for spring peak flood water level and flow

Summary of wave height measurements

The 457-m (1,500-ft) weir length at flood water level and flow allowed the largest measured energy through the weir. Water depth above the weir and weir length were directly related to the amount of wave energy measured in the inlet. Waves measured in the inlet were smaller than the maximum wave height considered for safe transit but the waves coming down the channel were smaller than would be present in the prototype because of model limitation. Basically, the weir allowed additional energy into the navigable portion of the inlet which would make navigating in Ponce DeLeon Inlet more difficult.

Velocity considerations

For the north jetty weir experiments, five velocity gauges were used (Figure 19). Gauge 1 was located in the middle of the channel mouth at the same location as velocity gauge 3 during south jetty experiments. Velocity gauge 2 was positioned at the center of the 152-m (500-ft) weir opening, which is the same location as gauge 4

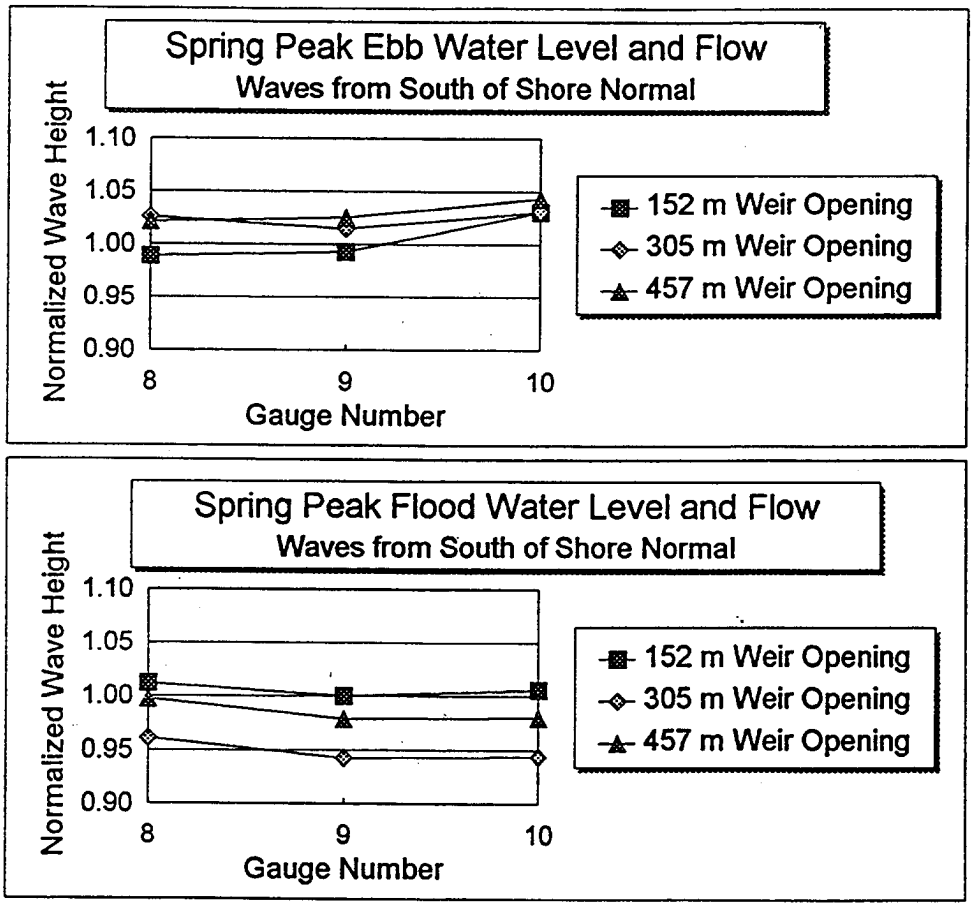

Figure 24. Wave heights normalized by the existing conditions and then averaged over the four navigation waves

used during the south jetty experimental phase. Gauges 3 and 4 were located adjacent to the 305-m (1,000-ft) and 457-m (1,500-ft) weir, respectively. Gauge 5 was located adjacent to the north spit in the area of high erosional pressure. The five velocity gauges were used to quantify the differences in the current patterns associated with the various north jetty weir openings.

Before the results of velocity measurements are presented, the reader needs to recall that the experimental uncertainty associated with the velocity measurements is on the order of 10 percent. Differences less than 10 percent can be attributed to experimental error.

Average or mean velocity values scaled to prototype units are presented. These values were calculated over the length of simulated conditions (1 hr 15 min prototype scale). Results for two navigation waves generated with the plunger wave machine (H_{m0} = 1.5 m, T_p = 8 sec, T_p = 12 sec, respectively) are presented in Figures 27 and 28 for the four different weir conditions studied. On spring peak ebb conditions, there is very little difference between the different weir openings except at velocity gauge 1 for navigation wave N2 and the 457-m (1,500-ft) weir opening. Further analysis of the time series data associated with this point indicates that the

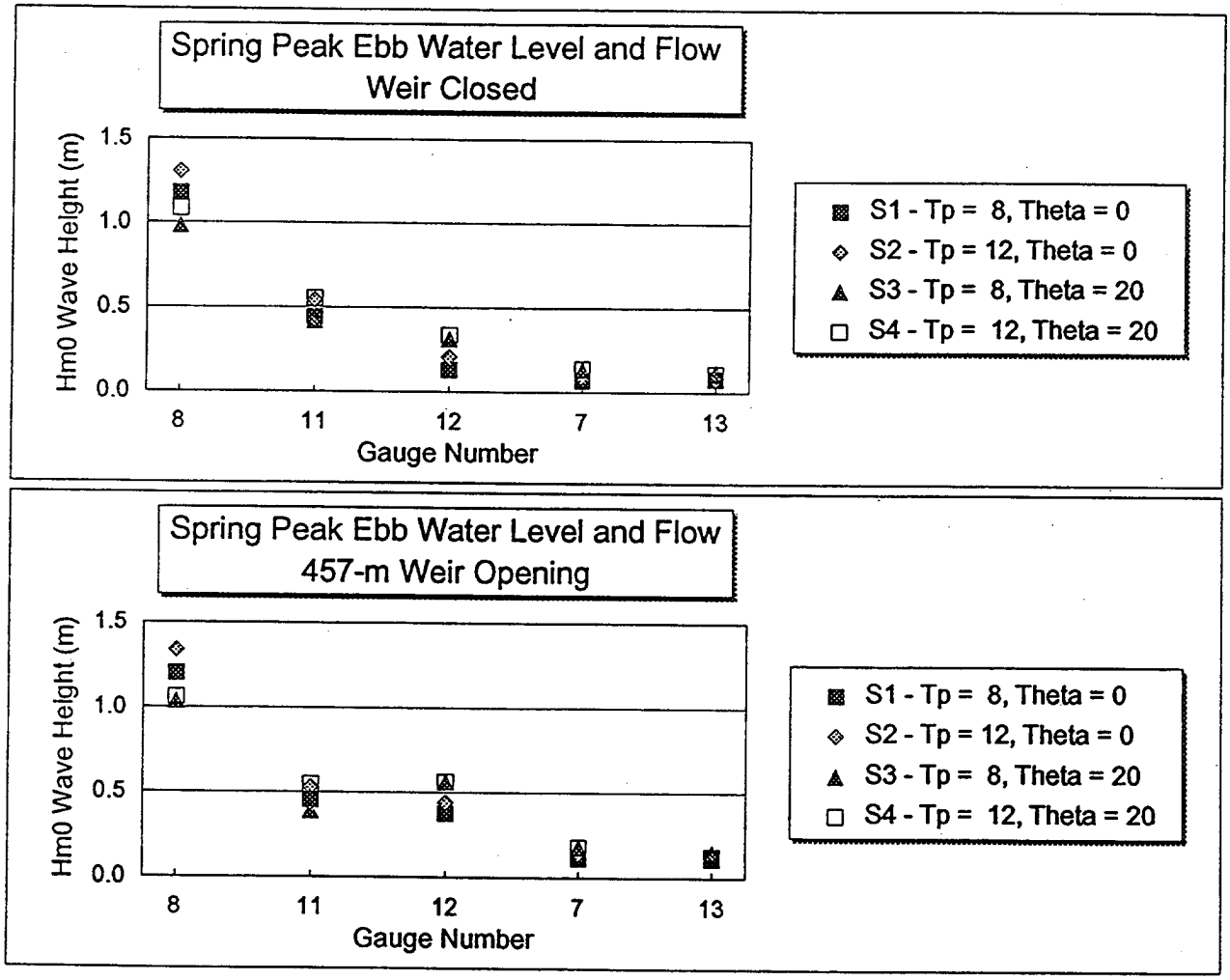

Figure 25. Wave attenuation with wave propagation down inlet channel for spring peak ebb water level for the weir closed and the 457-m (1,500-ft) weir opening

signal-to-noise ratio and correlation coefficient (measurements of statistical confidence in the measured results) are at the lower limits for acceptable results. The accuracy of this point is doubtful but it was retained for completeness. Increased seeding concentrations usually improve these measurements. For the spring peak ebb flow, seeding material (hollow sphere, see page 25) was added to the model adjacent to Rockhouse Creek. The majority of flow will pass adjacent to the north jetty with little movement across the width of the channel. For this reason, it was difficult to keep the seeding concentration high for the entire run, at the velocity gauge 1 position. These results are consistent with those found during the dye measurements. On spring peak ebb flow, the water is entrained in the channel and there is very little flow over the weir. No changes occur in the spring peak ebb flow conditions and typical waves should be encountered with different weir lengths under ebb conditions.

On flood flow there is a marked difference between the closed weir and the different weir openings. When the weir is opened, the velocity is lower throughout

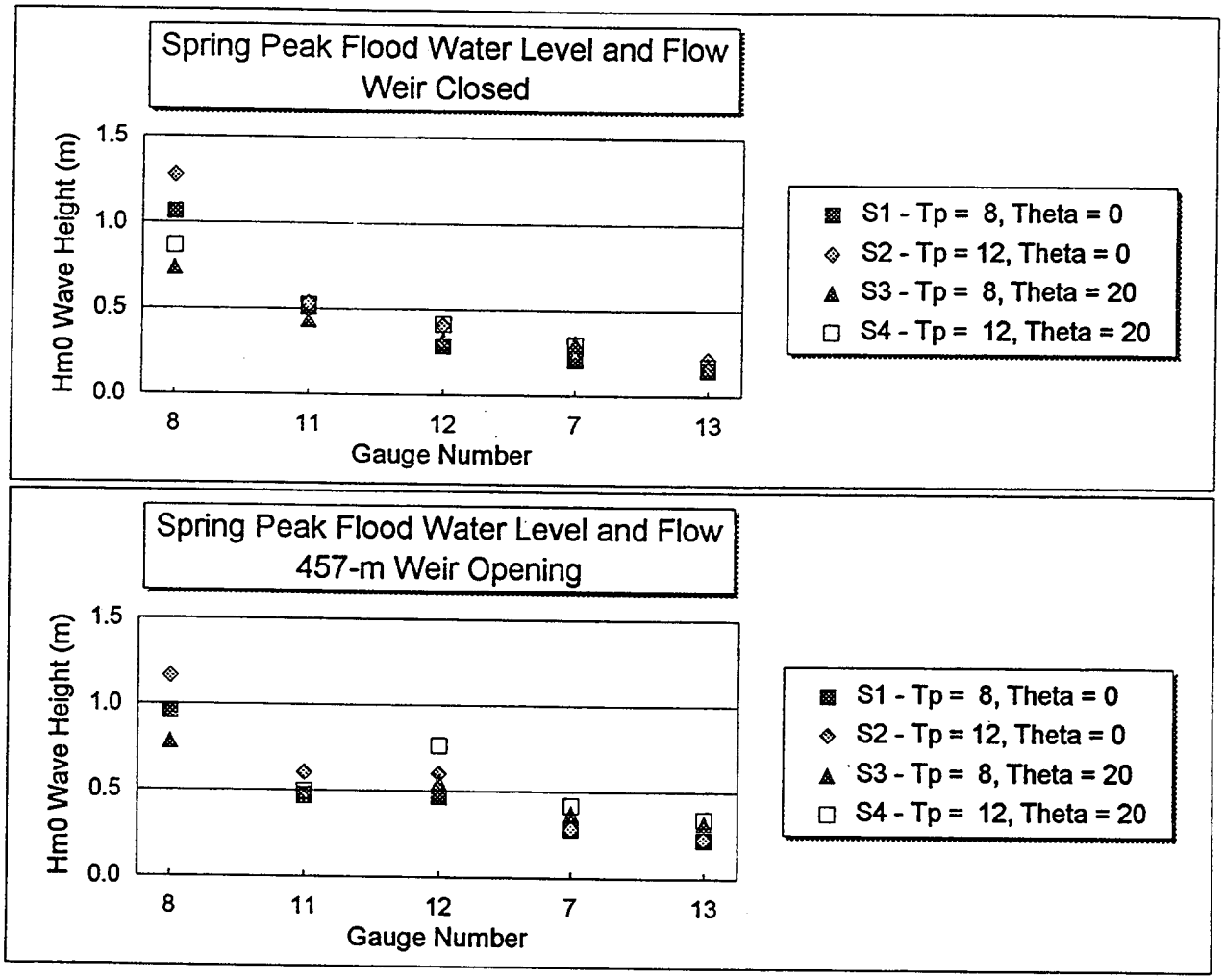

Figure 26. Wave attenuation with wave propagation down inlet channel for spring peak flood water level for the weir closed and the 457-m (1,500-ft) weir opening

the inlet. Differences between the open and closed weir are not as large at the inlet mouth as indicated by velocity gauge 1. Gauge 1 for navigation wave N1 for the 457-m (1,500-ft) weir opening exhibits the same low signal-to-noise ratio and correlation coefficients, which indicates questionable results for this gauge. Gauges 2-5 also exhibit marked differences between the closed-weir condition and the open-weir conditions. Gauge 2 located closest to the eastern tip of the north jetty exhibits the greatest differences between the closed weir and the open-weir condition. When the weir is closed, flood waters are transported down the inlet and past velocity gauge 2. However, when the weir is opened, a portion of the tidal flow is transported over the weir and not down the inlet. Differences between the four weir openings are not as great at velocity gauge 4, especially for wave case N1. Only a portion of the weir is opened shoreward of this position and this gauge records the velocity of water coming over the weir and down the channel.

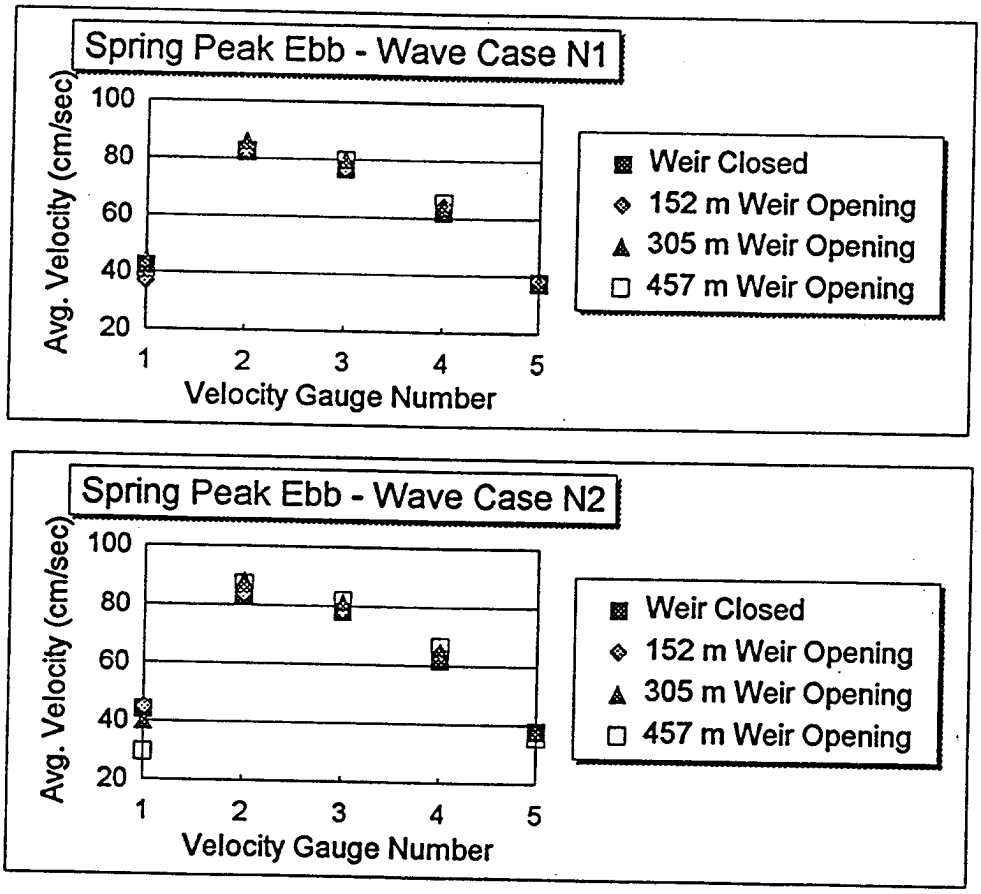

Figure 27. Velocity measurements for the four weir conditions for a spring peak ebb flow and water level for wave cases N1 and N2

Summary of velocity considerations

The velocity gauges indicated the same patterns seen in the dye runs. There was very little change in the flow characteristics between the existing (closed weir) condition and the open weir conditions for ebb flow. The ebb flow is entrained in the channel and very little water is diverted over the weir. However, flood flow and navigation type wave conditions from north of shore normal cause more water to flow over the weir and less down the inlet. The longer wave period, 12 sec, also pushes more water over the weir than the shorter, 8-sec wave period. On first appearance, opening the weir might help eliminate scour along the north interior spit, since the velocities decrease at gauge 5 (located adjacent to the spit). However, the dye indicated that water tended to flow even closer to the north interior spit to the south and west of gauge location 5.

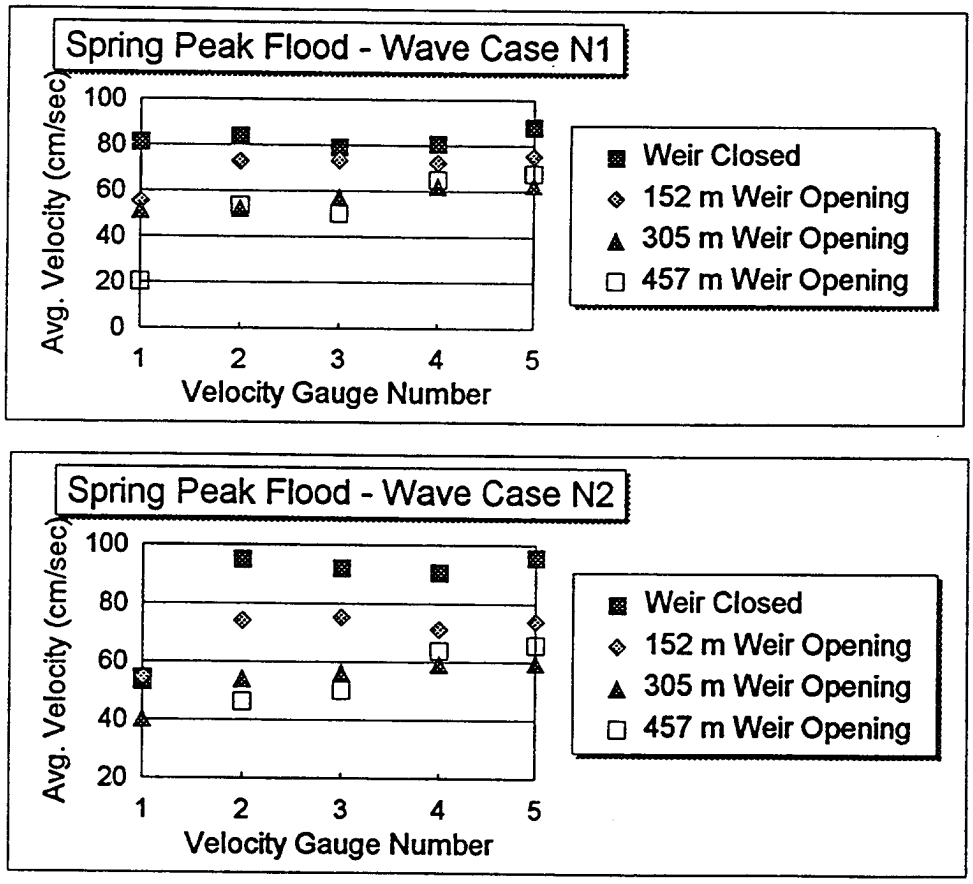

Figure 28. Velocity measurements for the four weir conditions for a spring peak flood flow and water level for wave cases N1 and N2

7 Conclusions and Recommendations

Conclusions and recommendations were made in concert with the numerical model results provided by Taylor Engineering as the project evolved. The south jetty extension length was chosen through feedback from the physical model, while results from the numerical model helped determine the orientation. The preferred weir condition became apparent from the results of both models and in light of the evolving configuration of the inlet.

The 305-m (1,000-ft) dogleg extension was the preferred south jetty extension. Based upon dye and tracer studies, the full 305-m extension was recommended. Both the straight and dogleg extensions provided somewhat equal capabilities in trapping northerly directed alongshore sediment transport. The numerical model, however, showed that the dogleg extension created better flow characteristics in the inlet. Also, the dogleg extension would not further restrict the width of the inlet opening, as would the straight extension. Another possible modification to aid in minimizing sediment transport into the inlet is to raise the elevation of the landward end of the south jetty. Sand appeared to be bypassing this end also. However, this could be an effect of a rubble-mound structure built upon a fixed bed model and problems in modeling the jetty porosity at its landward terminus. The south jetty extension also will not decrease wave heights seen at the north interior shoal. No significant changes in wave height were seen in the inlet throat between the existing condition and the preferred south jetty extension. Velocities did not appear to change significantly between existing conditions and the extension for the five gauge locations. Numerical model results show more detailed comparisons between plans.

No changes in the north jetty were recommended. The scour hole is probably caused by an ebb-dominated process and would not be helped by a mean low water weir. On ebb flow, water is entrained by the channel-dominated flow and very little water moved over the opened weir. The present evolution of the inlet suggests that the main navigation channel is rotating toward a more northwest/southeast alignment as the north spit is eroded. This rotation may reduce the scour pressure on the north jetty by "swinging" the main channel slightly away from the north jetty at the location of the present scour hole. Opening the weir would allow a supply of sand into the inlet; however, results indicated that currents behind the weir are strong and

can move material out of the area. The area behind any of the weir openings would not function well as an impoundment basin. There is no control over where the sediment is deposited and a portion of the material would be deposited in already shallow areas within the inlet. It would not seem prudent to allow an "unchecked" supply of sediment into the inlet through a weir, when also trying to prevent sand from reaching the inlet around the south jetty. Opening the weir increased the amount of wave energy inside the inlet. Although wave heights were below the safe navigation limits for the 1.5-m waves chosen at the 9.1-m (30-ft) limits, they were about twice as large as when the weir was closed. The direction of wave approach (across the weir) and any cross-currents through the weir would further increase the difficulty of navigating through the inlet. In summary, the negative impacts far outweigh any benefits that would be gained by opening the weir and thus it is recommended that the north jetty weir not be reopened.

References

Bottin, R. R., and Briggs, M. J. (1996). "Newport North Marina, Yaquina Bay, Oregon, design for wave protection," Technical Report CERC-96-2, U.S. Army Engineer Waterways Experiment Station, Vicksburg, MS.

Bottin, R. R., Jr., and Chatham, C. E., Jr. (1975). "Design for wave protection, flood control and prevention of shoaling, Cattaraugus Creek Harbor, New York; hydraulic model investigation," Technical Report H-75-18, U.S. Army Engineer Waterways Experiment Station, Vicksburg, MS.

Brasfield, C. W., and Ball, J. W. (1967). "Expansion of Santa Barbara Harbor, California; hydraulic model investigation," Technical Report 2-805, U.S. Army Engineer Waterways Experiment Station, Vicksburg, MS.

Brooks, R. M., and Brandon, W. A. (1995). "Hindcast wave information for the U.S. Atlantic coast: Update 1976-1993 with Hurricanes," WIS Report 33, U.S. Army Engineer Waterways Experiment Station, Vicksburg, MS.

Dai, Y.B., and Jackson, R.A. (1966). "Design for rubble-mound breakwaters, Dana Point Harbor, California; hydraulic model investigation," Technical Report 2-725, U.S. Army Engineer Waterways Experiment Station, Vicksburg, MS.

Giles, P. J., and Chatham, C. E., Jr. (1974). "Remedial plans for prevention of harbor shoaling, Port Orford, Oregon; hydraulic model investigation," Technical Report H-74-4, U.S. Army Engineer Waterways Experiment Station, Vicksburg, MS.

Harkins, G. S. (1991). "Sensitivity analysis for multi-element wavemakers," M.S. thesis, University of Delaware, Newark.

Hubertz, J. M.., Brooks, R. M., Brandon, W. A., and Tracy, B. A. (1993). "Hindcast wave information for the U. S. Atlantic coast," WIS Report 30, U.S. Army Engineer Waterways Experiment Station, Vicksburg, MS.

Jones, C. P., and Mehta, A. J. (1978). "Ponce DeLeon Inlet, glossary of Inlets Report No. 6," Florida Sea Grant Program, Gainesville, FL.

Le Méhauté, B. (1965). "Wave absorbers in harbors," Contract Report 2-122, U.S. Army Engineer Waterways Experiment Station, Vicksburg, MS, prepared by National Engineering Science Company, Pasadena, CA, under contract No. DA-22-079-CIVENG-64-81.

Noda, E. K. (1972). "Equilibrium beach profile scale-model relationship," *Journal Waterways, Harbors and Coastal Engineering Division*, American Society of Civil Engineers 98(WW4), 511-528.

Outlaw, D. G., and Briggs, M. J. (1986). "Directional irregular wave generator design for shallow wave basins." *21st American Towing Tank Conference*, August 7, Washington, DC, 1-6.

Taylor, R. B. (1989). "Program development Report for Port District Inlet Management Program," prepared by Taylor Engineering, Jacksonville, FL.

Taylor, R. B., and Hull, J. J. (1996). "Ponce DeLeon Inlet Feasibility Study, Numerical Modeling and Shoaling Analysis," Taylor Engineering, Inc., Jacksonville, FL.

Taylor, R. B., Yanez, M. A., Hull, T. J., and McFetridge, W. F. (1990). "Engineering evaluation of Ponce DeLeon Inlet, final Phase II report," Taylor Engineering, Inc., Jacksonville, FL.

U.S. Army Corps of Engineers. (1952). "Survey-review report on Ponce DeLeon Inlet, Florida," U.S. Army Engineer District, Jacksonville, FL.

_____. (1963). "Survey-review report on Ponce DeLeon Inlet, Florida," U.S. Army Engineer District, Jacksonville, FL.

_____. (1967). "General and detail design memorandum, Ponce DeLeon Inlet, Florida," U.S. Army Engineer District, Jacksonville, FL.

_____. (1983). "General and detail design memorandum, Ponce DeLeon Inlet, Florida, Addendum 1 (Adjustment of Weir)," U.S. Army Engineer District, Jacksonville, FL.

U.S. Department of Commerce, National Oceanic and Atmospheric Administration, National Ocean Service. (1992). "United States Coast Pilot Atlantic Coast: Cape Henry to Key West."

Appendix A
Water Level Data

Table A1
Constituents for the Interior South Site (TDR156.DTD)

Constituent	A_i (m)	ω_i (deg/hr)	$v\phi u_i$ (deg) 1994	k_i (deg)
M2-1	0.4464	28.9841	278.0	236.5
S2-2	0.0599	30.0000	0.0	253.9
N2-3	0.0835	28.4397	334.9	230.3
K1-4	0.0741	15.0411	18.0	133.0
O1-5	0.0529	13.9430	256.1	138.2
P1-6	0.0233	14.9589	349.6	113.8
K2-7	0.0145	30.0821	215.4	248.0

Table A2
Constituents for the Interior North Site (TDR408.TMS)

Constituent	A_i (m)	ω_i (deg/hr)	$v\phi u_i$ (deg) 1994	k_i (deg)
M2-1	0.3578	28.9841	278.0	247.0
S2-2	0.0455	30.0000	0.0	264.9
N2-3	0.0653	28.4397	334.9	238.6
K1-4	0.0588	15.0411	18.0	141.8
O1-5	0.0470	13.9430	256.1	151.8
P1-6	0.0177	14.9589	349.6	138.1
K2-7	0.0162	30.0821	215.4	258.0

Table A3
Constituents for the Inlet Throat Site (TDR88.TMS)

Constituent	A_i (m)	ω_i (deg/hr)	$v\phi u_i$ (deg) 1994	k_i (deg)
M1-1	0.4614	28.9841	278.0	232.2
S2-2	0.0785	30.0000	0.0	243.3
N2-3	0.1105	28.4397	334.9	211.6
K1-4	0.0739	15.0411	18.0	126.1
O1-5	0.0478	13.9430	256.1	141.4
P1-6	0.0287	14.9589	349.6	123.3
K2-7	0.0282	30.0821	215.4	257.2

Table A4
Constituents for the Rockhouse Creek Site (TDR154.TMS)

Constituent	A_i (m)	ω_i (deg/hr)	$v\phi u_i$ (deg) 1994	k_i (deg)
M2-1	0.4413	28.9841	278.0	236.4
S2-2	0.0564	30.0000	0.0	249.7
N2-3	0.0869	28.4397	334.9	227.5
K1-4	0.0723	15.0411	18.0	131.5
O1-5	0.0548	13.9430	256.1	139.7
P1-6	0.0221	14.9589	349.6	123.1
K2-7	0.0213	30.0821	215.4	250.9

Table A5
Constituents for the Offshore North Site (TDR328.TMS)

Constituent	A_i (m)	ω_i (deg/hr)	$v\phi u_i$ (deg) 1994	k_i (deg)
M2-1	0.5847	28.9841	278.0	223.7
S2-2	0.0849	30.0000	0.0	236.3
N2-3	0.1226	28.4397	334.9	213.8
K1-4	0.0926	15.0411	18.0	122.0
O1-5	0.0627	13.9430	256.1	127.1
P1-6	0.0273	14.9589	349.6	117.6
K2-7	0.0221	30.0821	215.4	253.4

Table A6
Constituents for the Offshore South Site, TDR85.DTD

Constituent	A_i (m)	ω_i (deg/hr)	$v\phi u_i$ (deg) 1994	k_i (deg)
M2-1	0.5790	28.9841	278.0	223.0
S2-2	0.0683	30.0000	0.0	240.3
N2-3	0.1180	28.4397	334.9	211.5
K1-4	0.0970	15.0411	18.0	124.5
O1-5	0.0631	13.9430	256.1	125.0
P1-6	0.0233	14.9589	349.6	134.5
K2-7	0.0262	30.0821	215.4	214.3

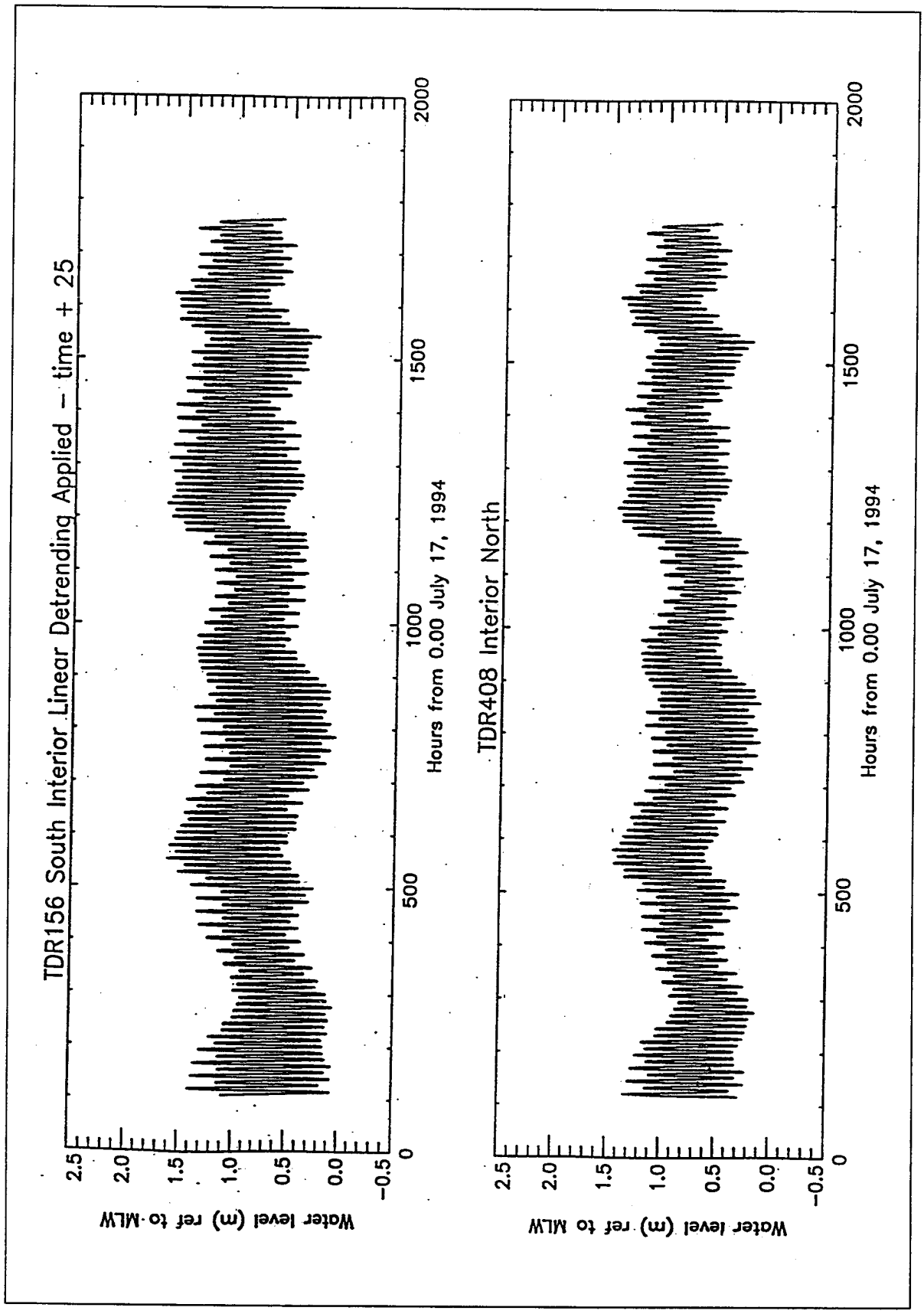

Figure A1. Water level data at South and North Interior Sites

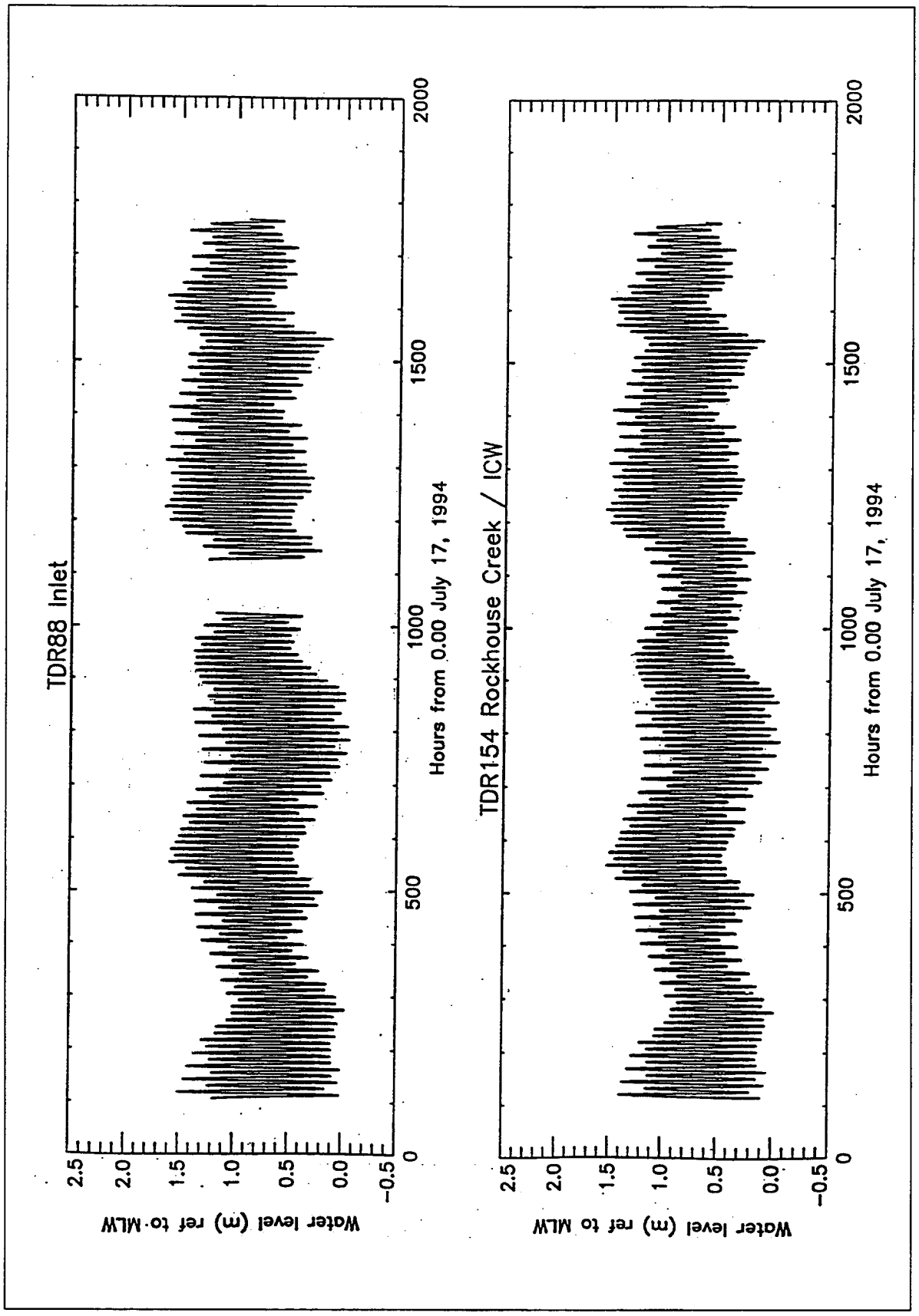

Figure A2. Water level data at Inlet Throat and Rockhouse Creek Sites

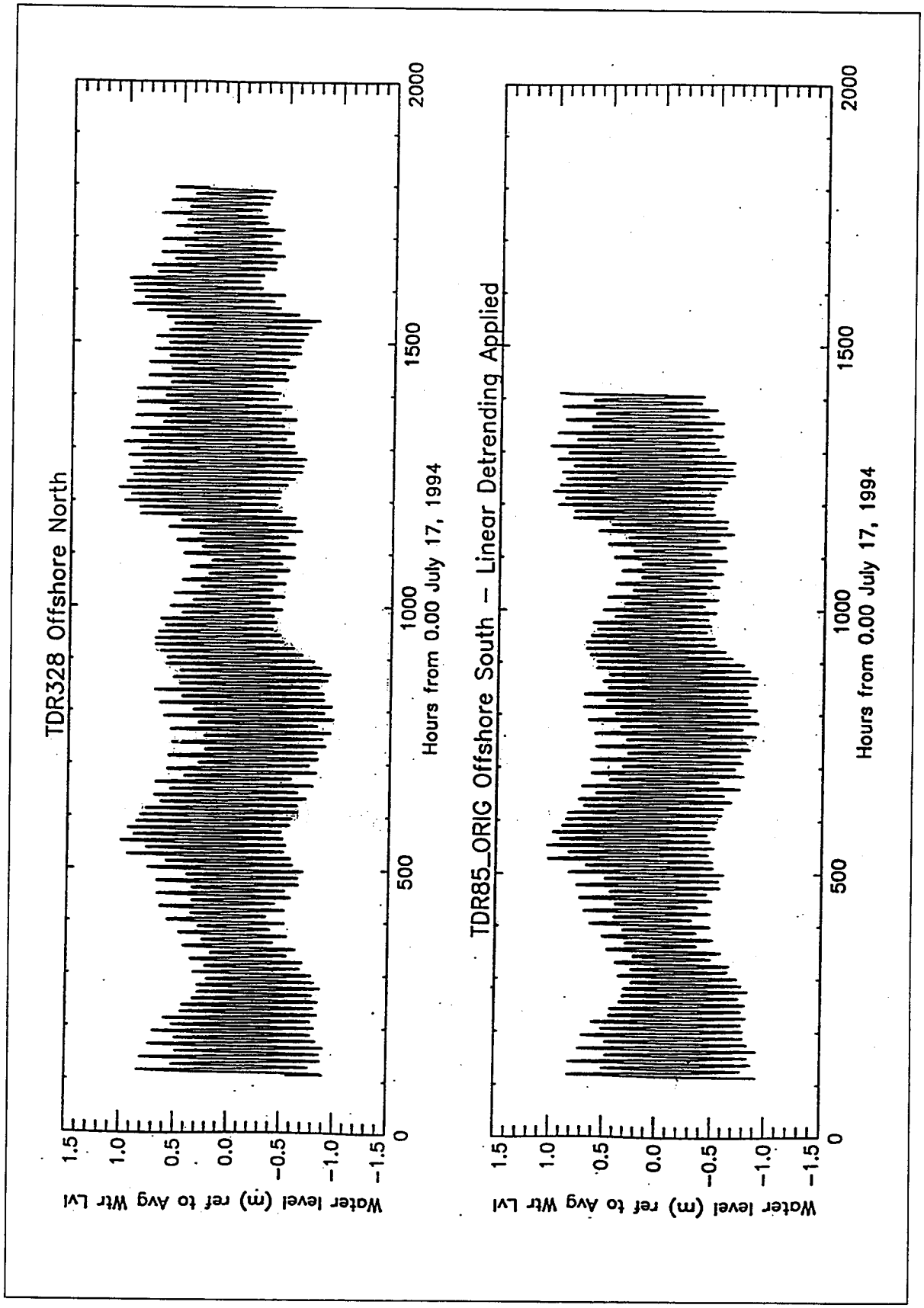

Figure A3. Water level data at North and South Offshore Sites

Appendix B
BBADCP - Data Range A - H

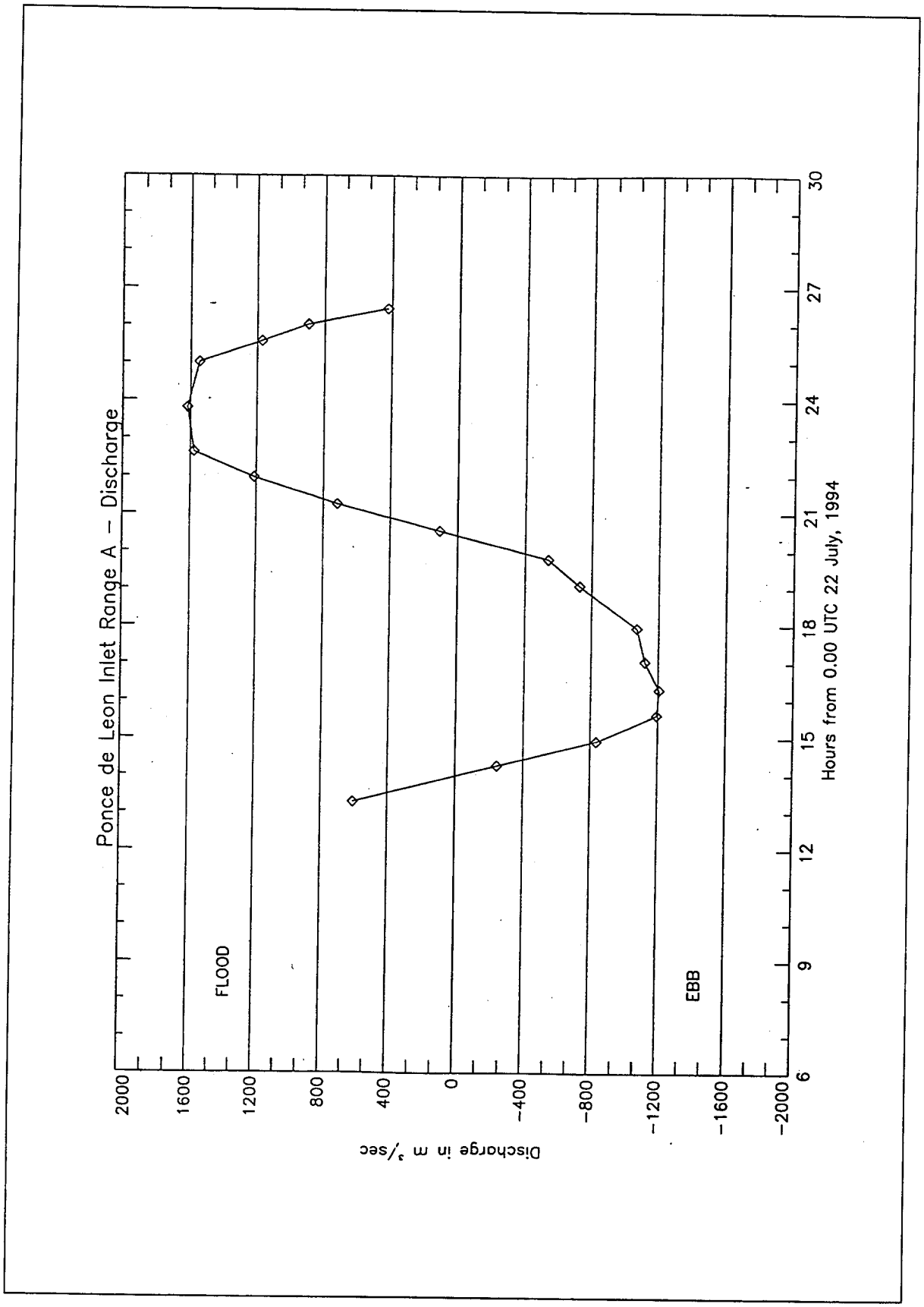

Figure B1. Discharge, Range A

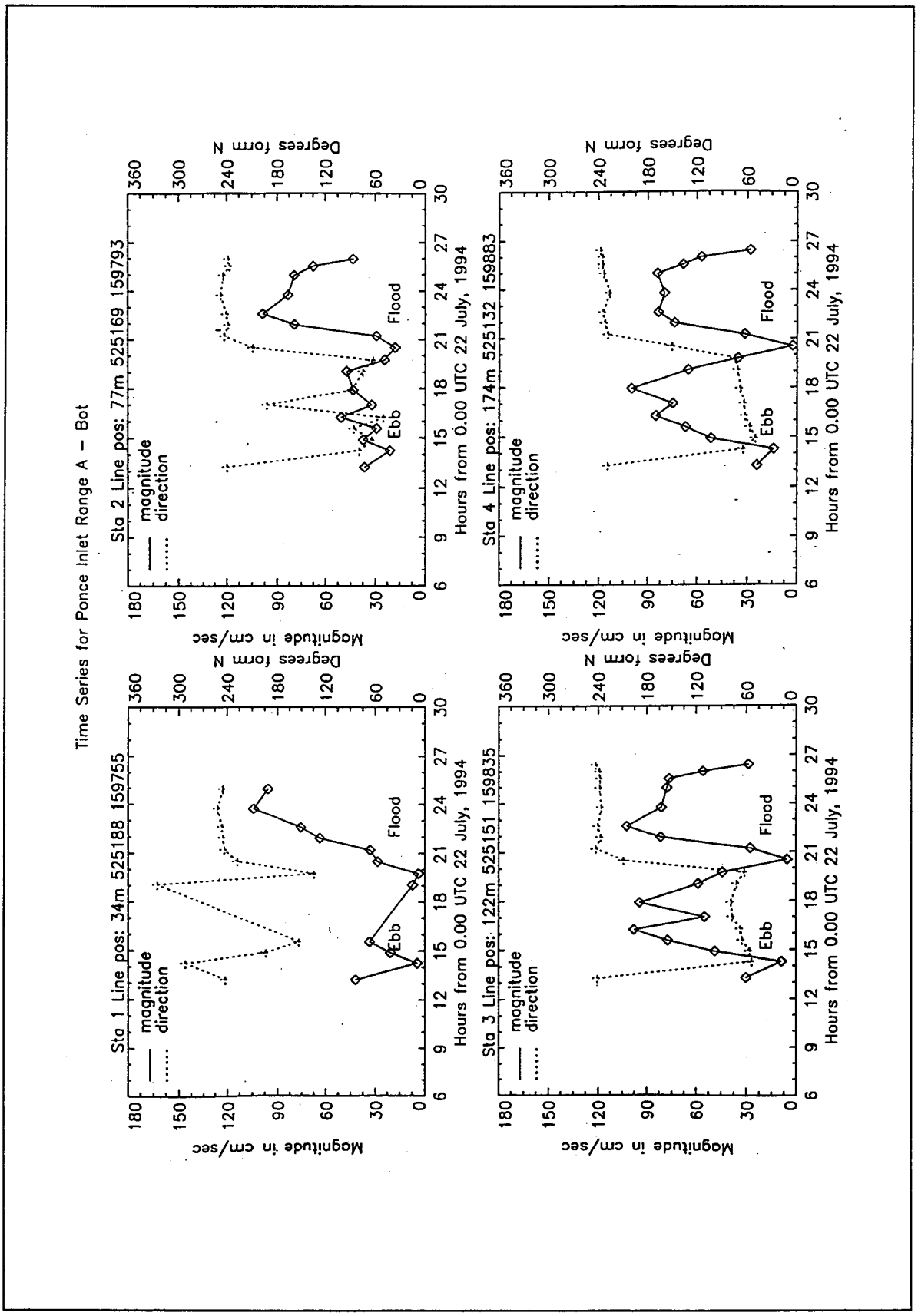

Figure B2. Time series, Range A, stations 1-4

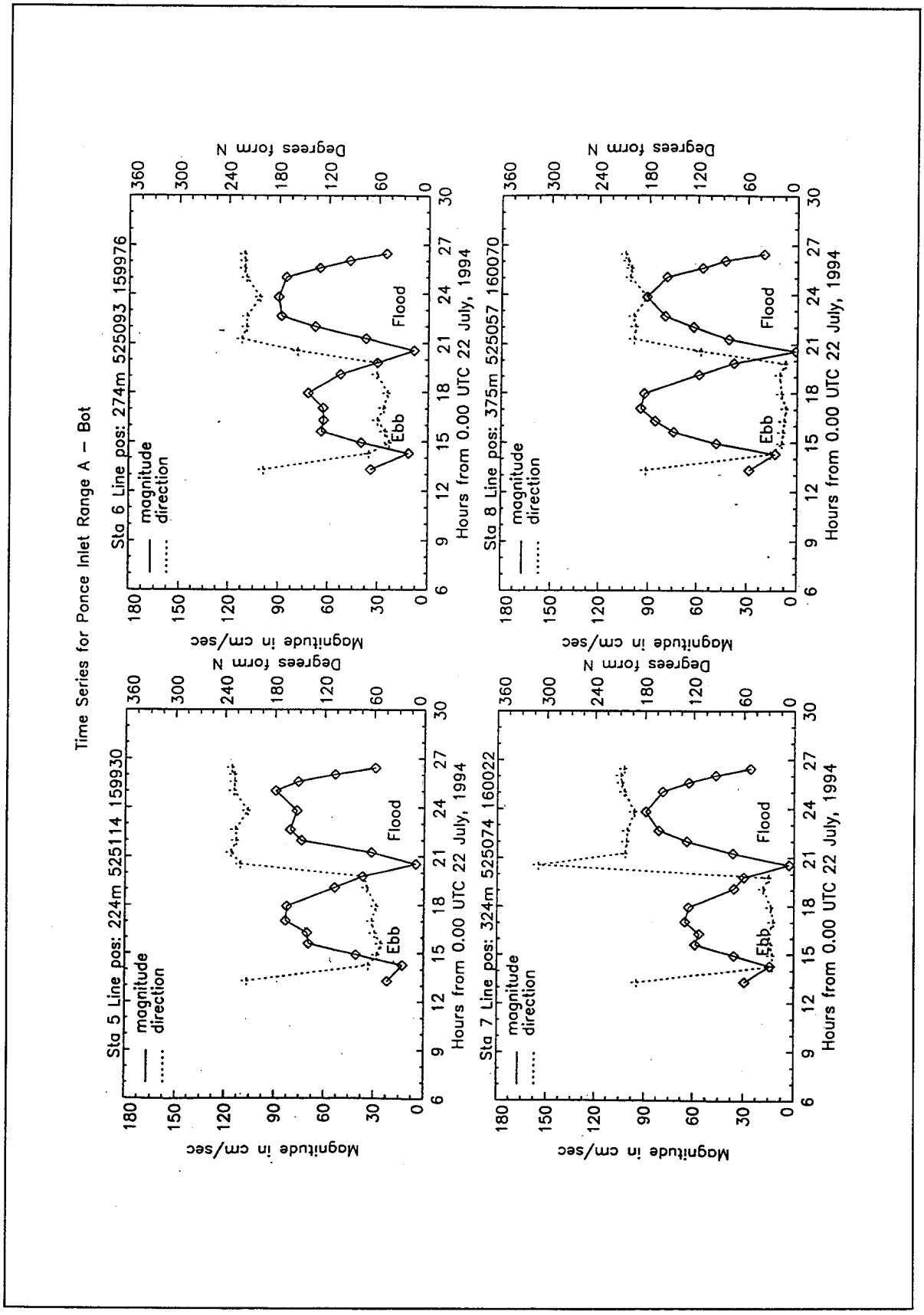

Figure B3. Time series, Range A, stations 5-8

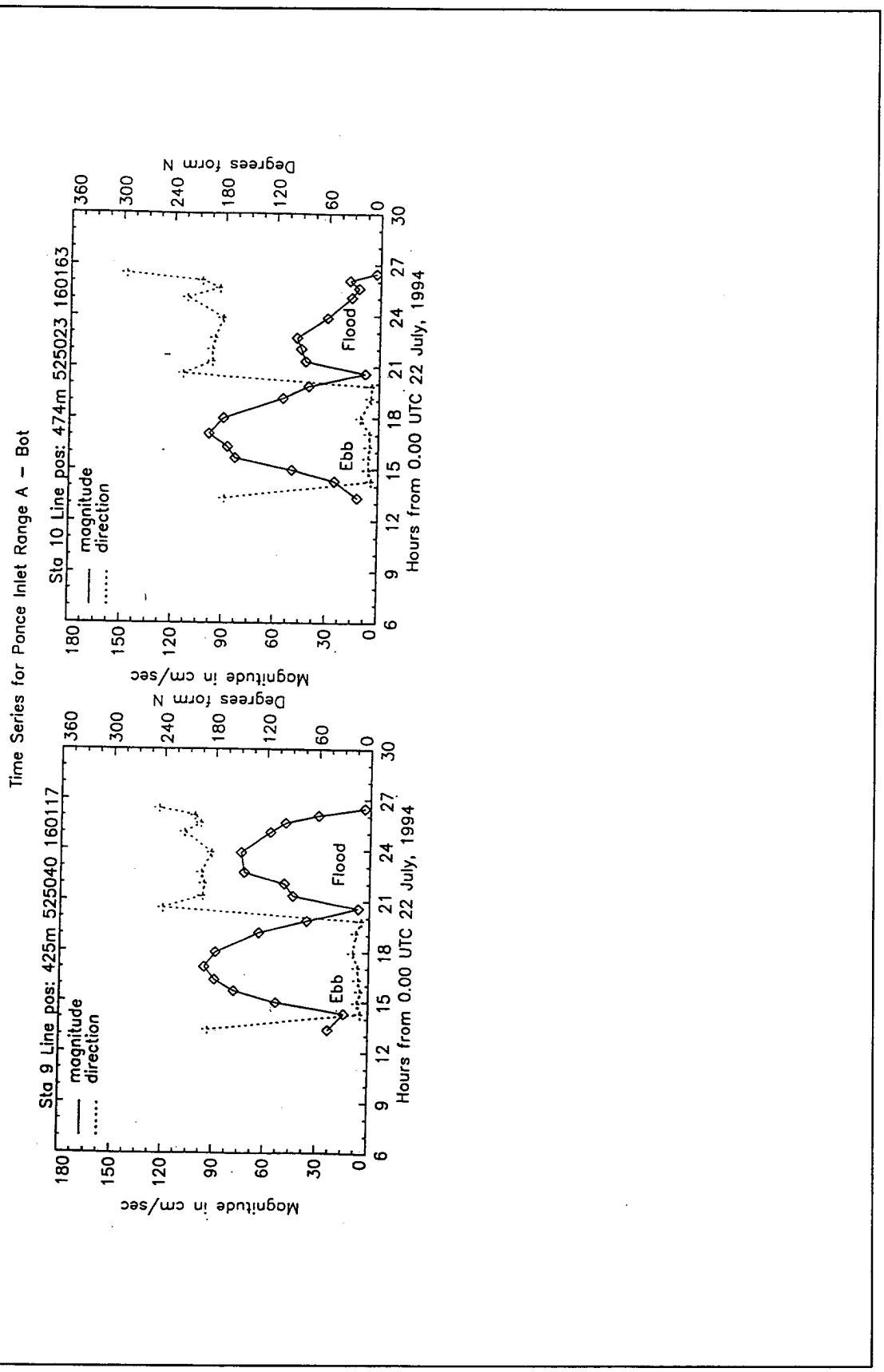

Figure B4. Time series, Range A, stations 9 and 10

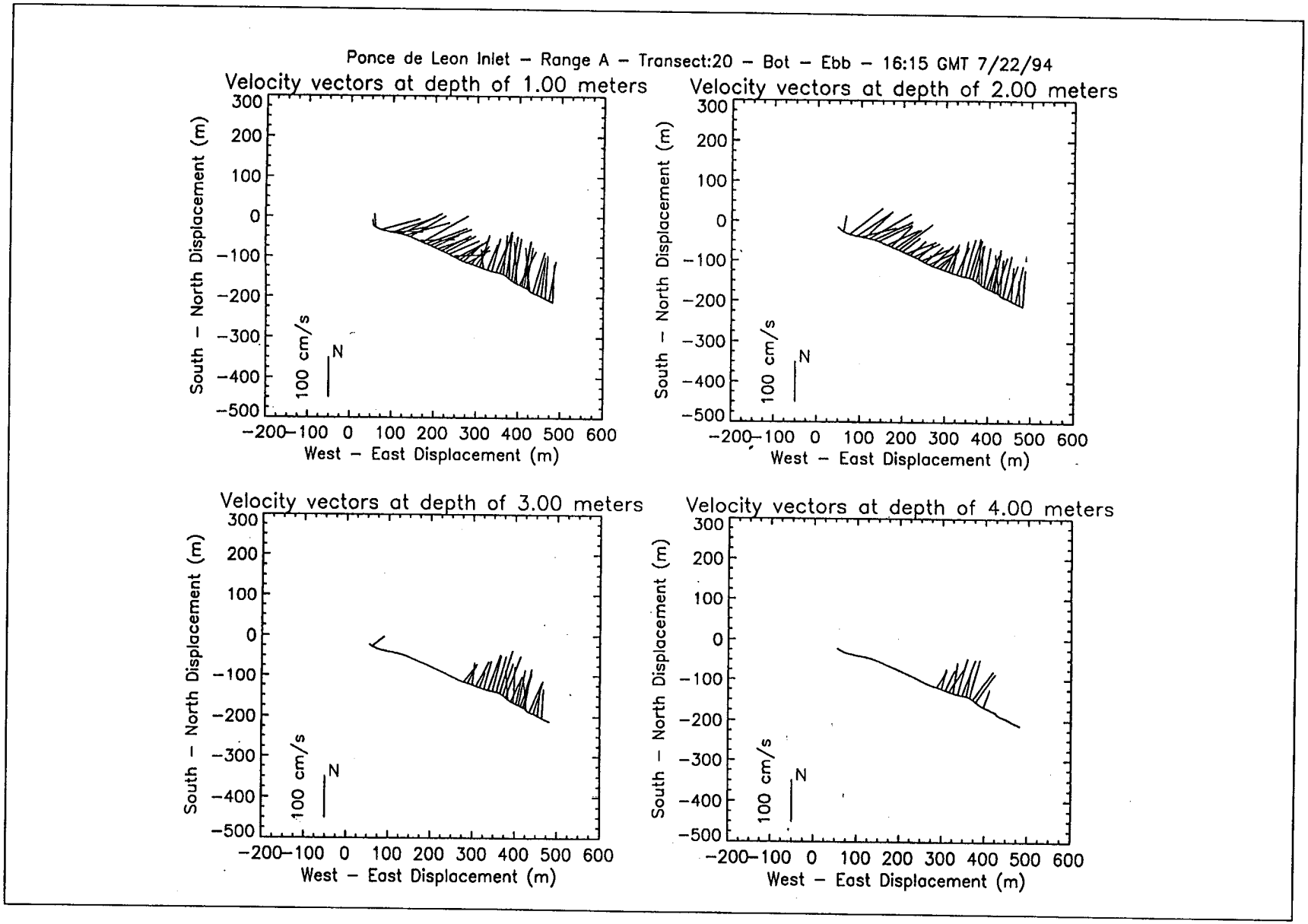

Figure B5. Velocity vector plots for peak ebb conditions, Range A

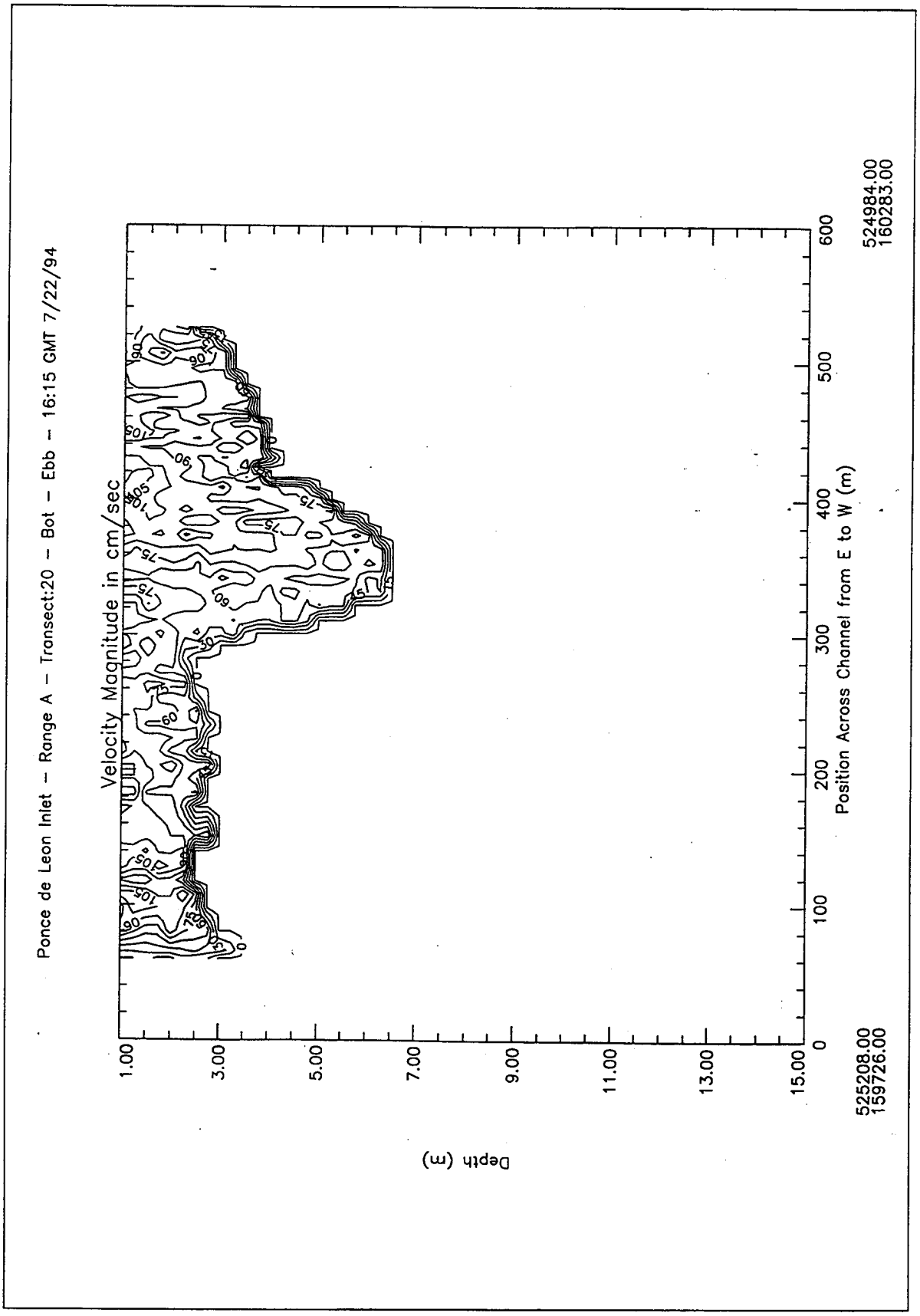

Figure B6. Contour plot of water magnitudes at peak ebb conditions, Range A

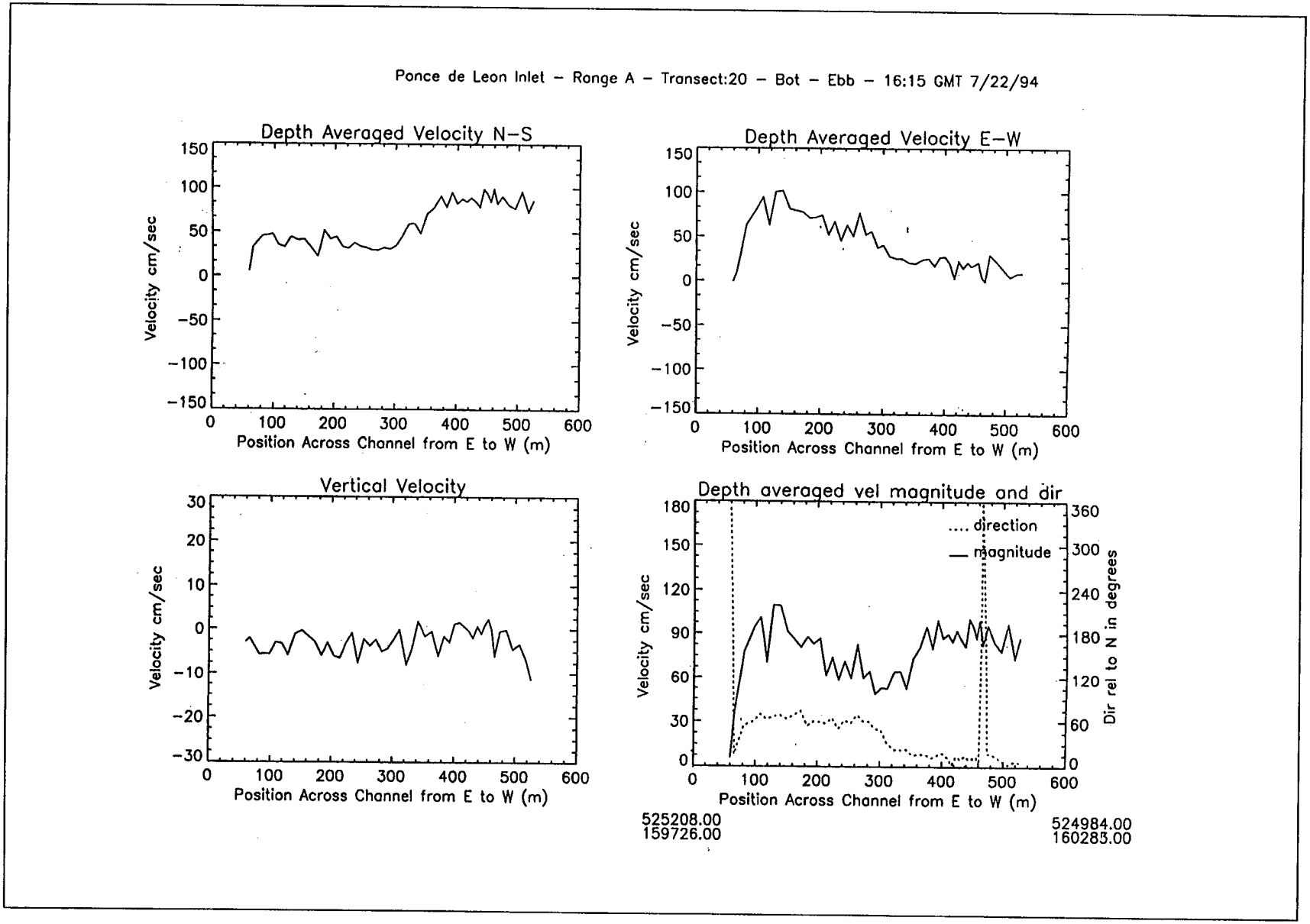

Figure B7. Depth average water velocities at peak ebb conditions, Range A

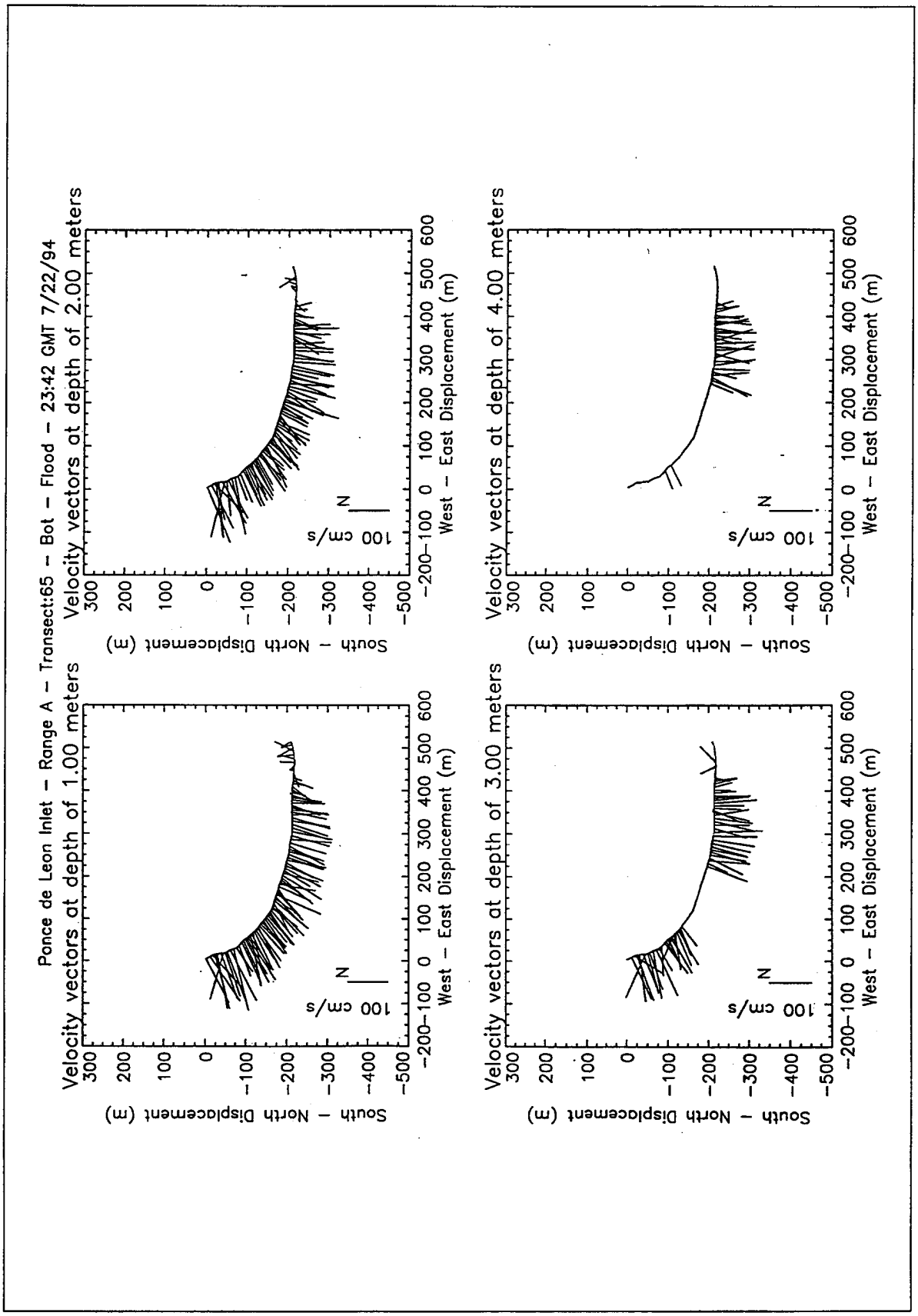

Figure B8. Velocity vector plots for peak flood conditions, Range A

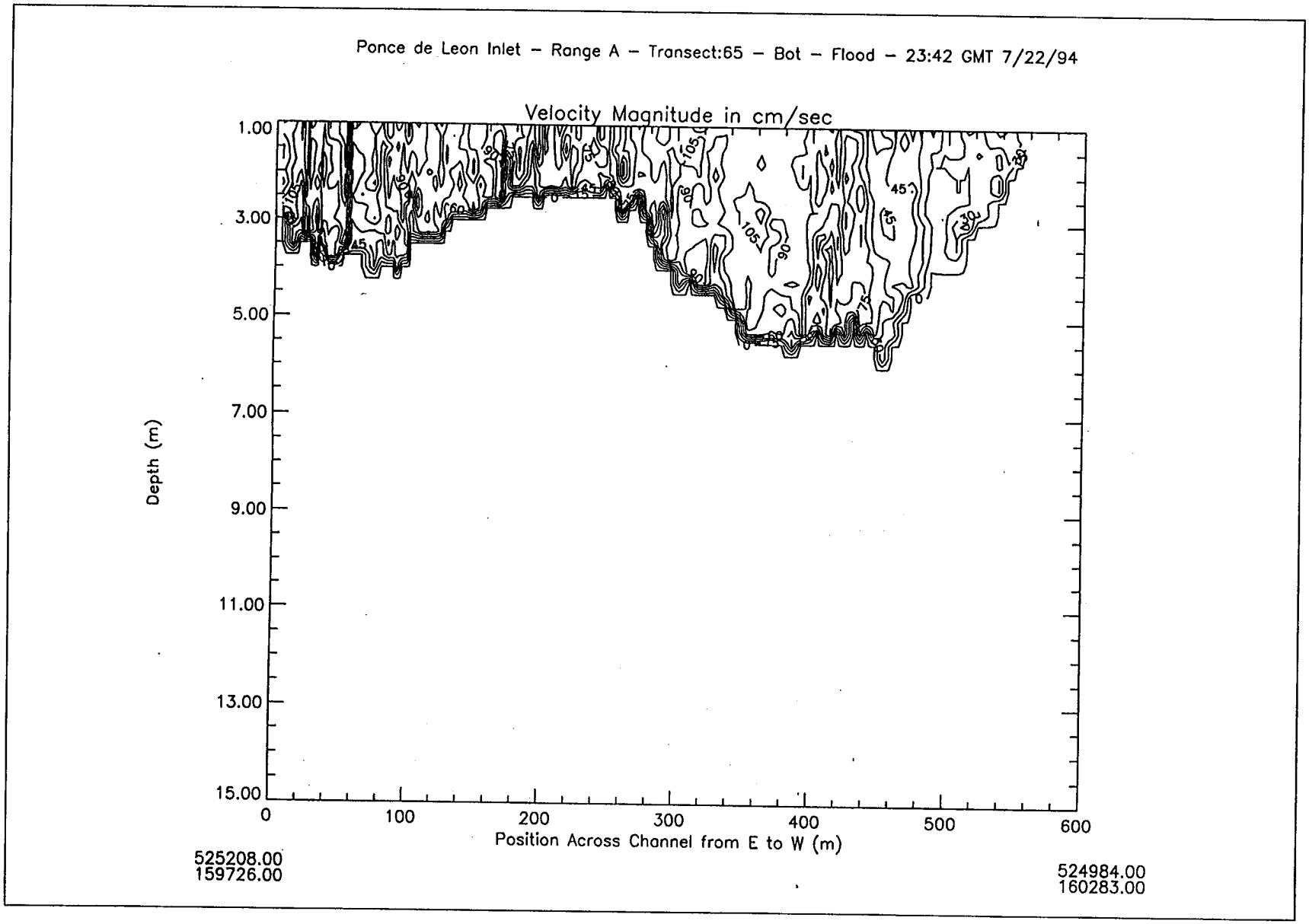

Figure B9. Contour plot of water magnitudes at peak flood conditions, Range A

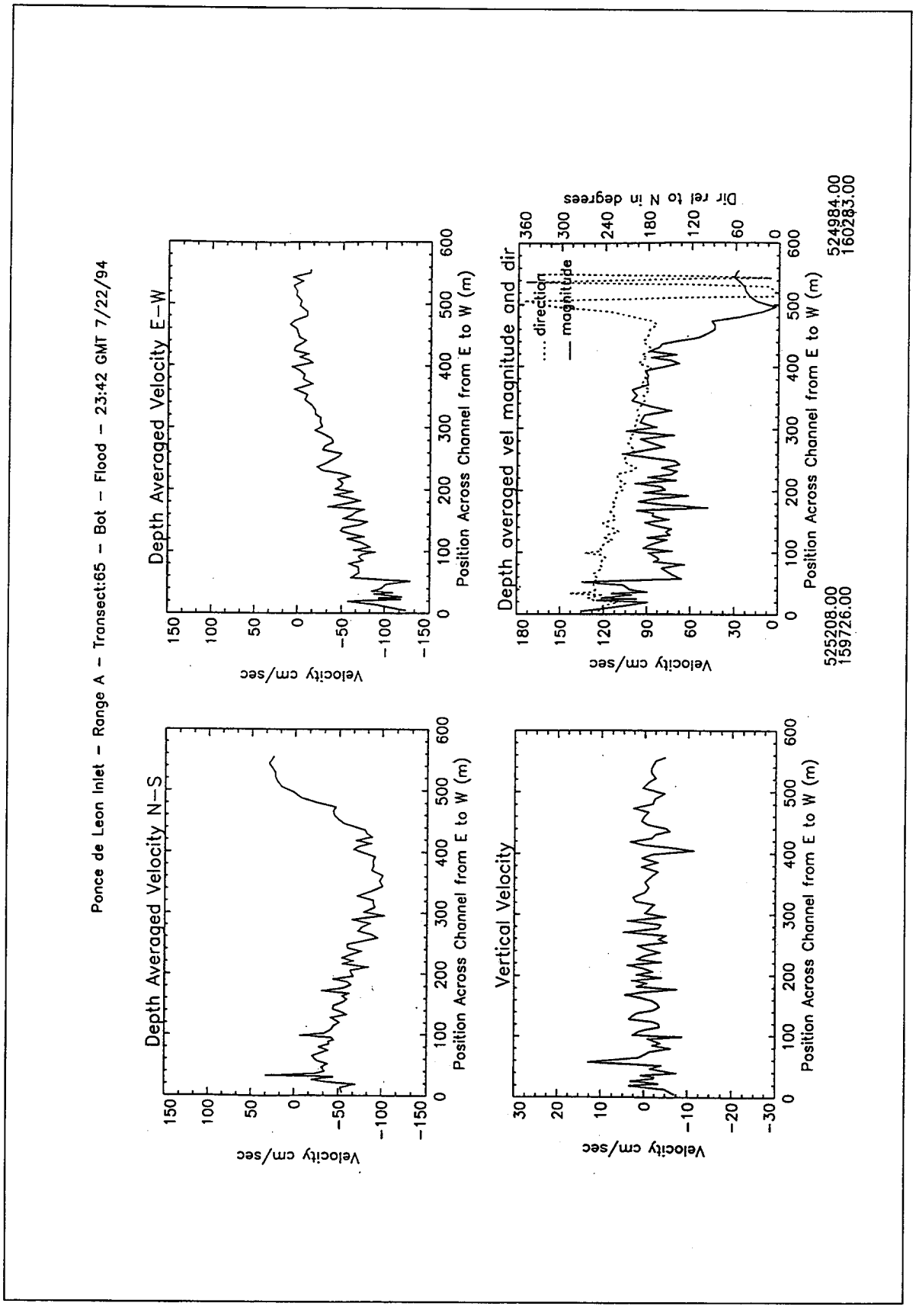

Figure B10. Depth average water velocities at peak flood conditions, Range A

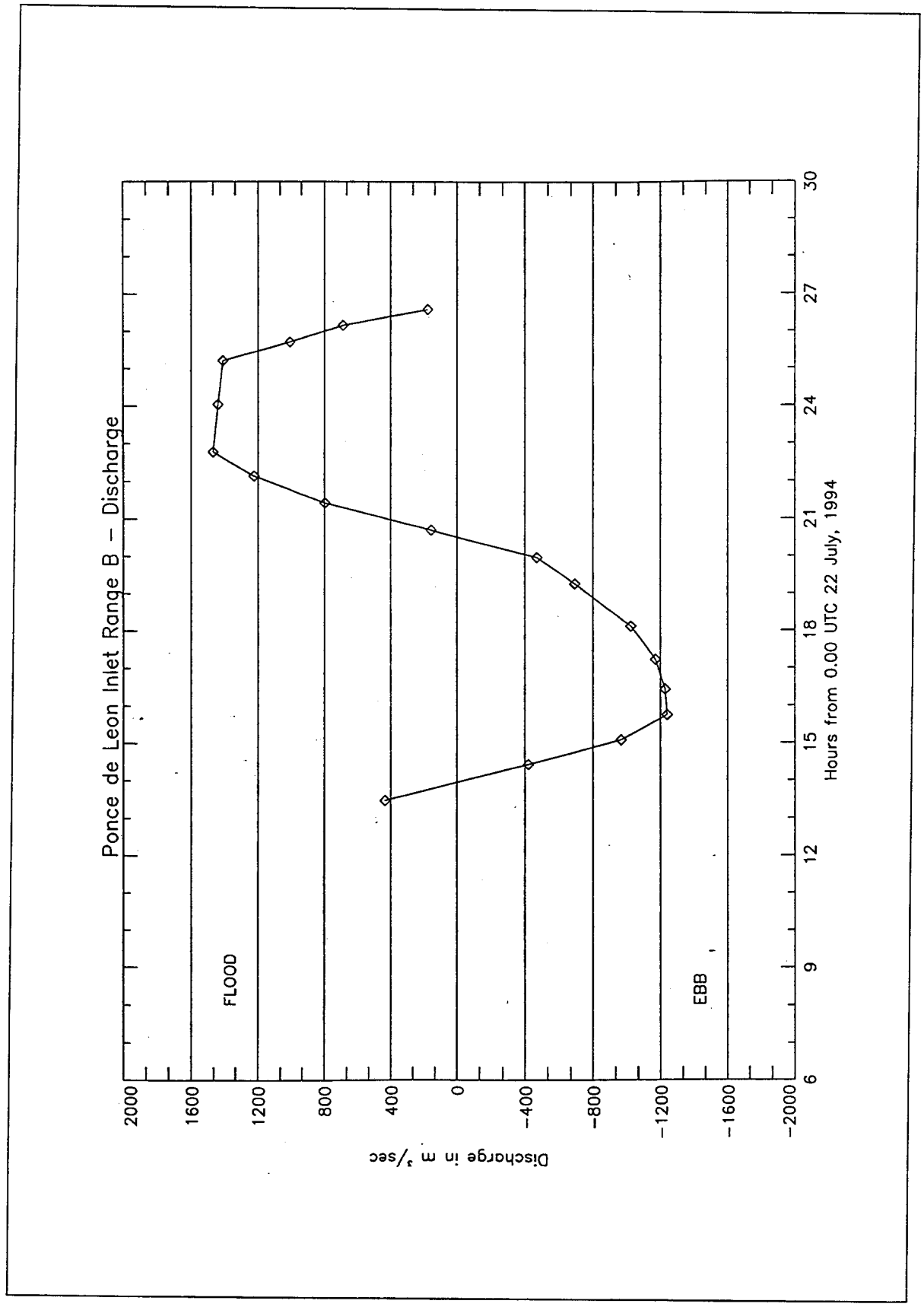

Figure B11. Discharge, Range B

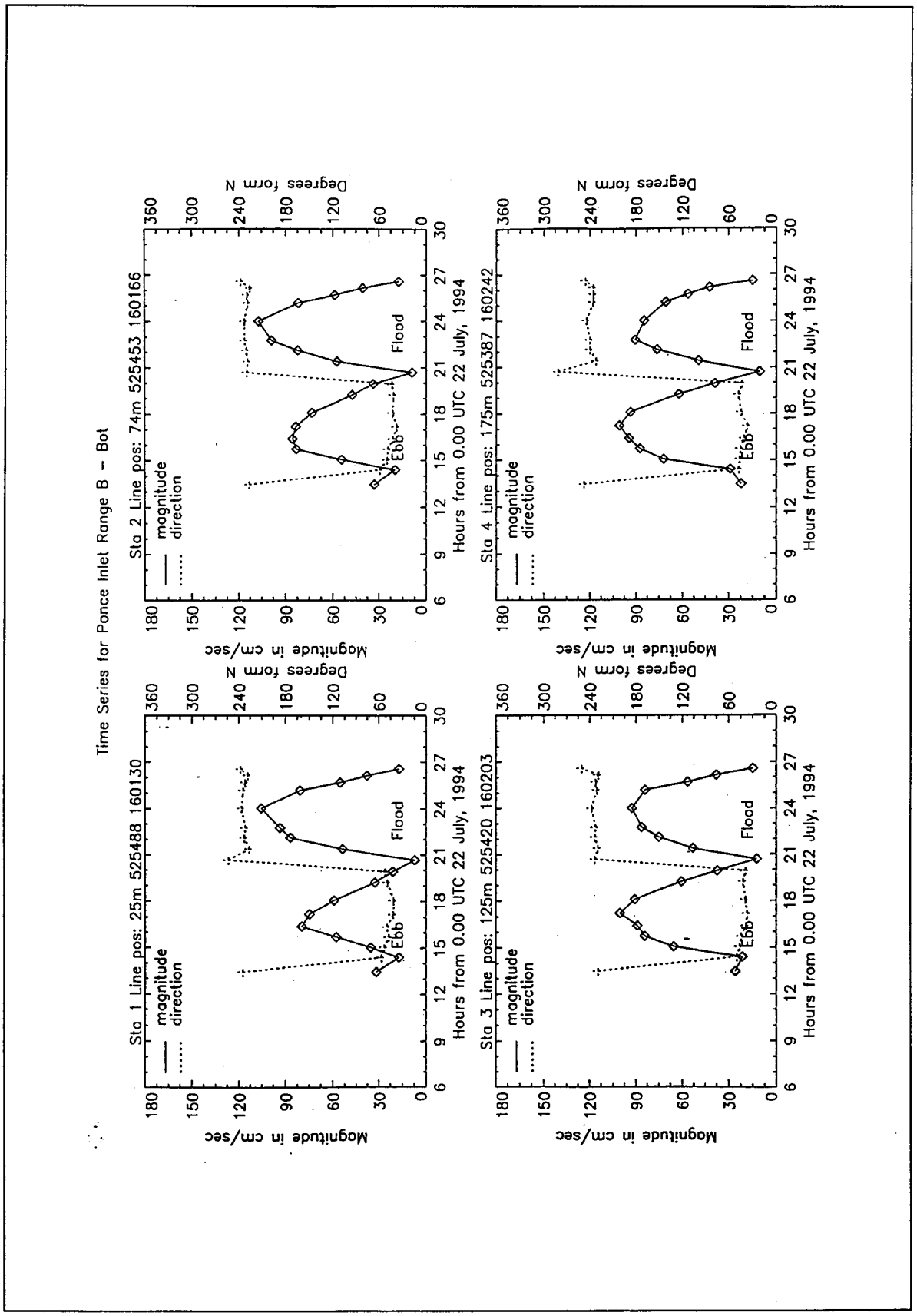

Figure B12. Time series, Range B, stations 1-4

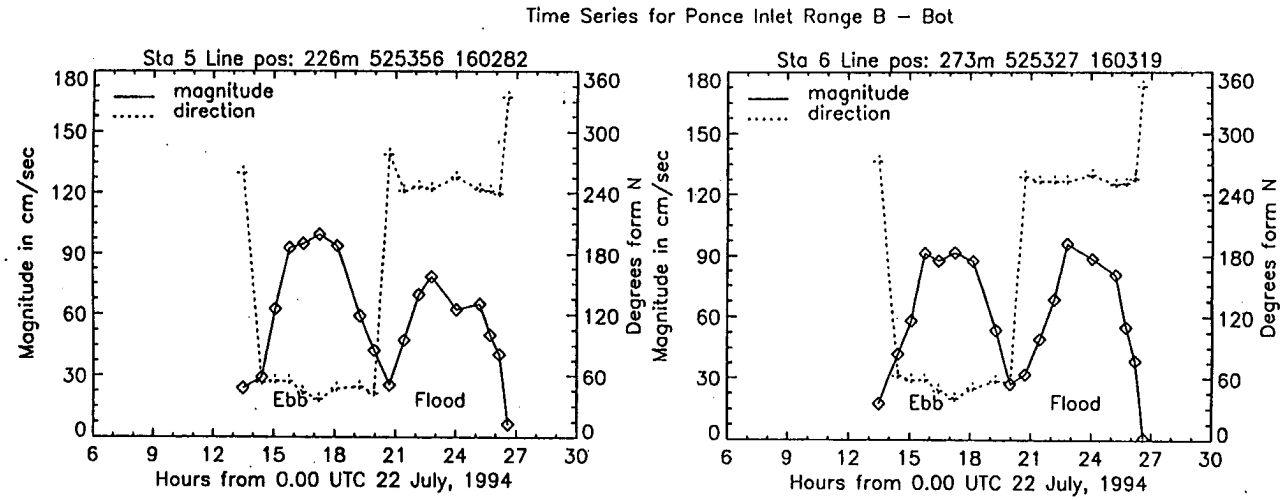

Figure B13. Time series, Range B, stations 5 and 6

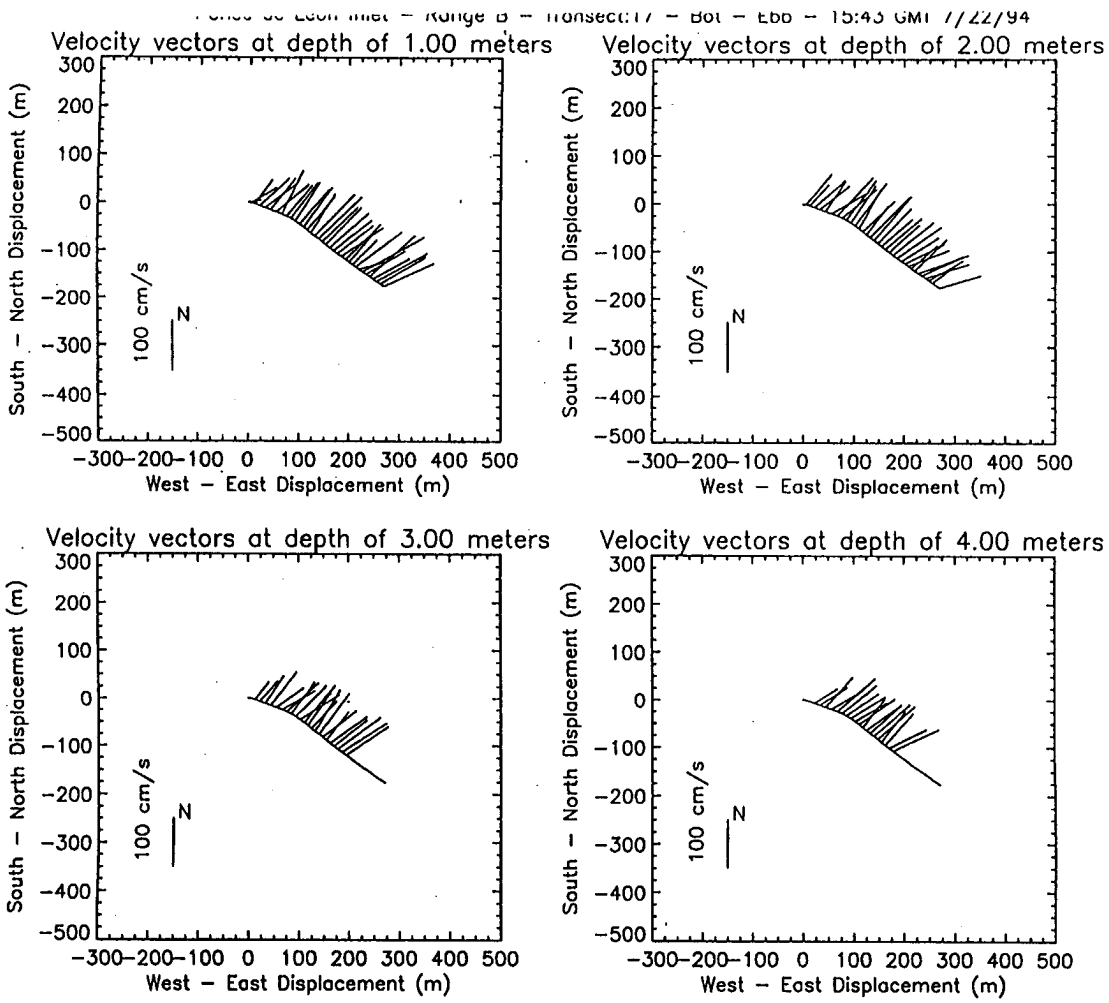

Figure B14. Velocity vector plots at peak ebb conditions, Range B

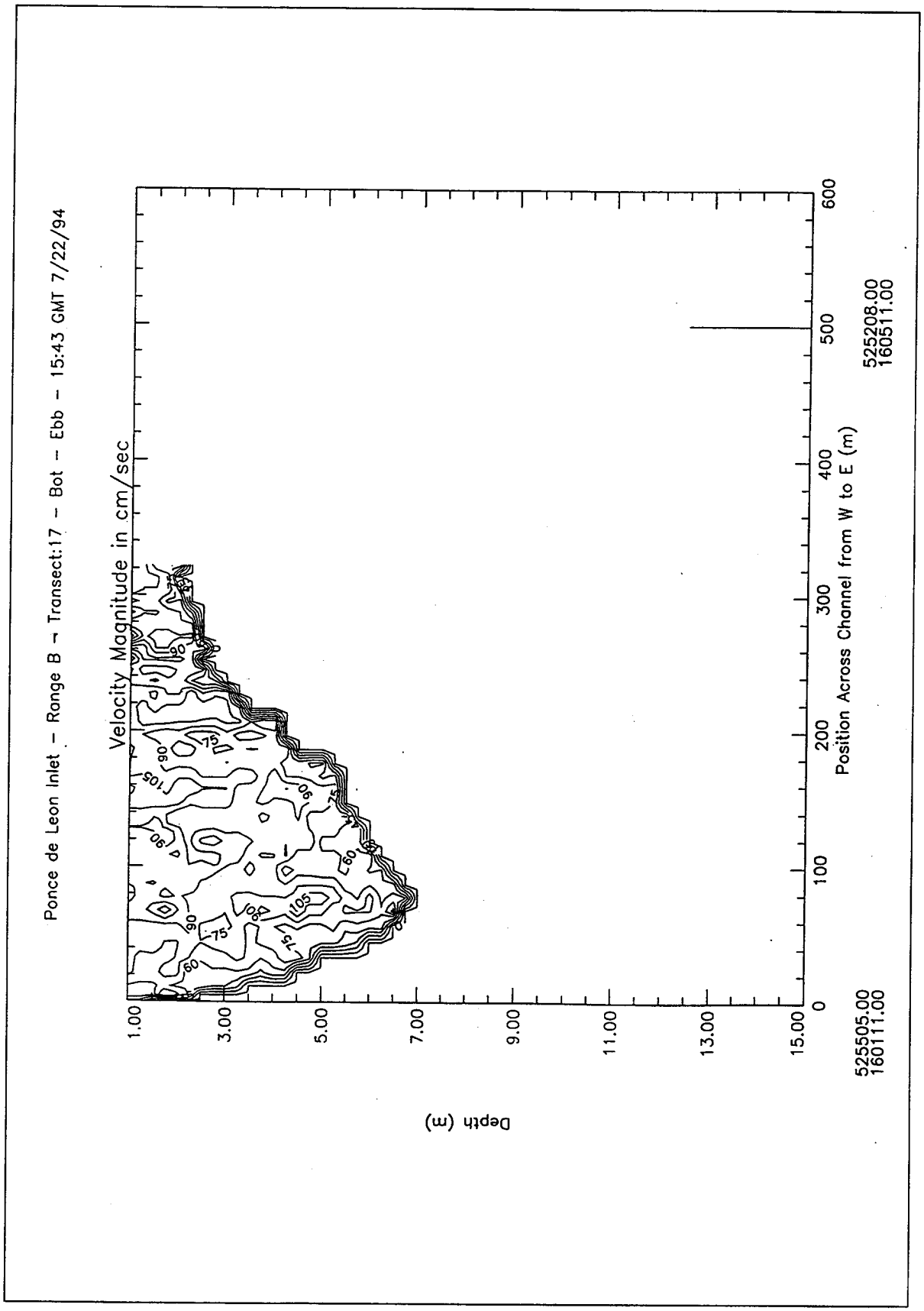

Figure B15. Contour plot of water magnitudes at peak ebb conditions, Range B

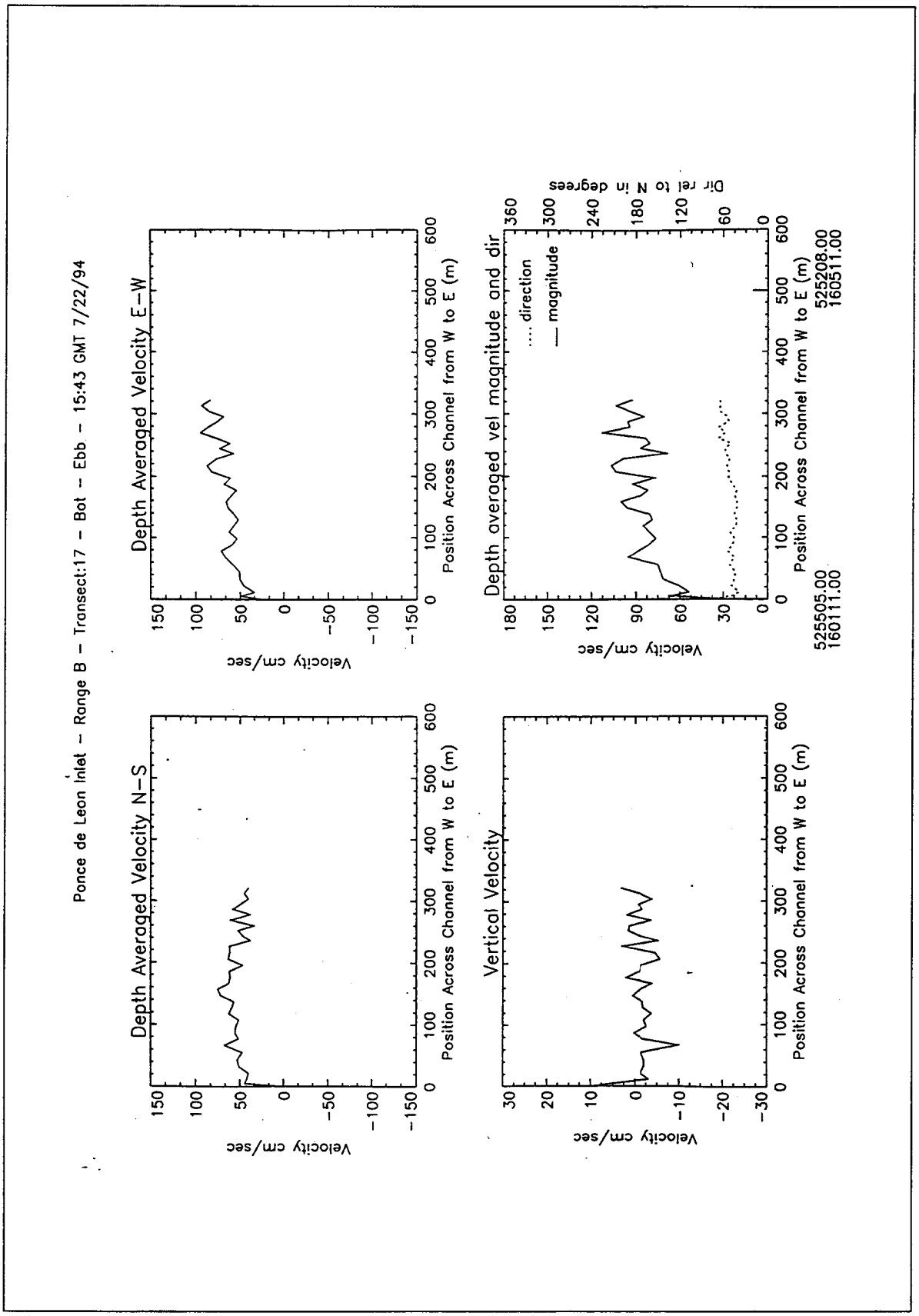

Figure B16. Depth average water velocities at peak ebb conditions, Range B

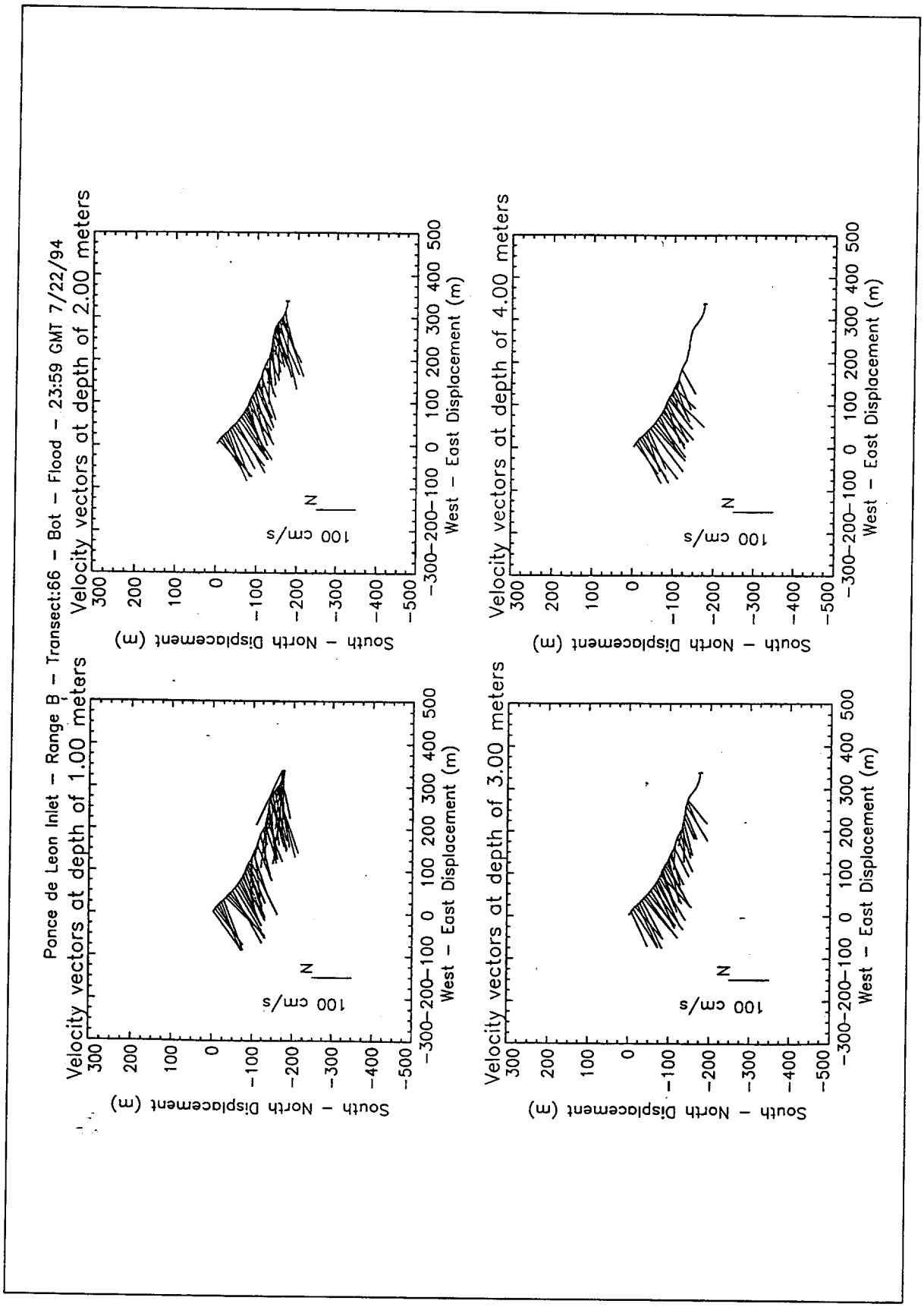

Figure B17. Velocity vector plots at peak ebb conditions, Range B

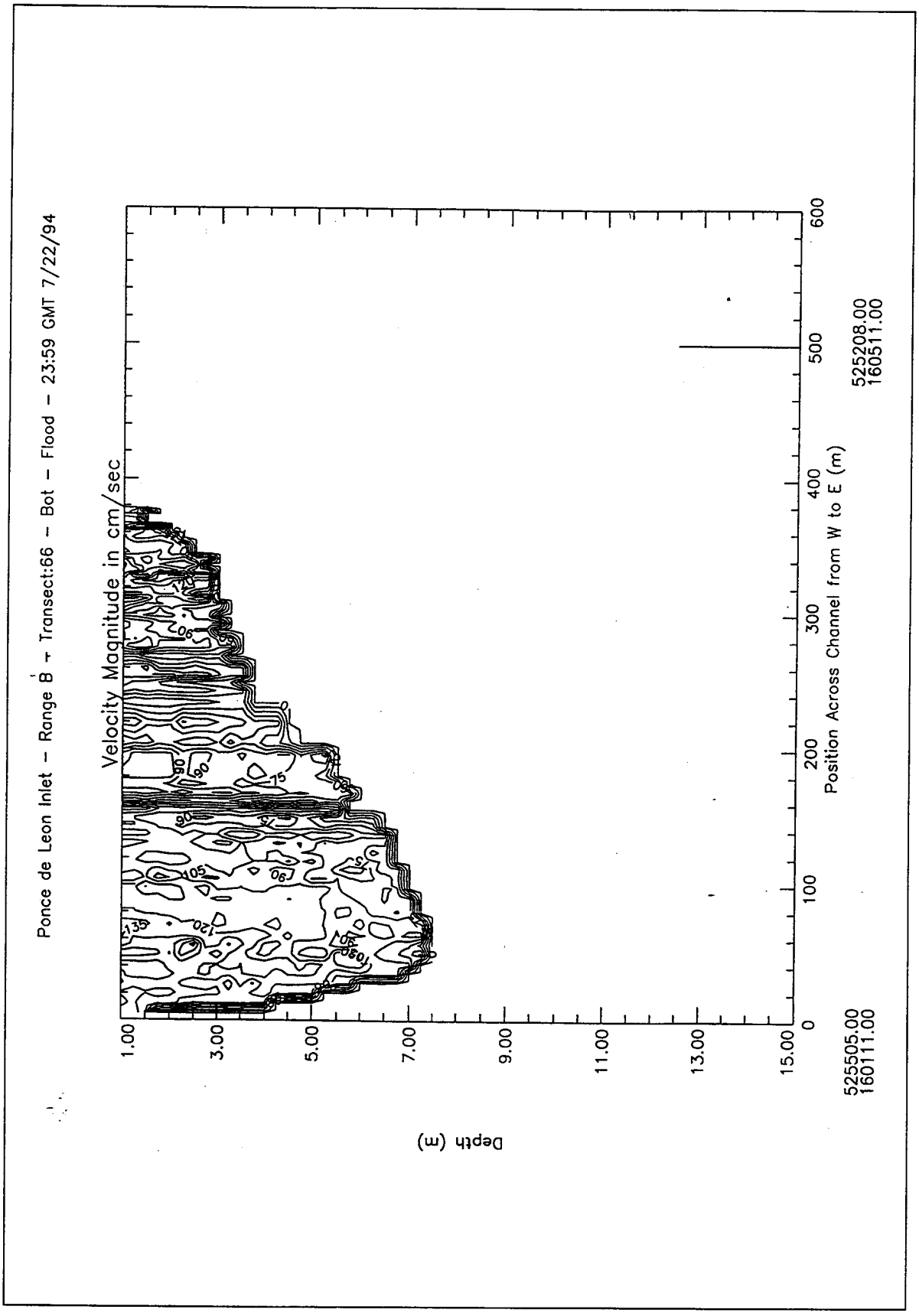

Figure B18. Contour plot of water magnitudes at peak ebb conditions, Range B

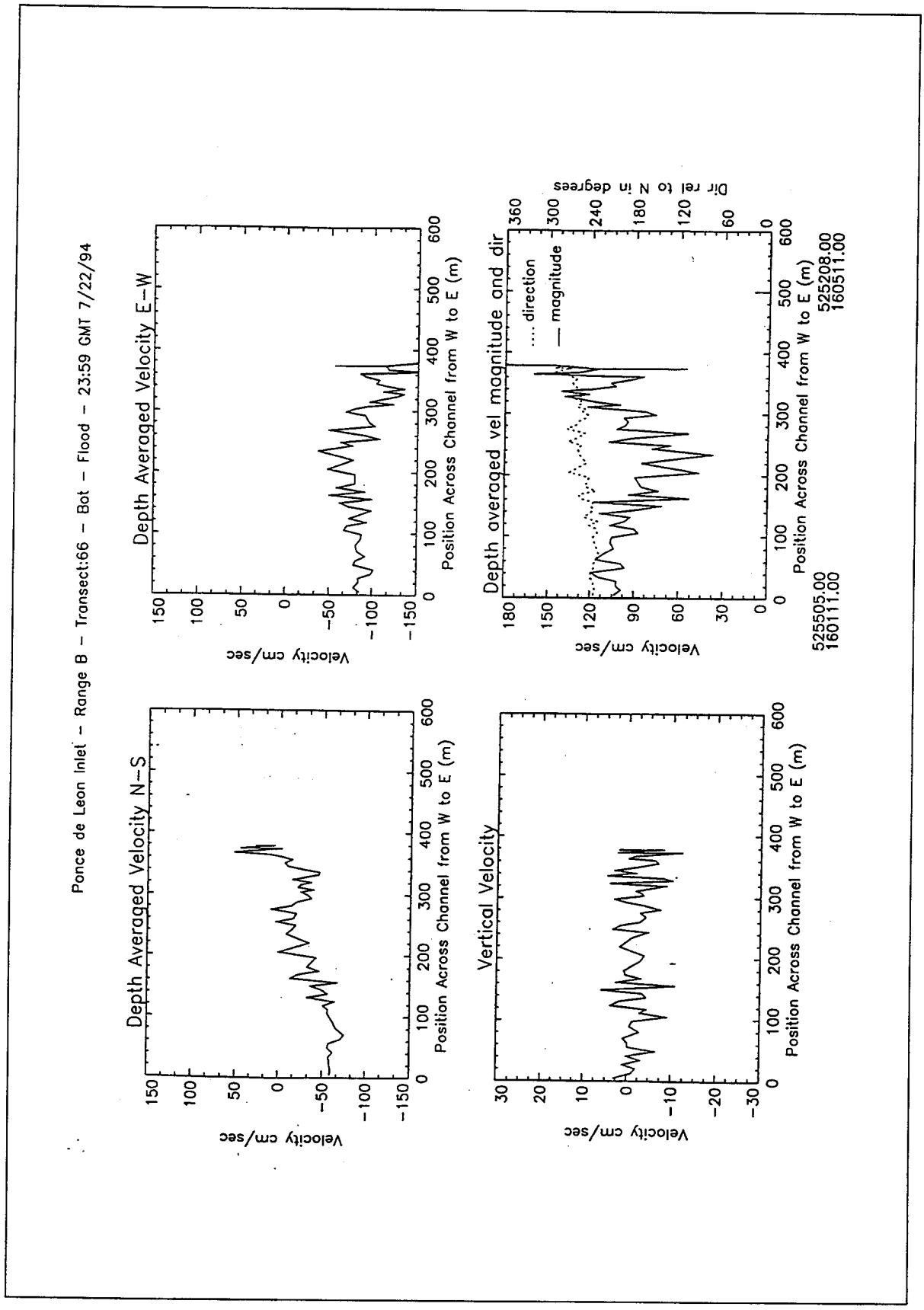

Figure B19. Depth average water velocities at peak ebb conditions, Range B

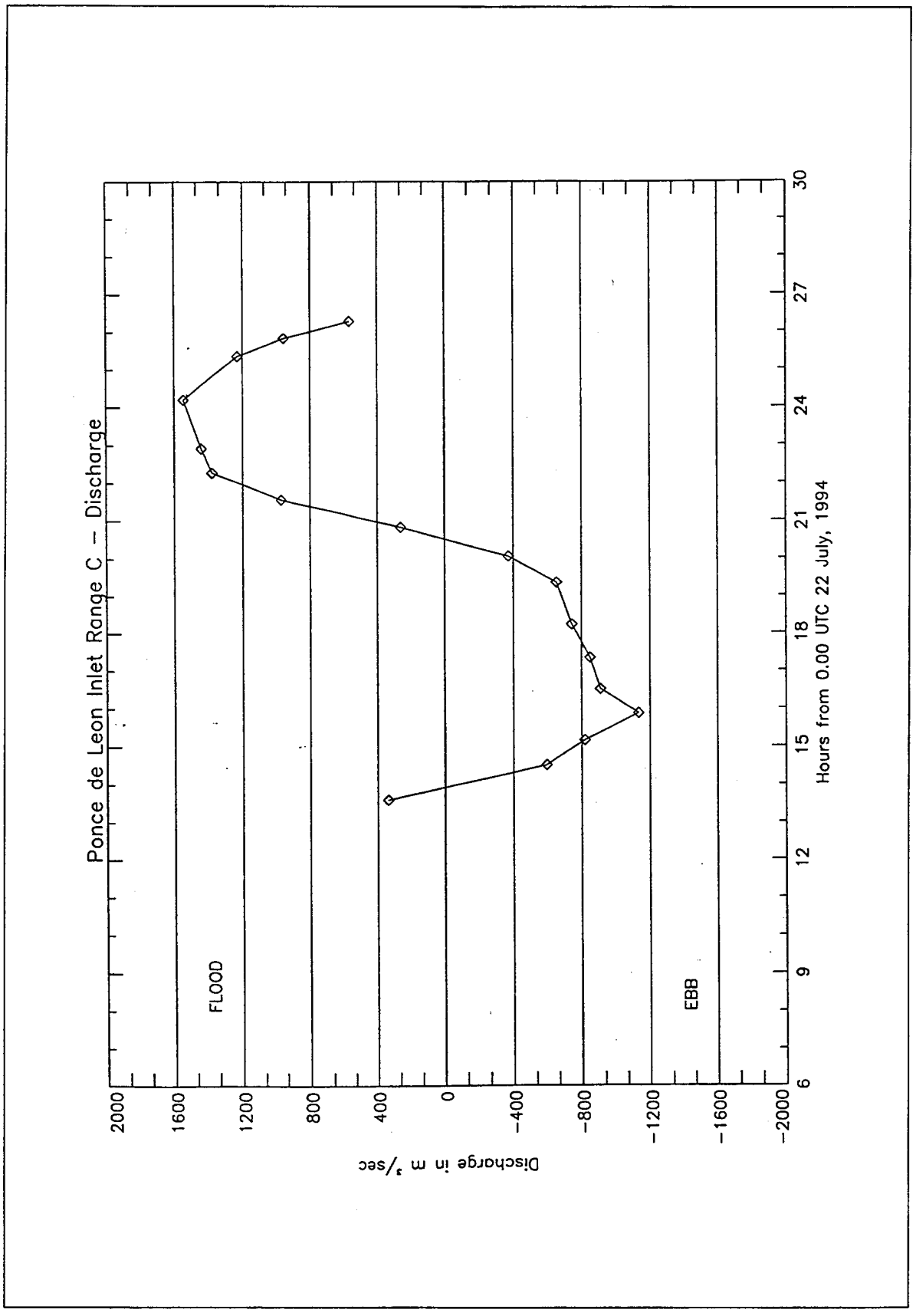

Figure B20. Discharge, Range C

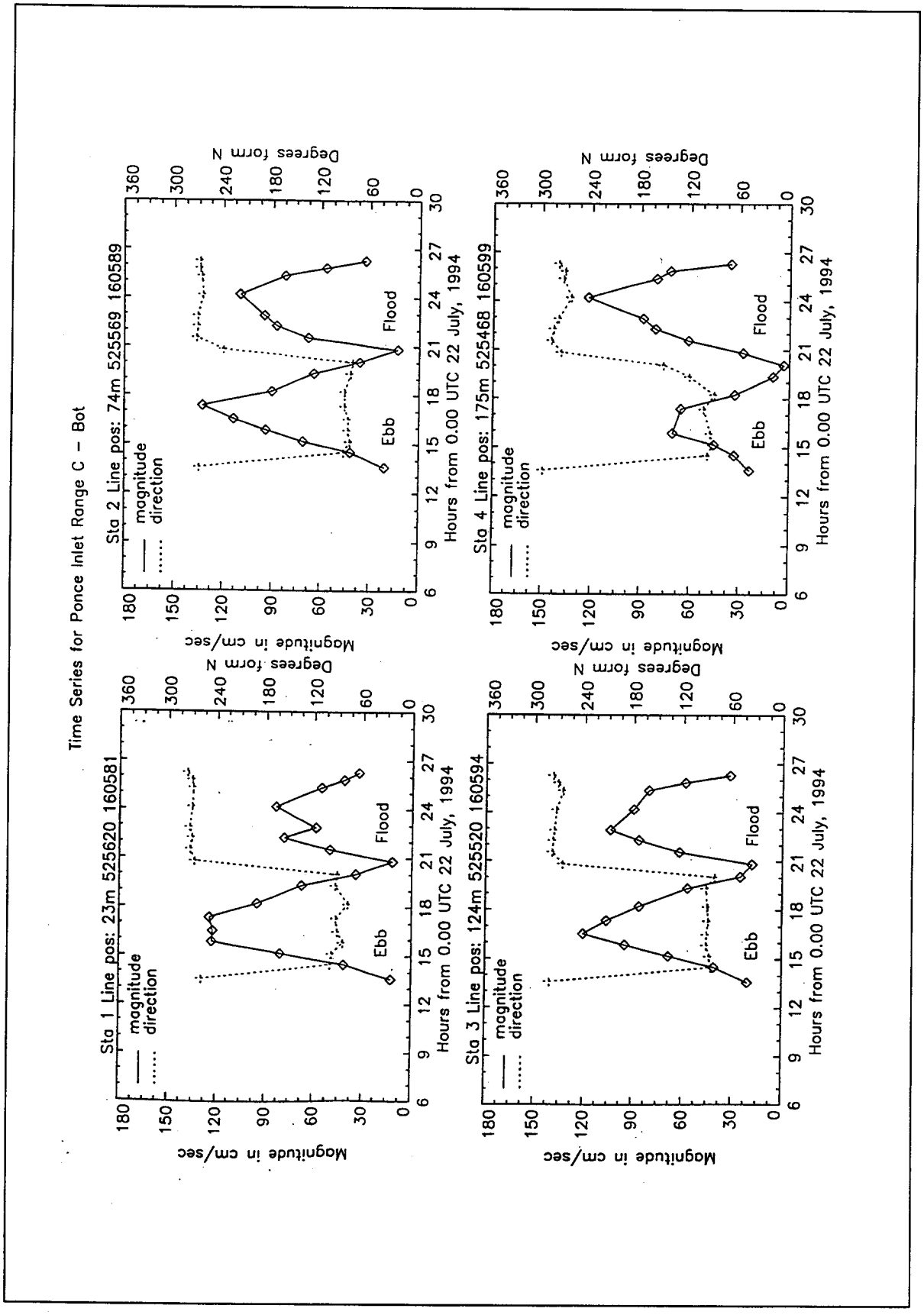

Figure B21. Time series, Range C, stations 1-4

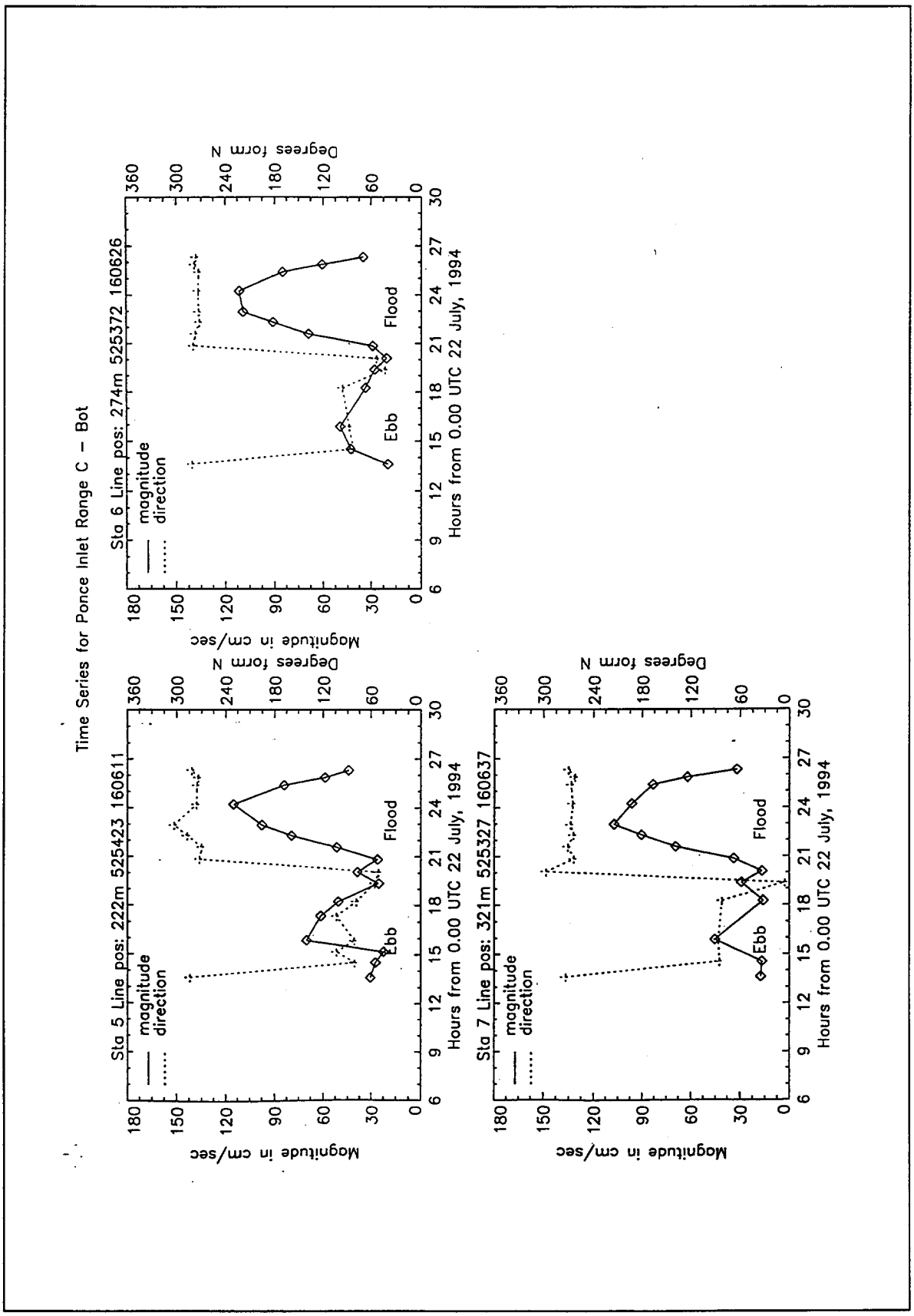

Figure B22. Time series, Range C, stations 5-7

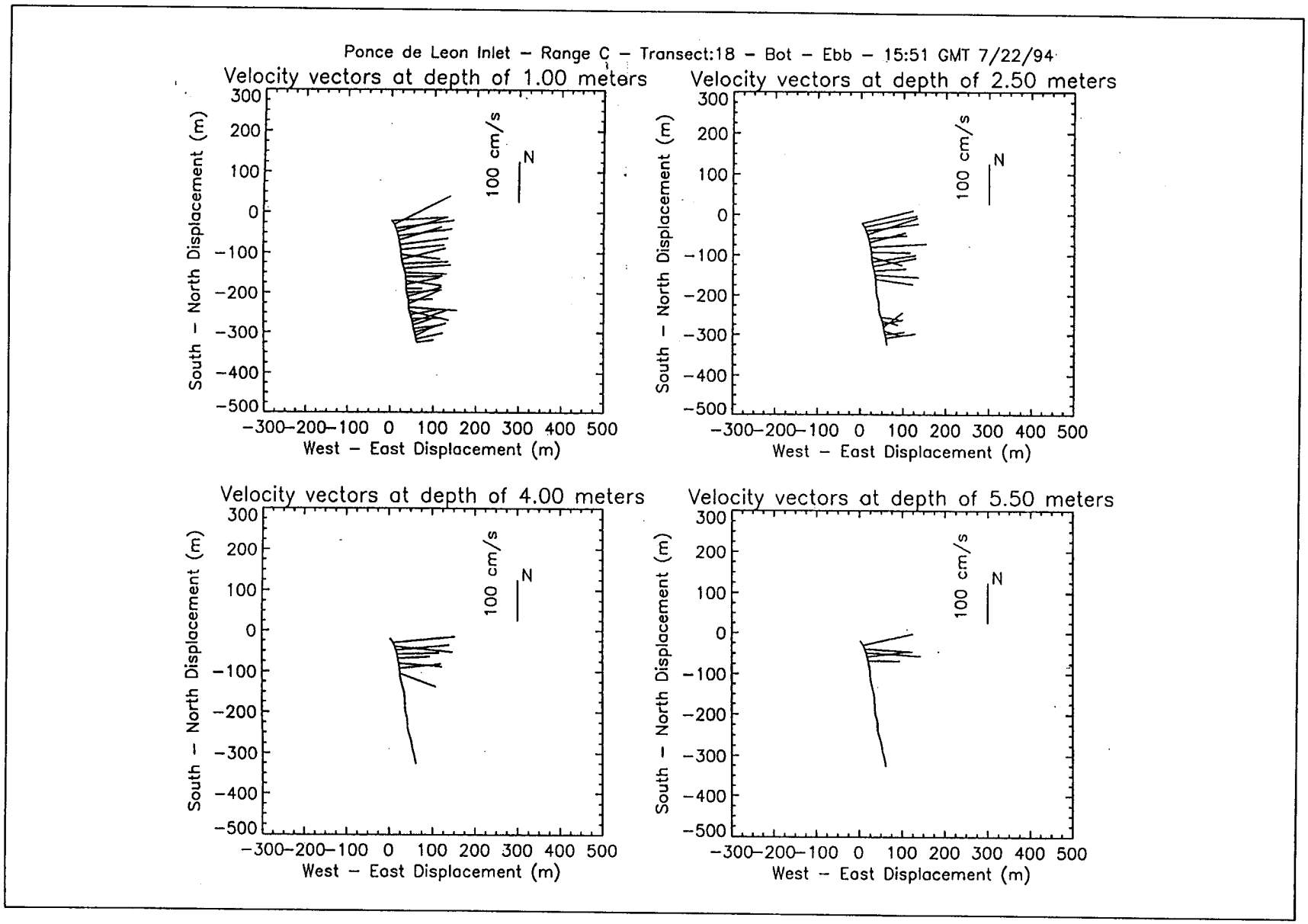

Figure B23. Velocity vector plots at peak ebb conditions, Range C

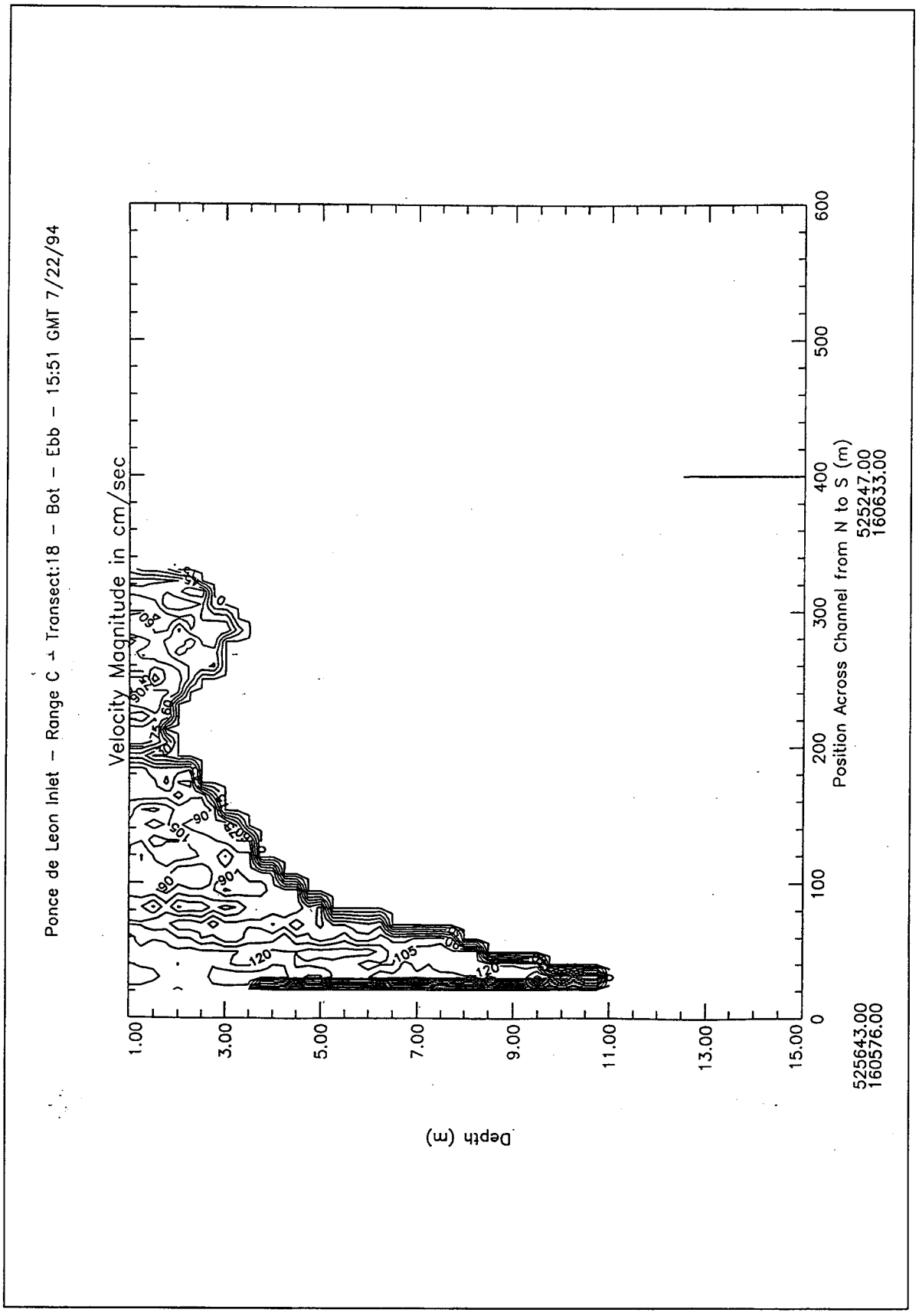

Figure B24. Contour plot of water magnitudes at peak ebb conditions, Range C

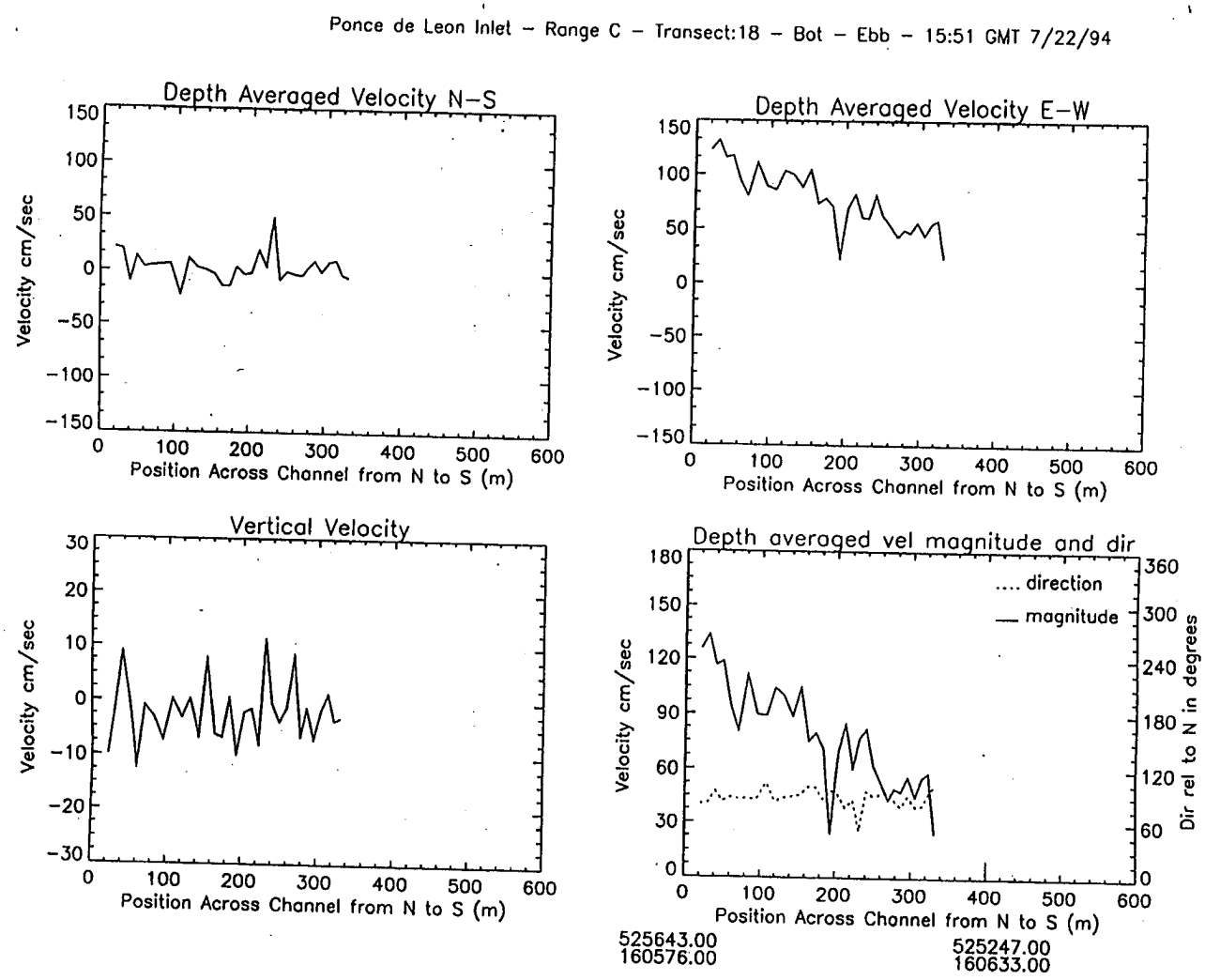

Figure B25. Depth average water velocities at peak ebb conditions, Range C

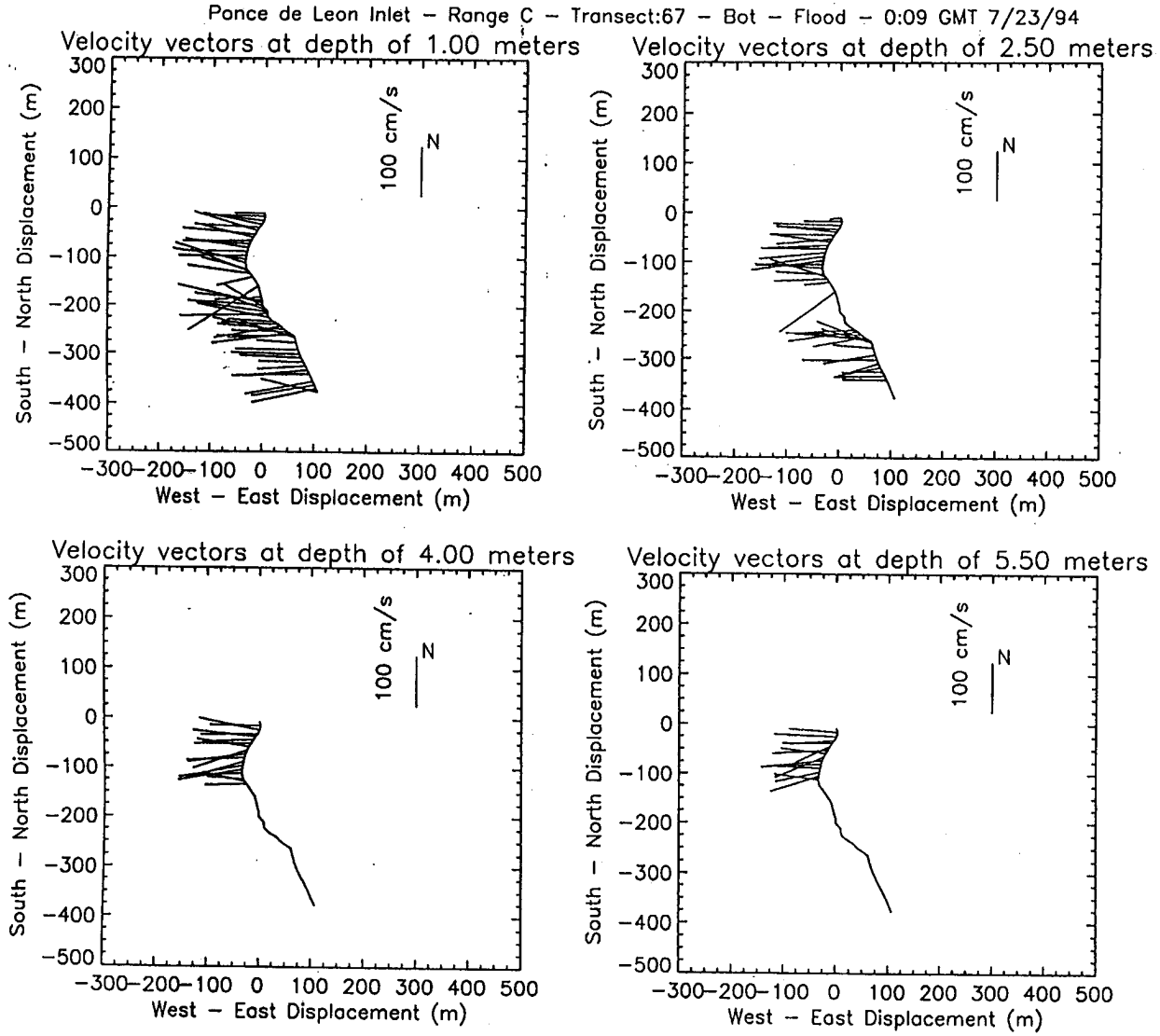

Figure B26. Velocity vector plots at peak flood conditions, Range C

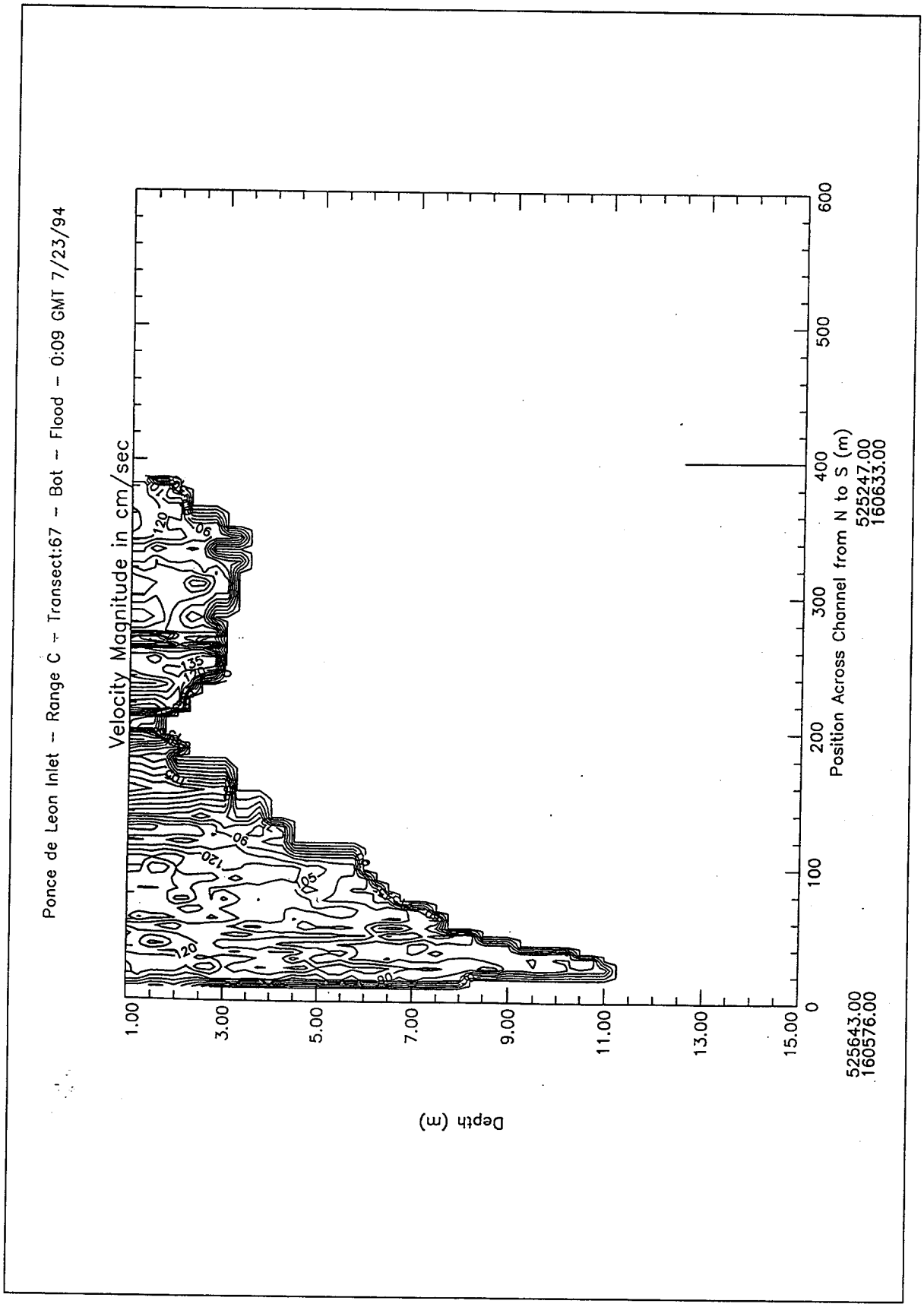

Figure B27. Contour plot of water magnitudes at peak flood conditions, Range C

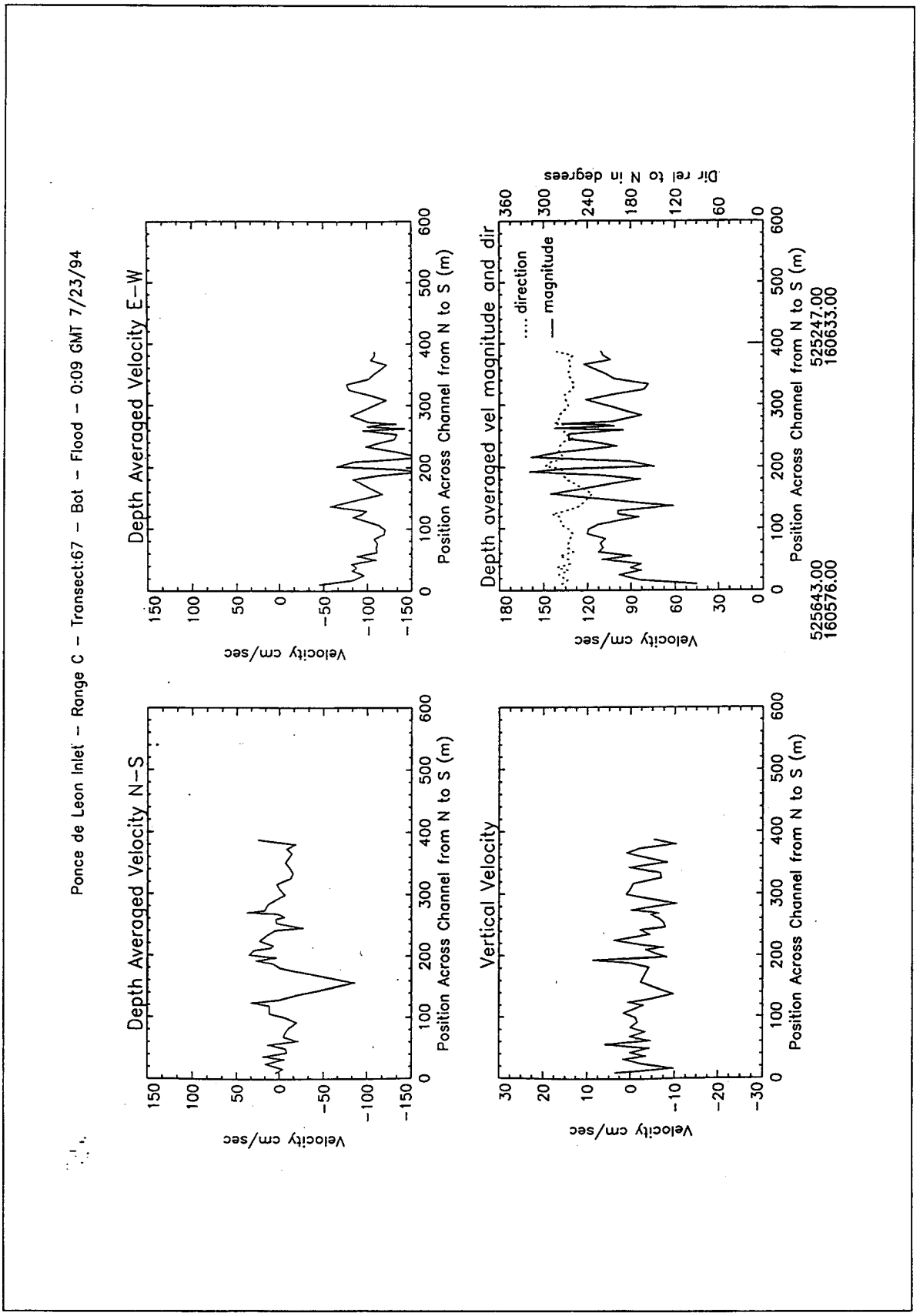

Figure B28. Depth average water velocities at peak flood conditions, Range C

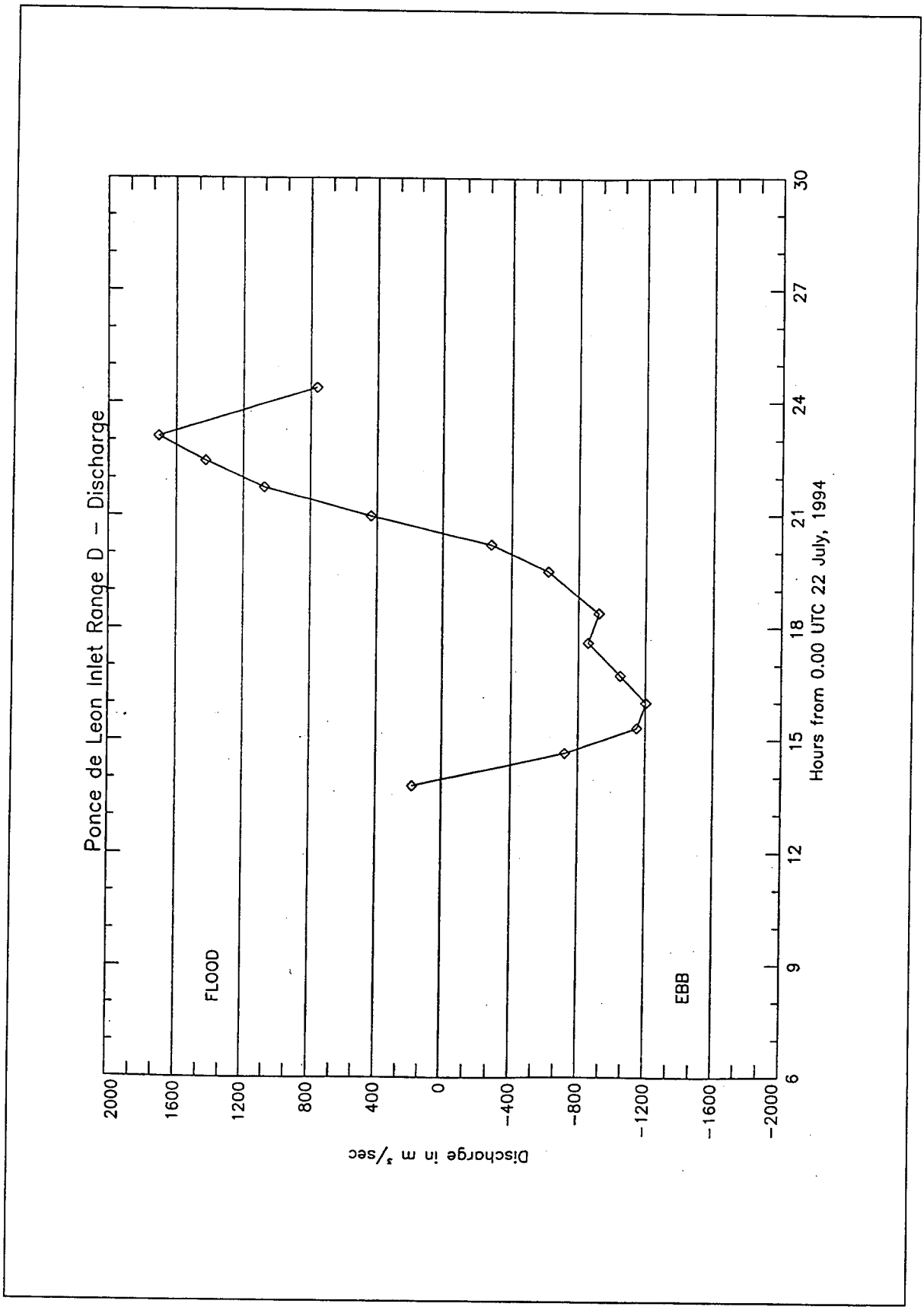

Figure B29. Discharge, Range D

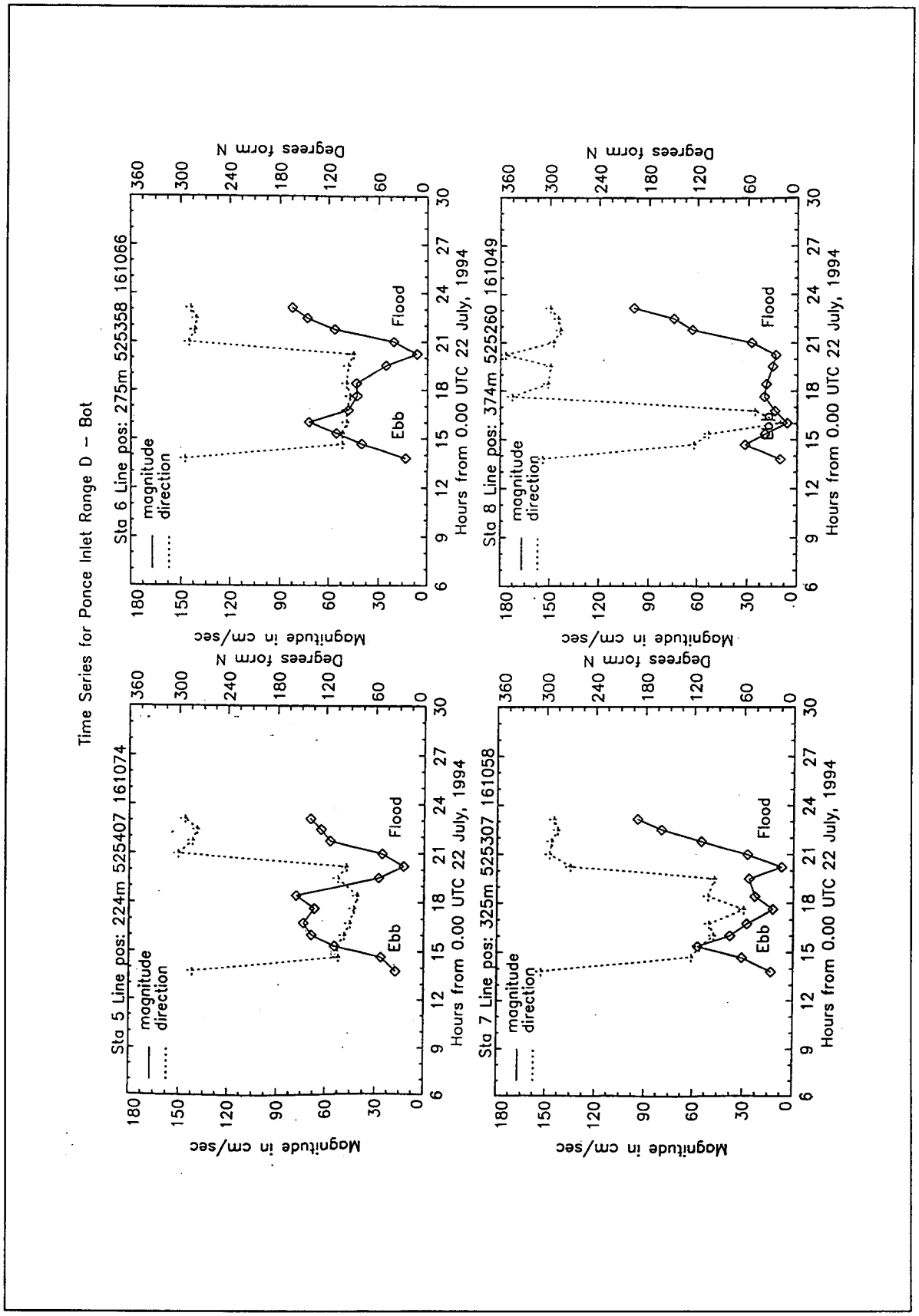

Figure B30. Time series, Range D, stations 5-8

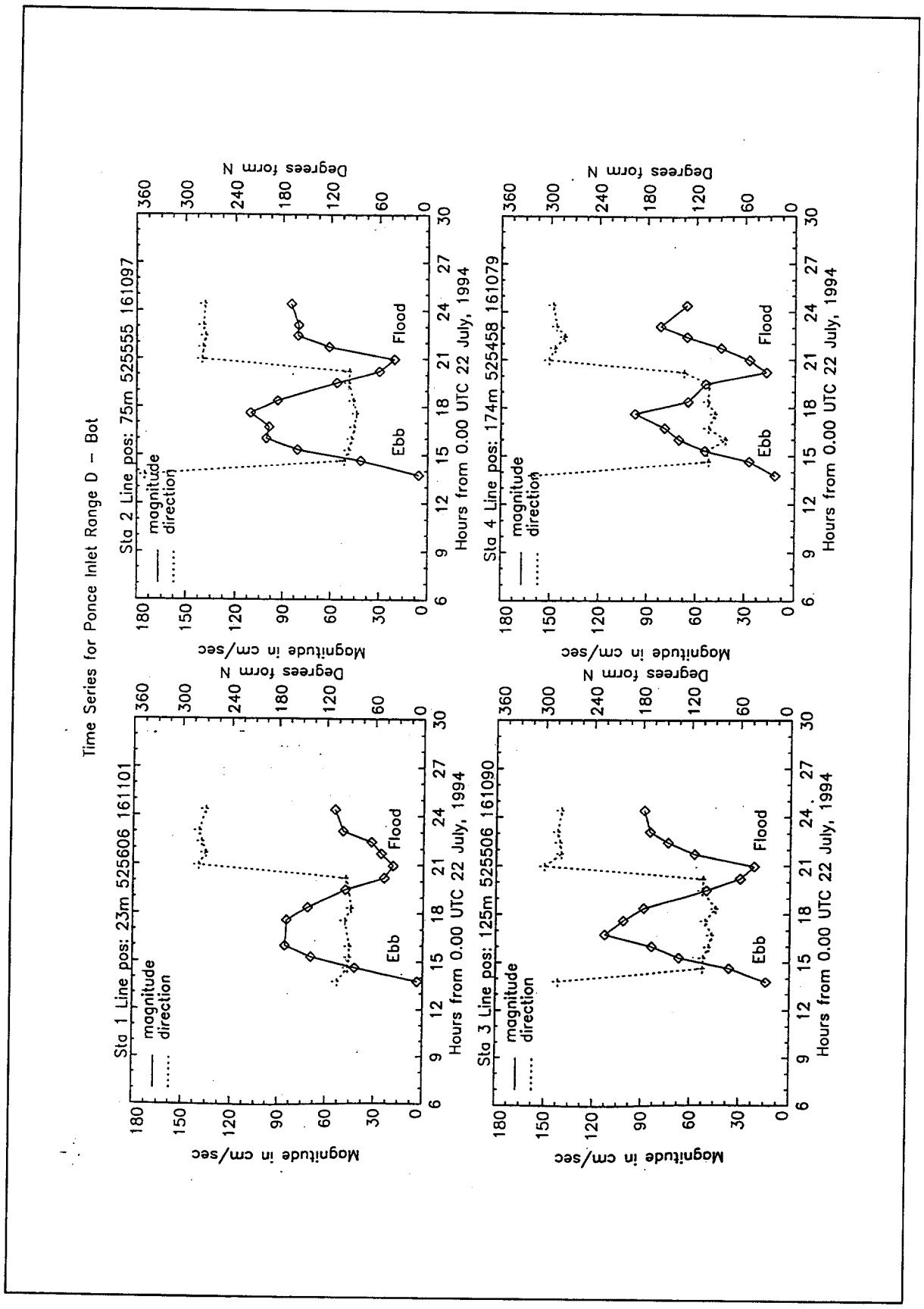

Figure B31. Time series, Range D, stations 1-4

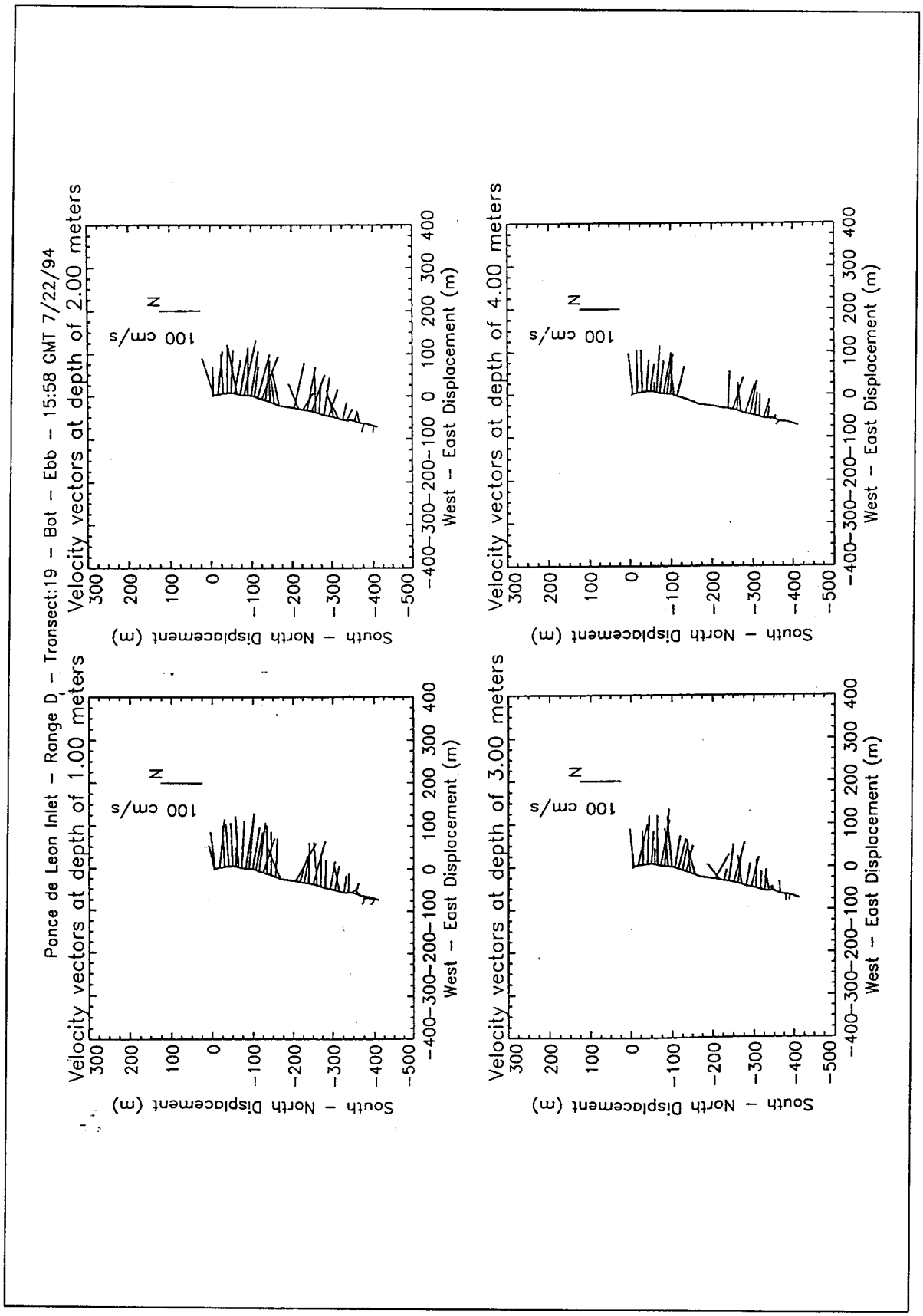

Figure B32. Velocity vector plots at peak ebb conditions, Range D

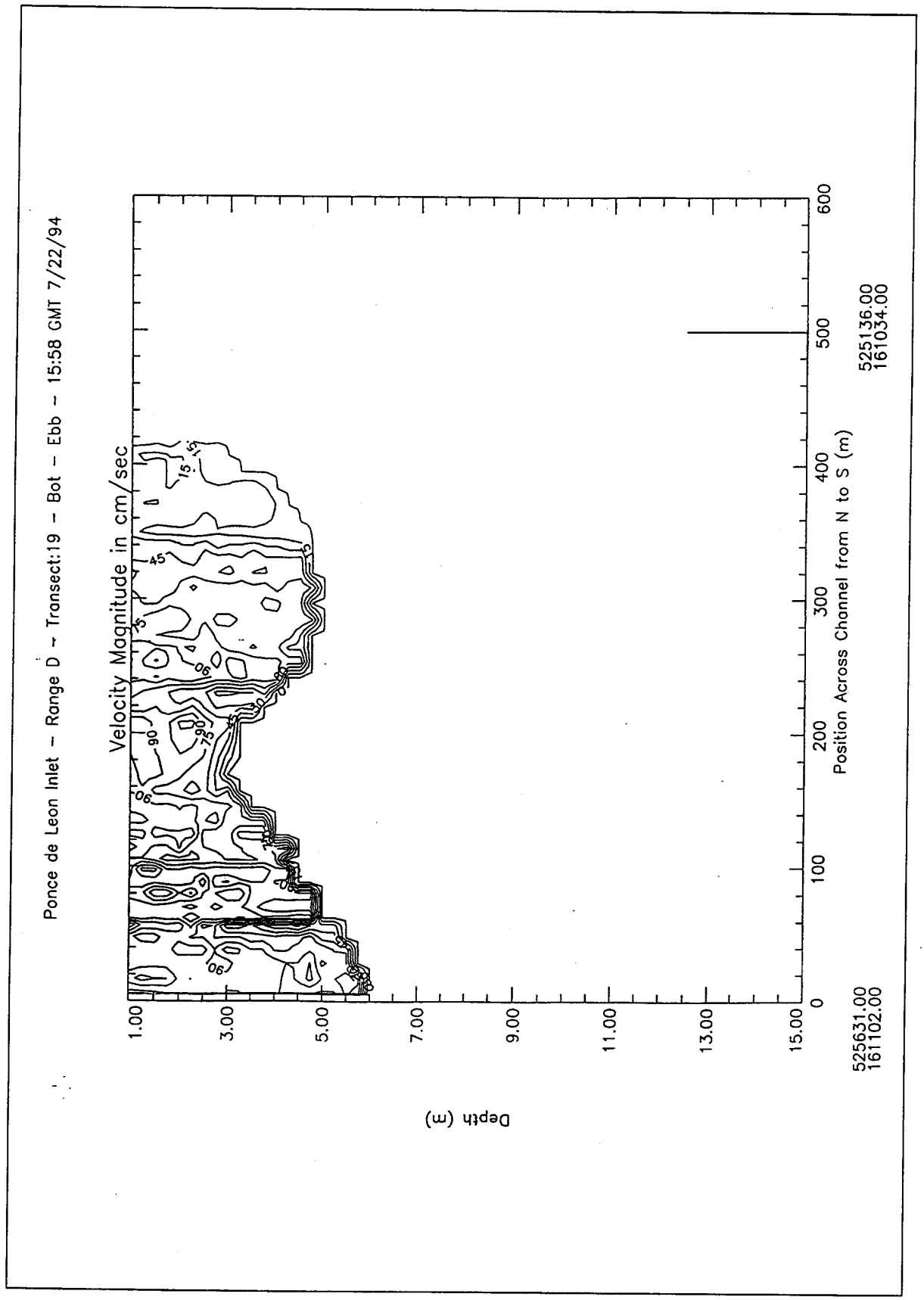

Figure B33. Contour plot of water magnitudes at peak ebb conditions, Range D

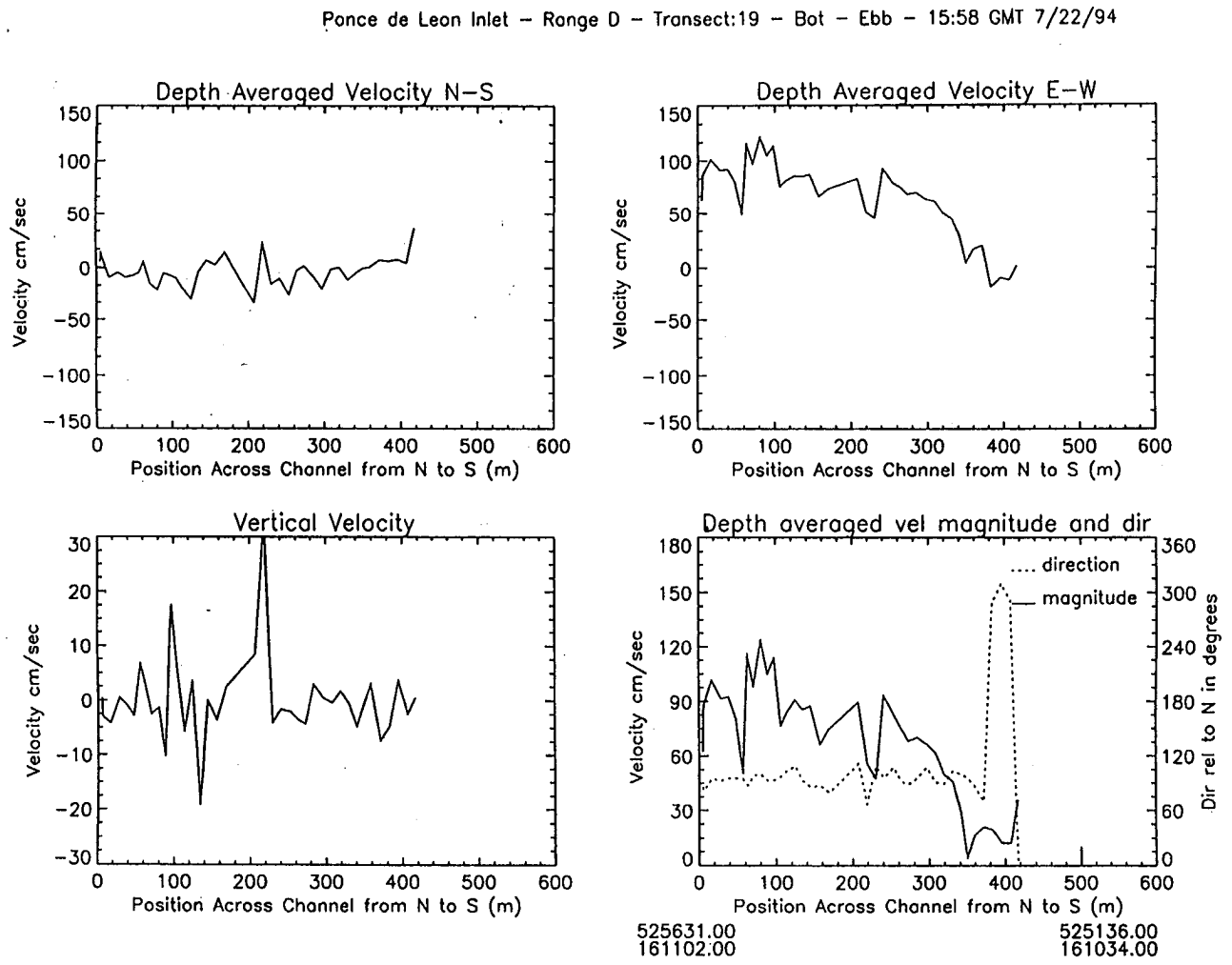

Figure B34. Depth average water velocities at peak ebb conditions, Range D

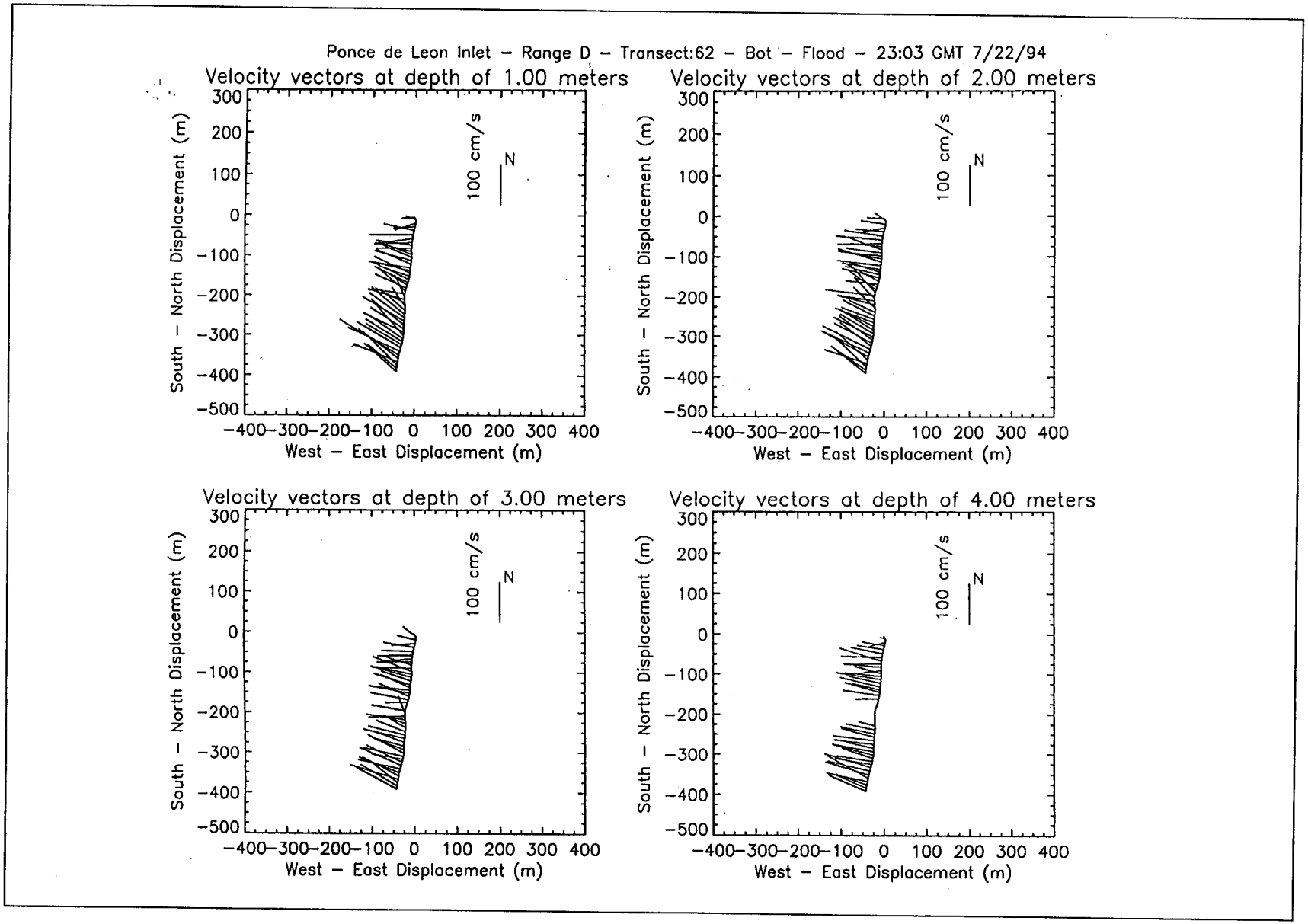

Figure B35. Velocity vector plots at peak flood conditions, Range D

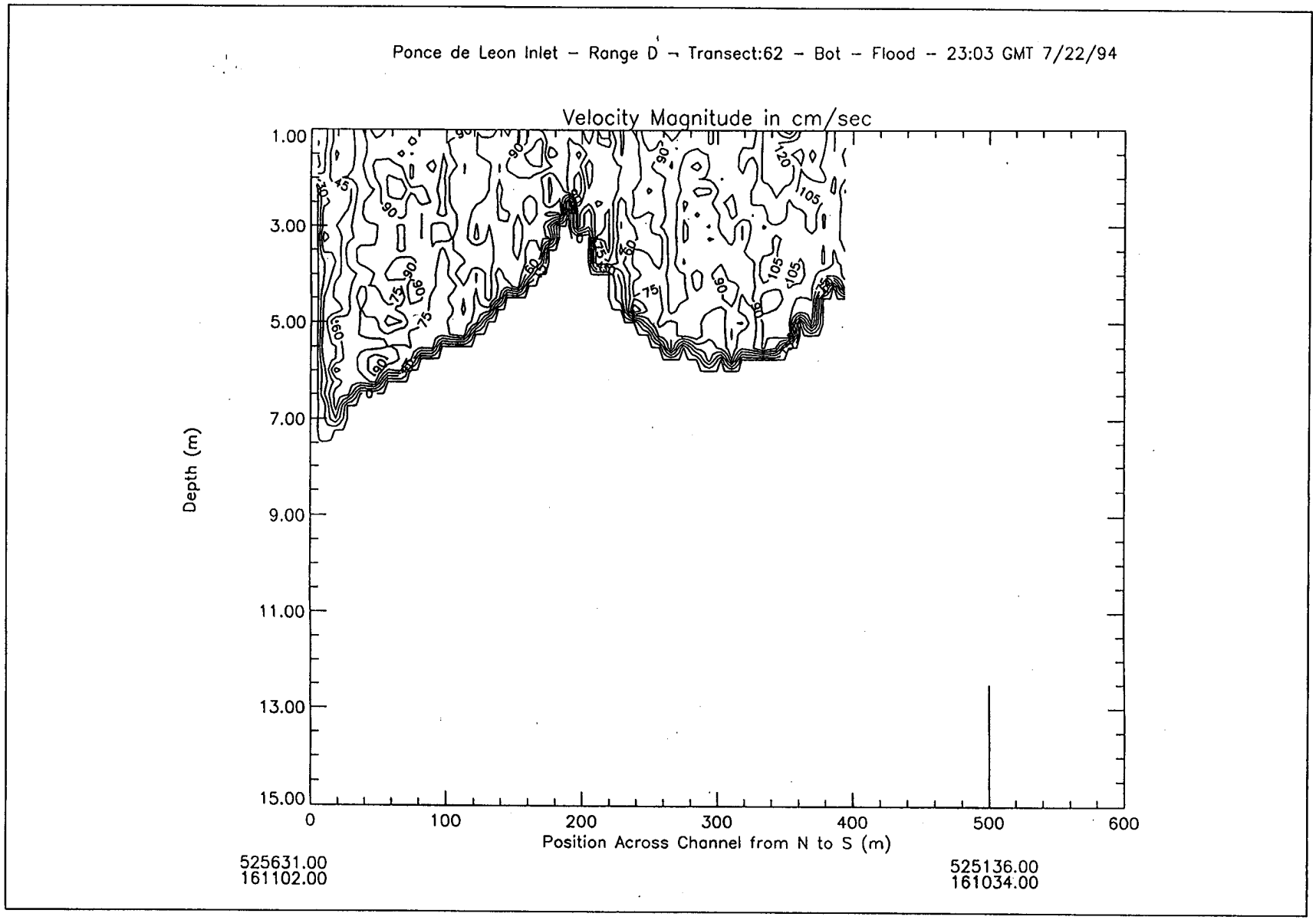

Figure B36. Contour plot of water magnitudes at peak flood conditions, Range D

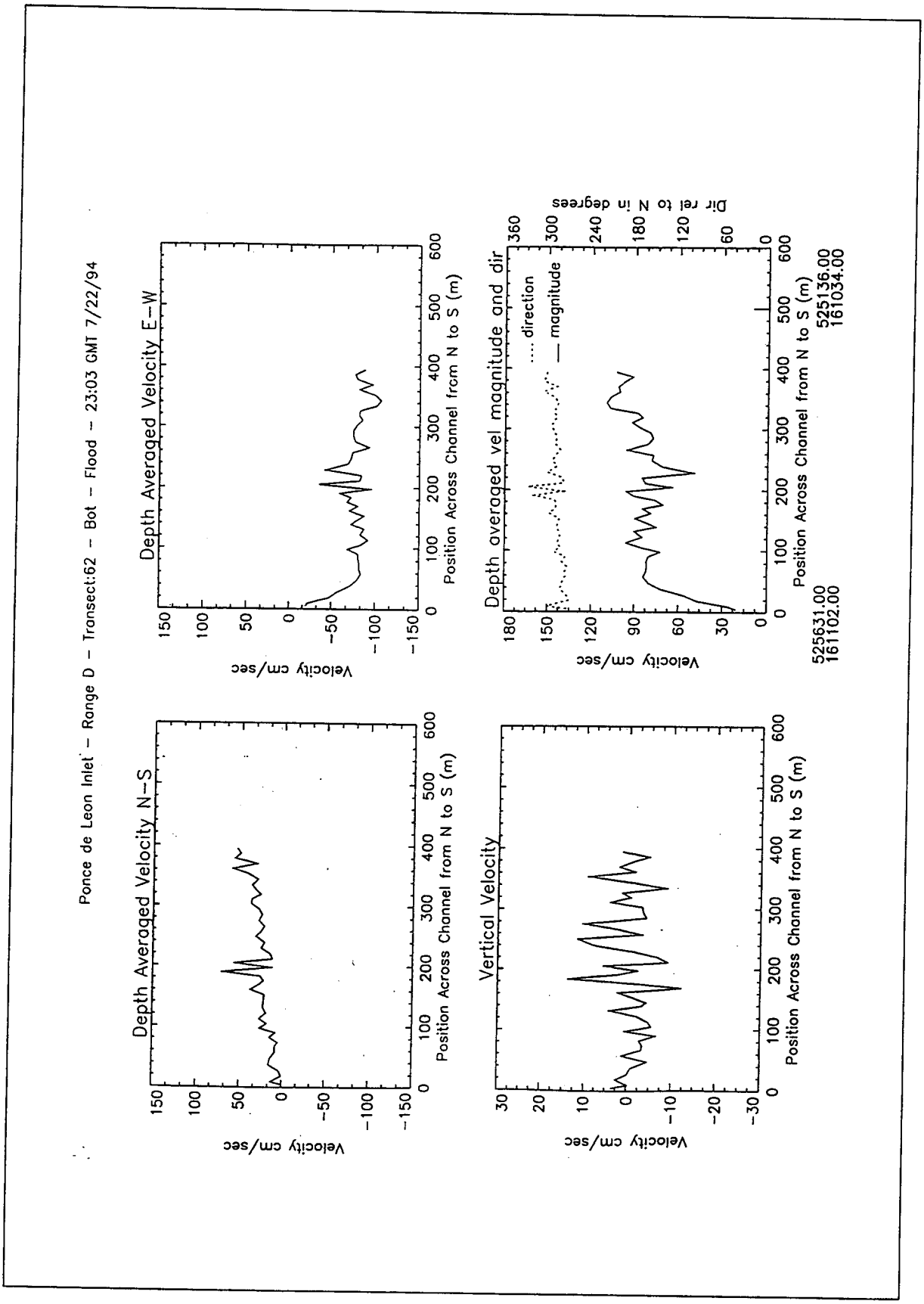

Figure B37. Depth average water velocities at peak flood conditions, Range D

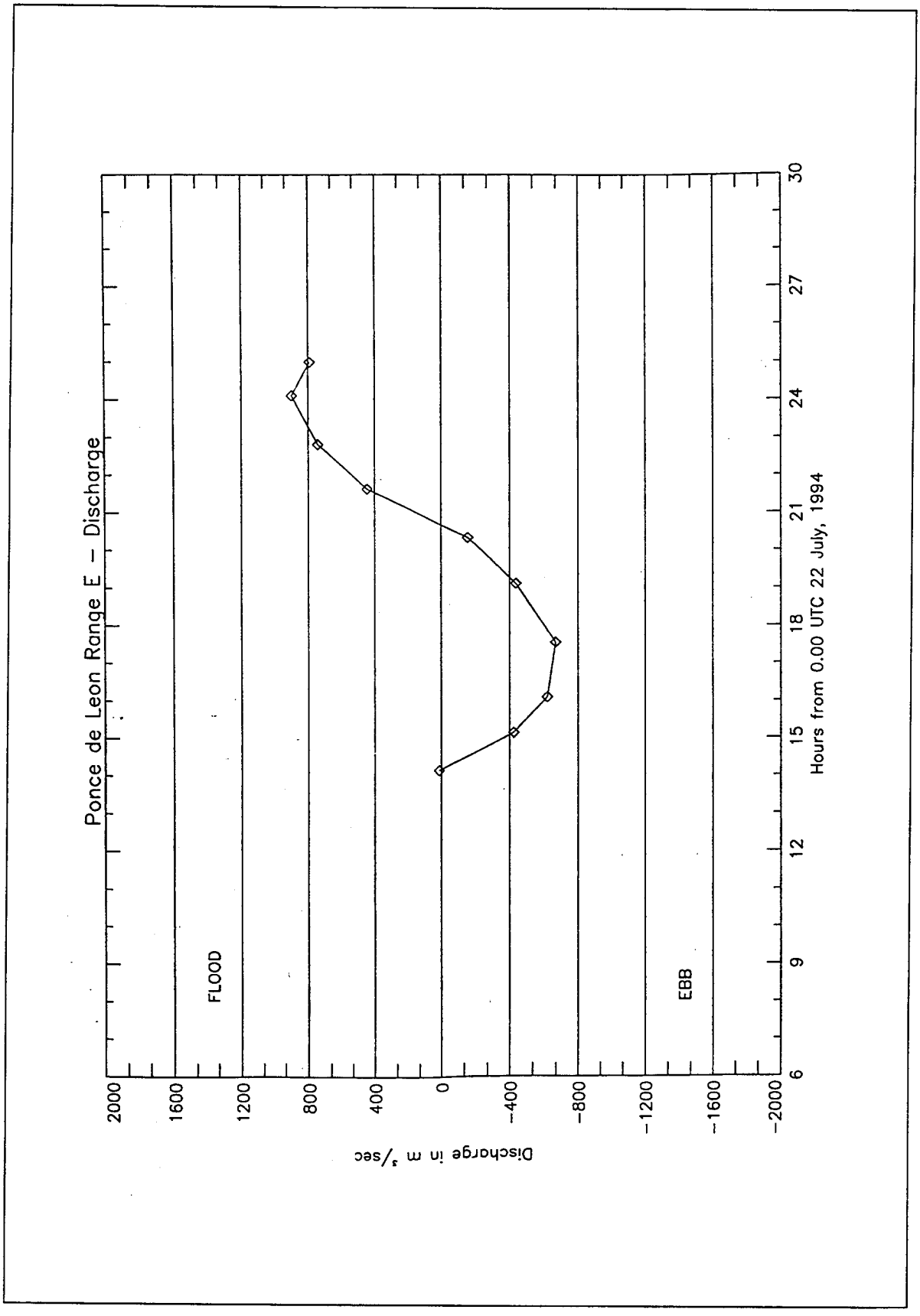

Figure B38. Discharge, Range E

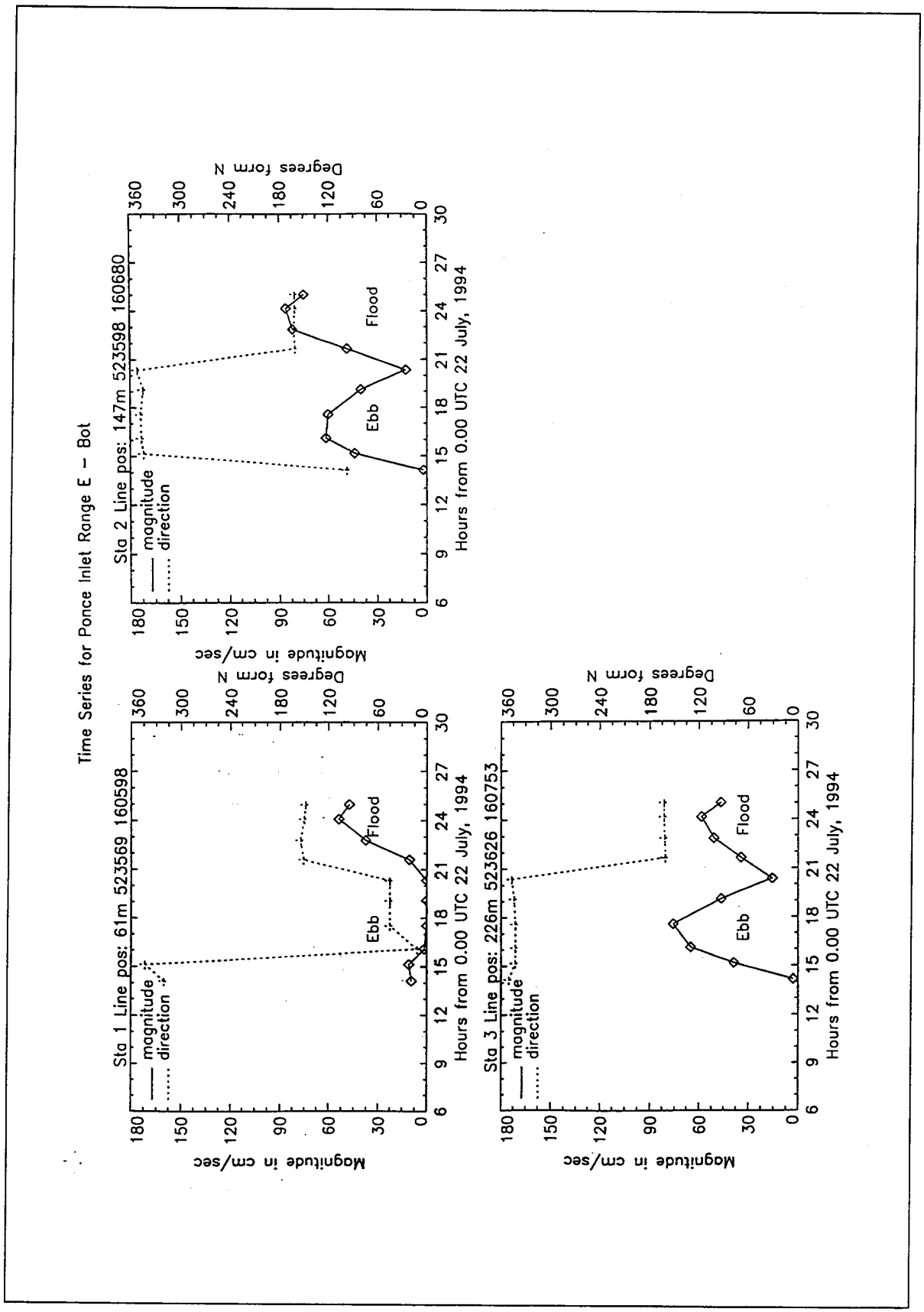

Figure B39. Time series, Range E

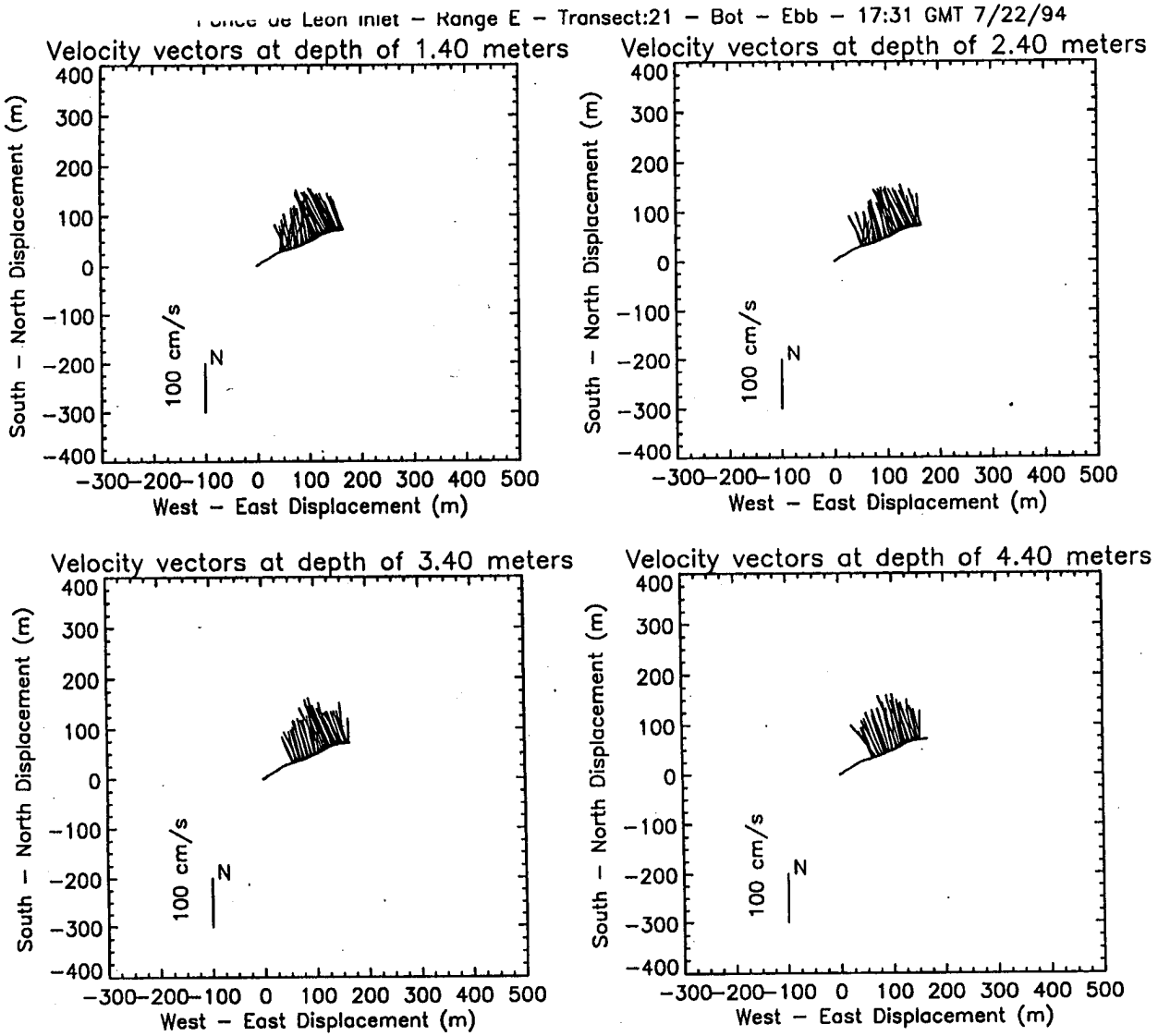

Figure B40. Velocity vector plots at peak ebb conditions, Range E

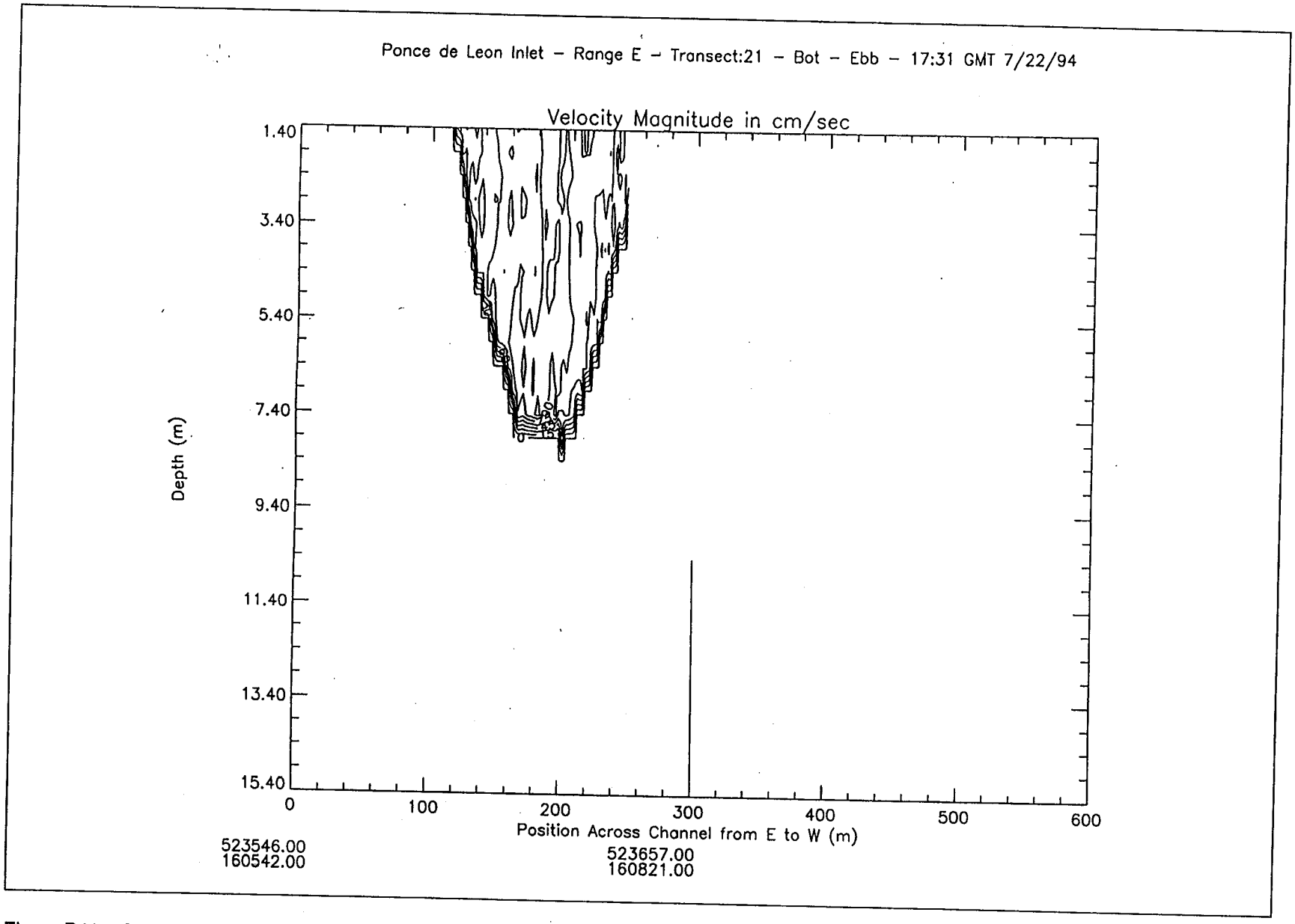

Figure B41. Contour plot of water magnitudes at peak ebb conditions, Range E

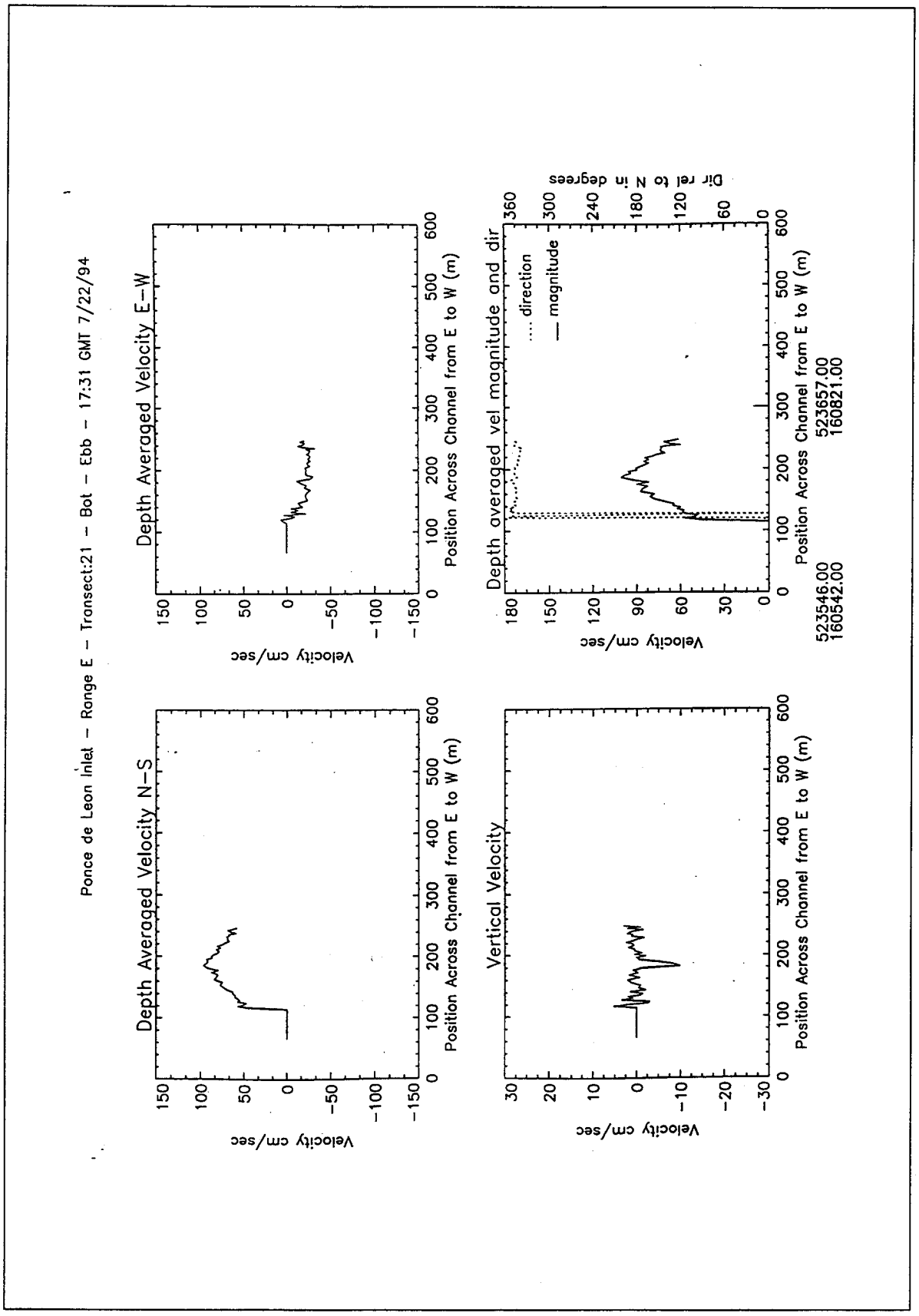

Figure B42. Depth average water velocities at peak ebb conditions, Range E

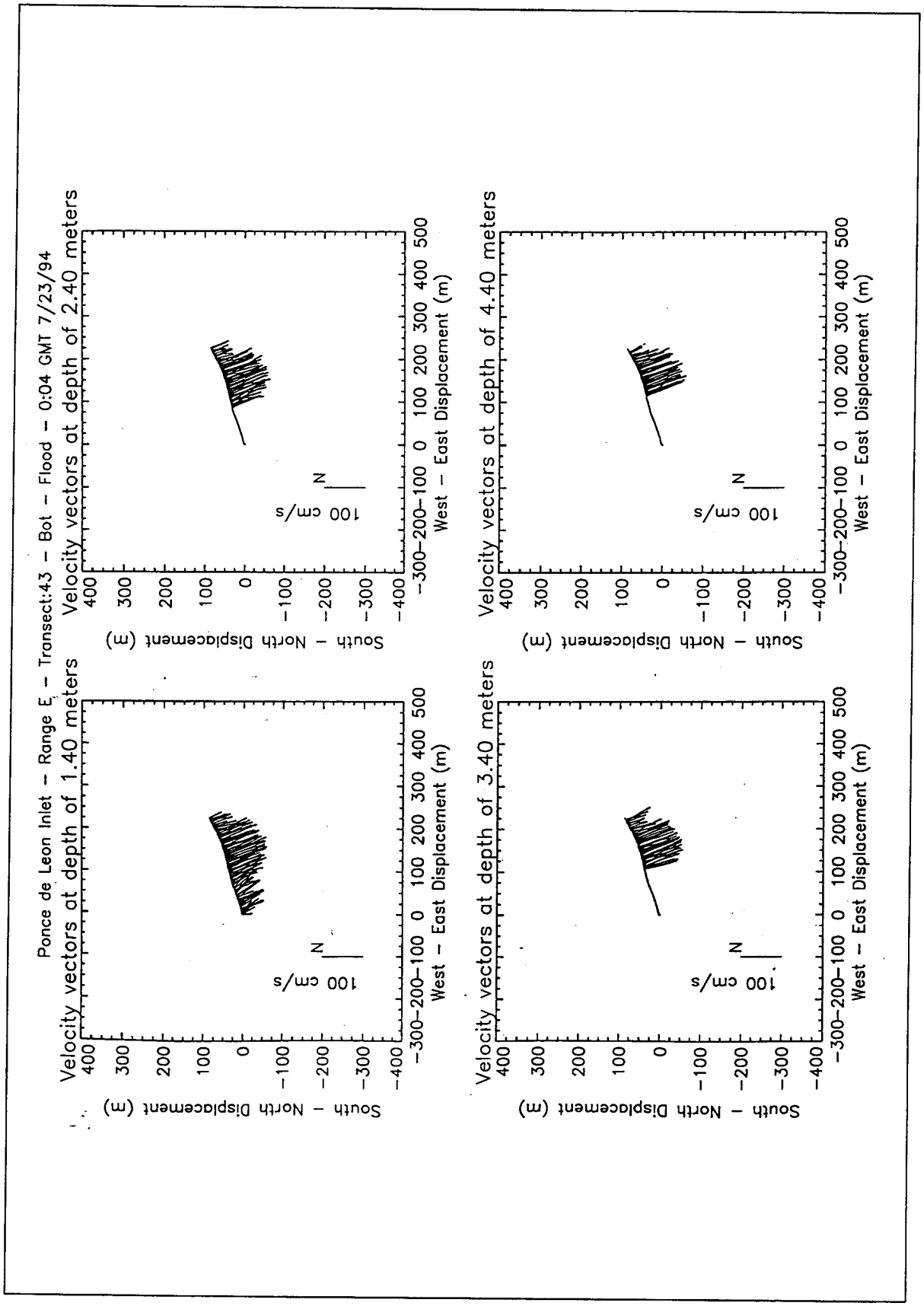

Figure B43. Velocity vector plots at peak flood conditions, Range E

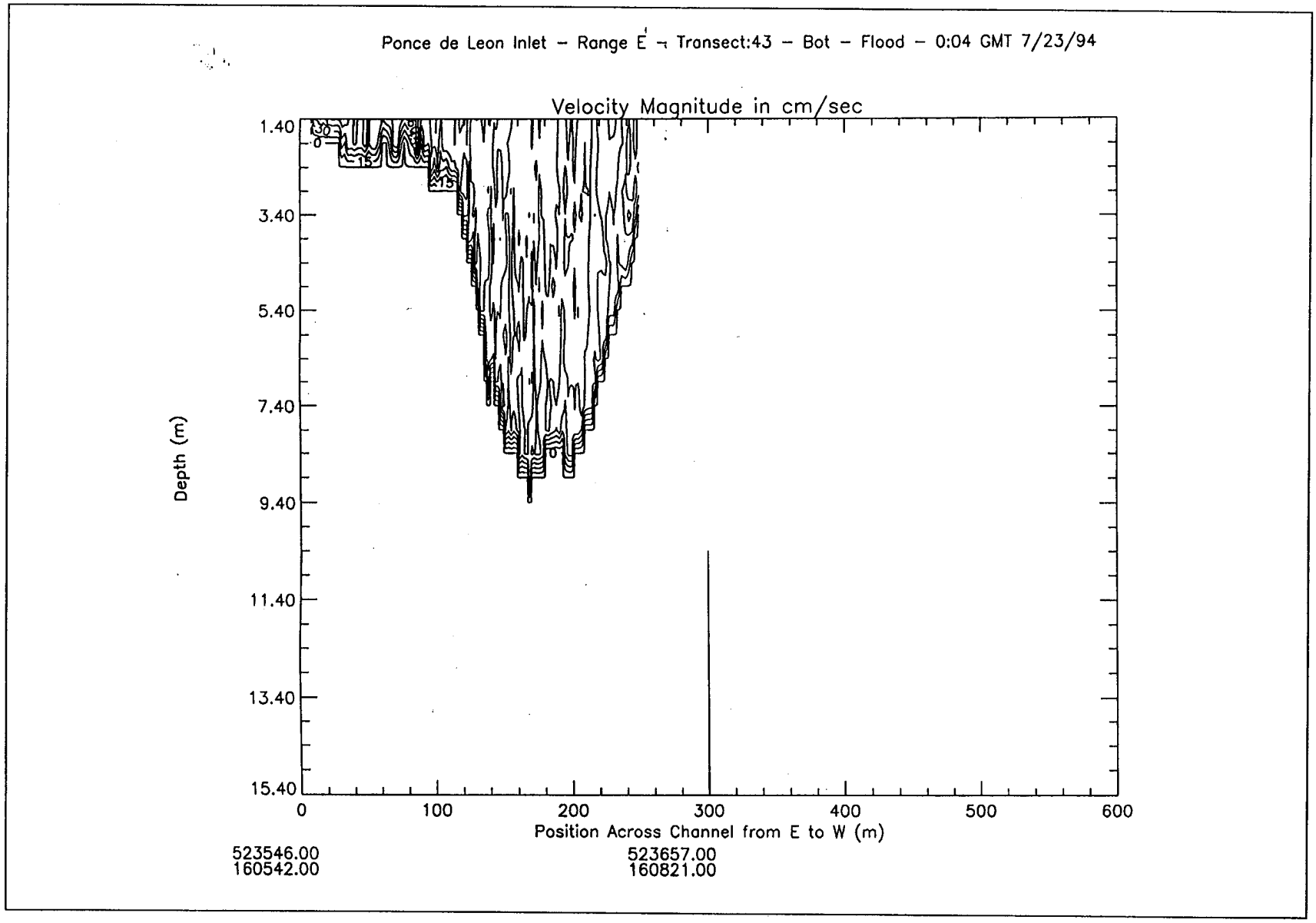

Figure B44. Contour plot of water magnitudes at peak flood conditions, Range E

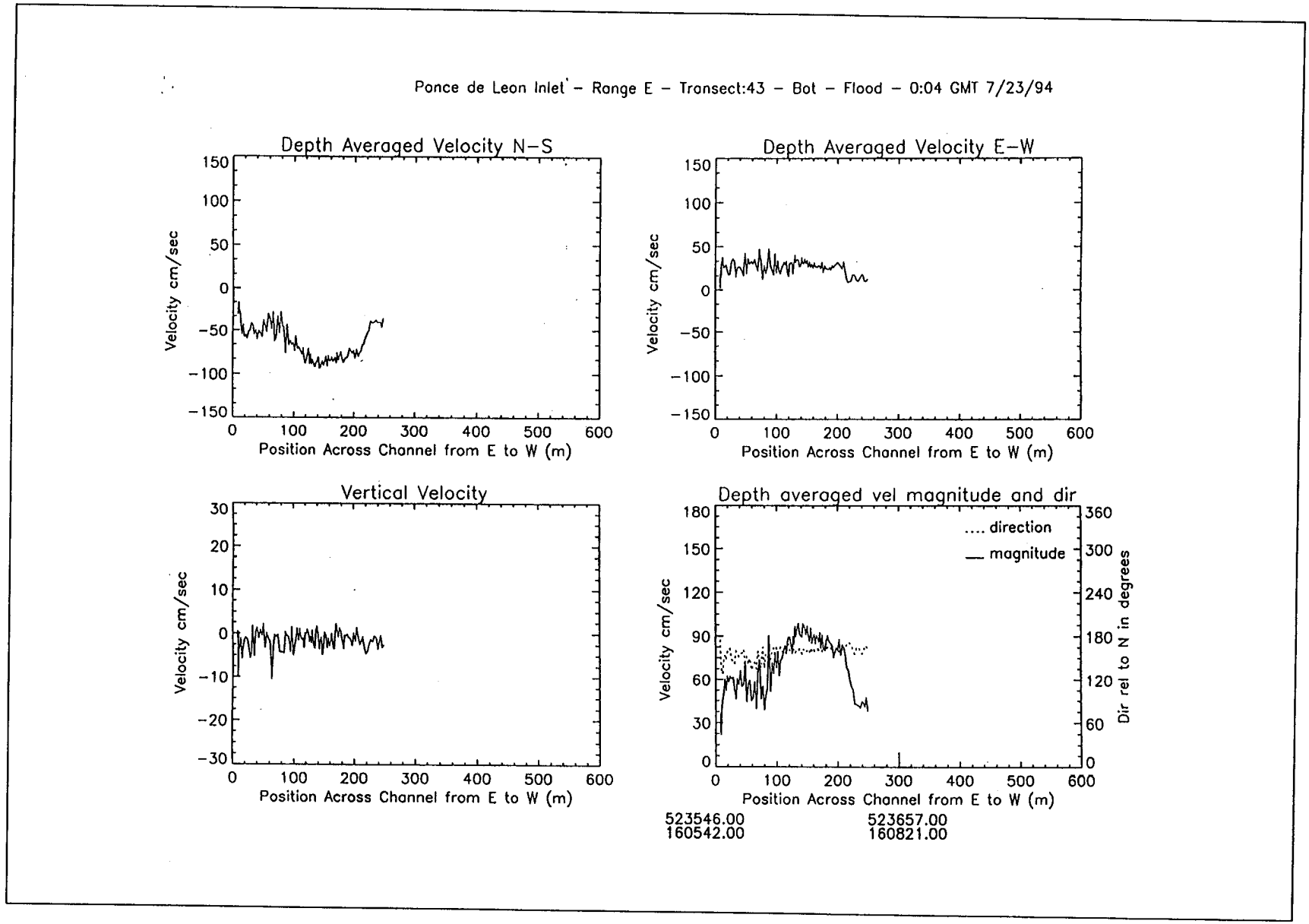

Figure B45. Depth average water velocities at peak flood conditions, Range E

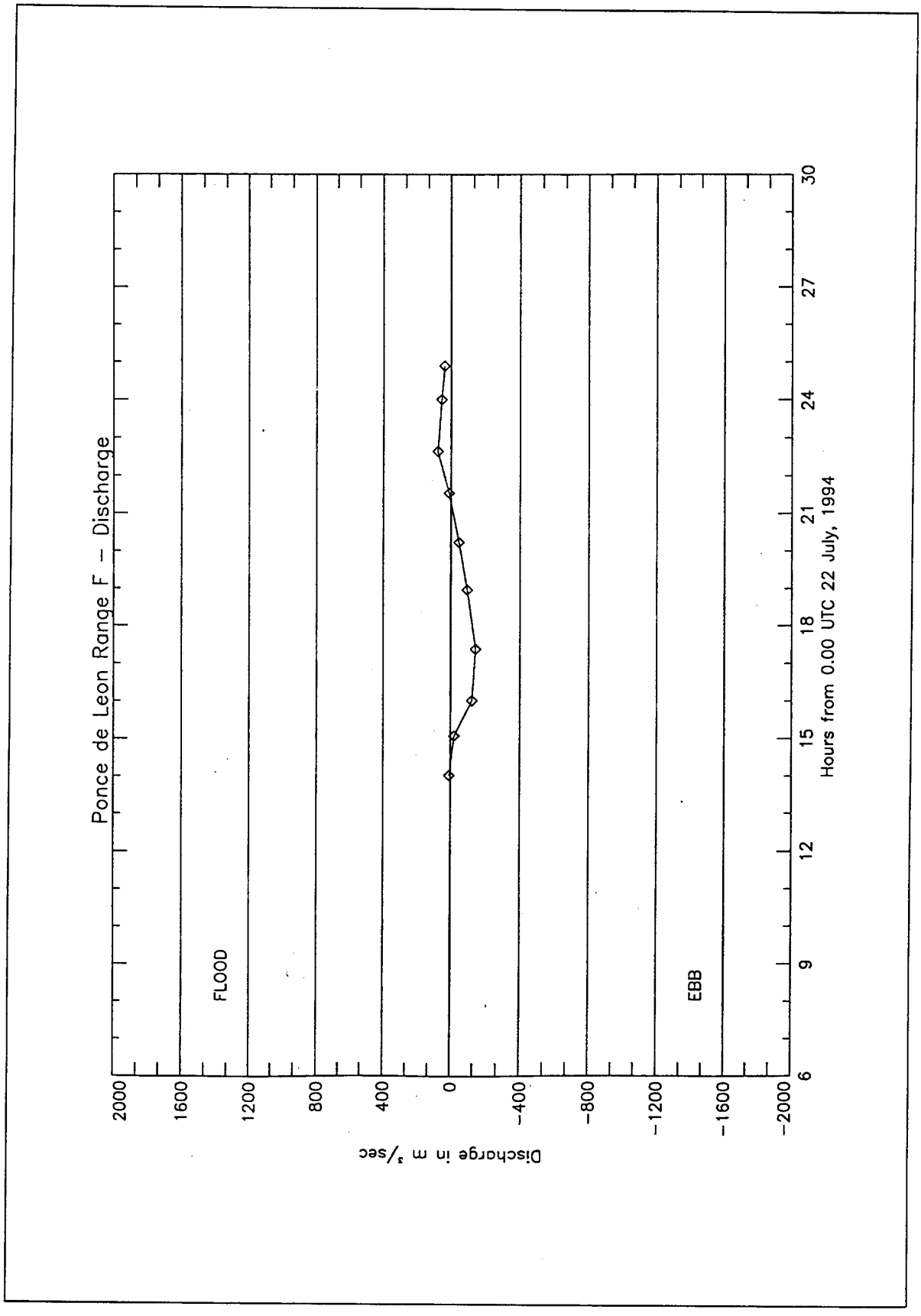

Figure B46. Discharge, Range F

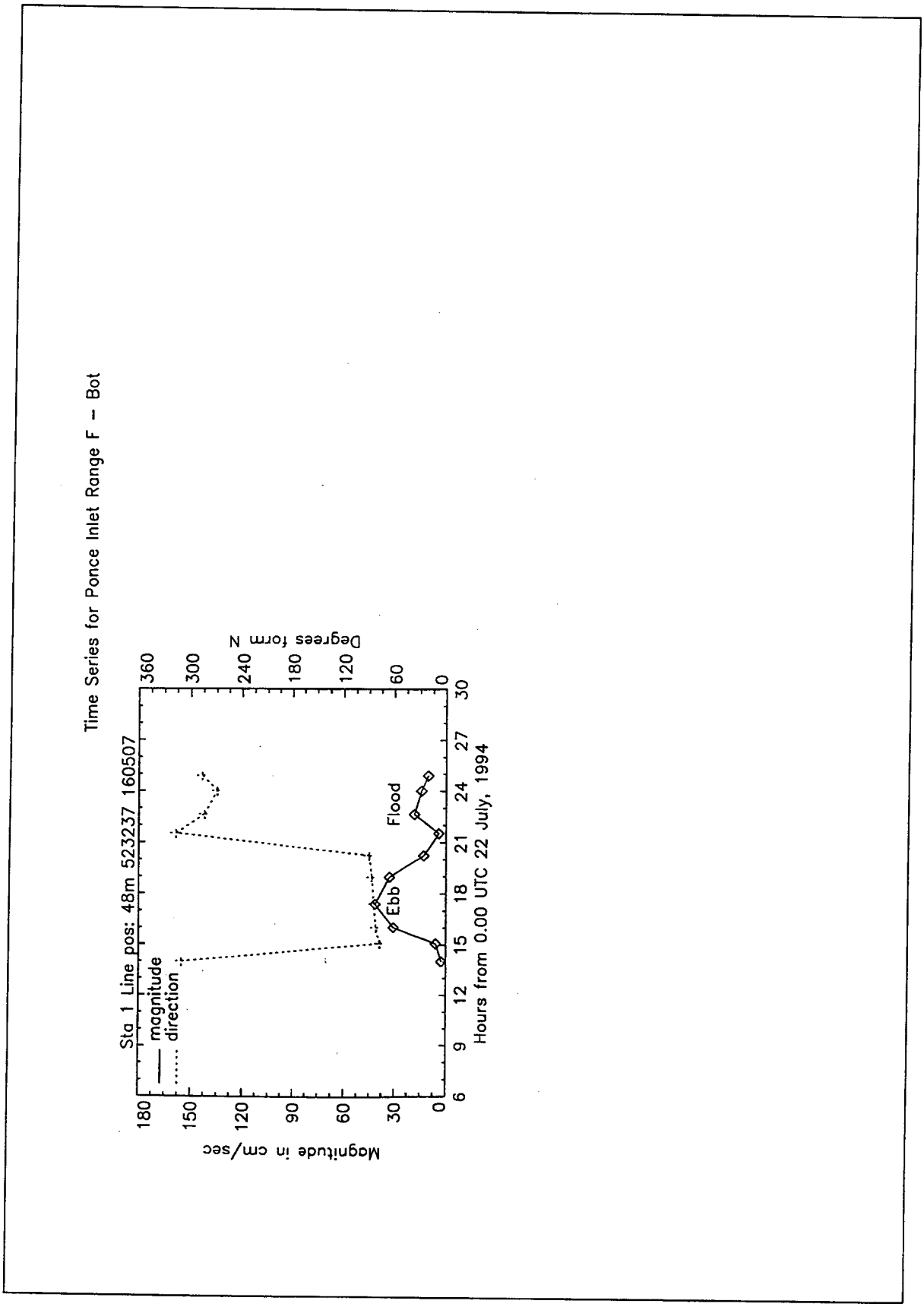

Figure B47. Time series, Range F

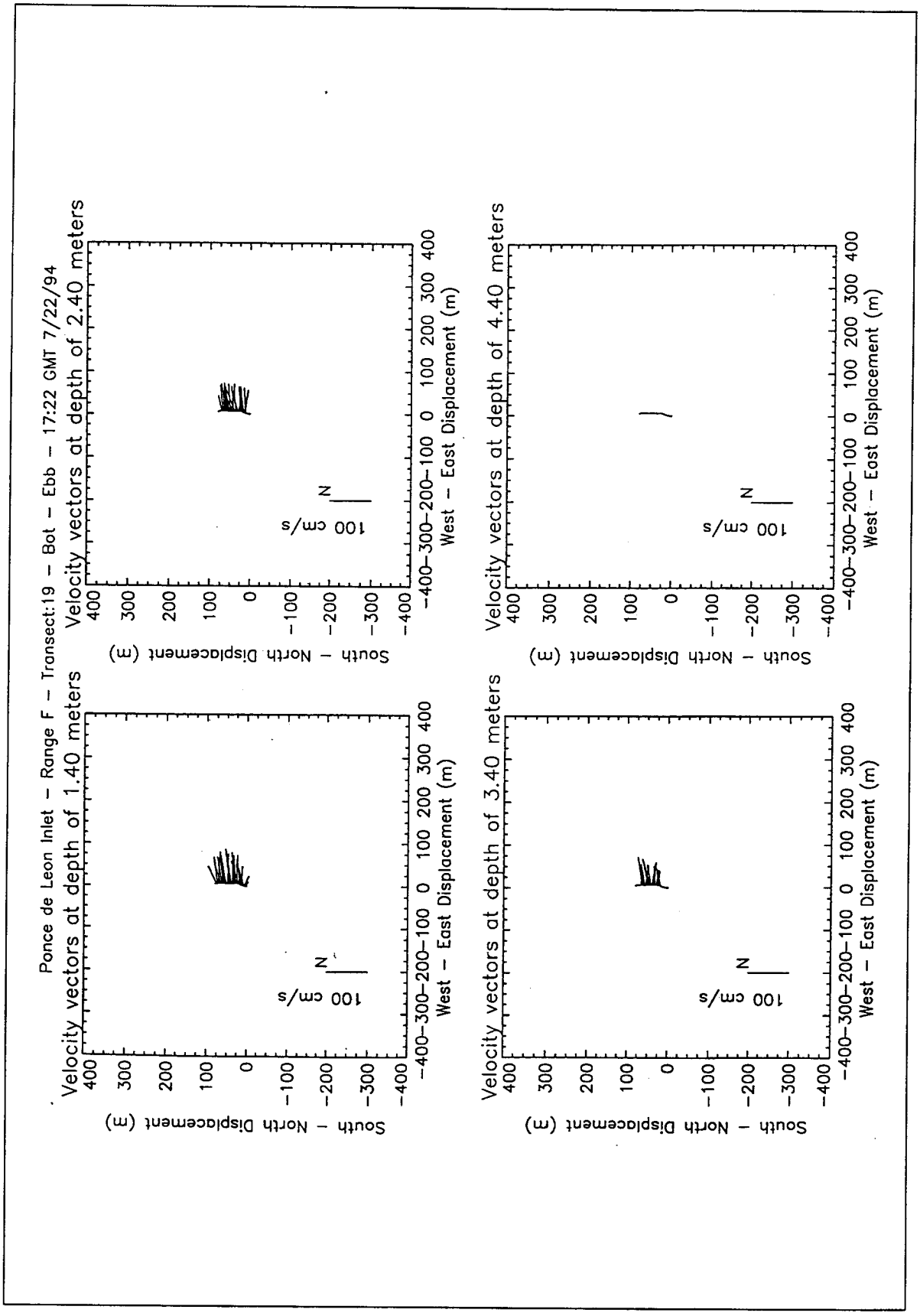

Figure B48. Velocity vector plots at peak ebb conditions, Range F

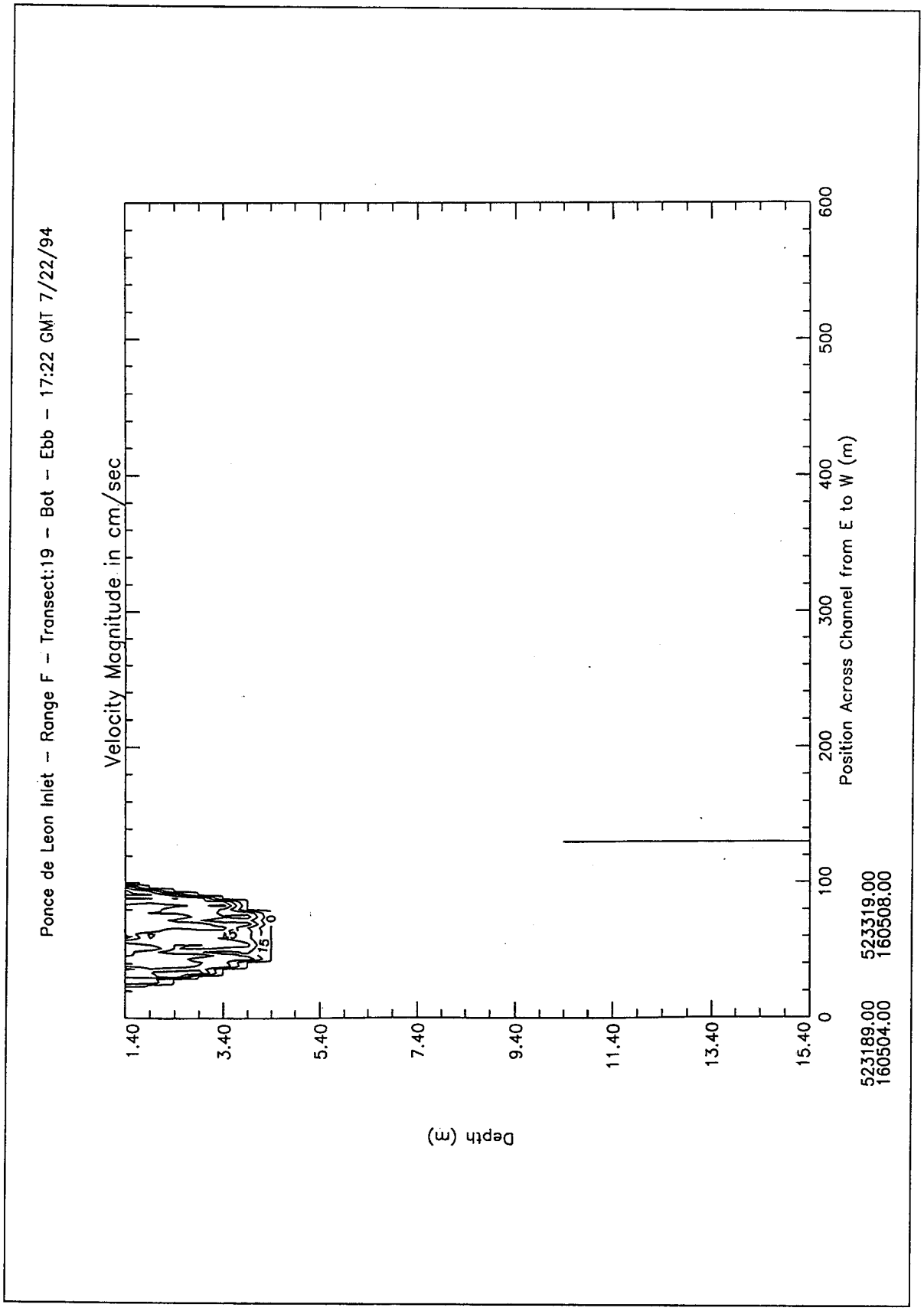

Figure B49. Contour plot of water magnitudes at peak ebb conditions, Range F

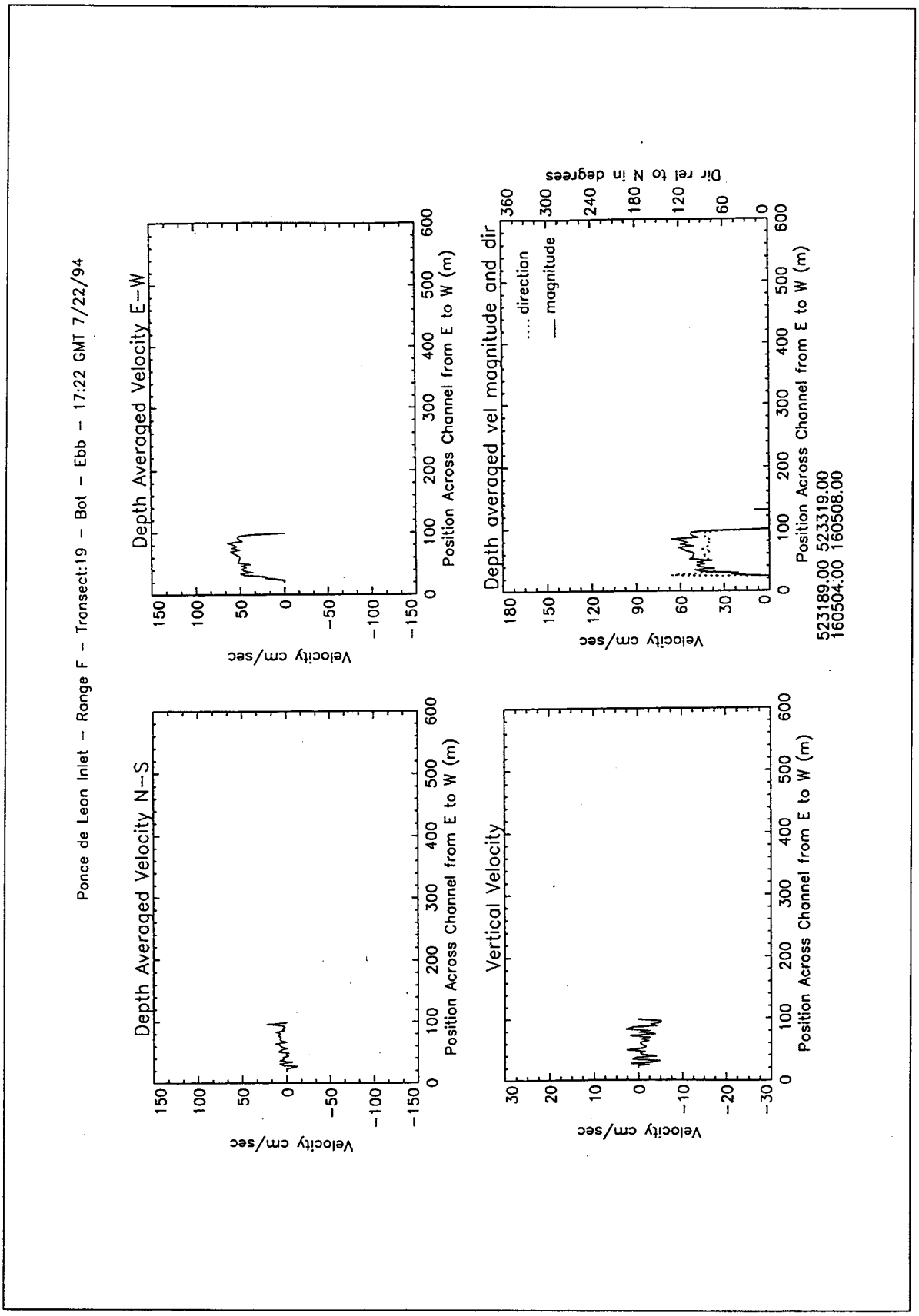

Figure B50. Depth average water velocities at peak ebb conditions, Range F

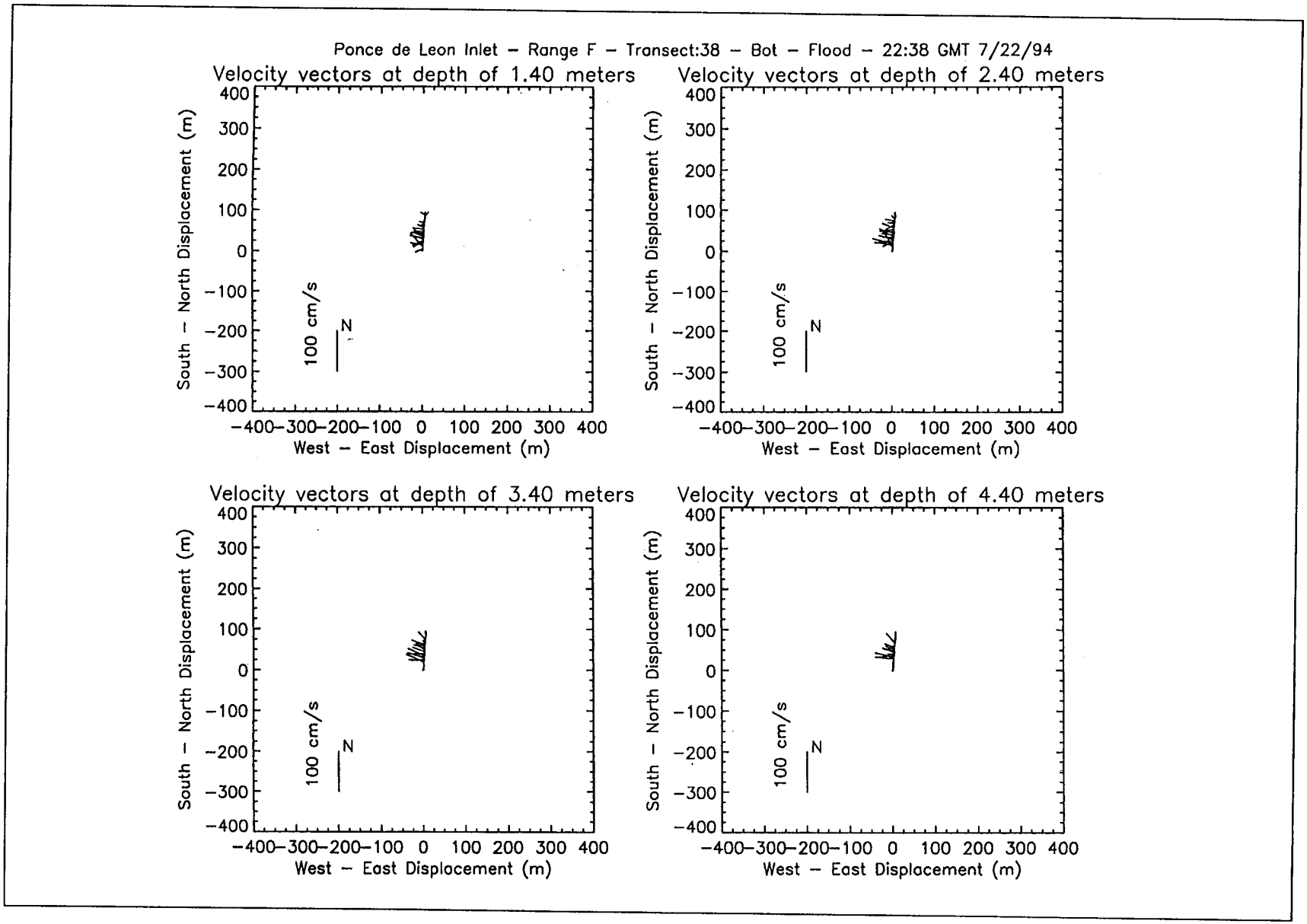

Figure B51. Velocity vector plots at peak flood conditions, Range F

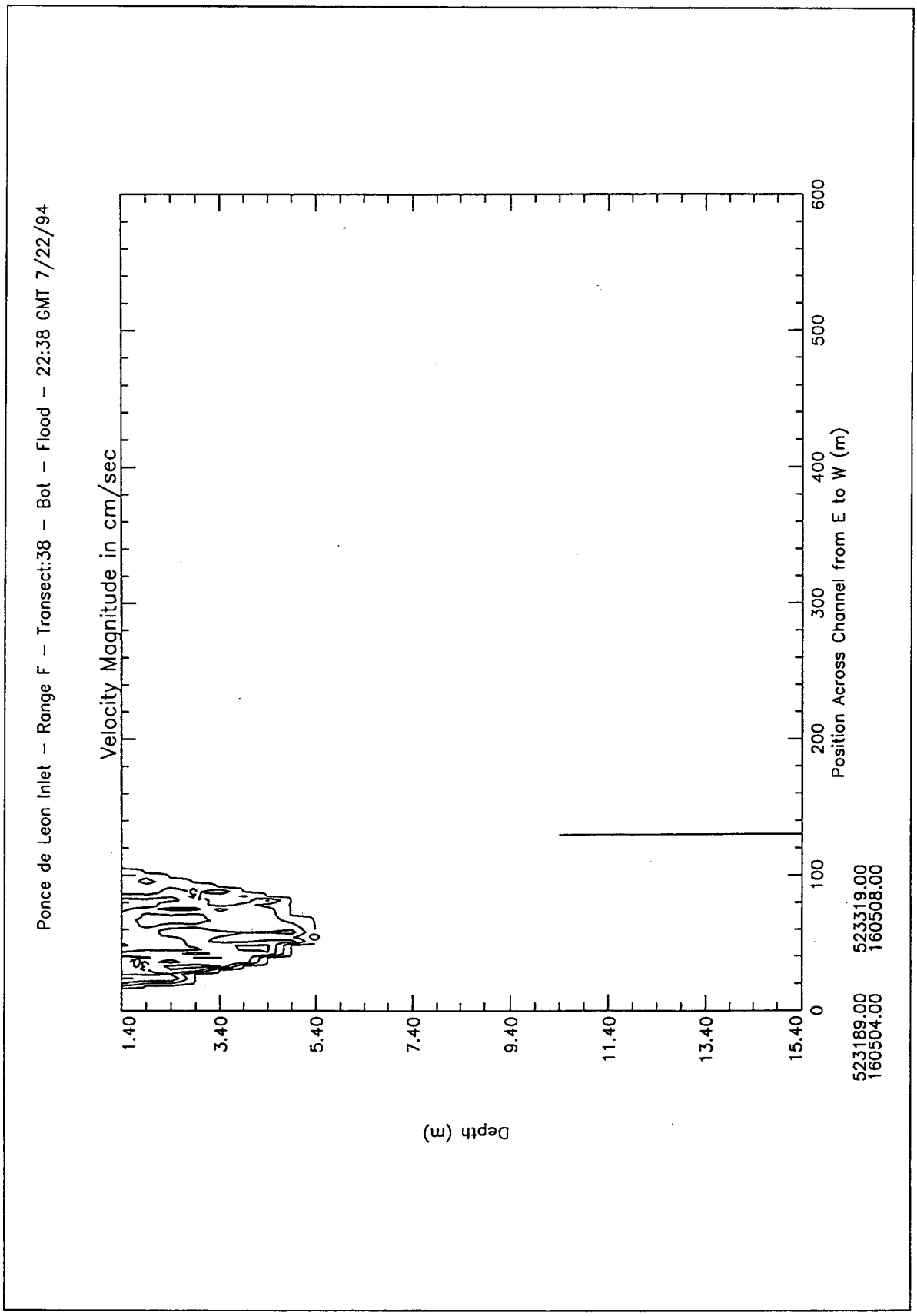

Figure B52. Contour plot of water magnitudes at peak flood conditions, Range F

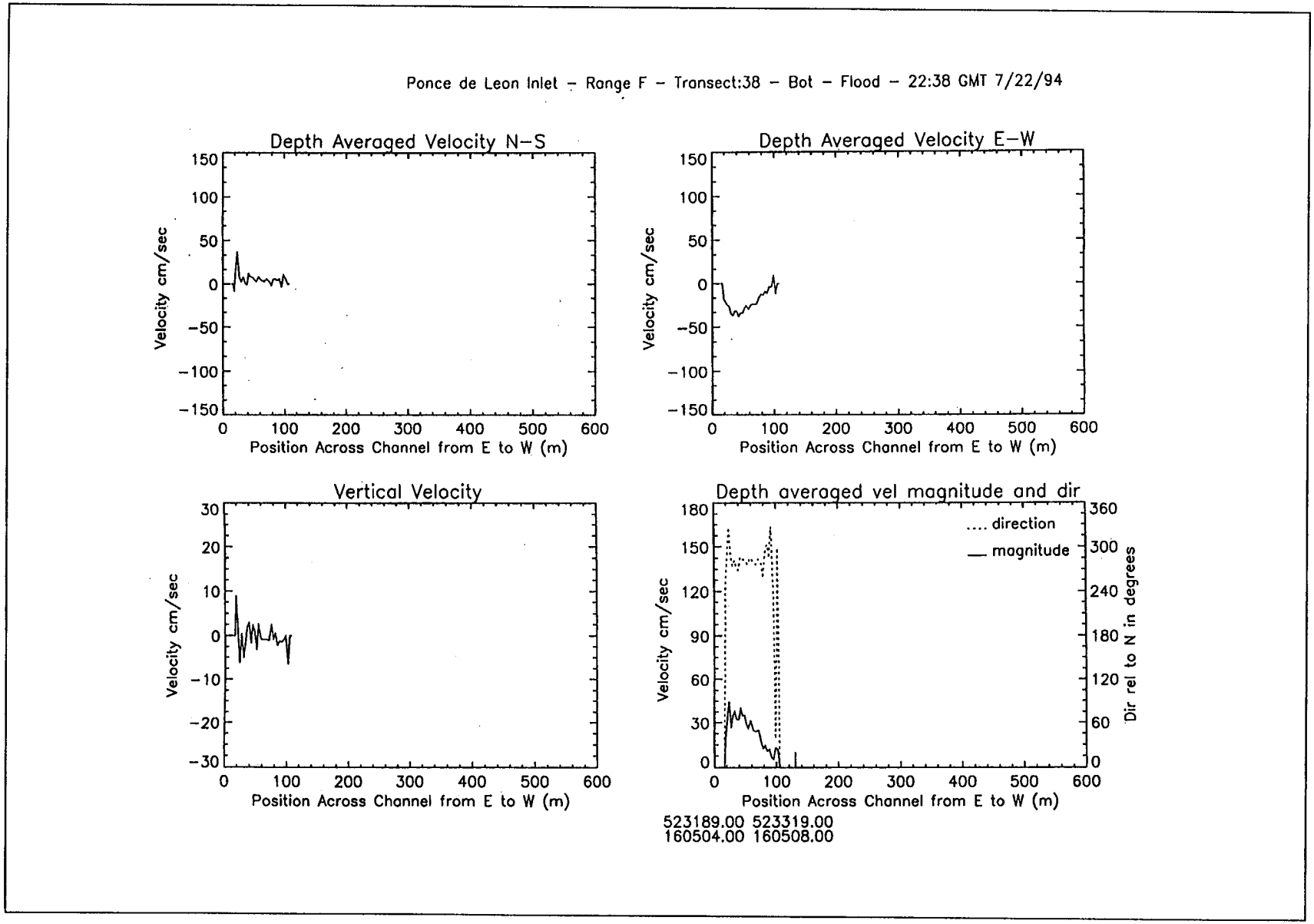

Figure B53. Depth average water velocities at peak flood conditions, Range F

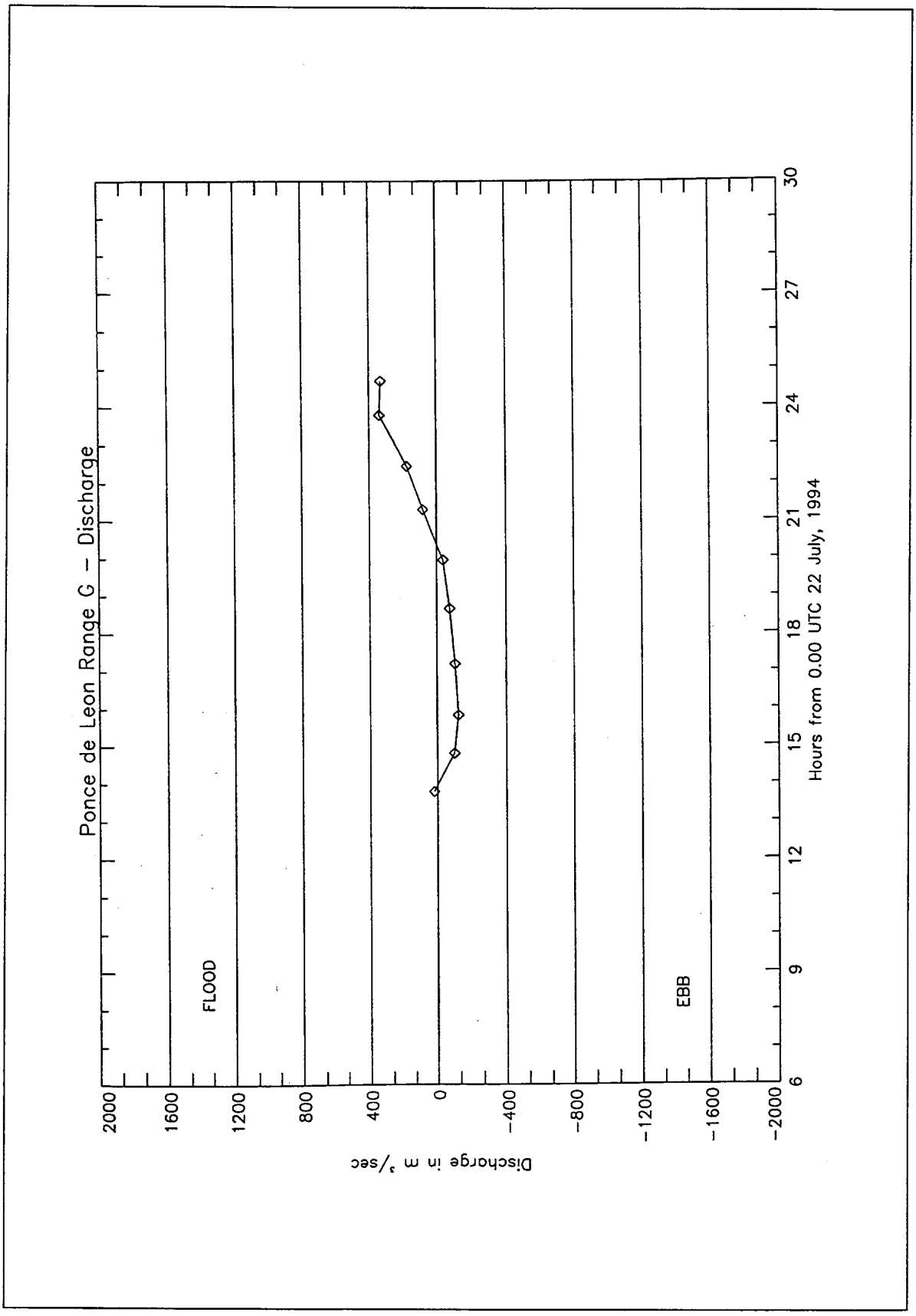

Figure B54. Discharge, Range G

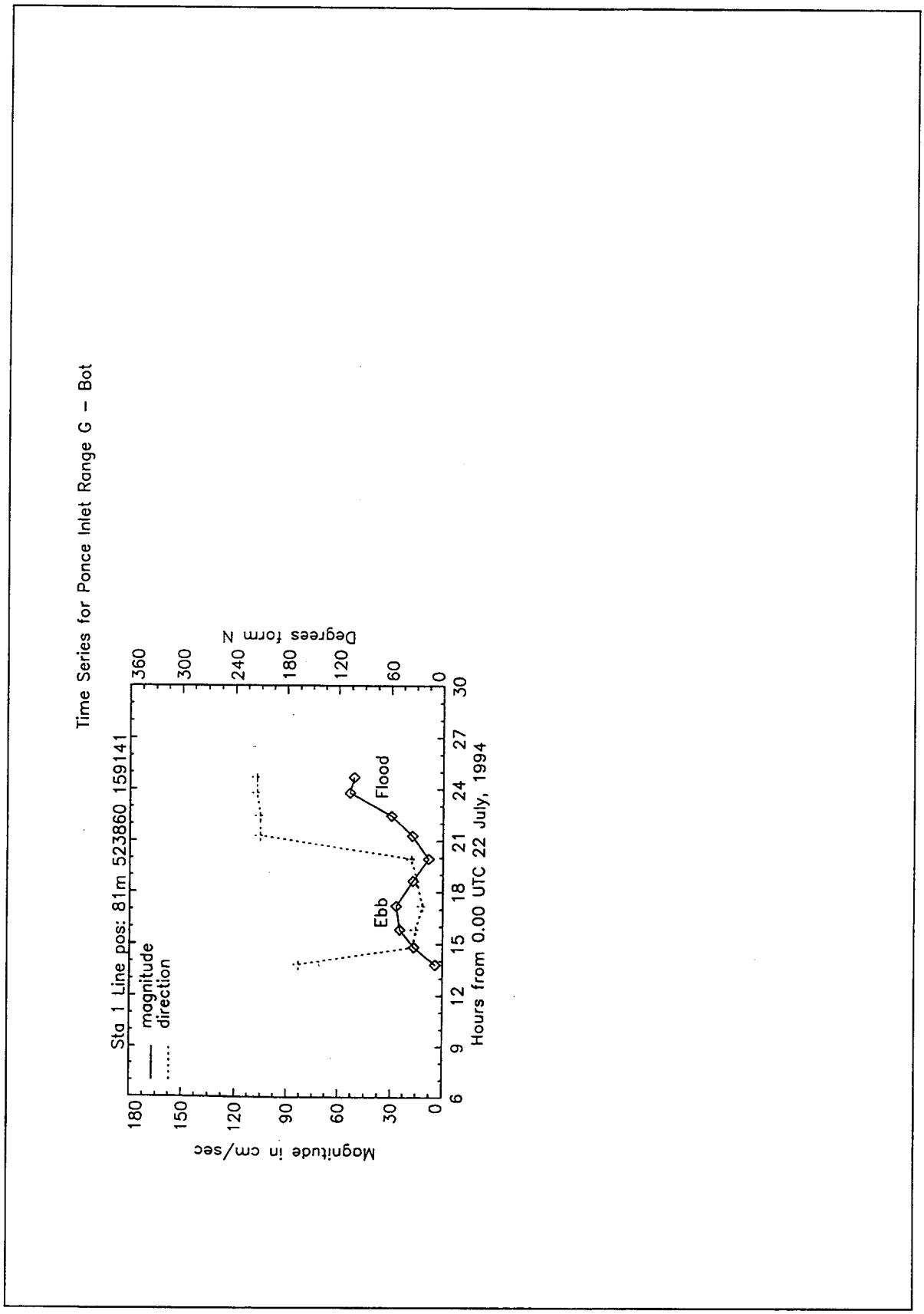

Figure B55. Time series, Range G

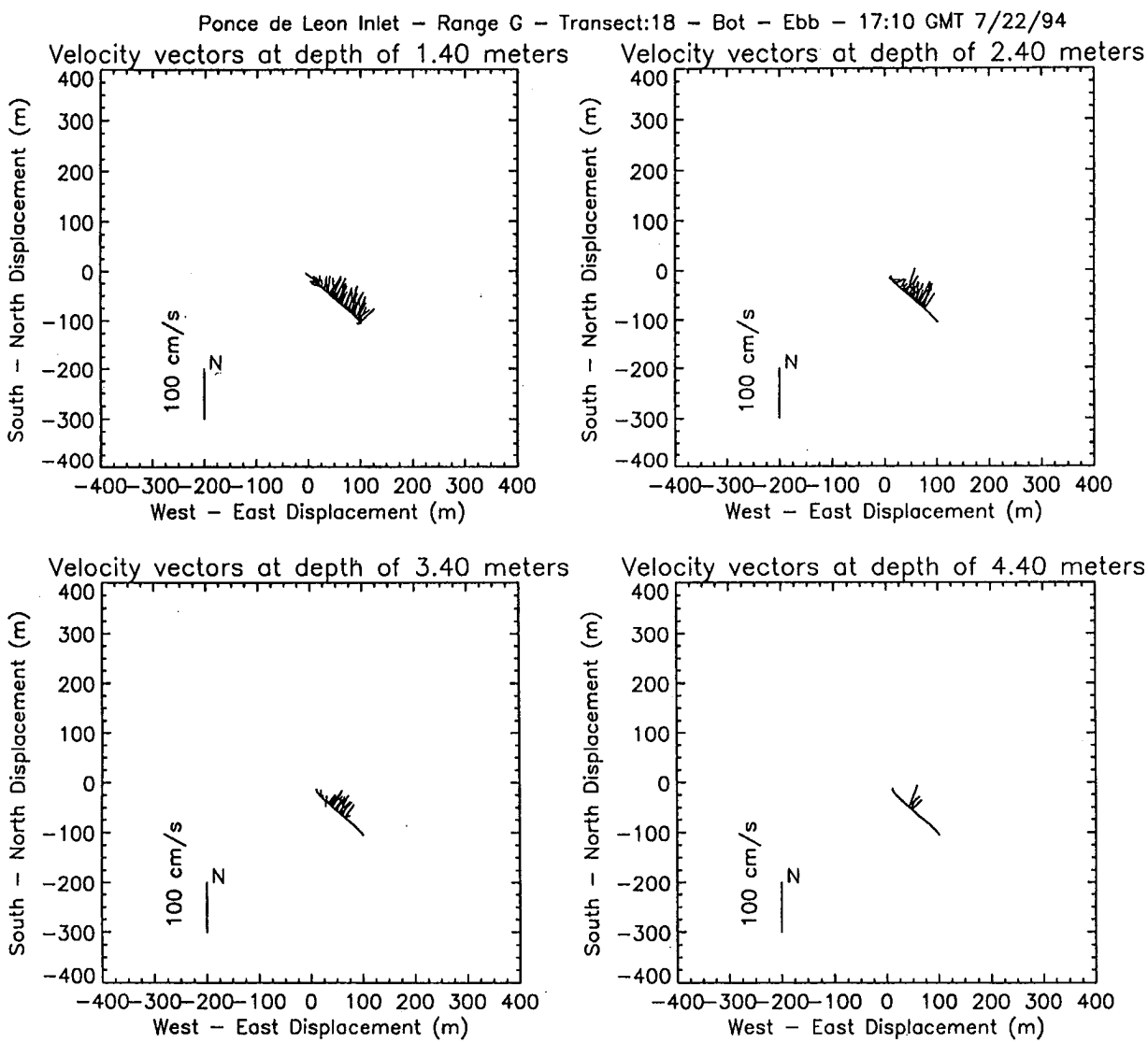

Figure B56. Velocity vector plots at peak ebb conditions, Range G

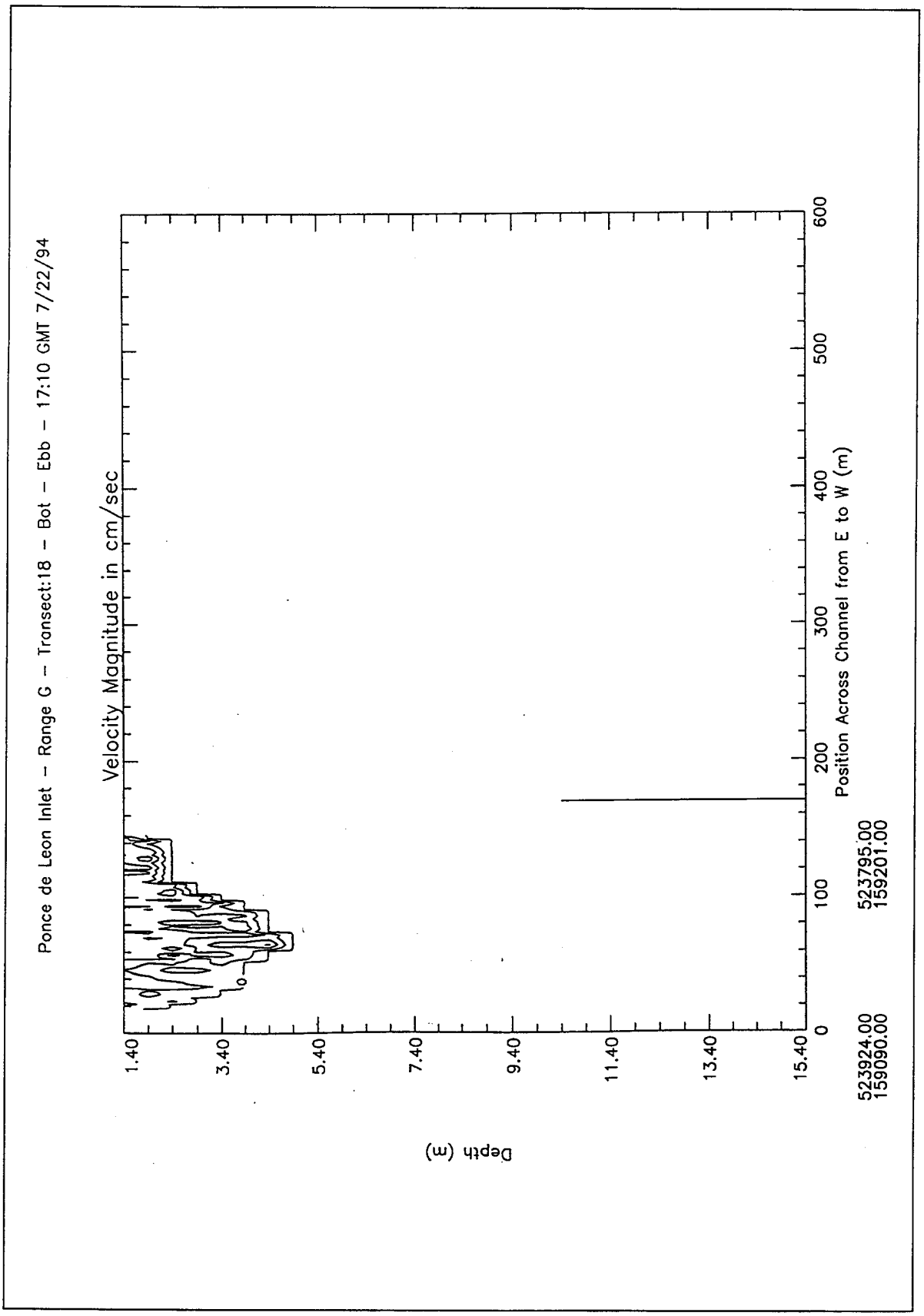

Figure B57. Contour plot of water magnitudes at peak ebb conditions, Range G

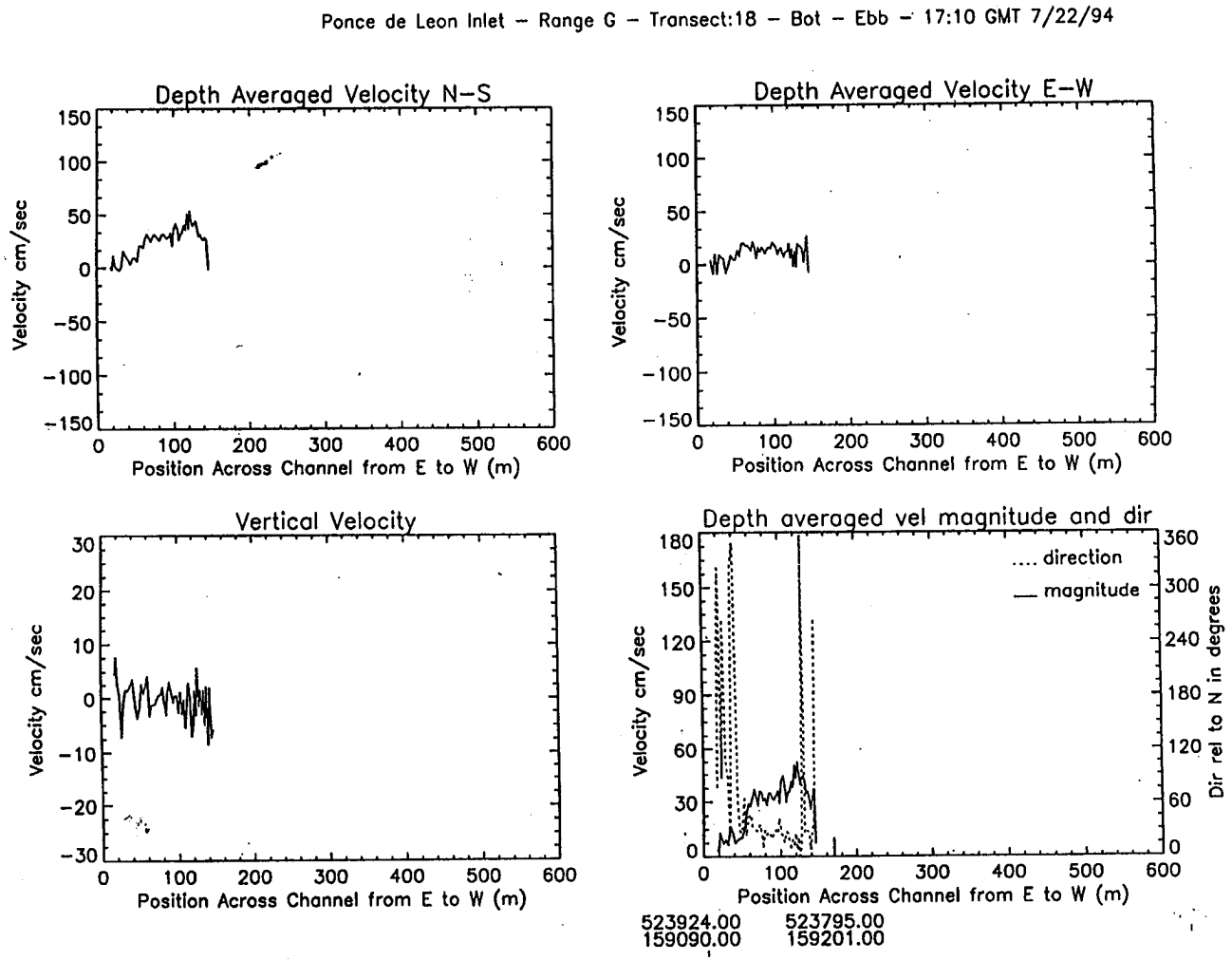

Figure B58. Depth average water velocities at peak ebb conditions, Range G

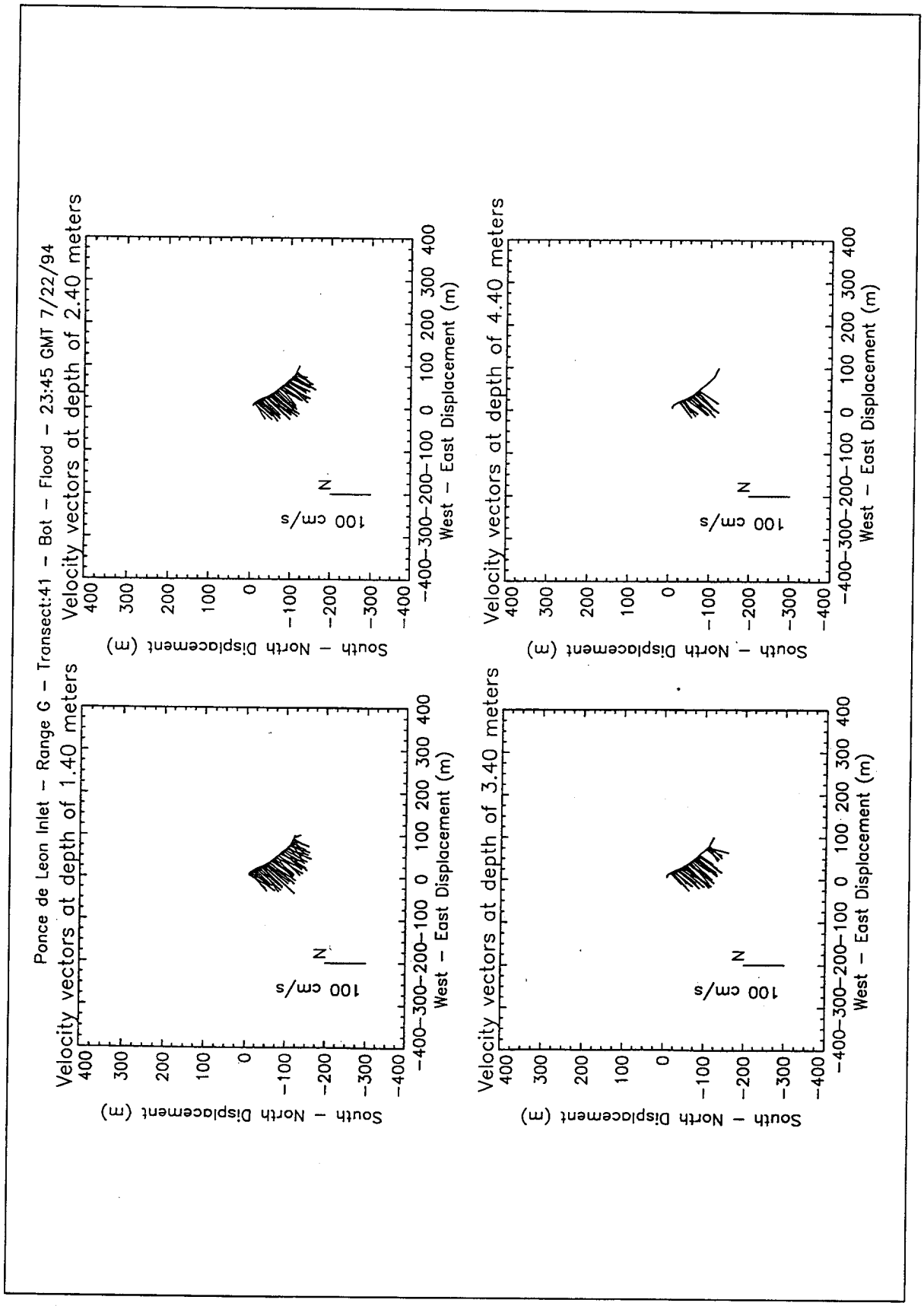

Figure B59. Velocity vector plots at peak flood conditions, Range G

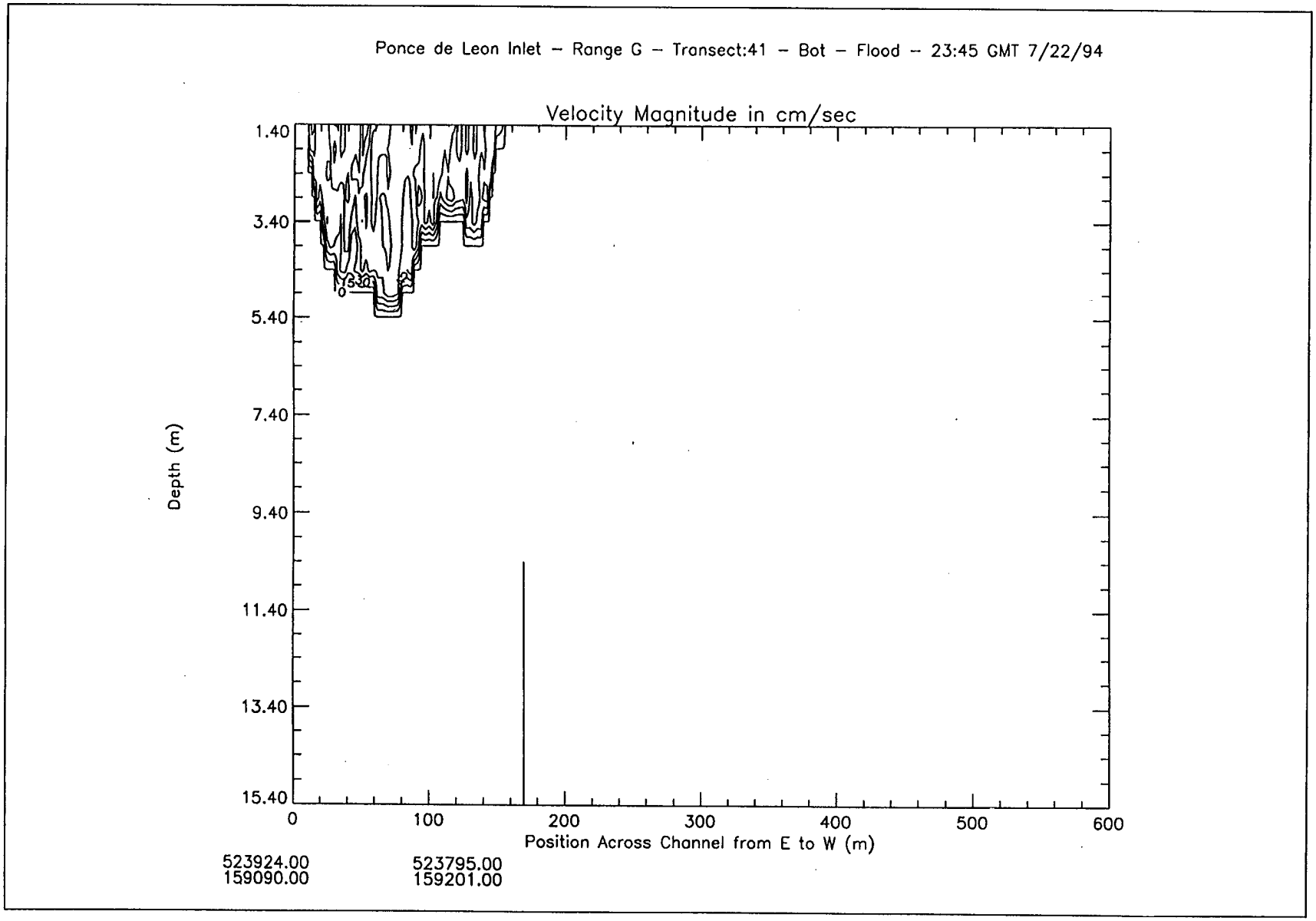

Figure B60. Contour plot of water magnitudes at peak flood conditions, Range G

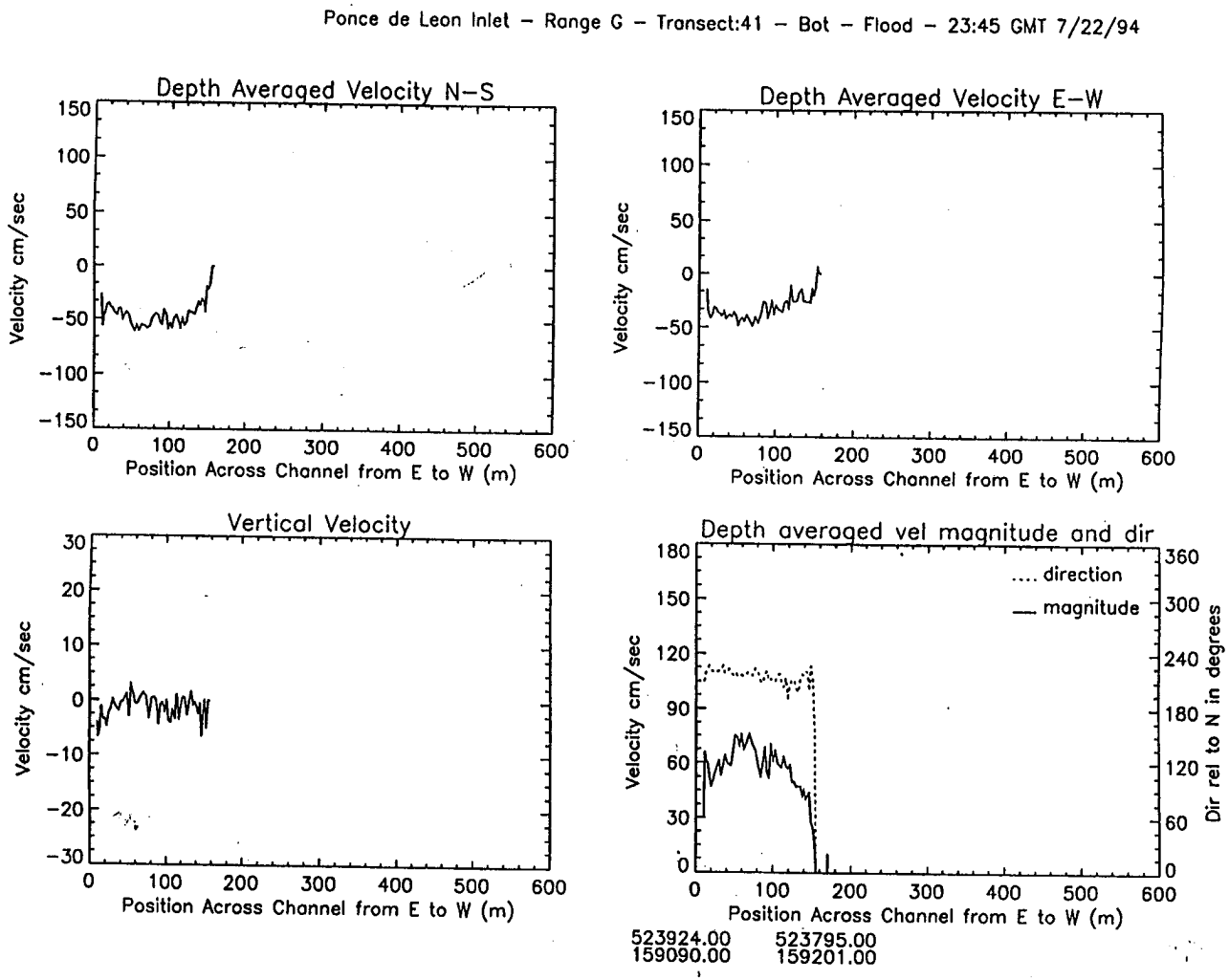

Figure B61. Depth average water velocities at peak flood conditions, Range G

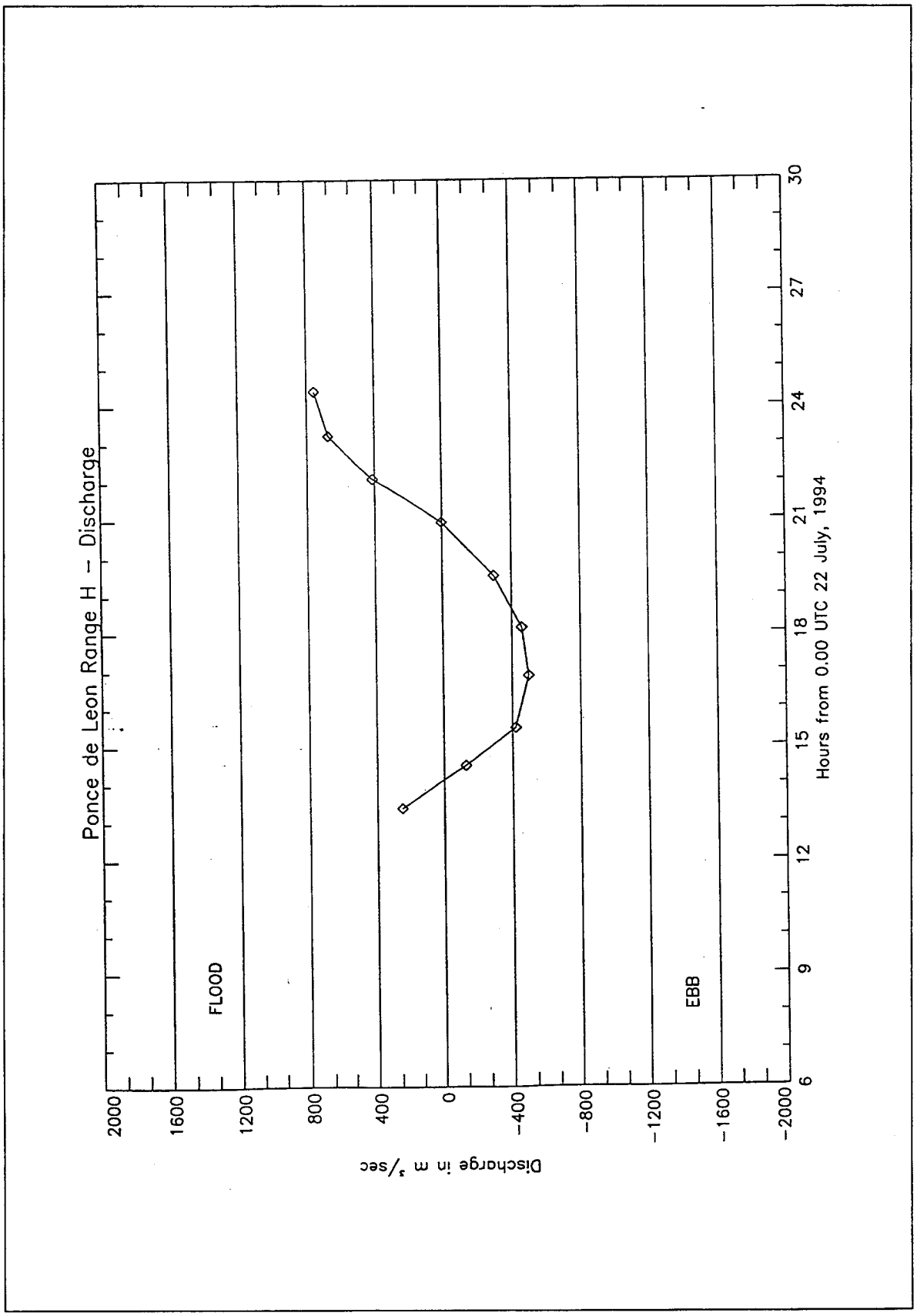

Figure B62. Discharge, Range H

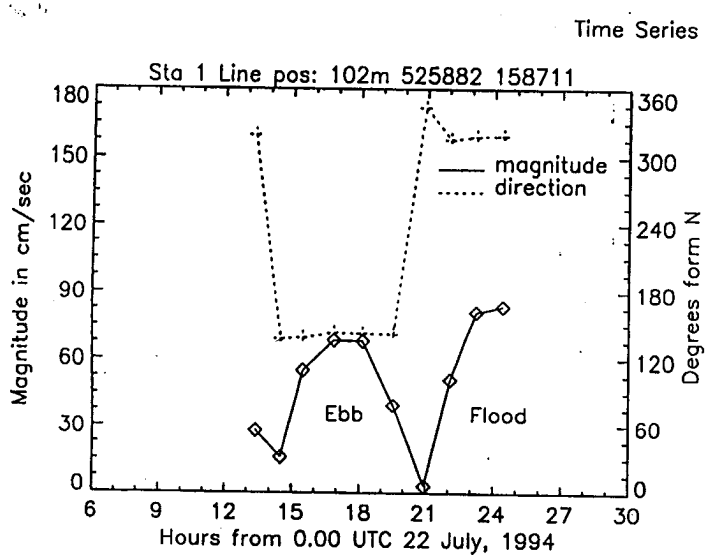

Figure B63. Time series, Range H

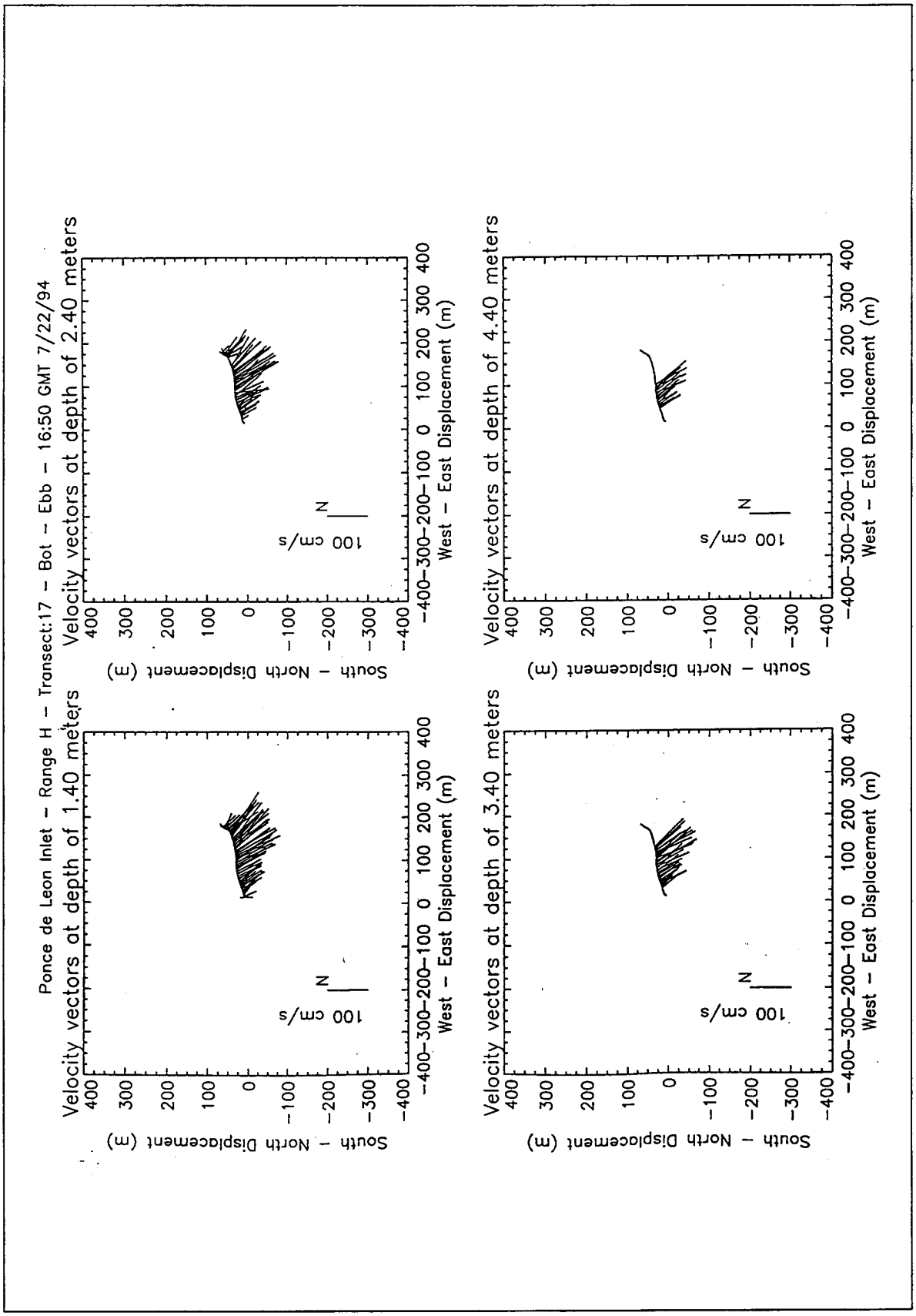

Figure B64. Velocity vector plots at peak ebb conditions, Range H

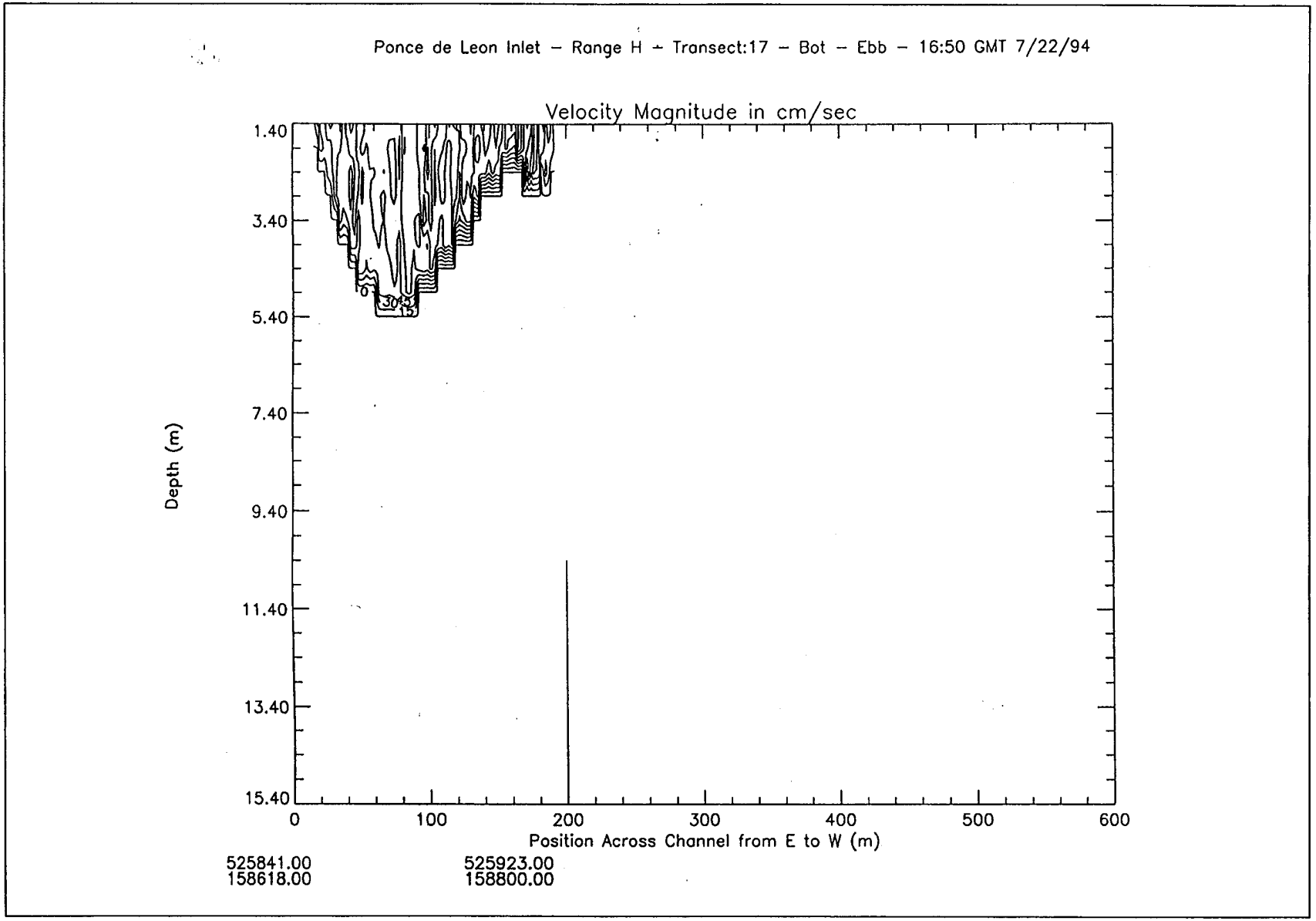

Figure B65. Contour plot of water magnitudes at peak ebb conditions, Range H

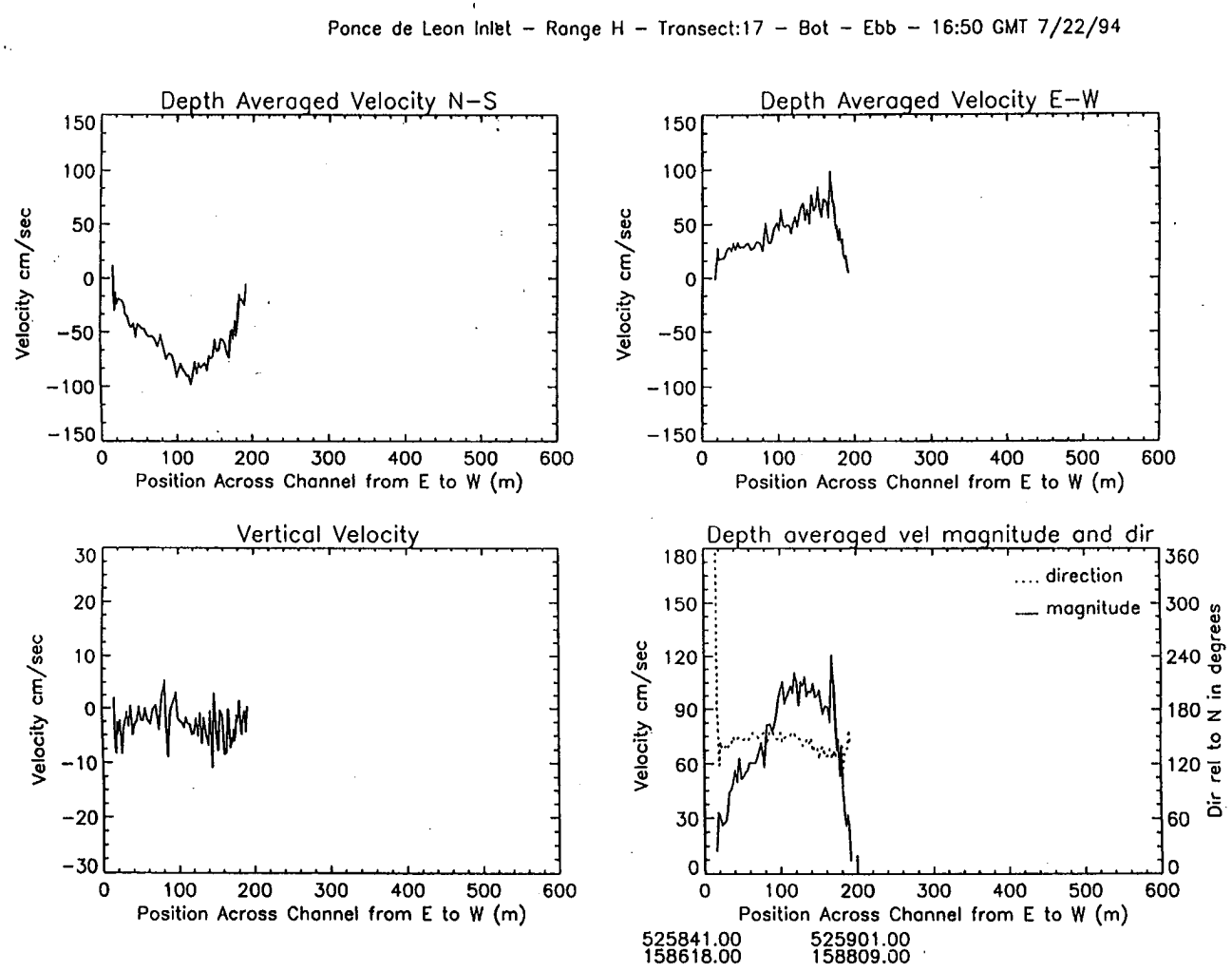

Figure B66. Depth average water velocities at peak ebb conditions, Range H

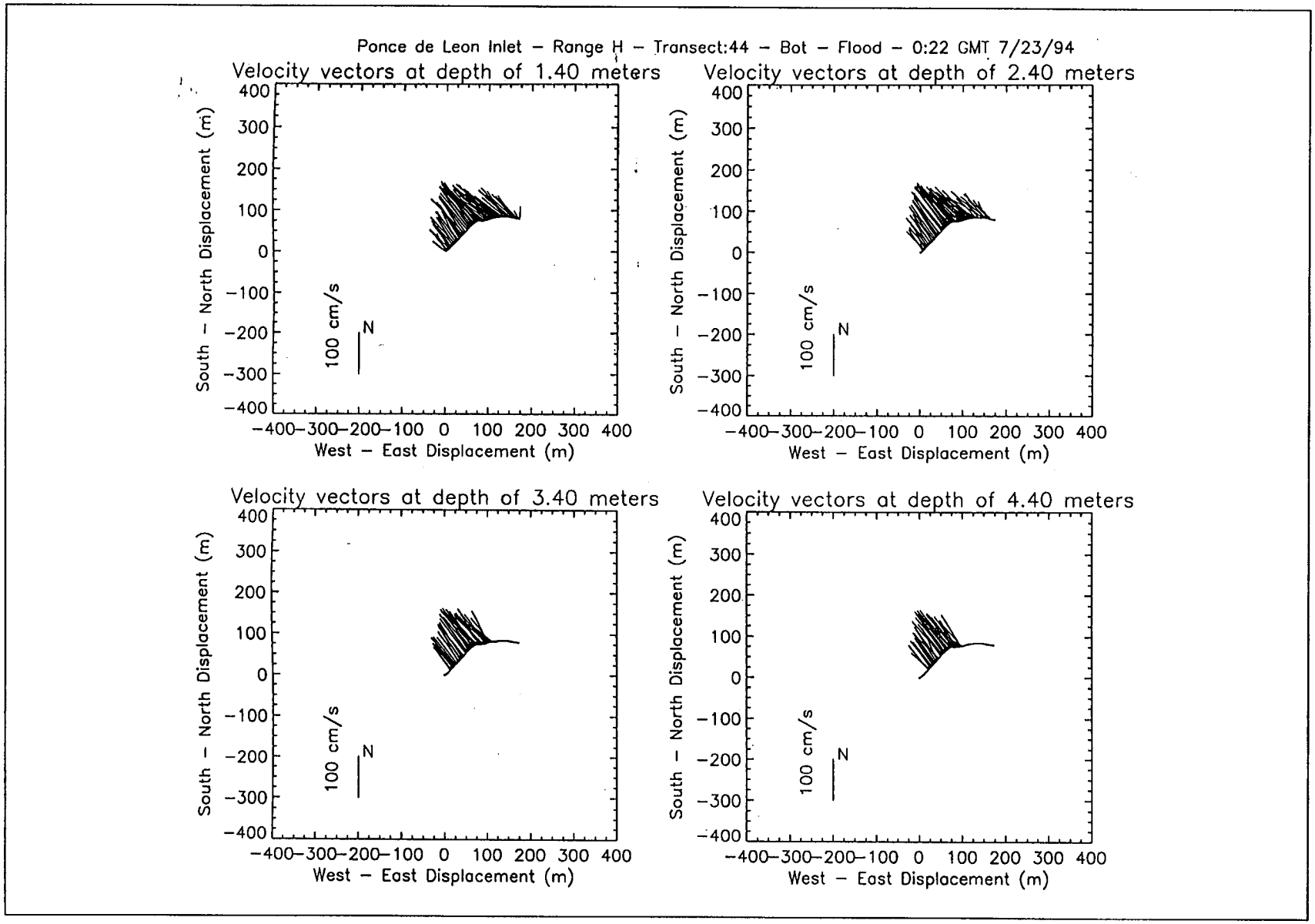

Figure B67. Velocity vector plots at peak flood conditions, Range H

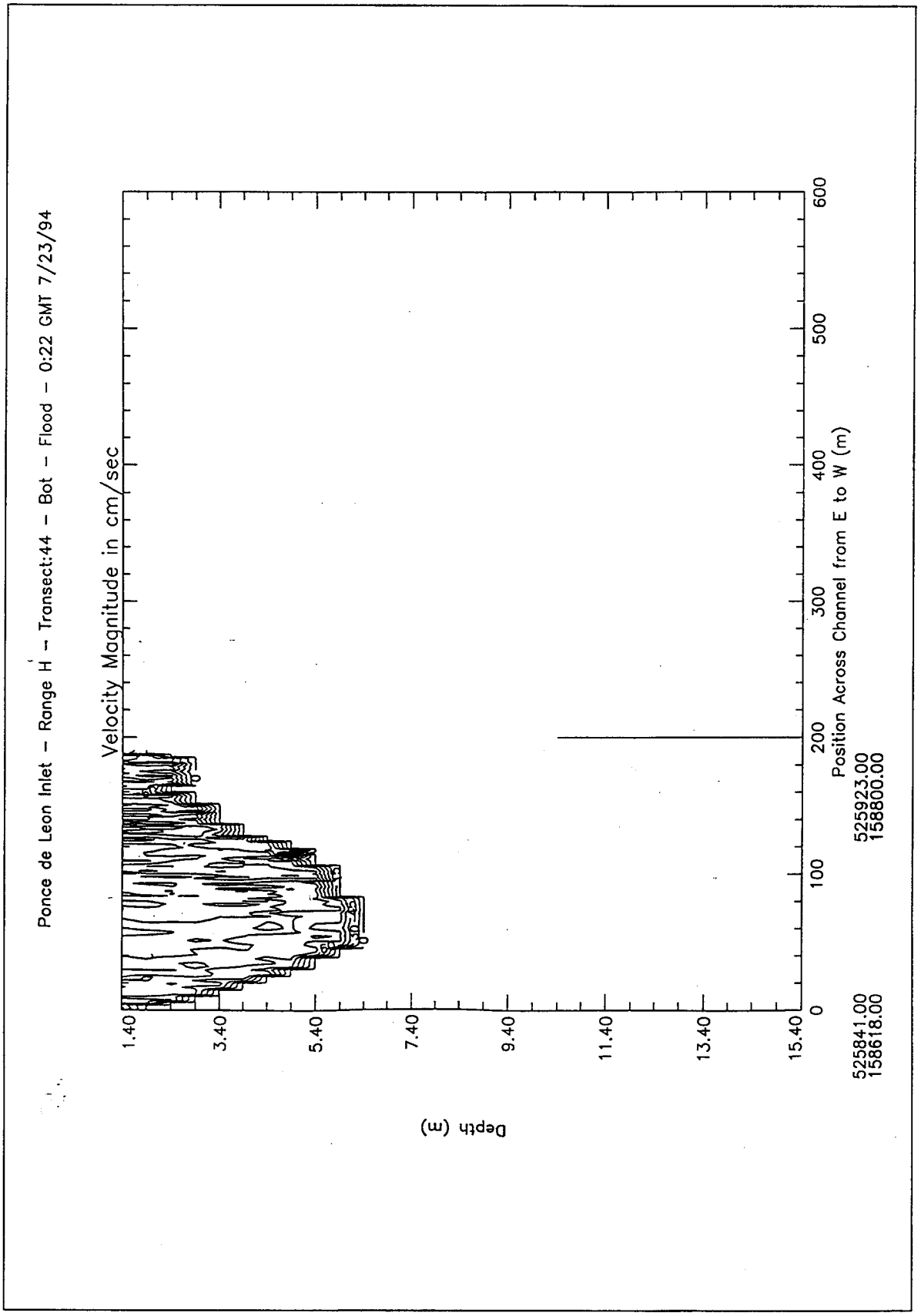

Figure B68. Contour plot of water magnitudes at peak flood conditions, Range H

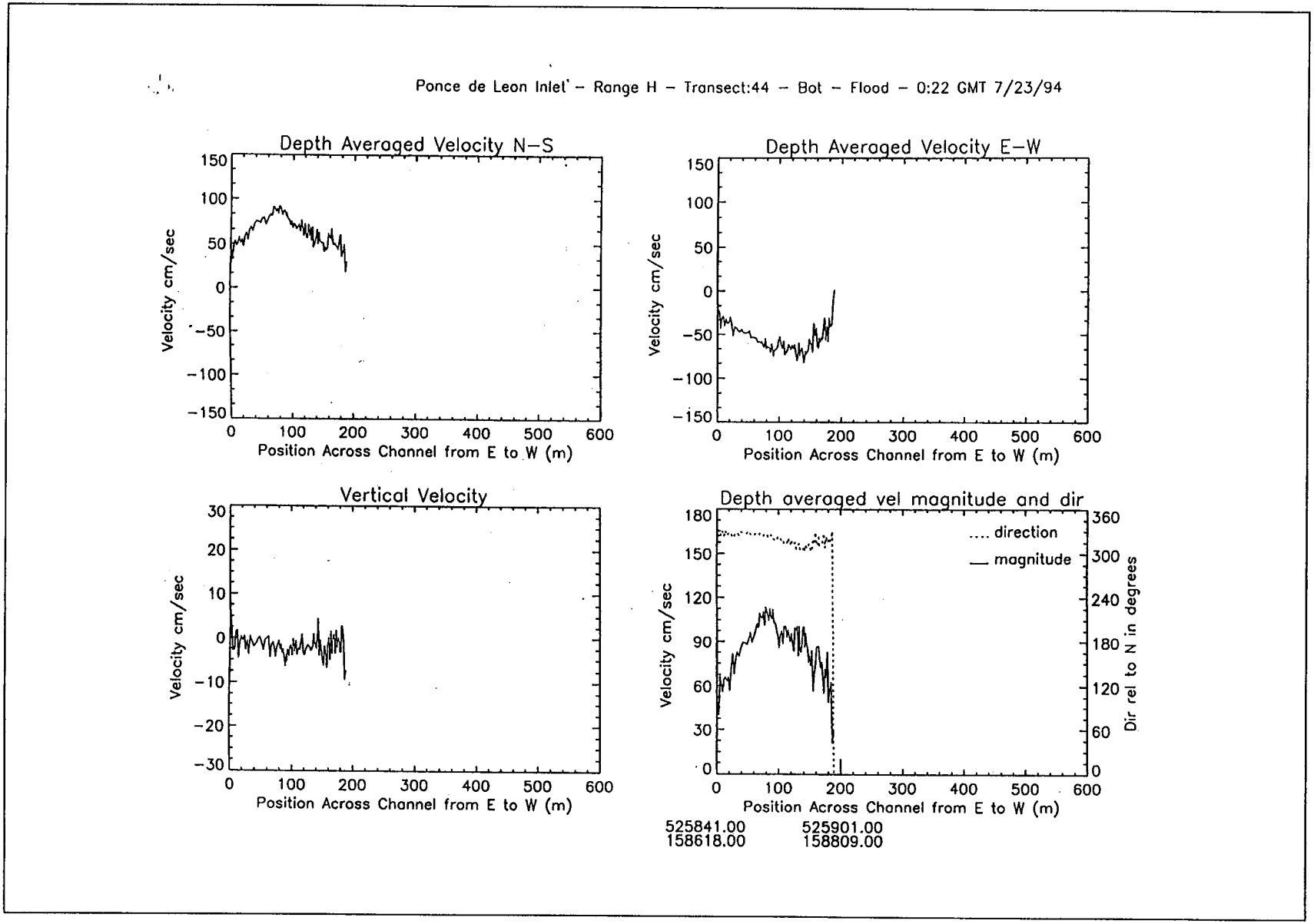

Figure B69. Depth average water velocities at peak flood conditions, Range H

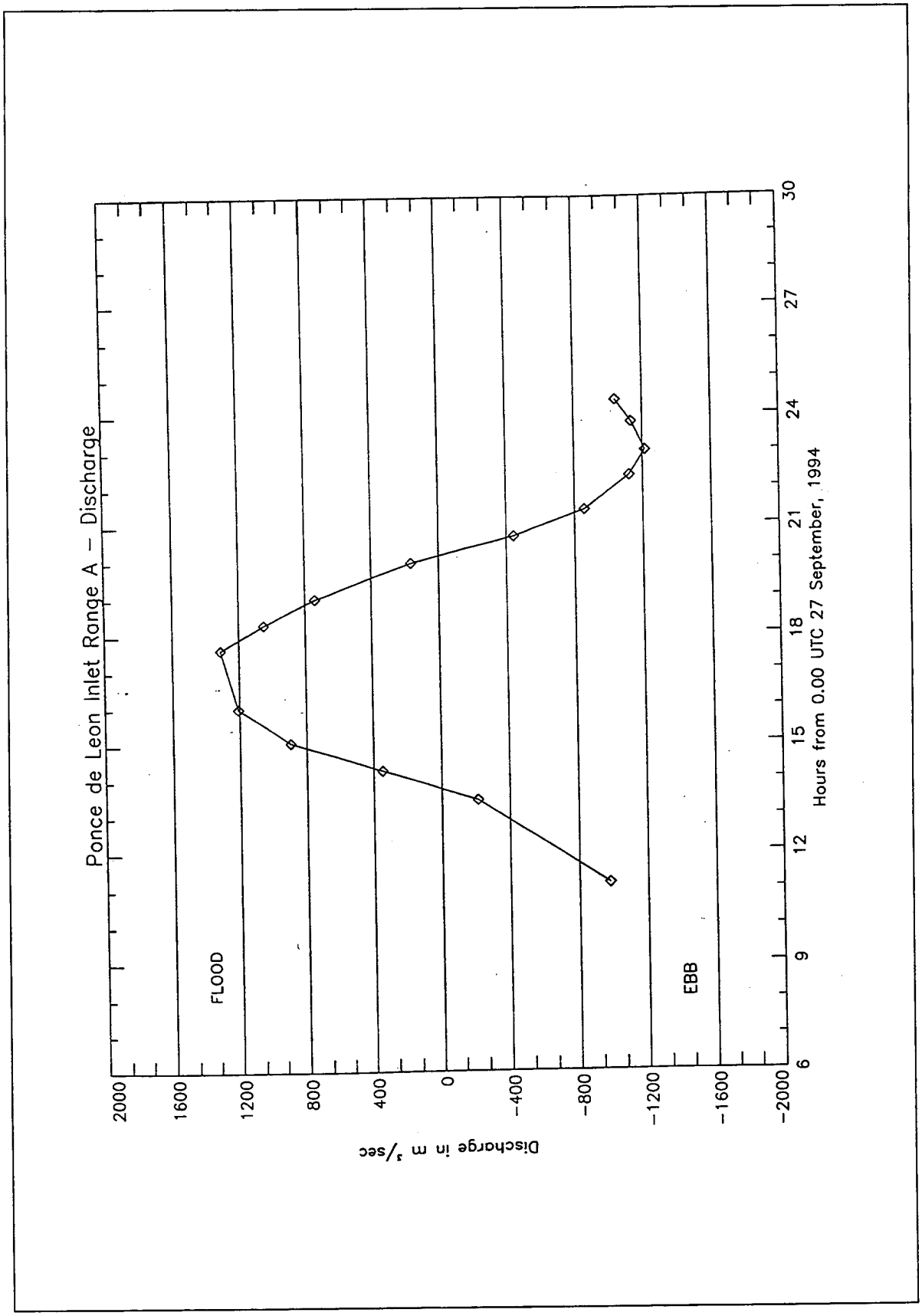

Figure B70. Discharge, Range A, September

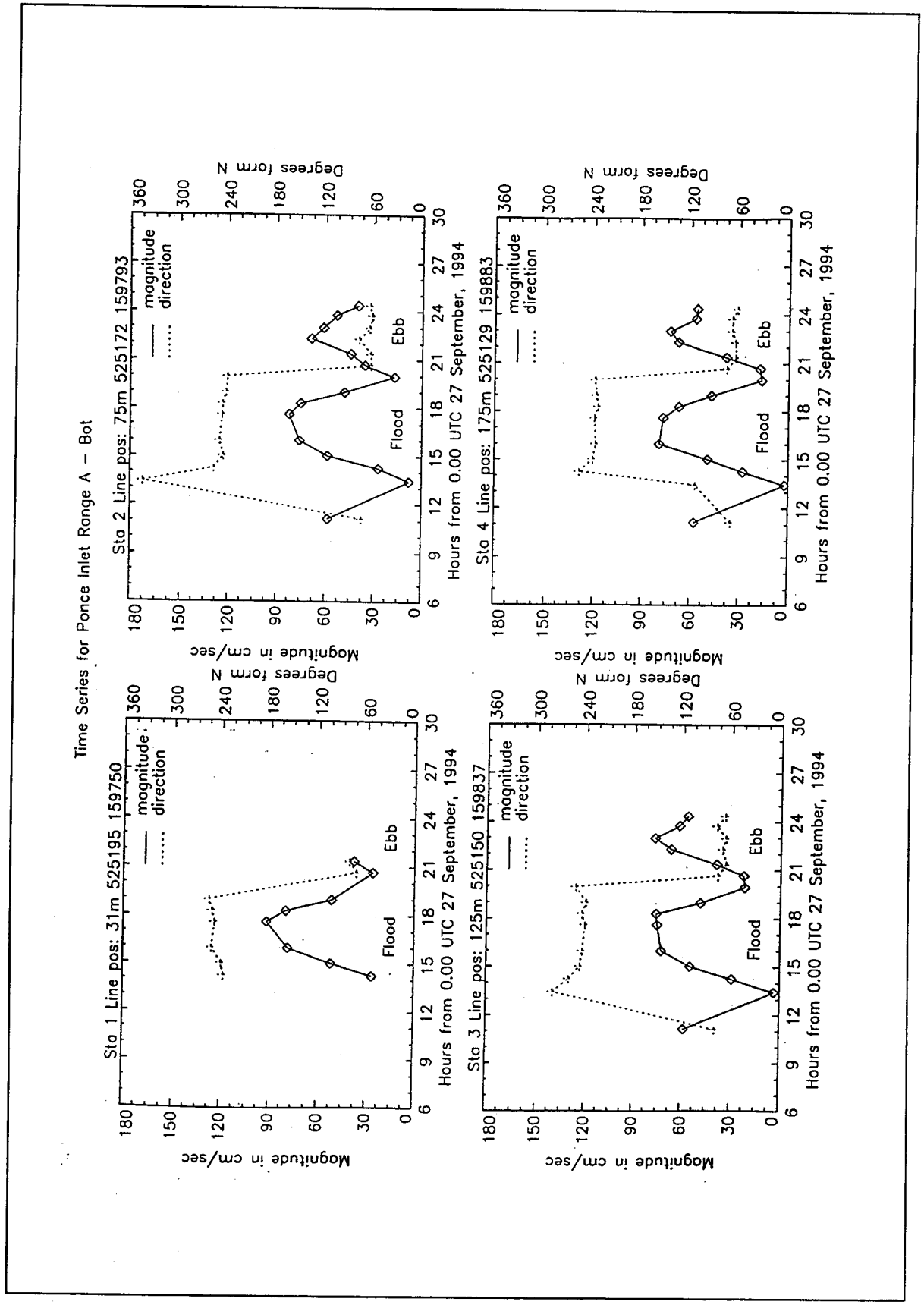

Figure B71. Time series, Range A, September, stations 1-4

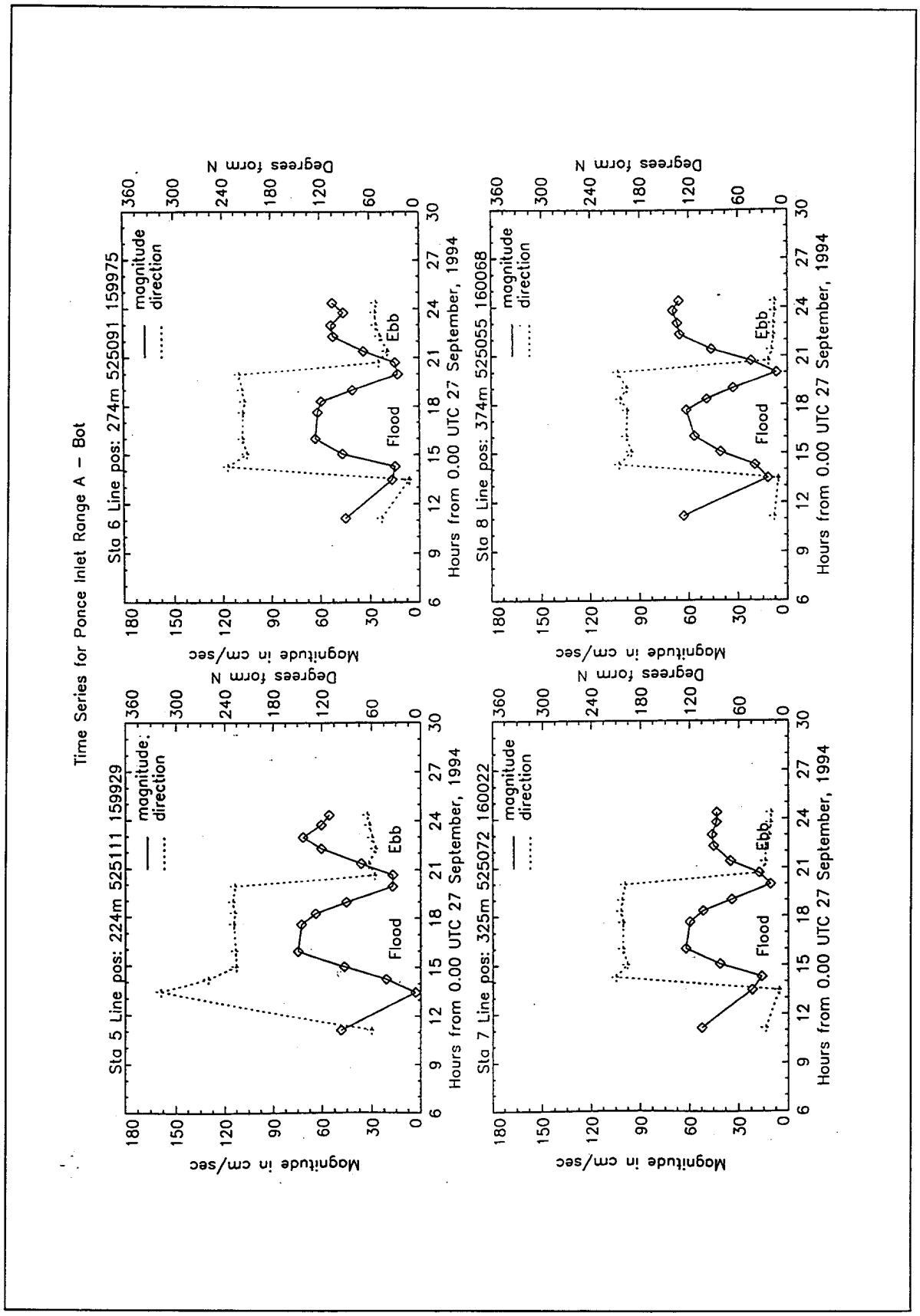

Figure B72. Time series, Range A, September, stations 5-8

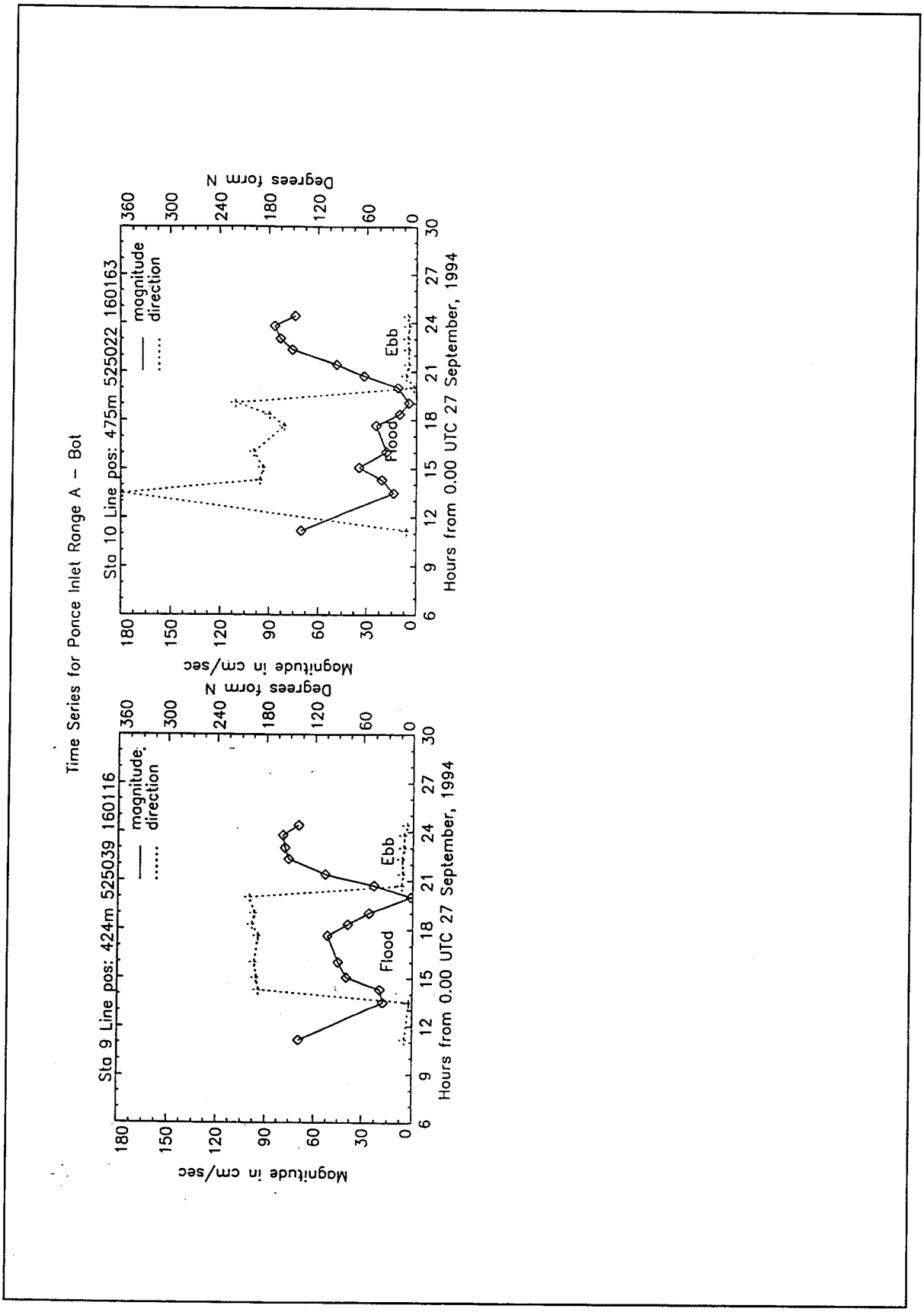

Figure B73. Time series, Range A, September, stations 9 and 10

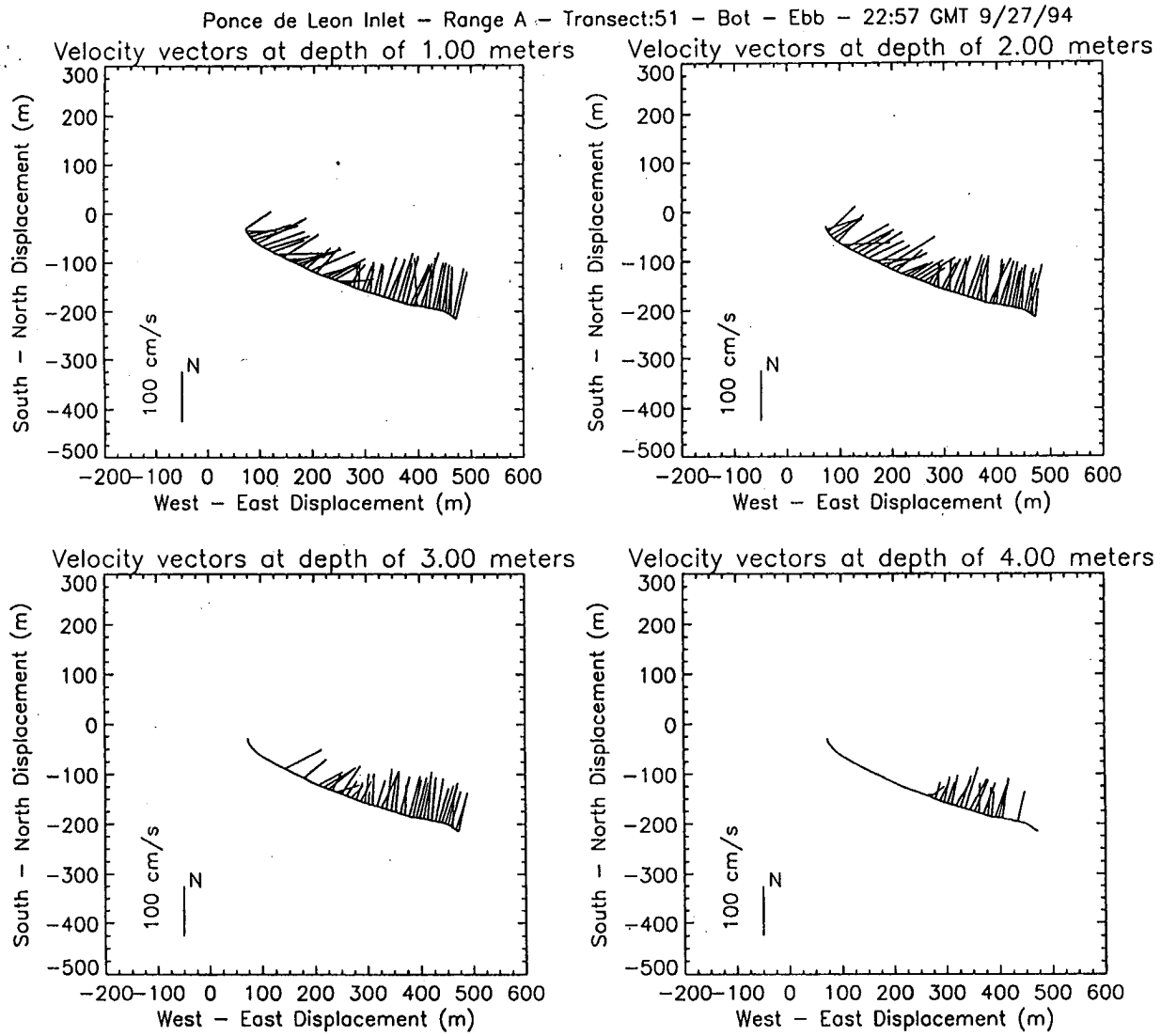

Figure B74. Velocity vector plots at peak ebb conditions, Range A, September

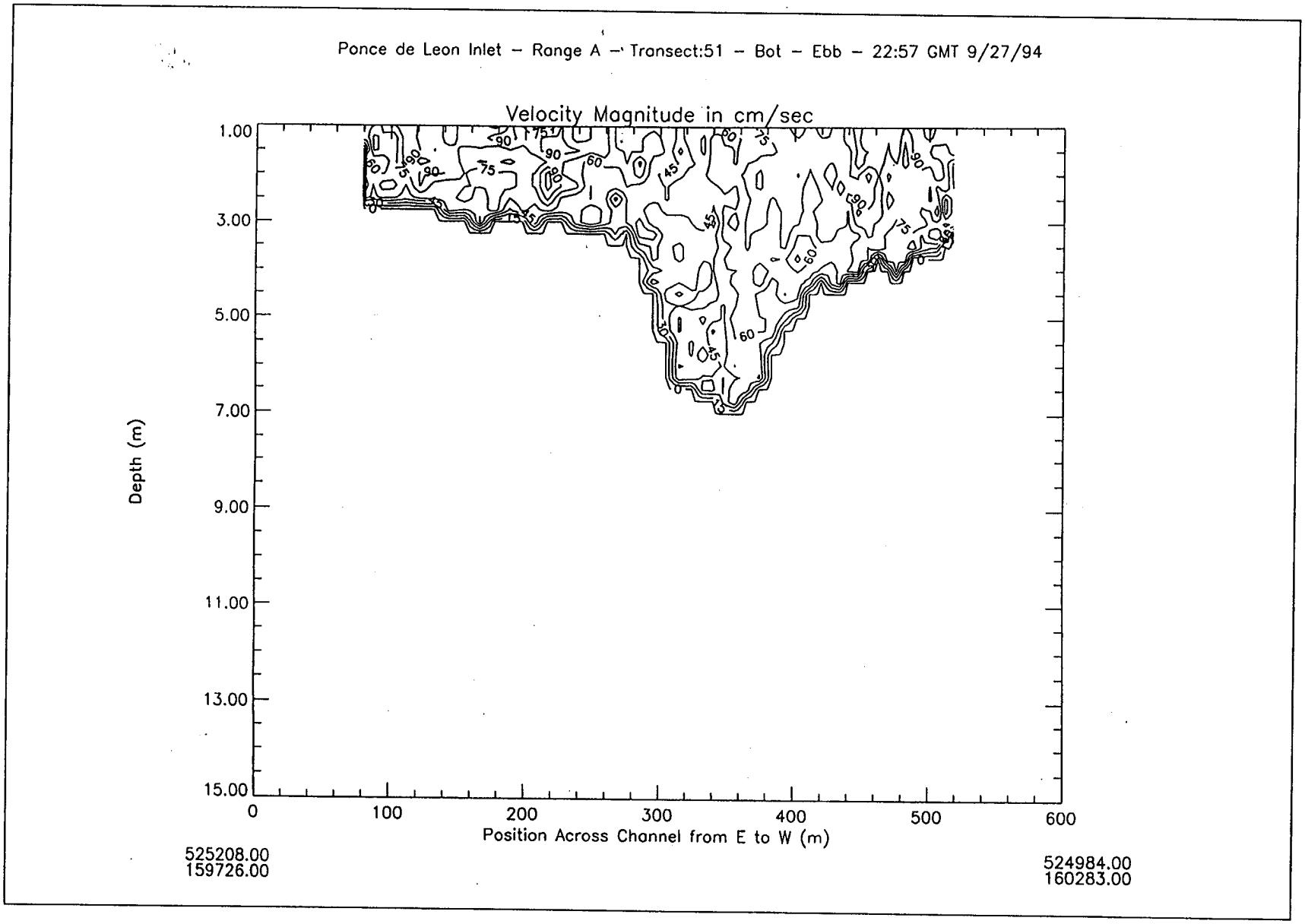

Figure B75. Contour plot of water magnitudes at peak ebb conditions, Range A, September

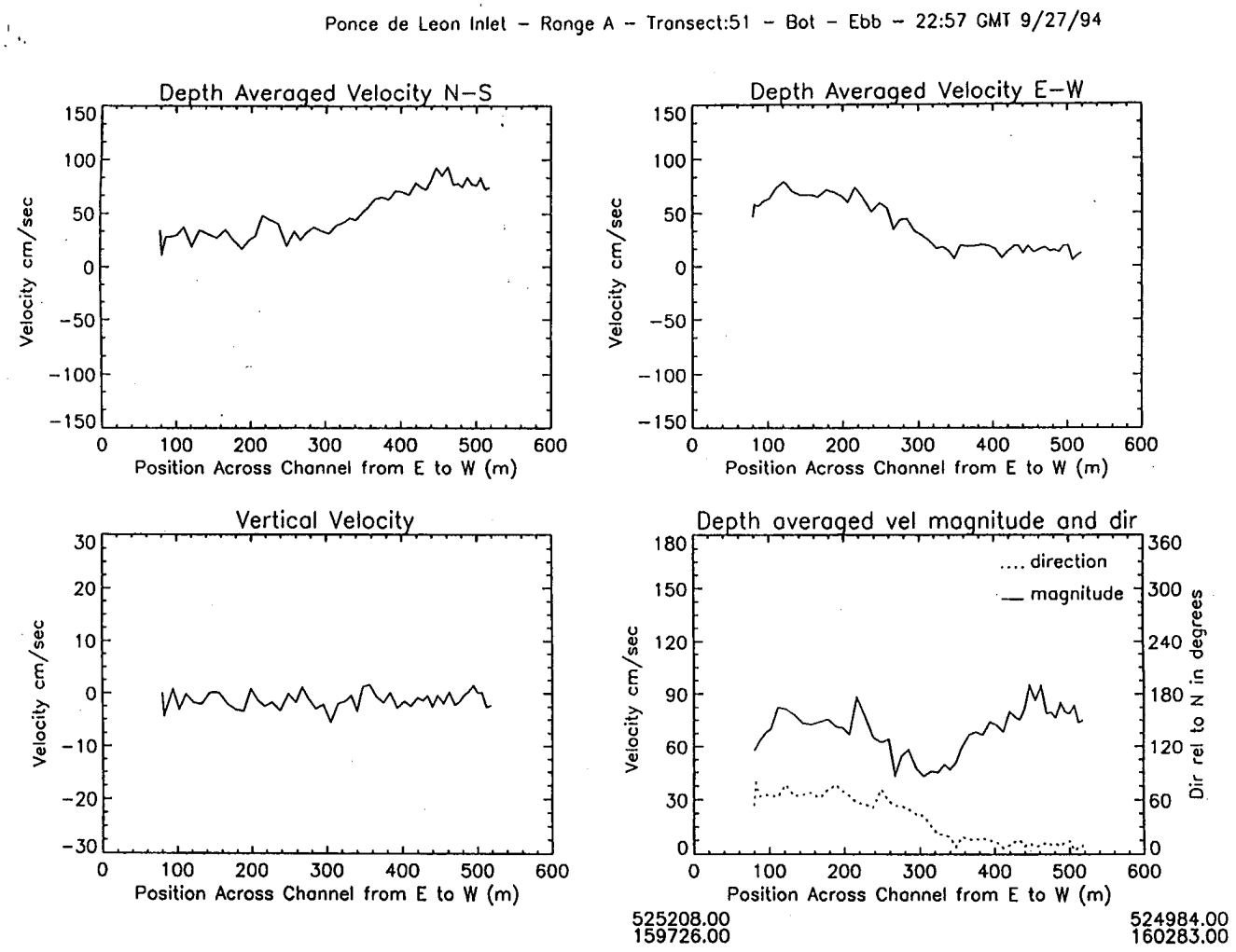

Figure B76. Depth average water velocities at peak ebb conditions, Range A, September

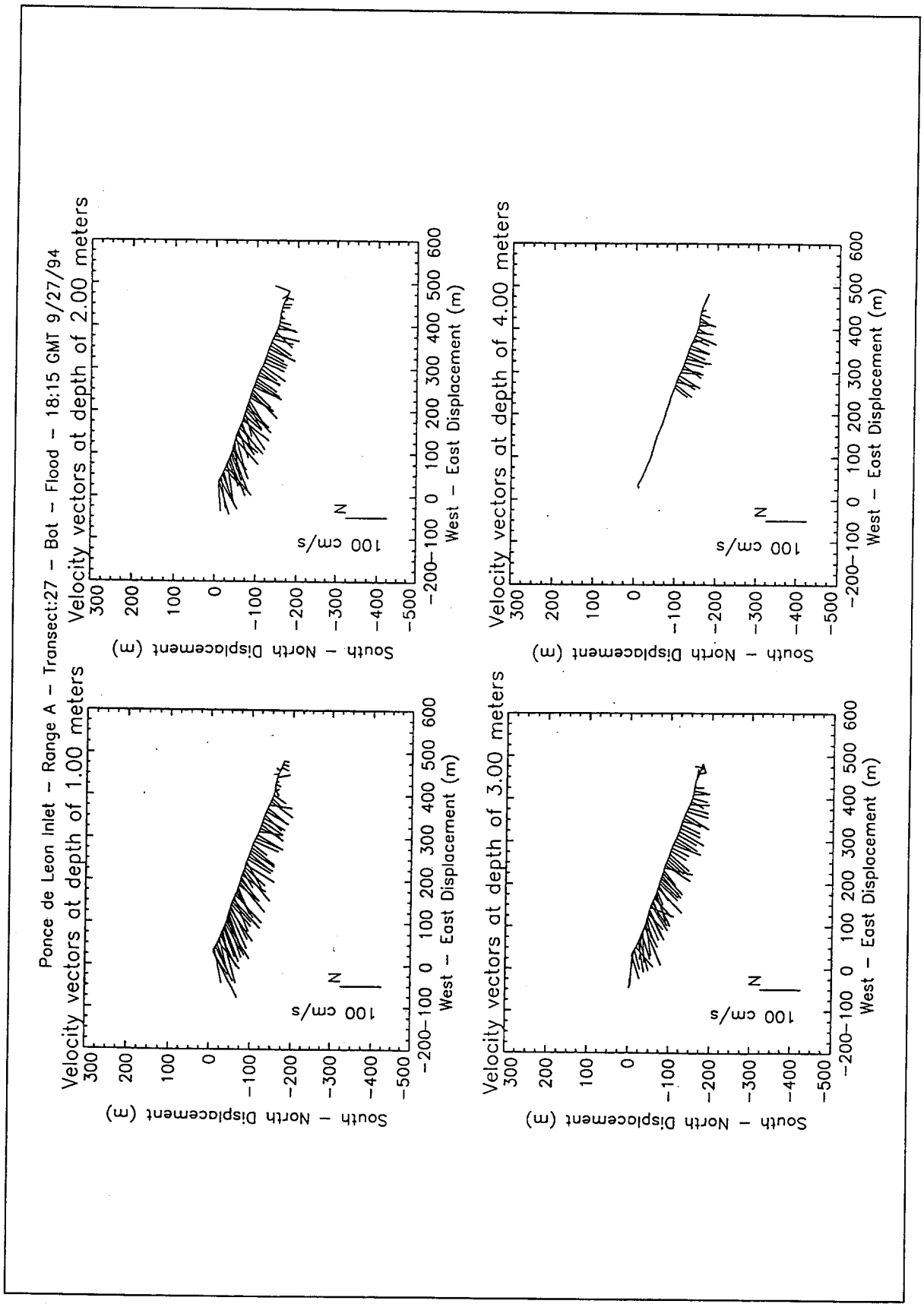

Figure B77. Velocity vector plots at peak flood conditions, Range A, September

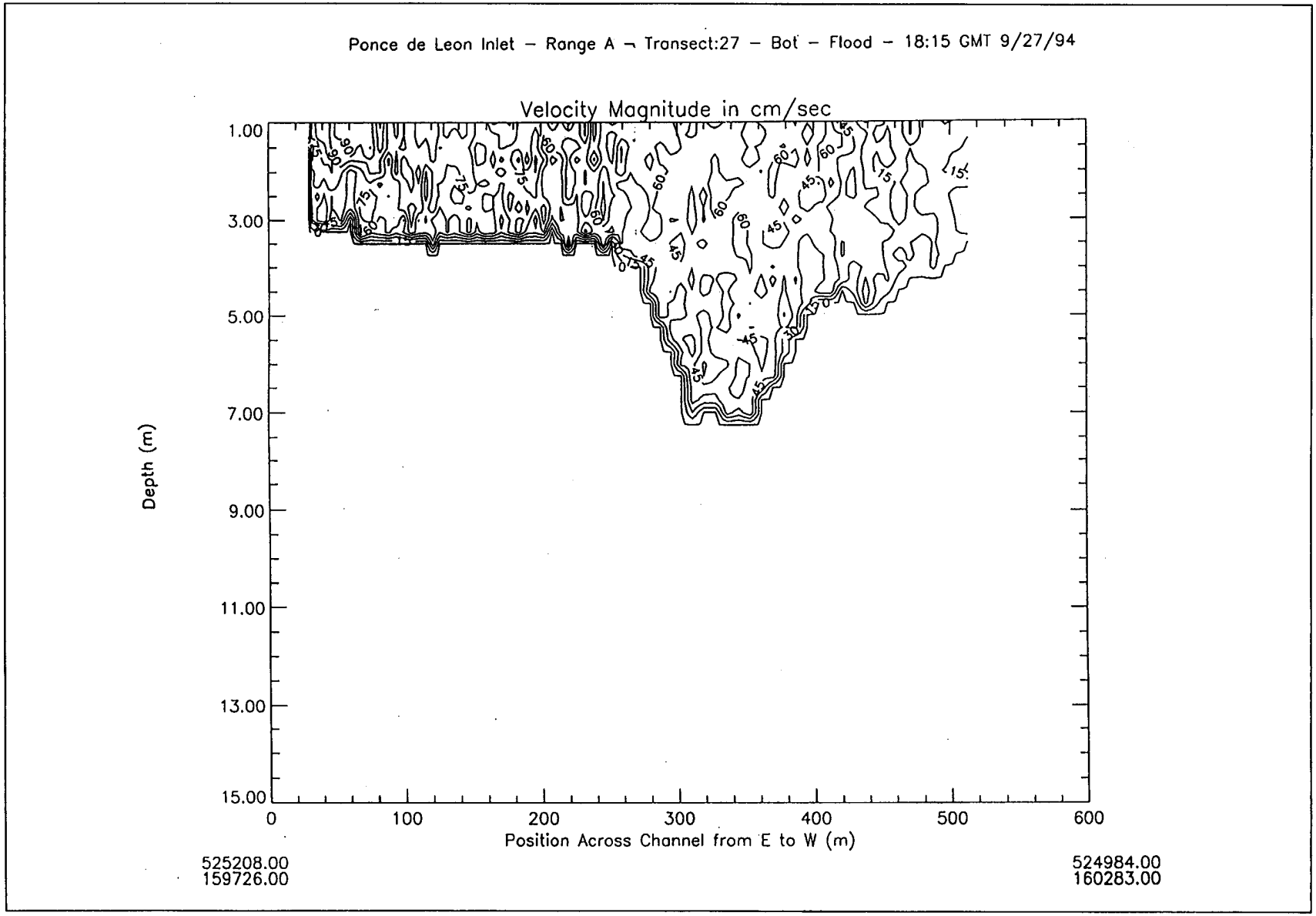

Figure B78. Contour plot of water magnitudes at peak flood conditions, Range A, September

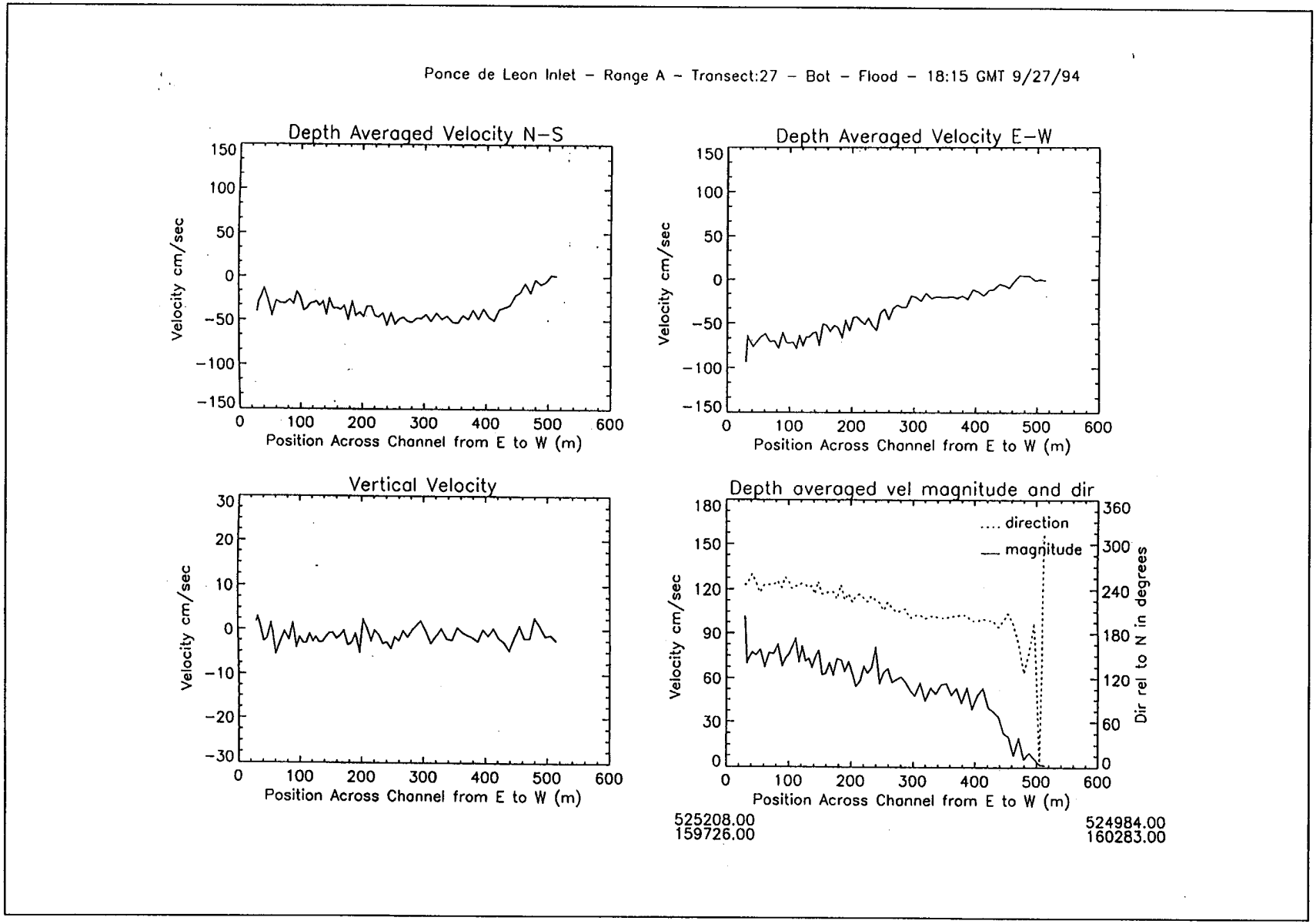

Figure B79. Depth average water velocities at peak flood conditions, Range A, September

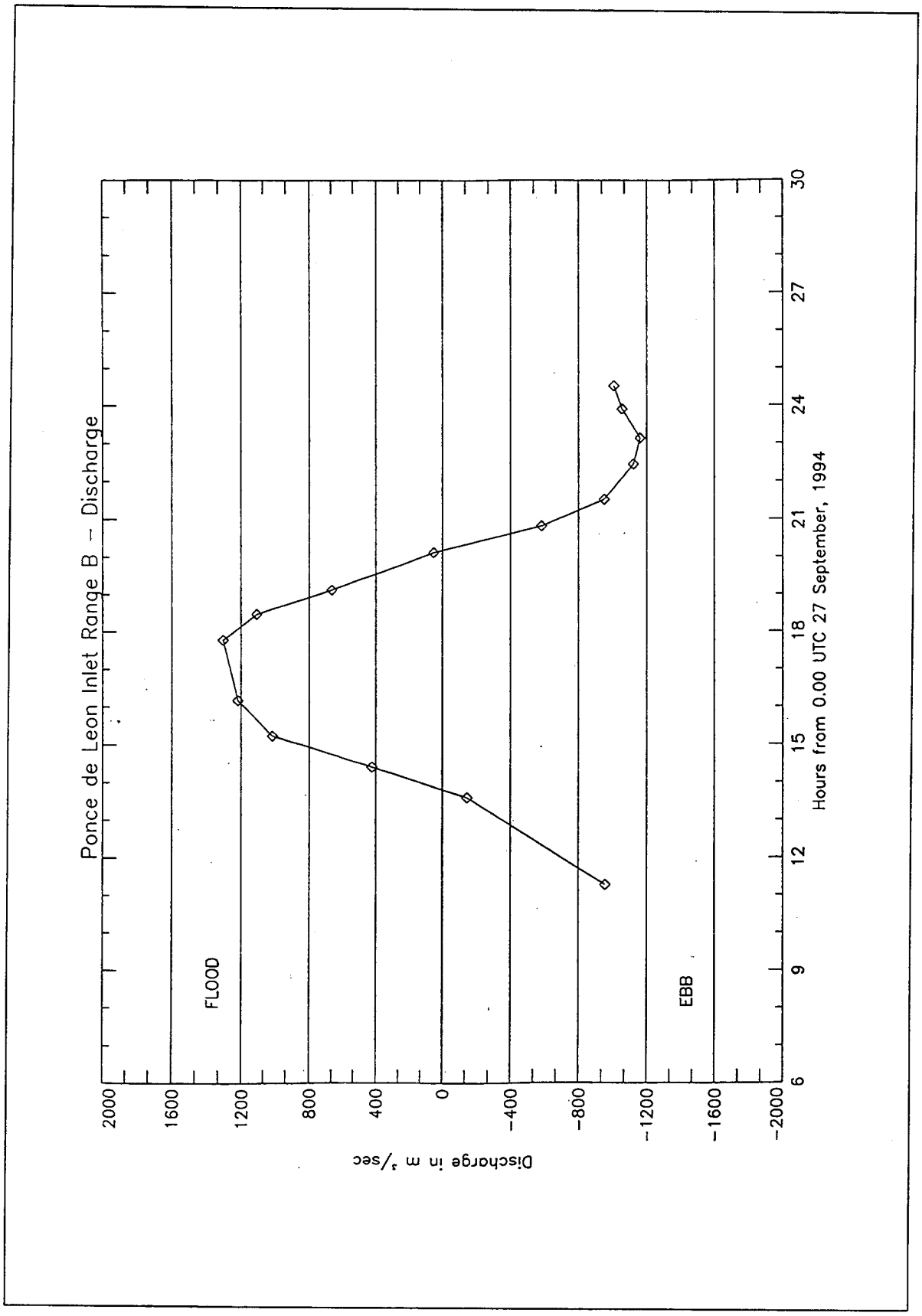

Figure B80. Discharge, Range B, September

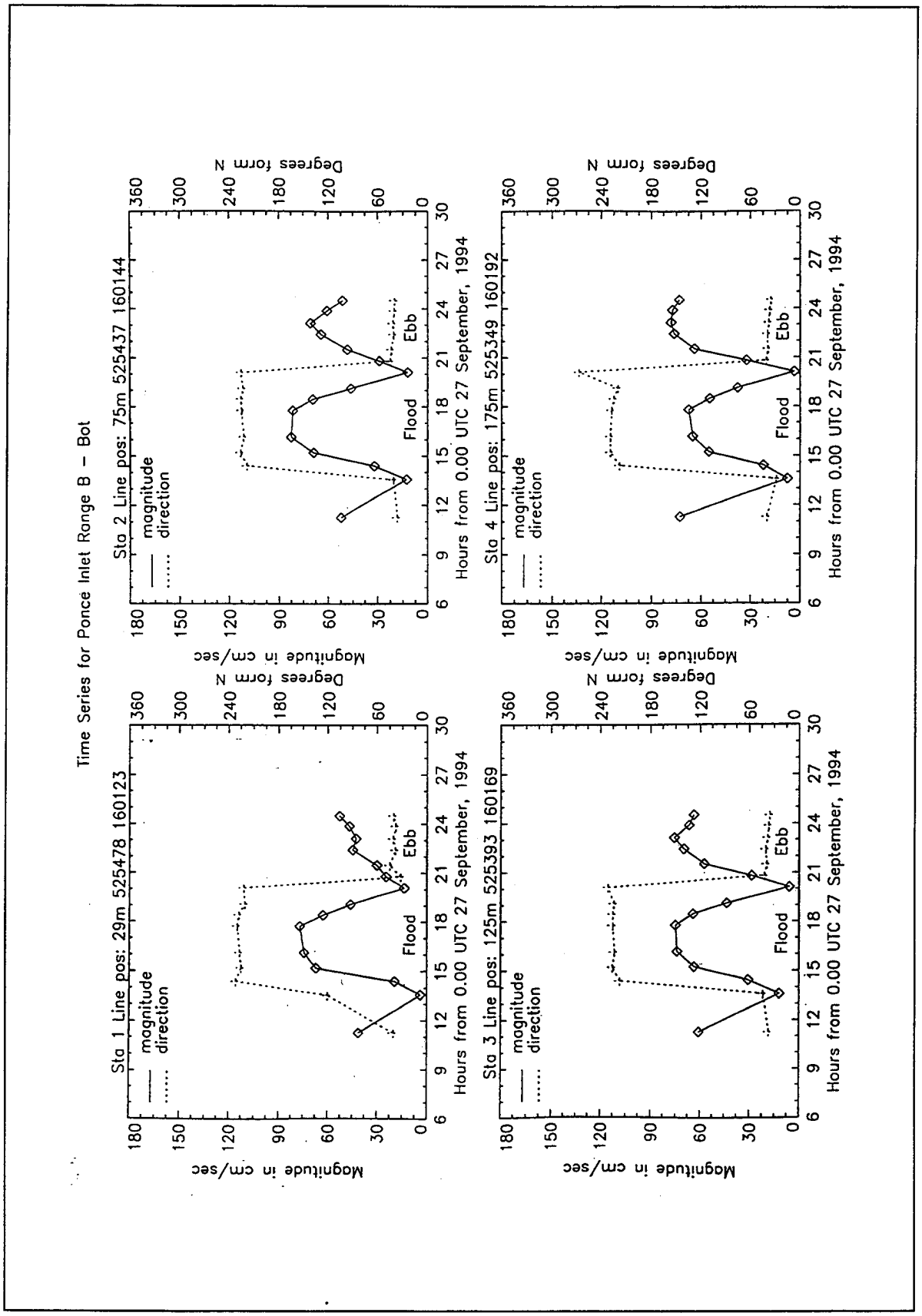

Figure B81. Time series, Range B, September, stations 1-4

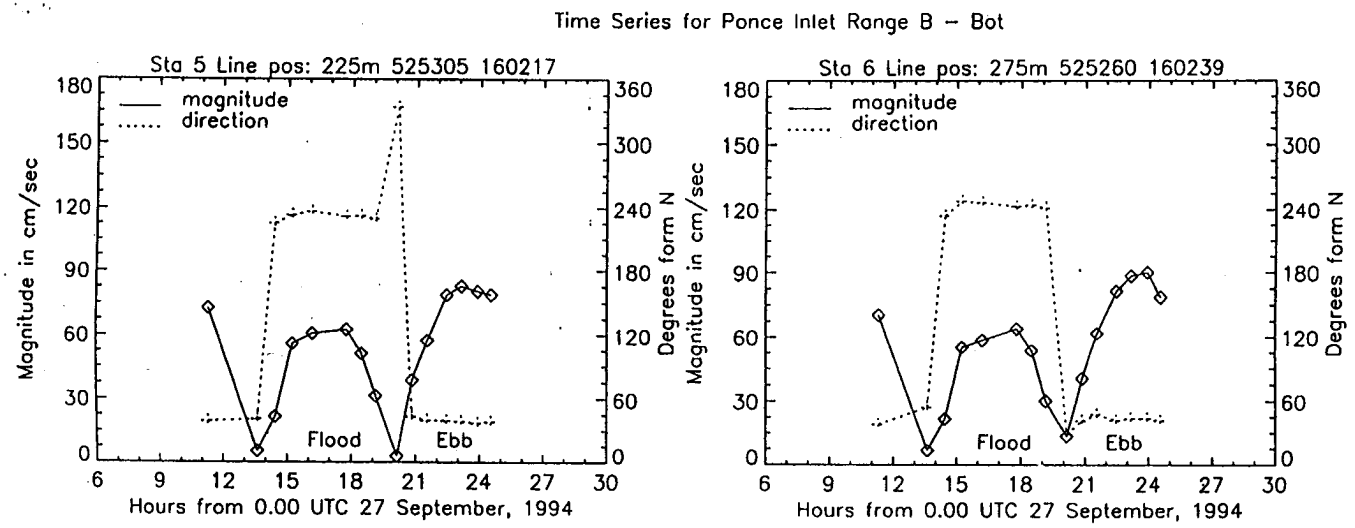

Figure B82. Time series, Range B, September, stations 5 and 6

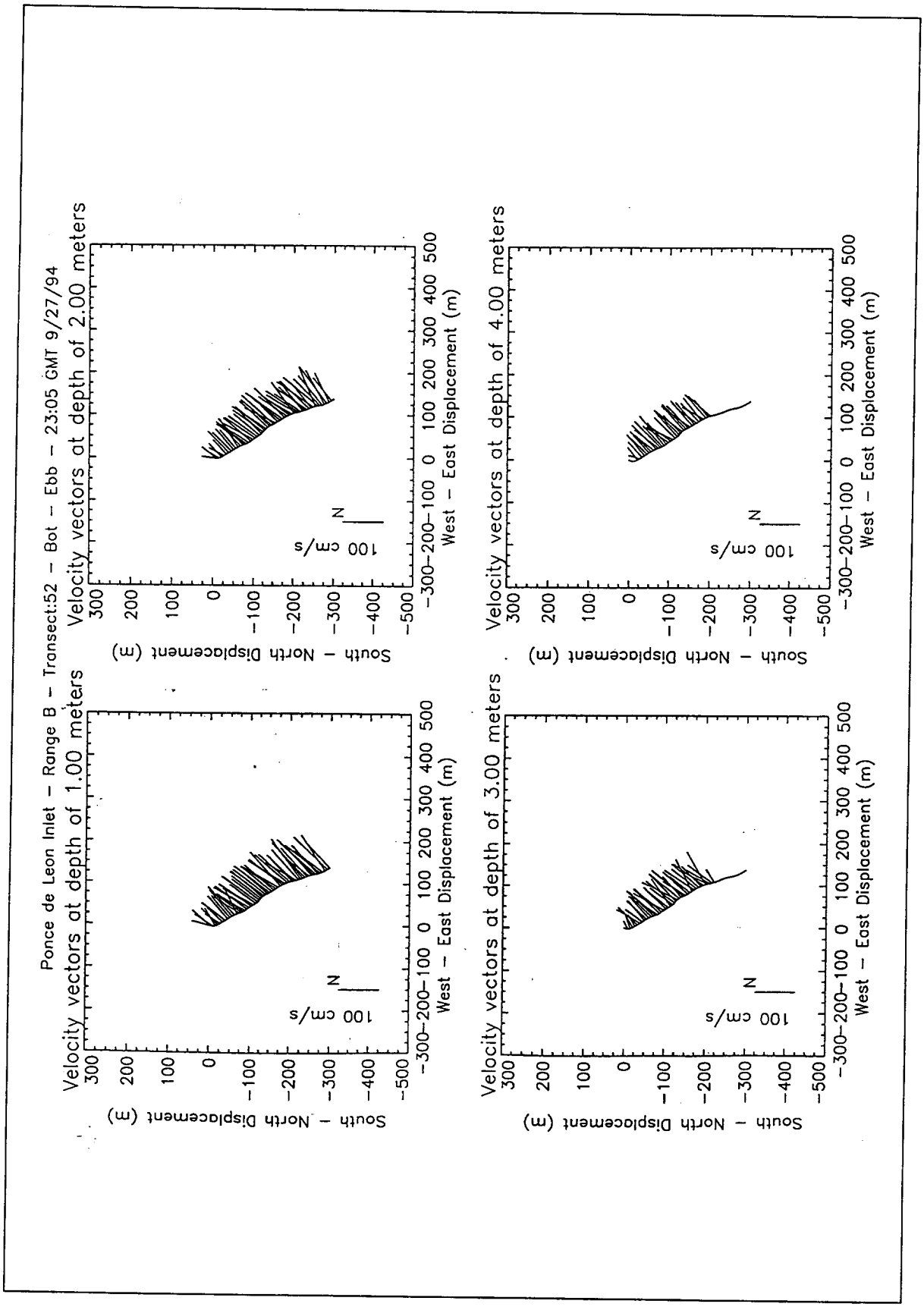

Figure B83. Velocity vector plots at peak ebb conditions, Range B, September

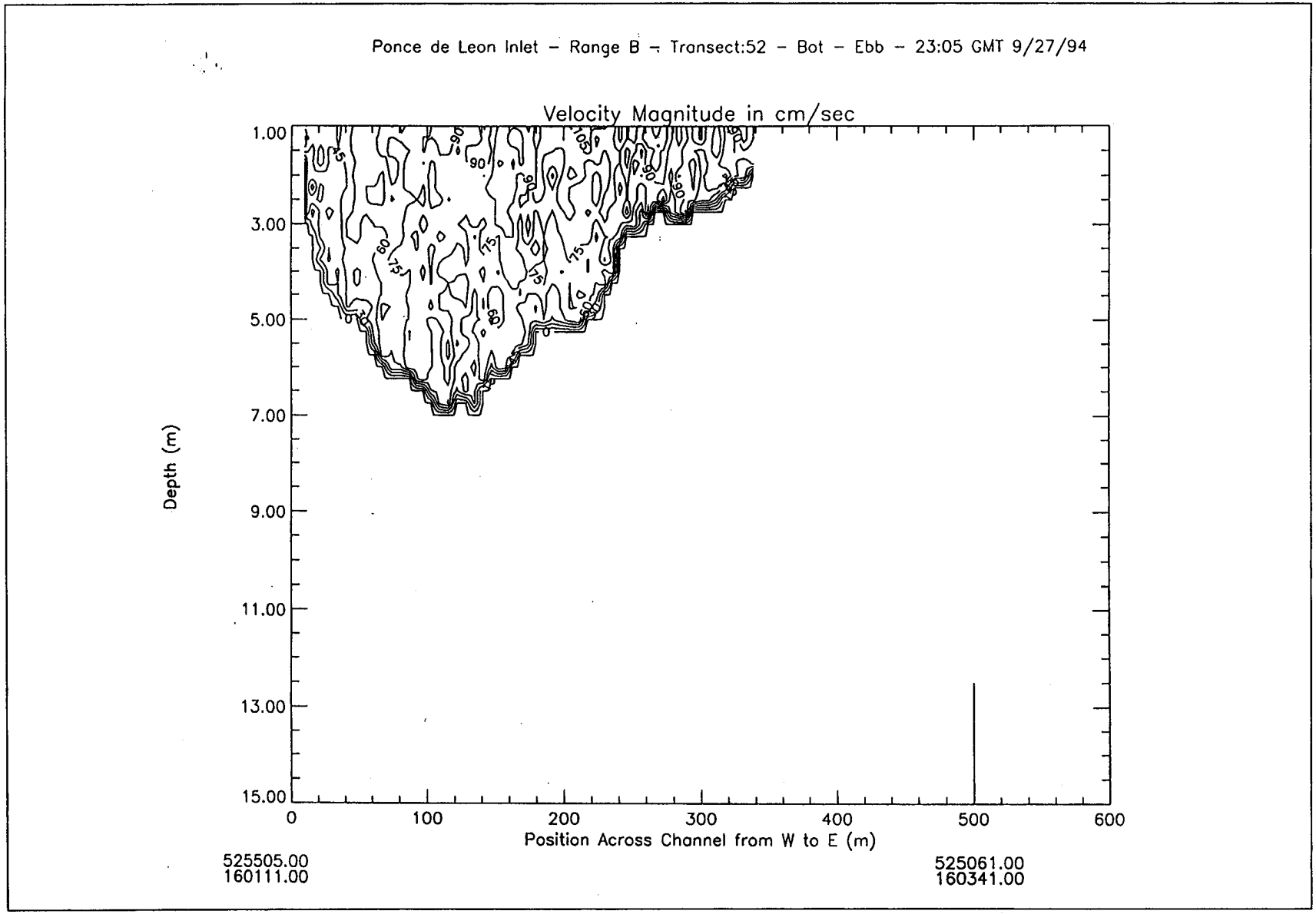

Figure B84. Contour plot of water magnitudes at peak ebb conditions, Range B, September

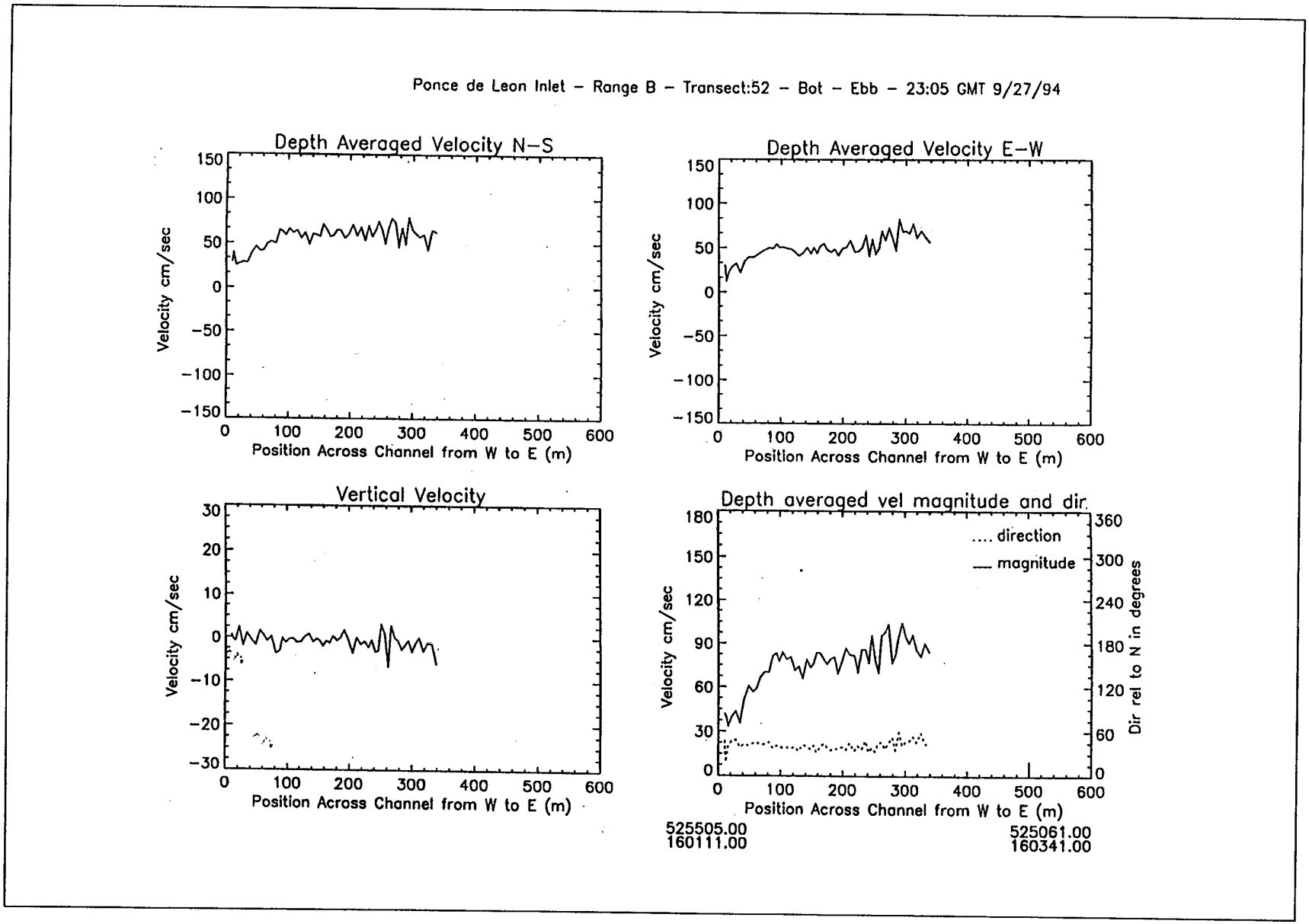

Figure B85. Depth average water velocities at peak ebb conditions, Range B, September

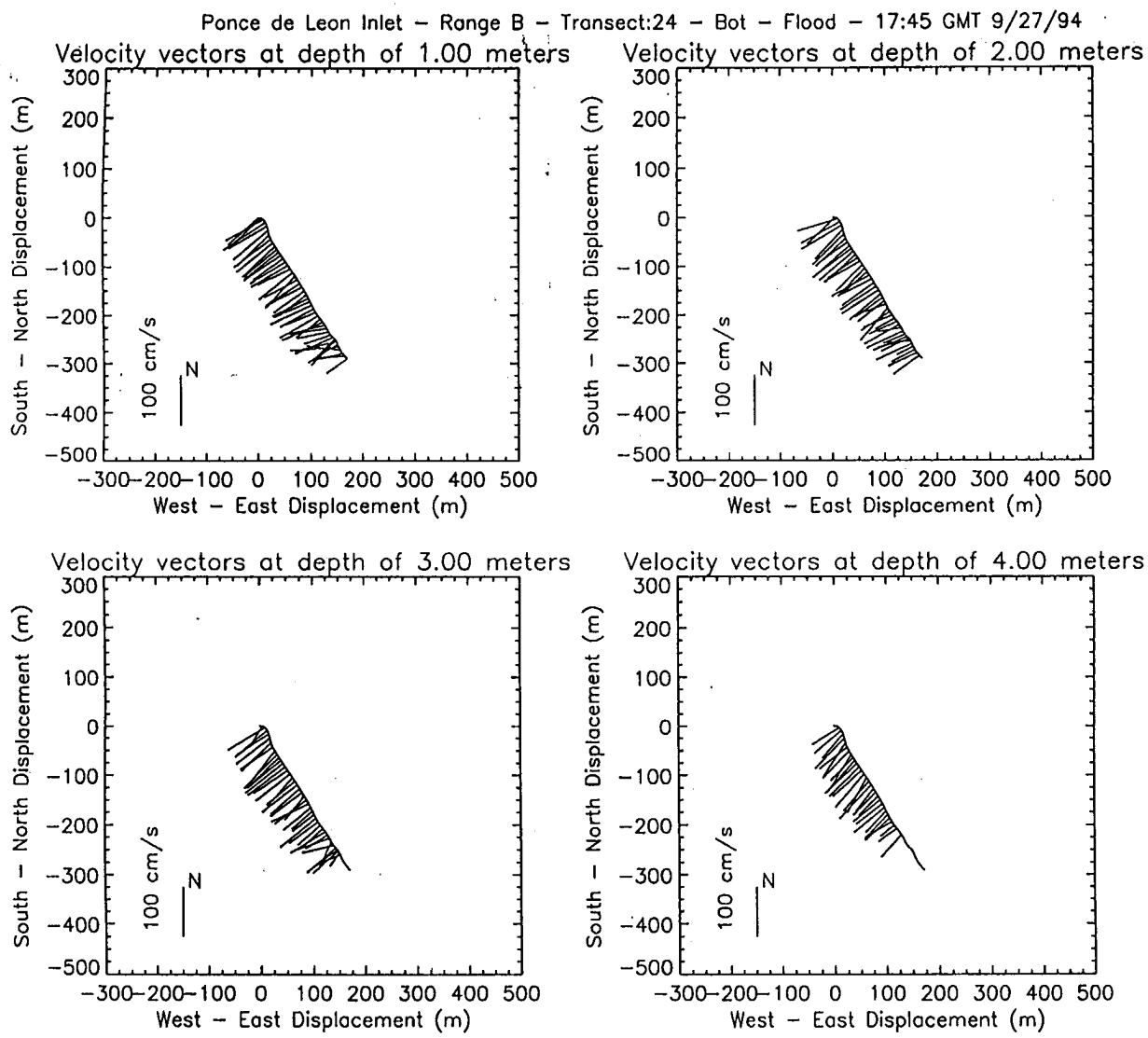

Figure B86. Velocity vector plots at peak flood conditions, Range B, September

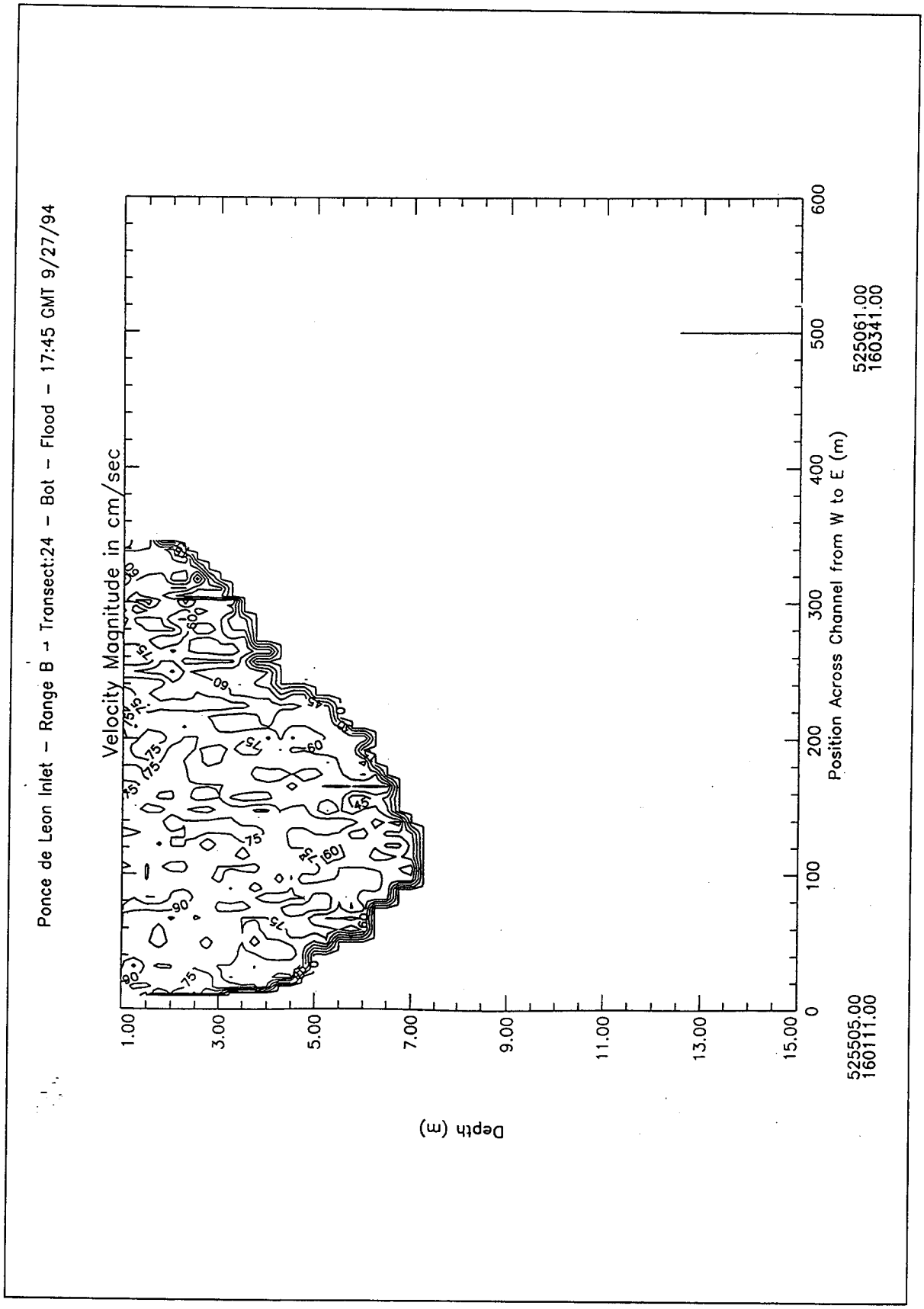

Figure B87. Contour plot of water magnitudes at peak flood conditions, Range B, September

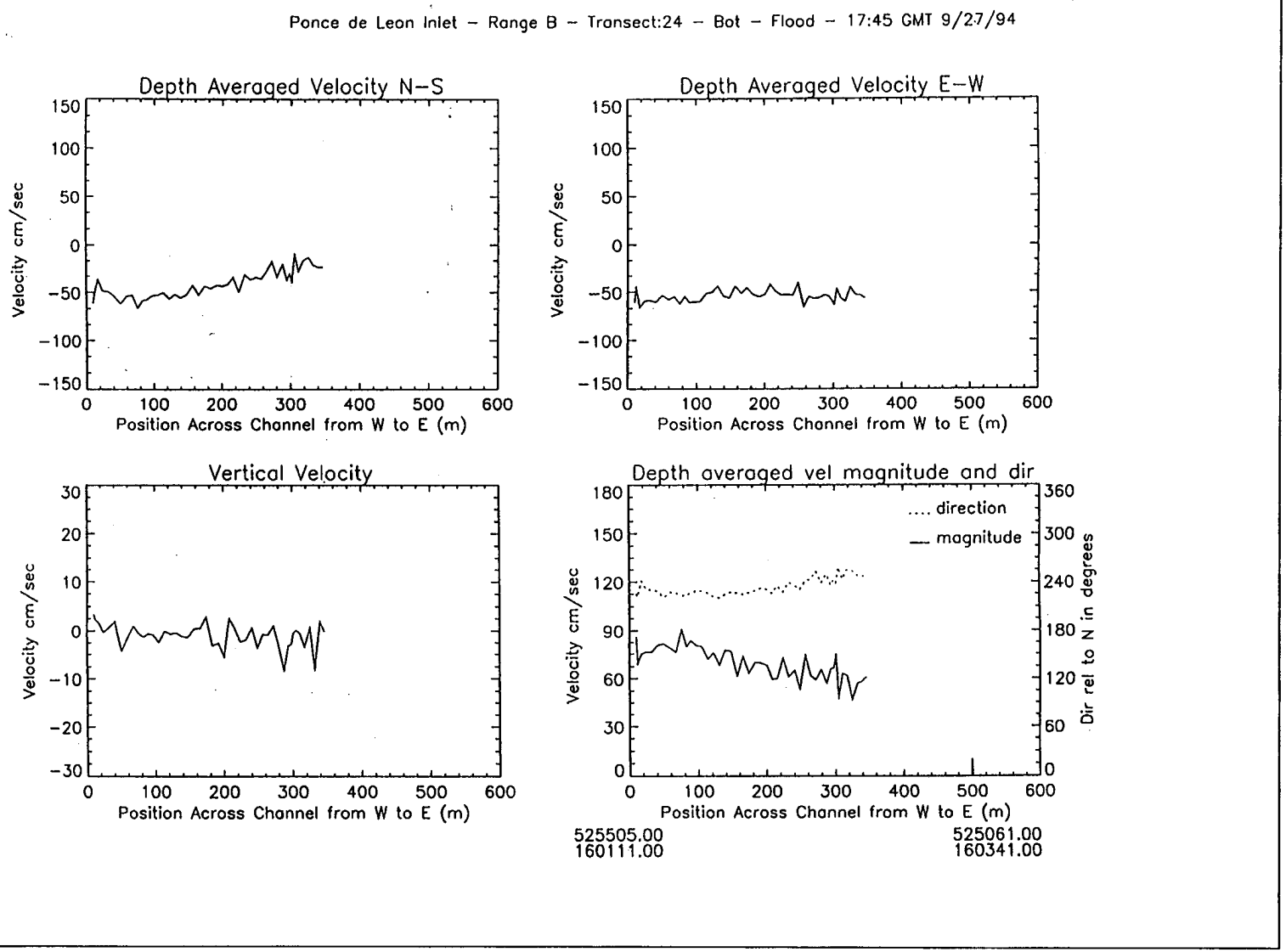

Figure B88. Depth average water velocities at peak flood conditions, Range B, September

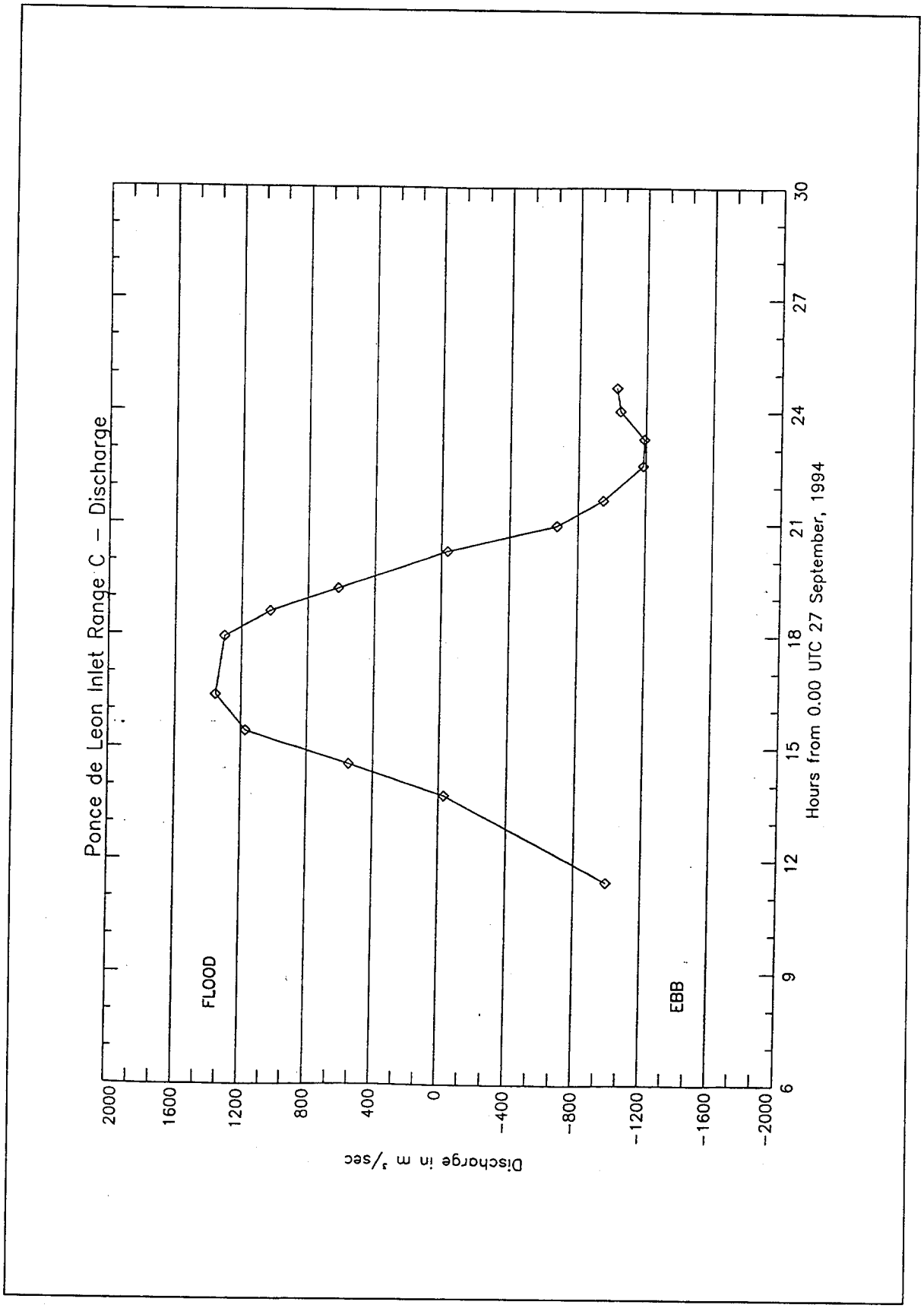

Figure B89. Discharge, Range C, September

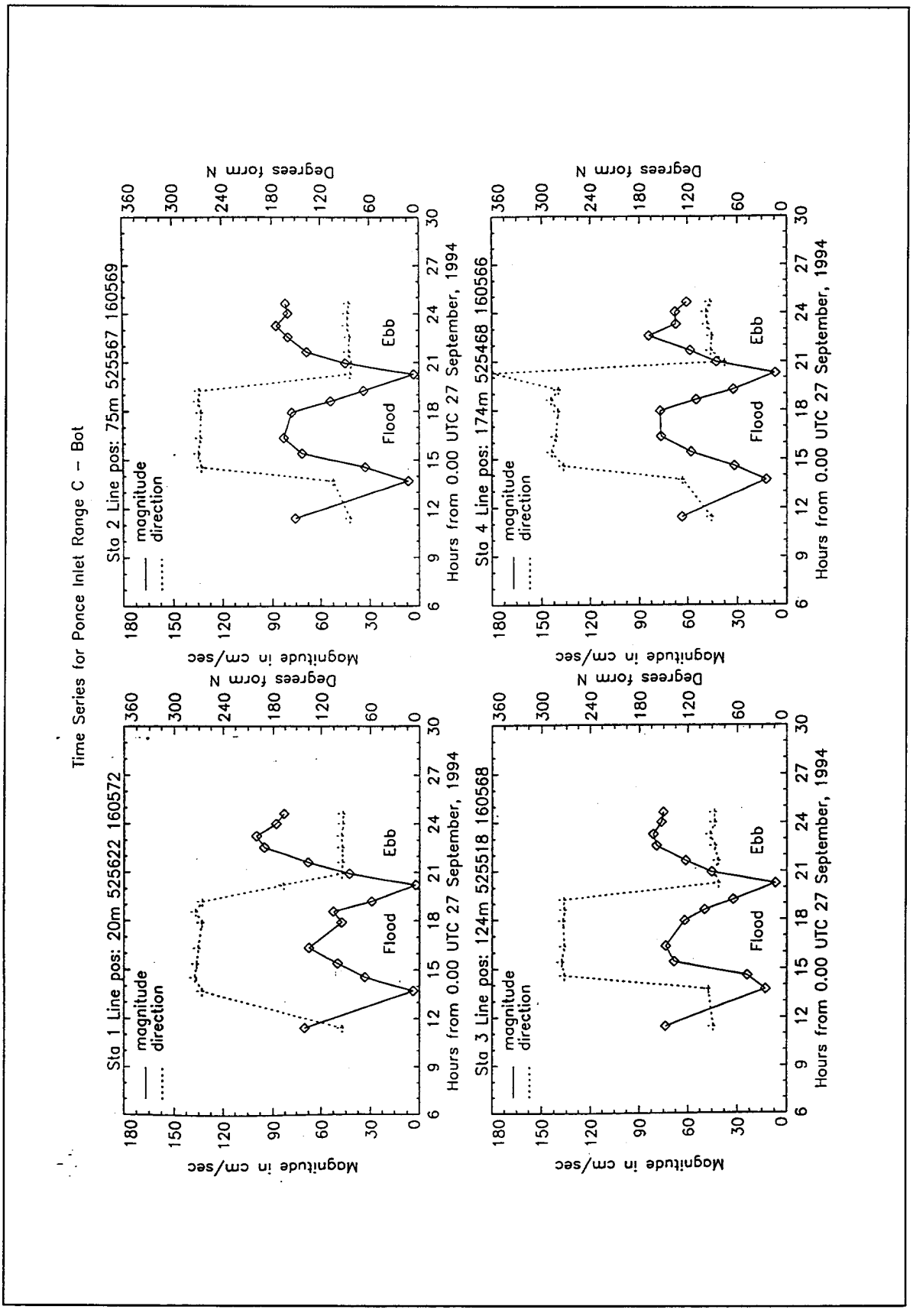

Figure B90. Time series, Range C, September, stations 1-4

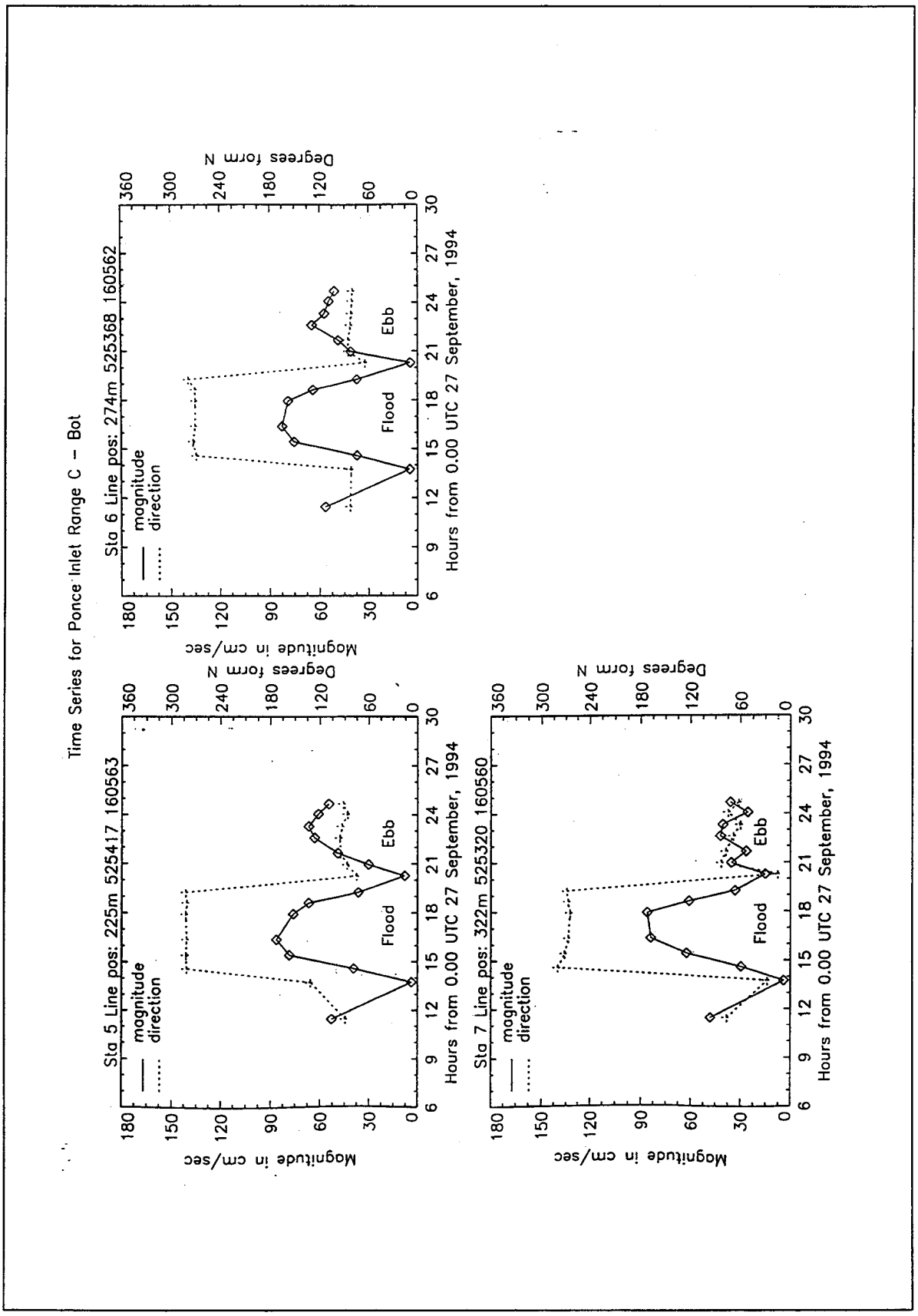

Figure B91. Time series, Range C, September, stations 5-7

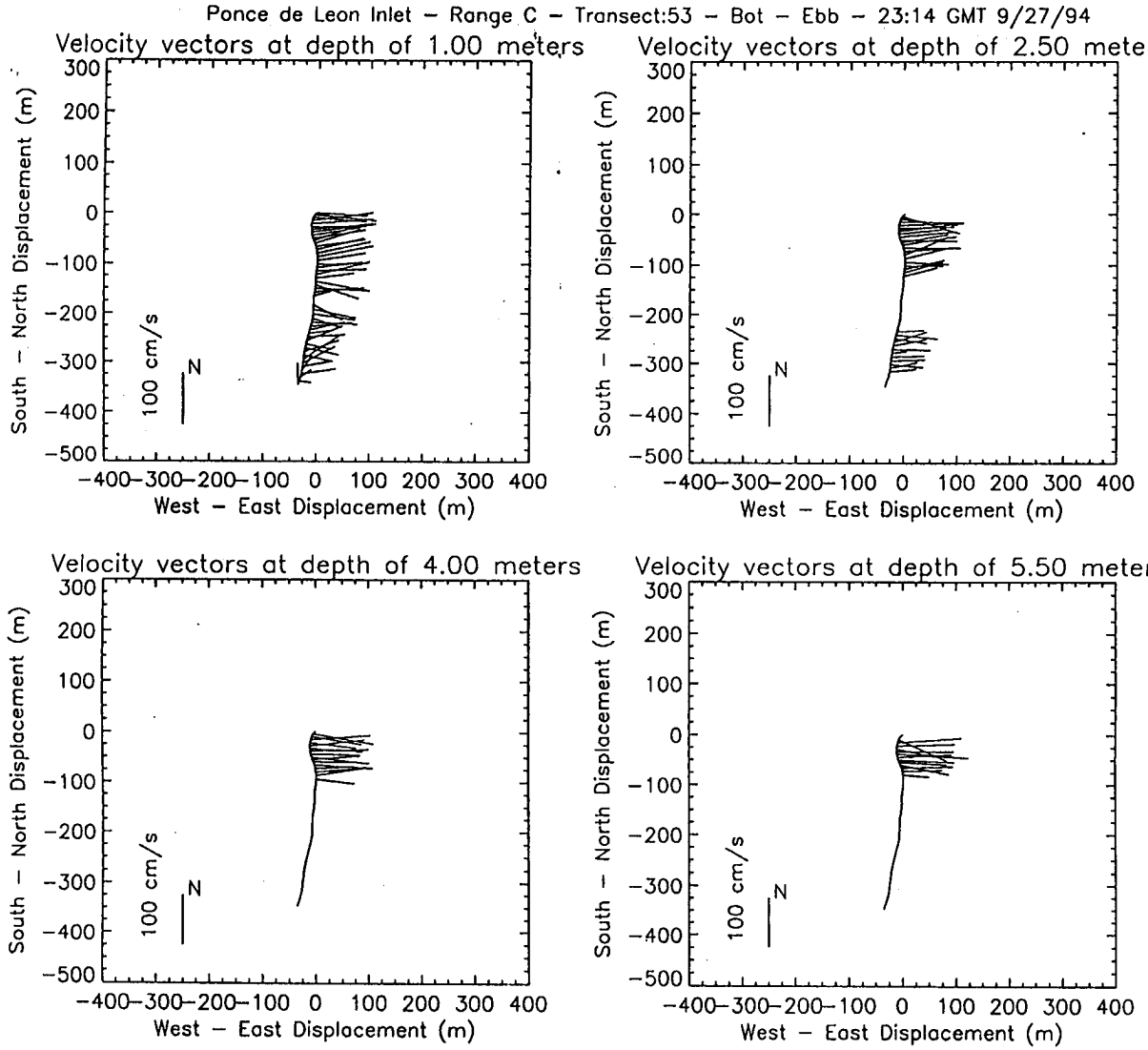

Figure B92. Velocity vector plots at peak ebb conditions, Range C, September

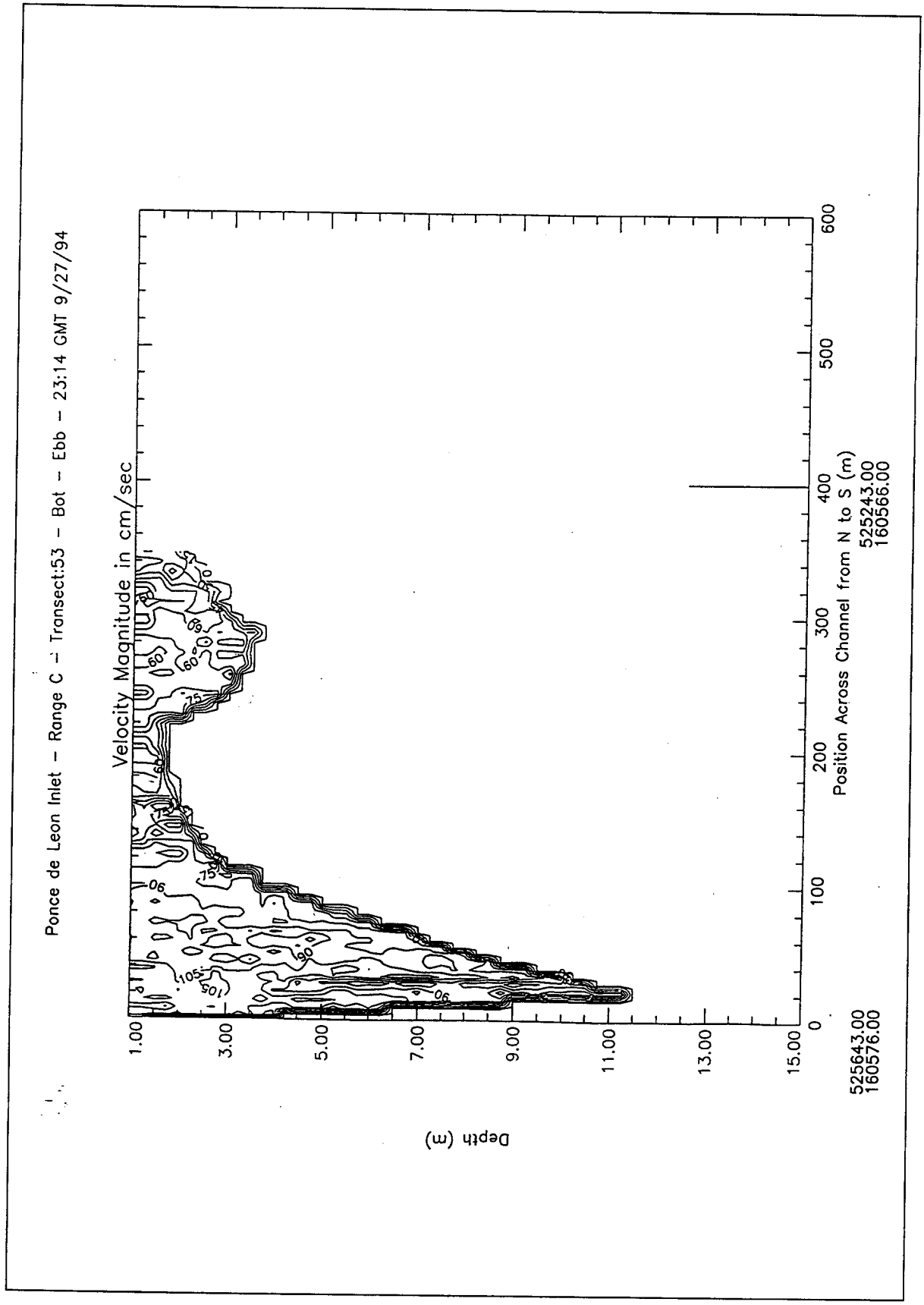

Figure B93. Contour plot of water magnitudes at peak ebb conditions, Range C, September

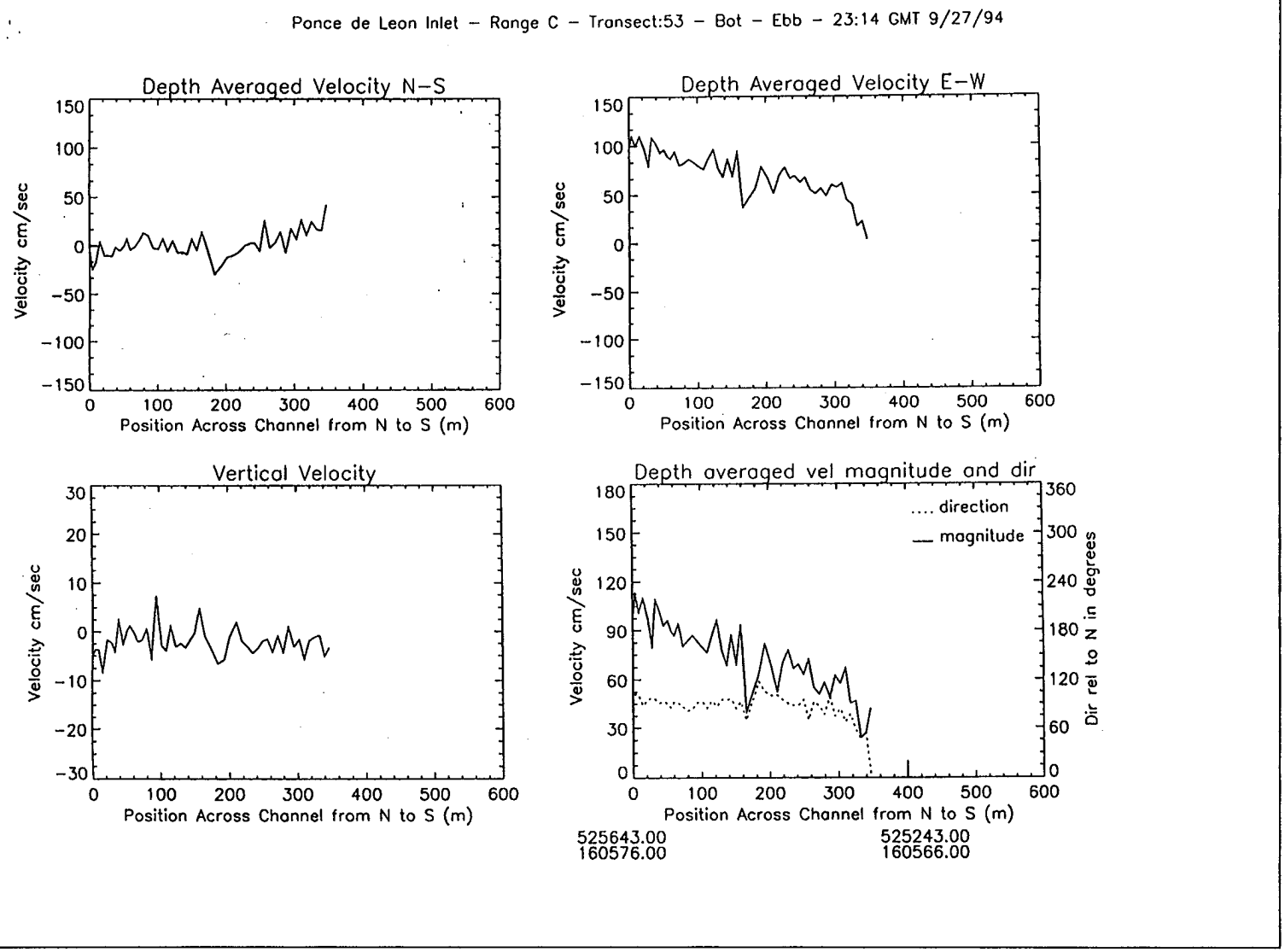

Figure B94. Depth average water velocities at peak ebb conditions, Range C, September

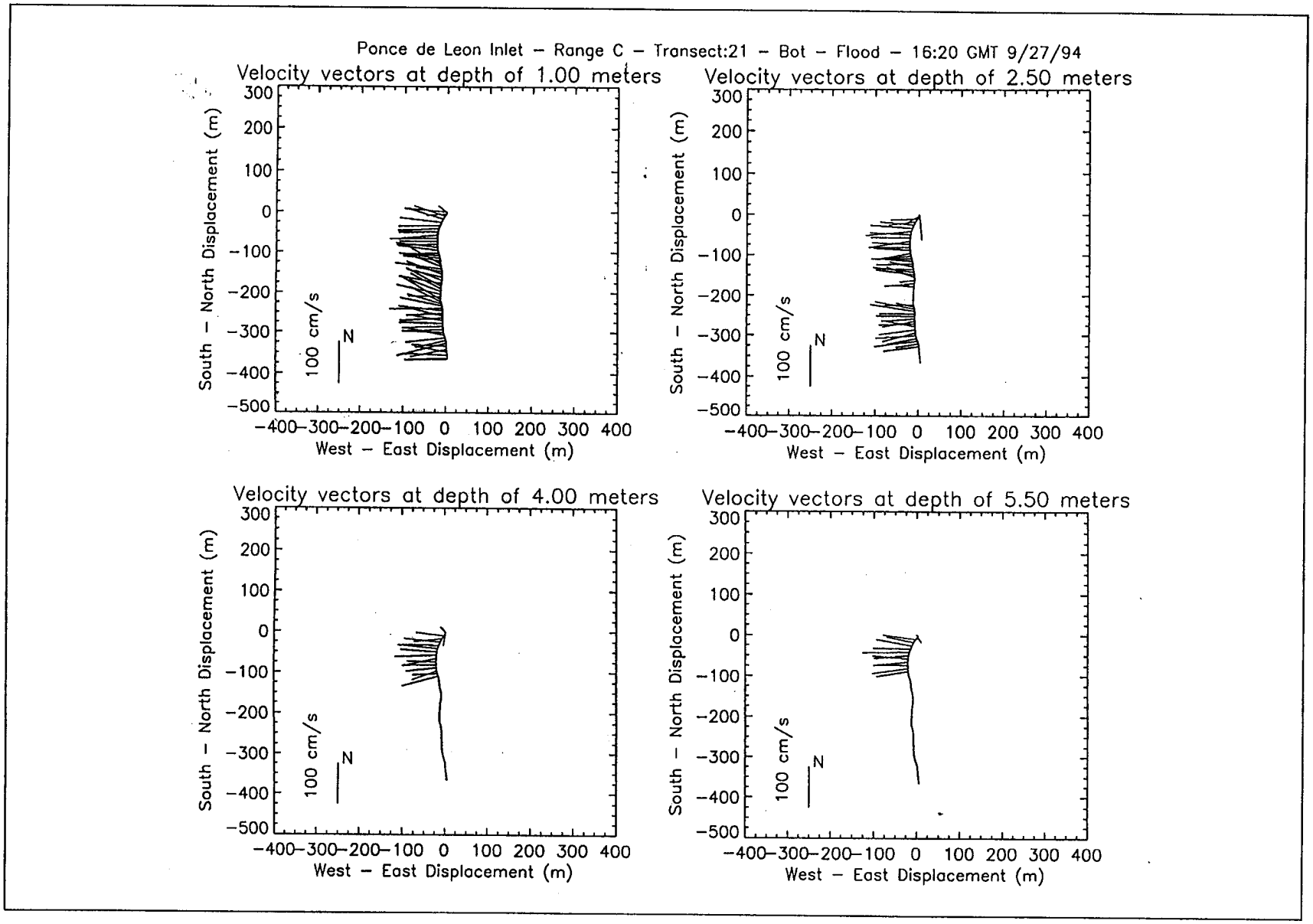

Figure B95. Velocity vector plots at peak flood conditions, Range C, September

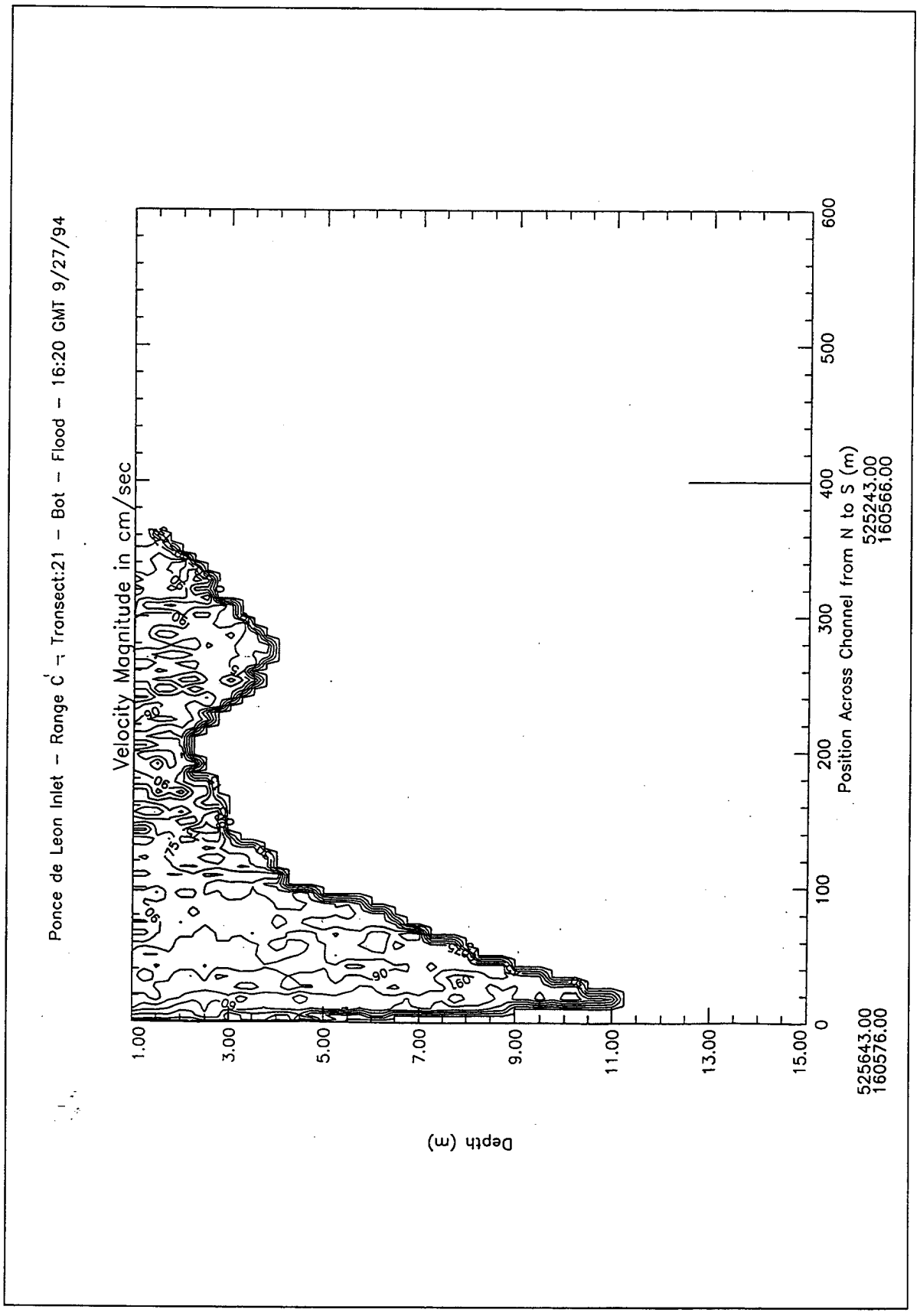

Figure B96. Contour plot of water magnitudes at peak flood conditions, Range C, September

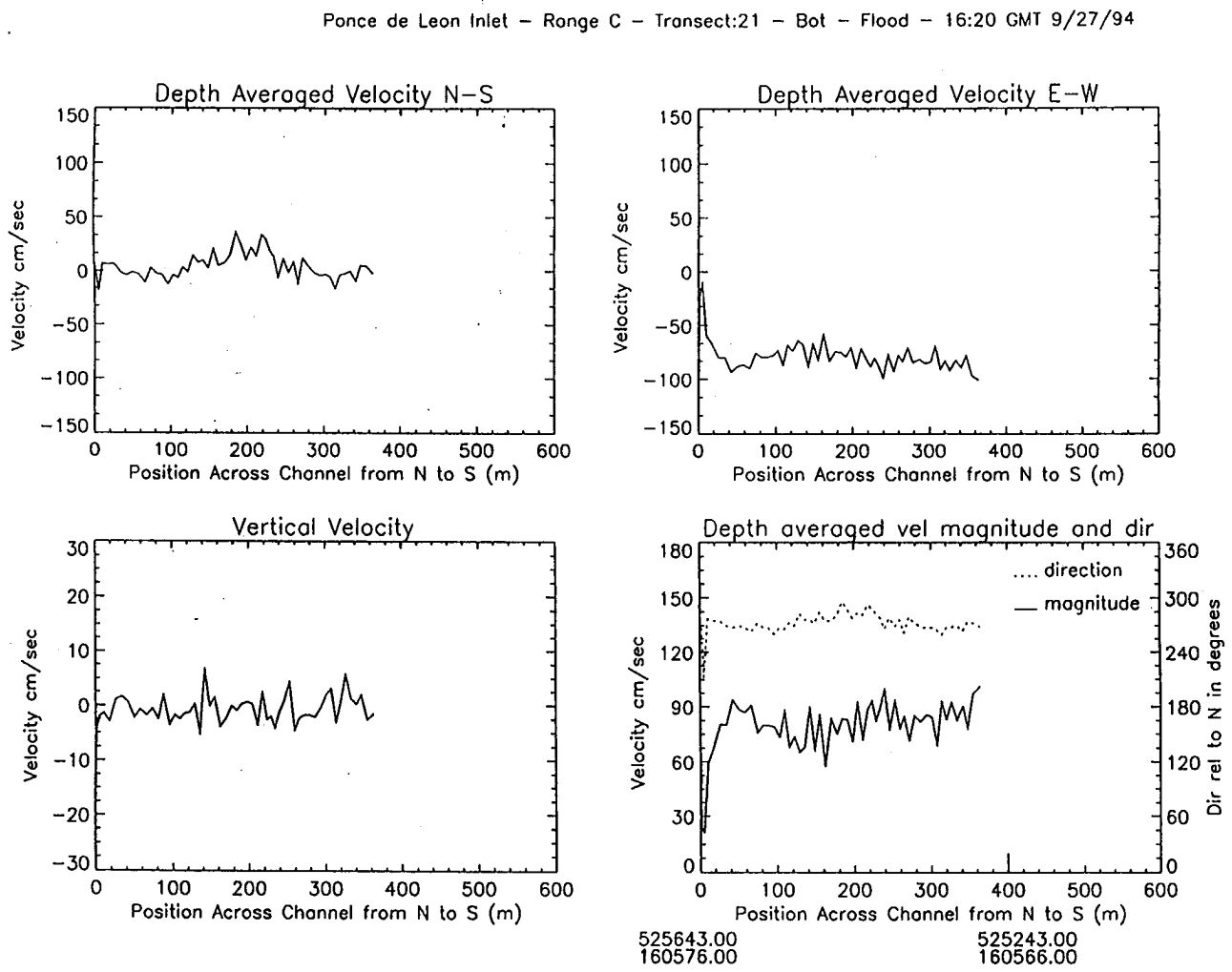

Figure B97. Depth average water velocities at peak flood conditions, Range C, September

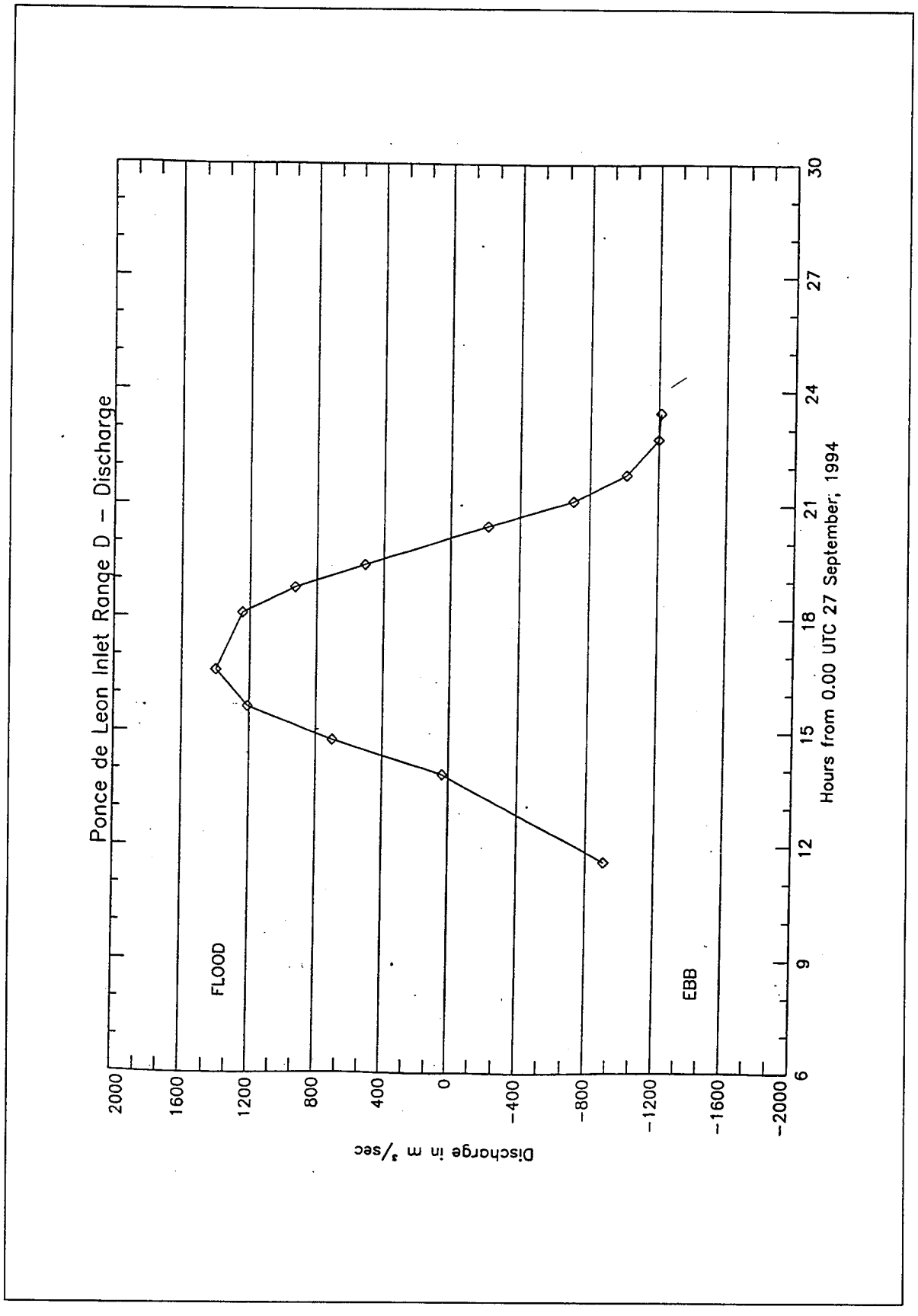

Figure B98. Discharge, Range D, September

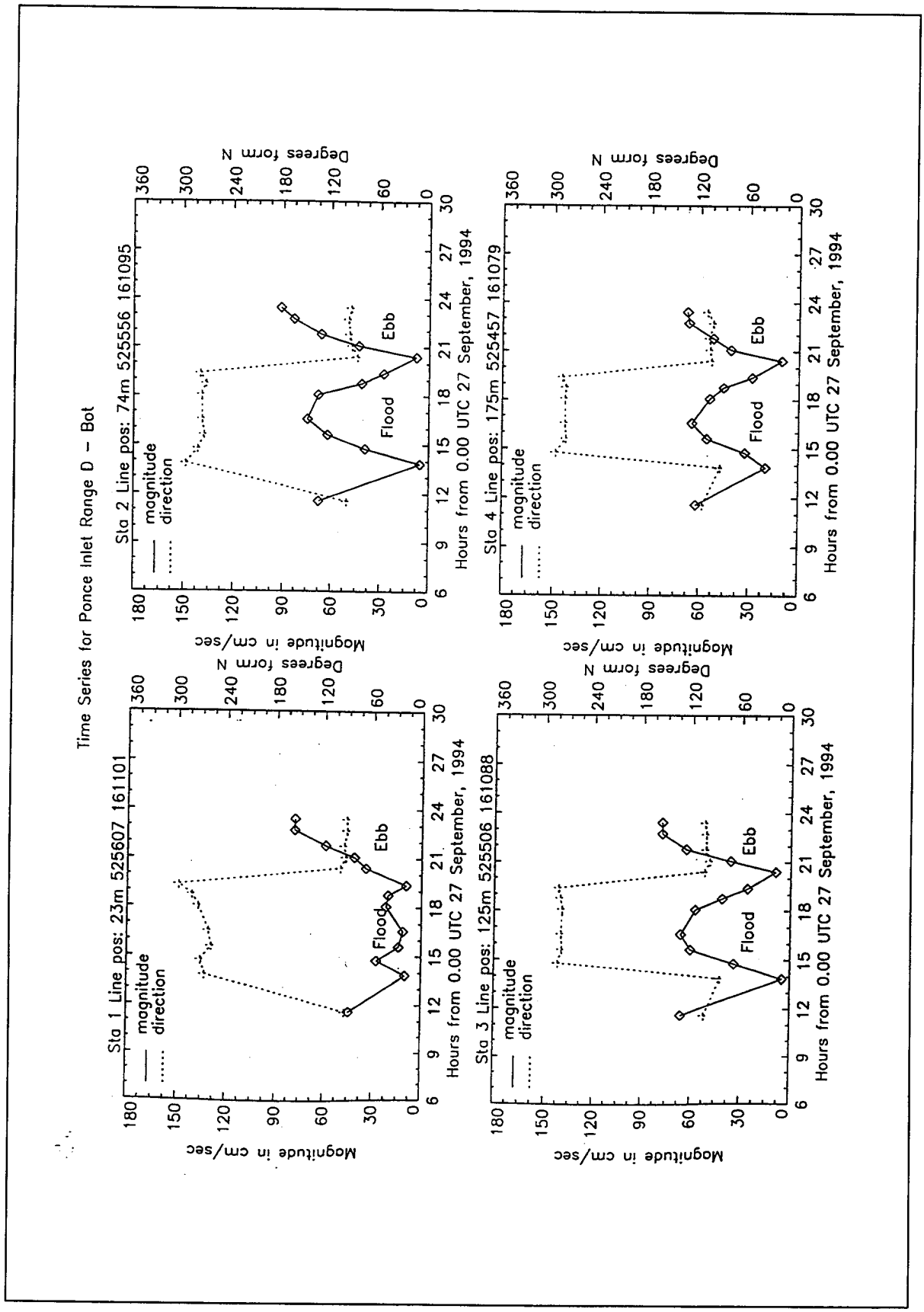

Figure B99. Time series, Range D, September, stations 1-4

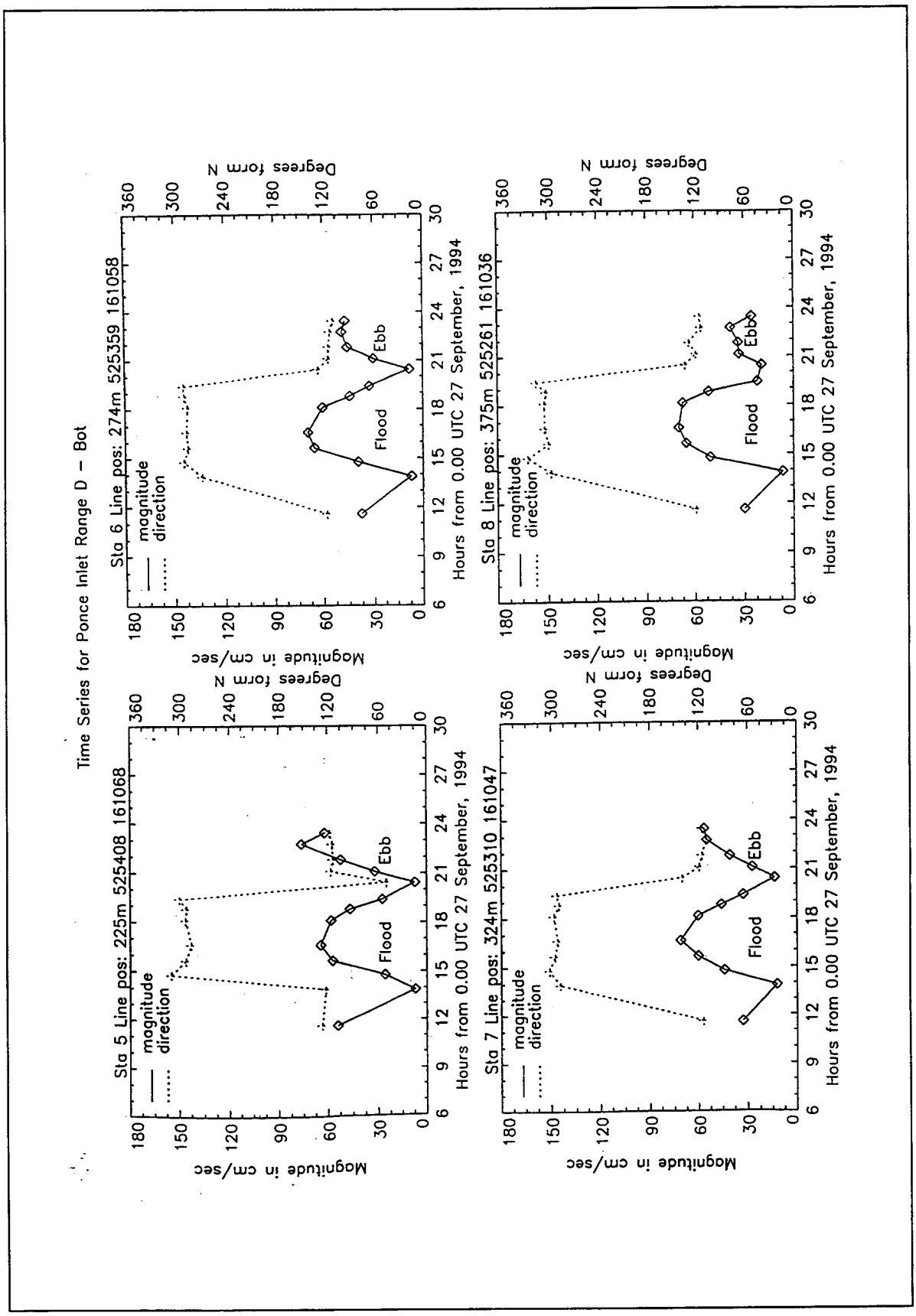

Figure B100. Time series, Range D, September, stations 5-8

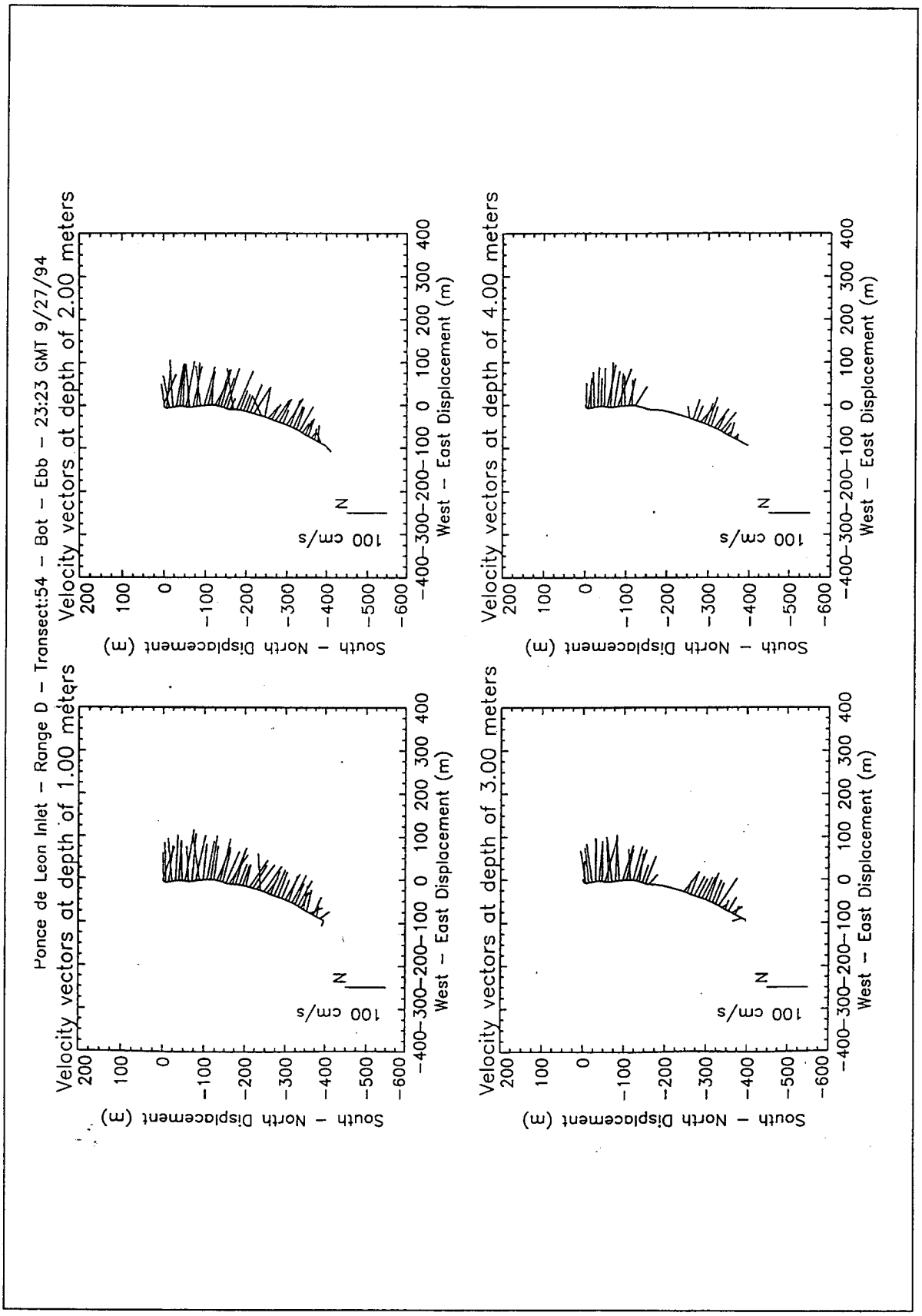

Figure B101. Velocity vector plots at peak ebb conditions, Range D, September

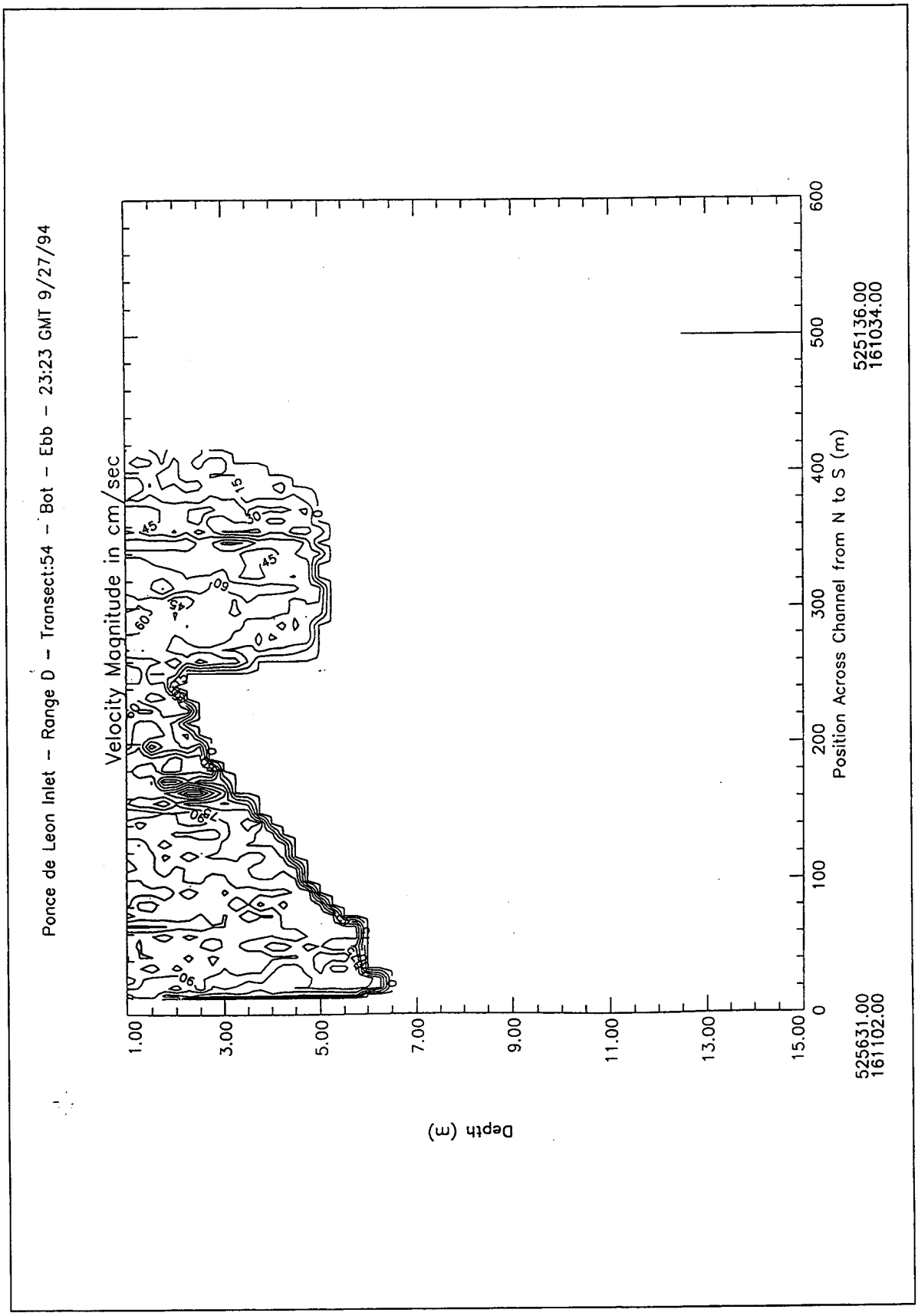

Figure B102. Contour plot of water magnitudes at peak ebb conditions, Range D, September

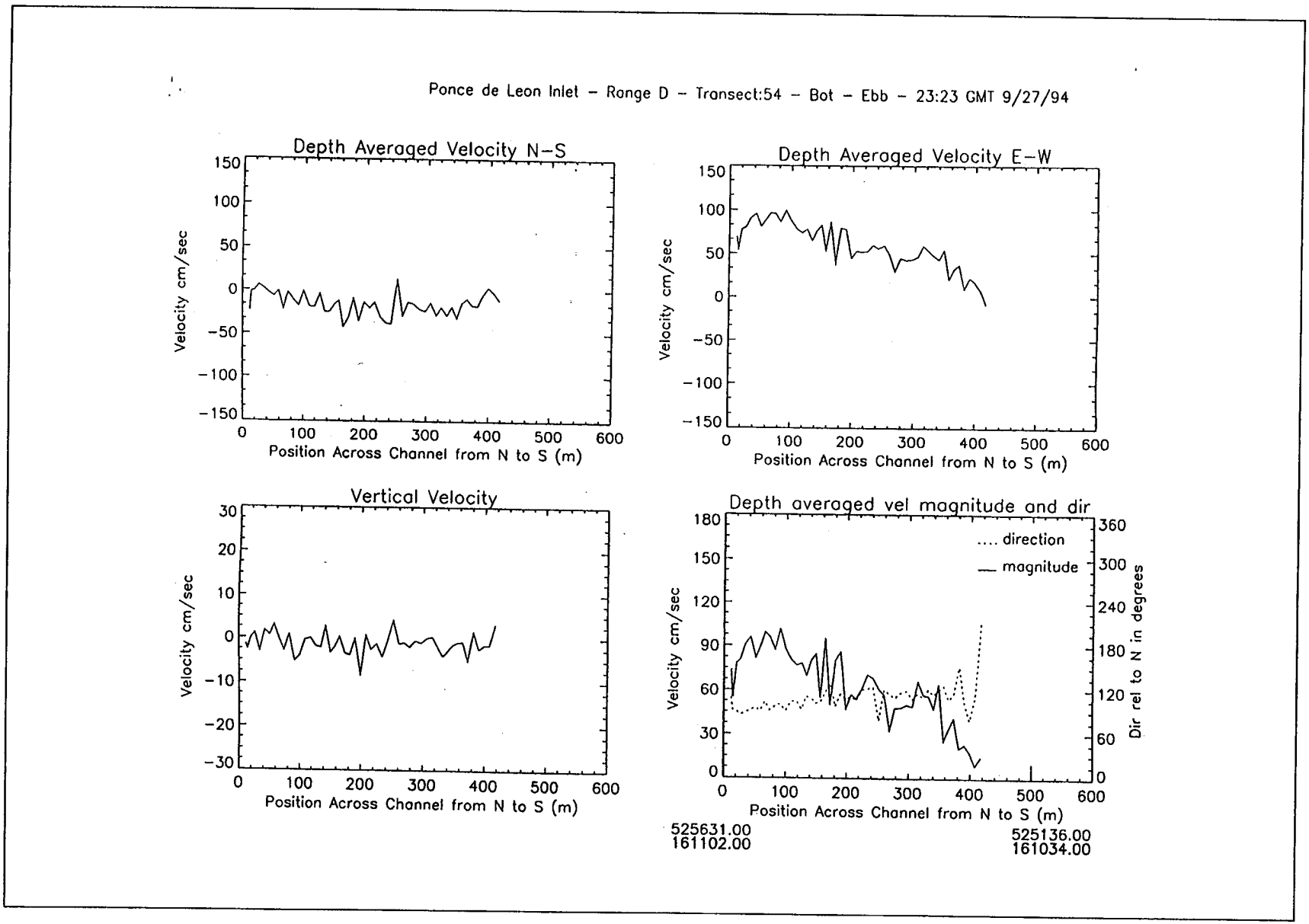

Figure B103. Depth average water velocities at peak ebb conditions, Range D, September

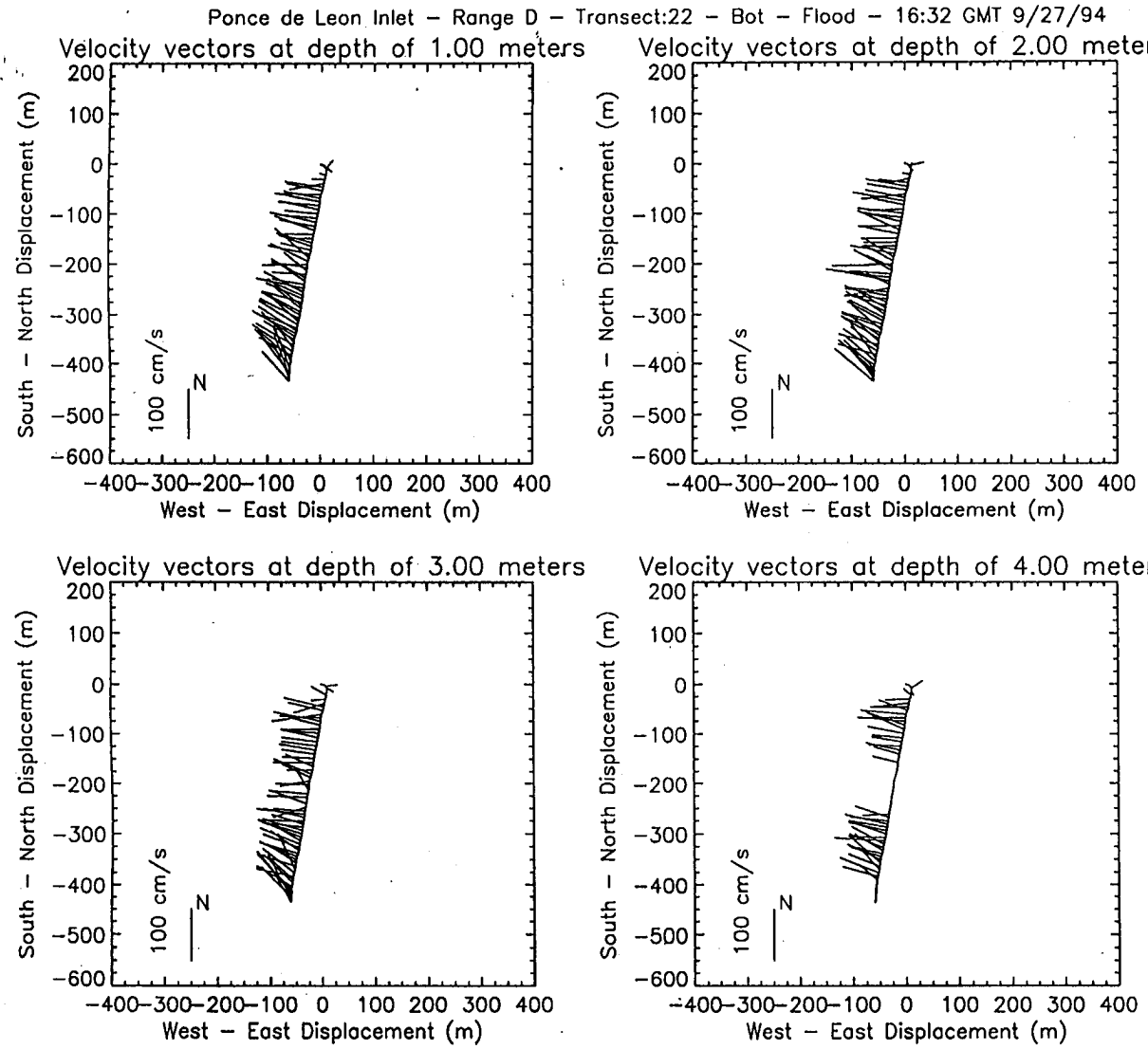

Figure B104. Velocity vector plots at peak flood conditions, Range D, September

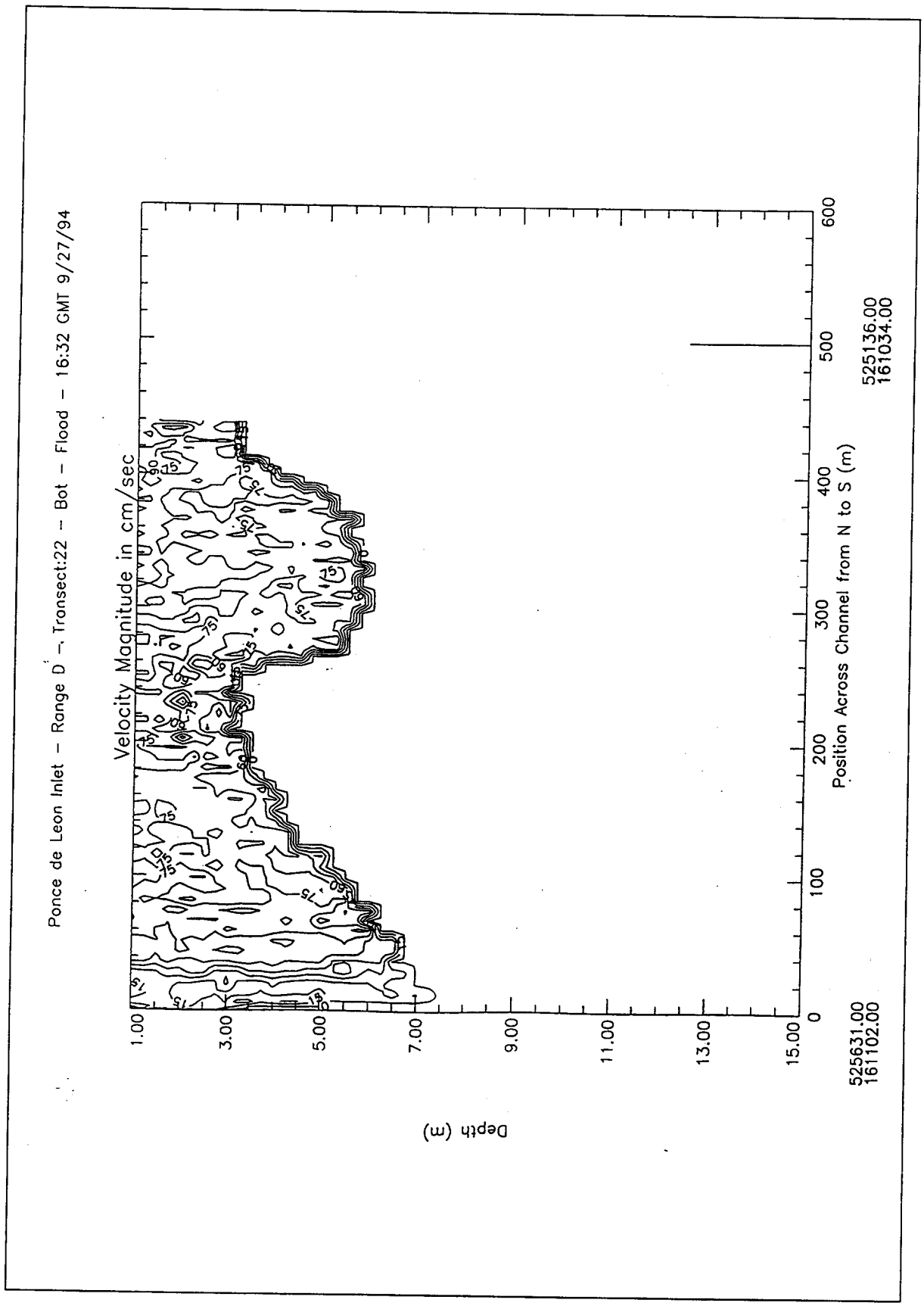

Figure B105. Contour plot of water magnitudes at peak flood conditions, Range D, September

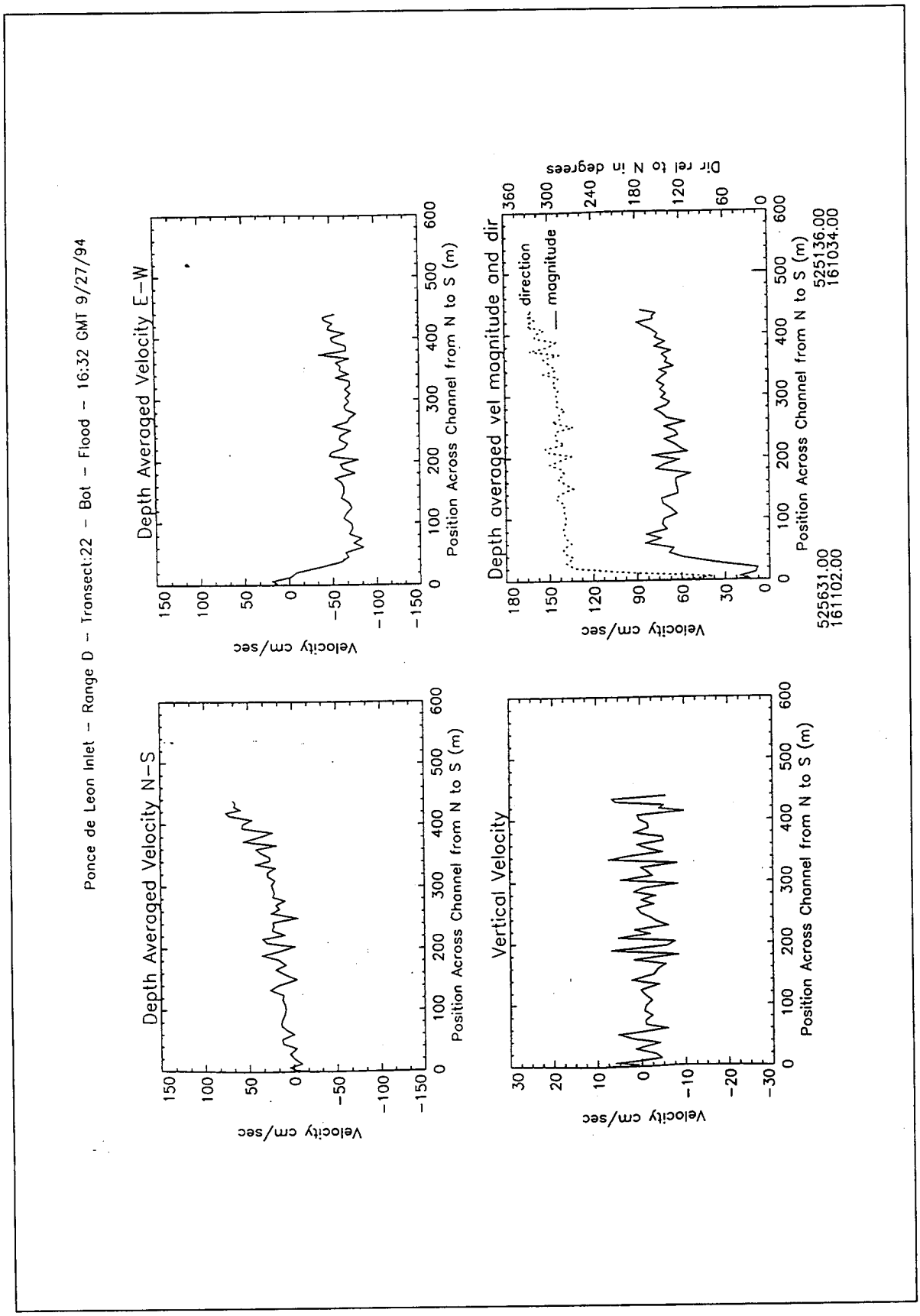

Figure B106. Depth average water velocities at peak flood conditions, Range D, September

Appendix C
Endeco Current Meter Data

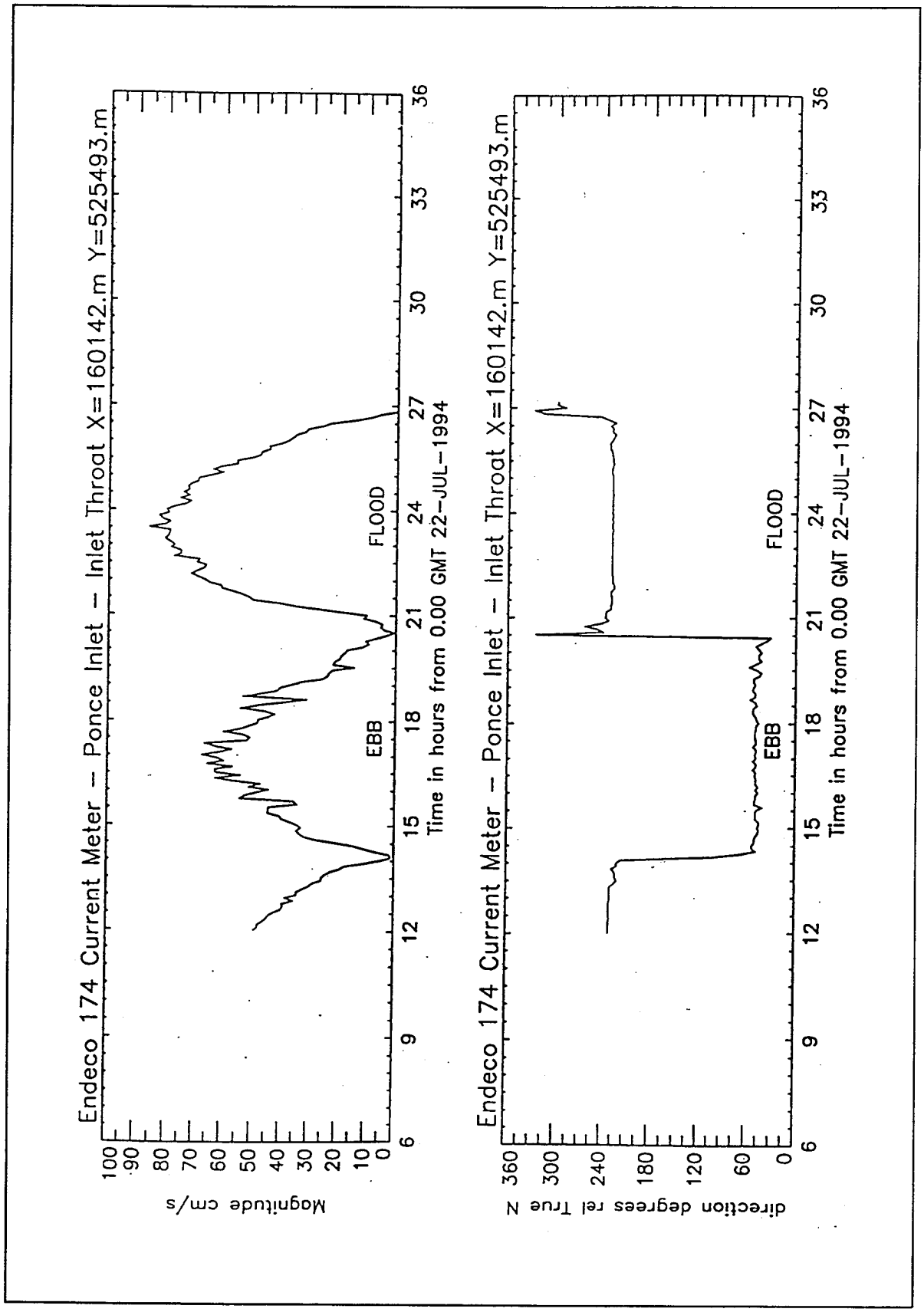

Figure C1. Current measurements at inlet throat for July deployment

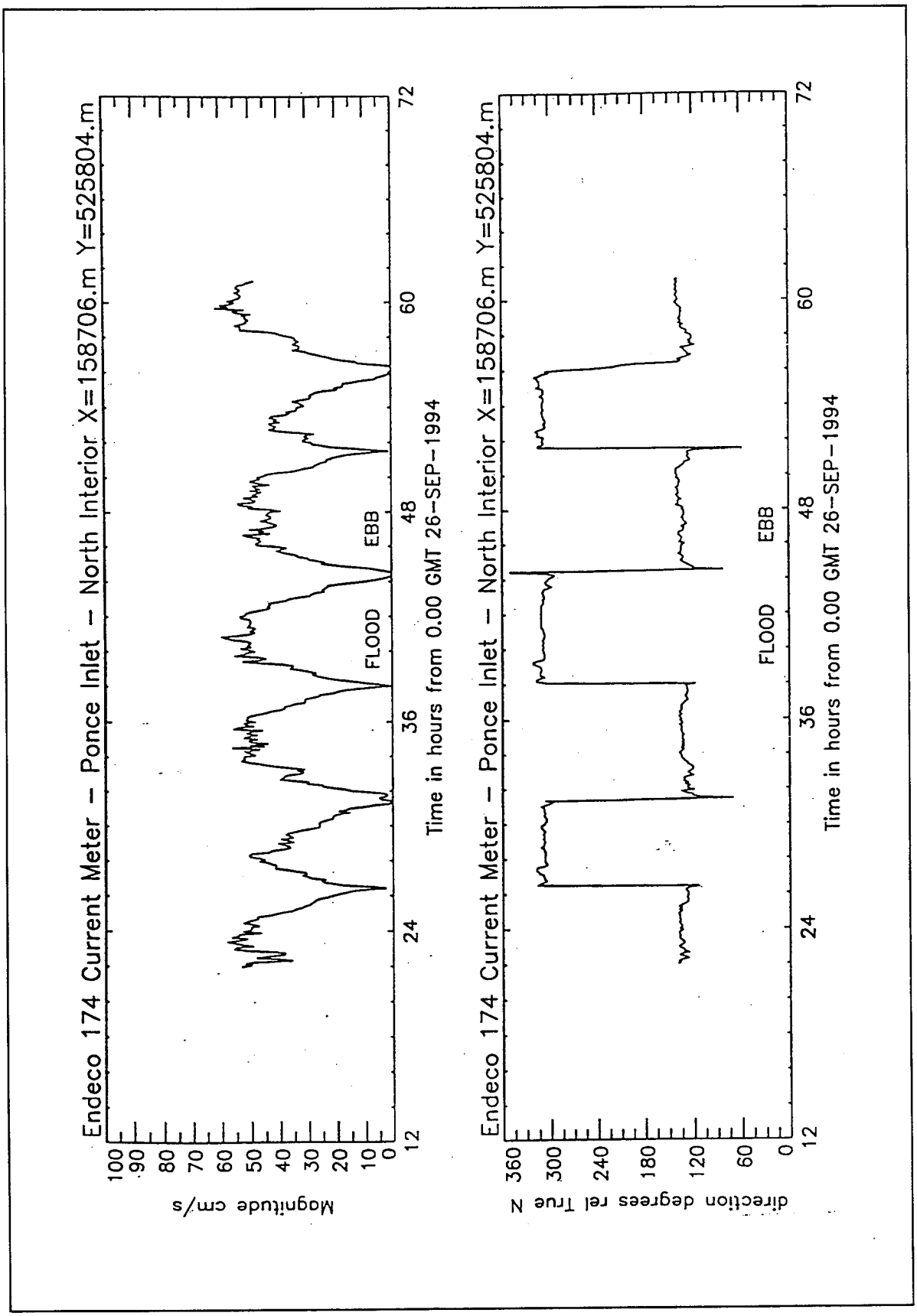

Figure C2. Current measurements at North Interior Site for September deployment

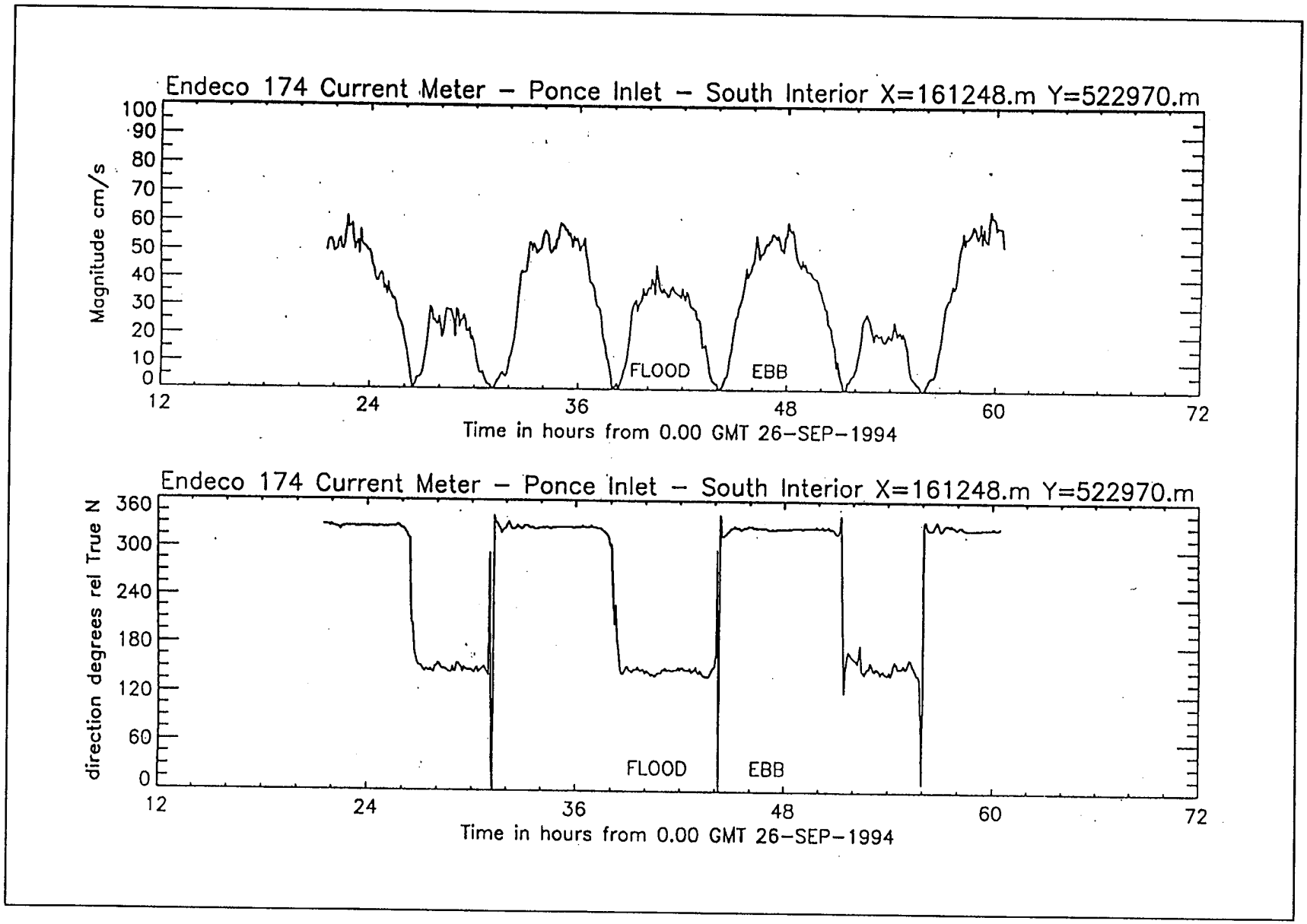

Figure C3. Current measurements at South Interior Site for September deployment

Appendix D
South Jetty Photos

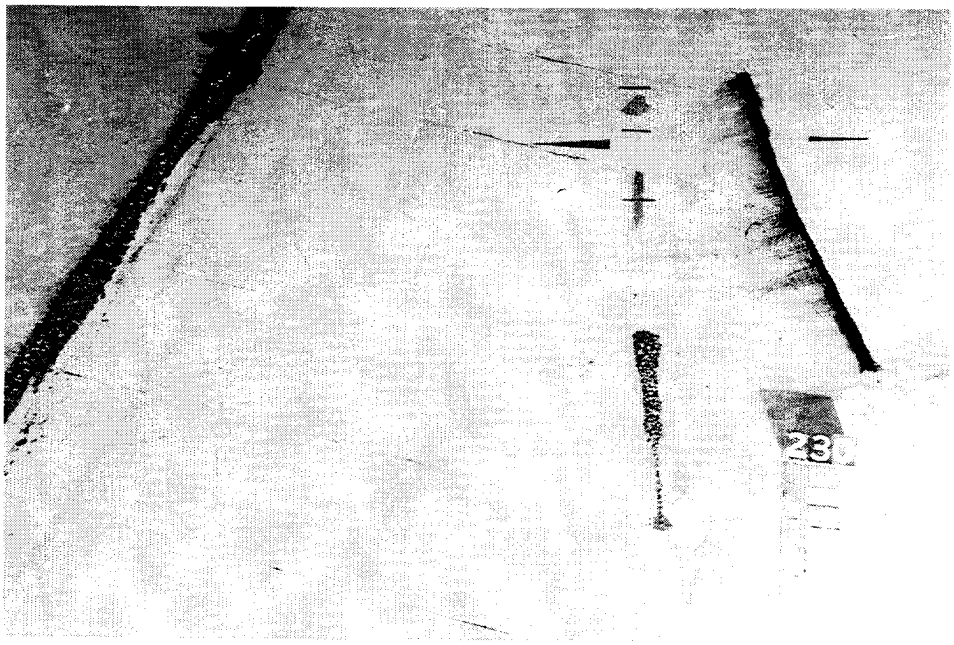

Figure D1. Initial placement of tracer material for the existing south jetty conditions

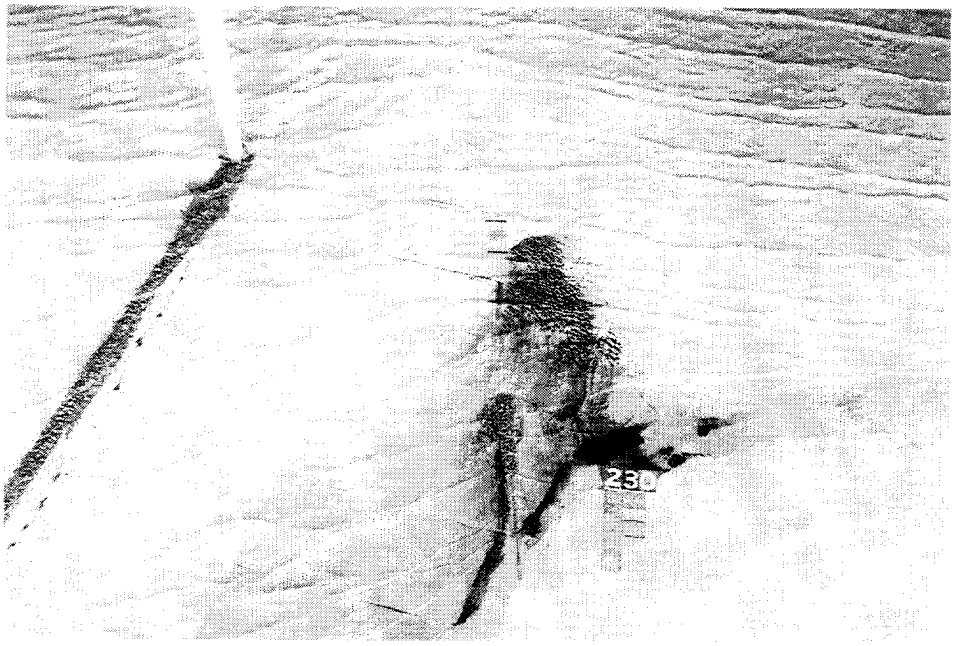

Figure D2. Tracer position after a prototype equivalent of 1 hr 15 min

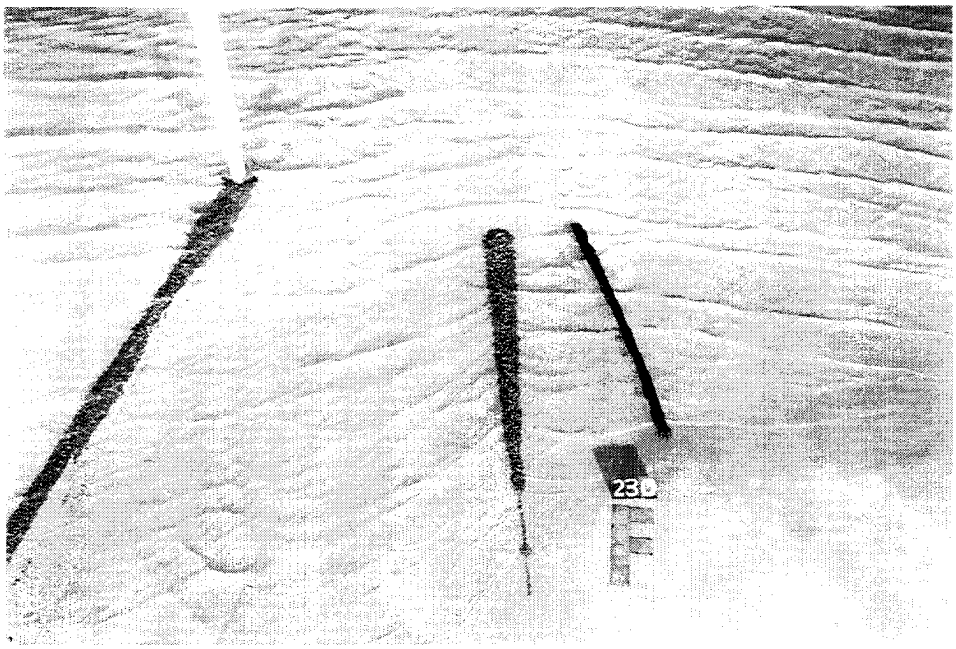

Figure D3. Initial placement of tracer material with 305-m (1,000-ft) south jetty straight extension

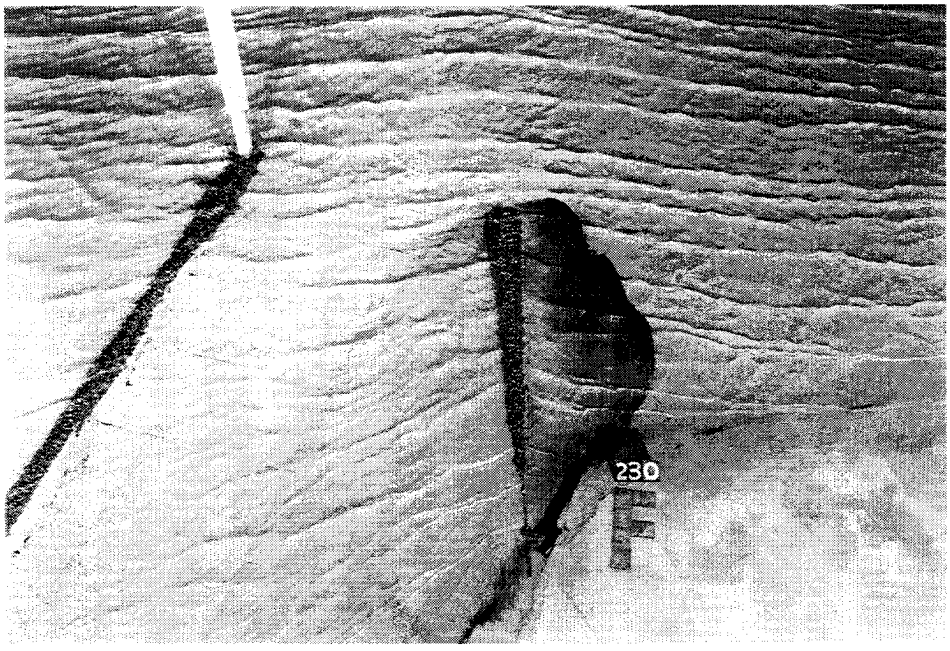

Figure D4. Tracer motion after 1 hr 15 min

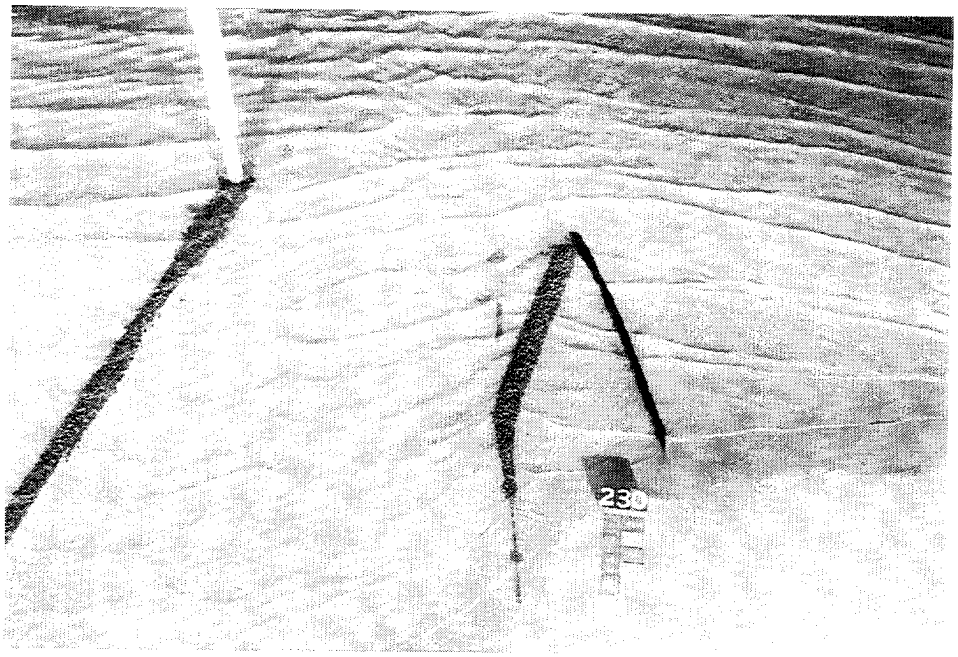

Figure D5. Initial placement of tracer material with 305-m (1,000-ft) south jetty dogleg extension

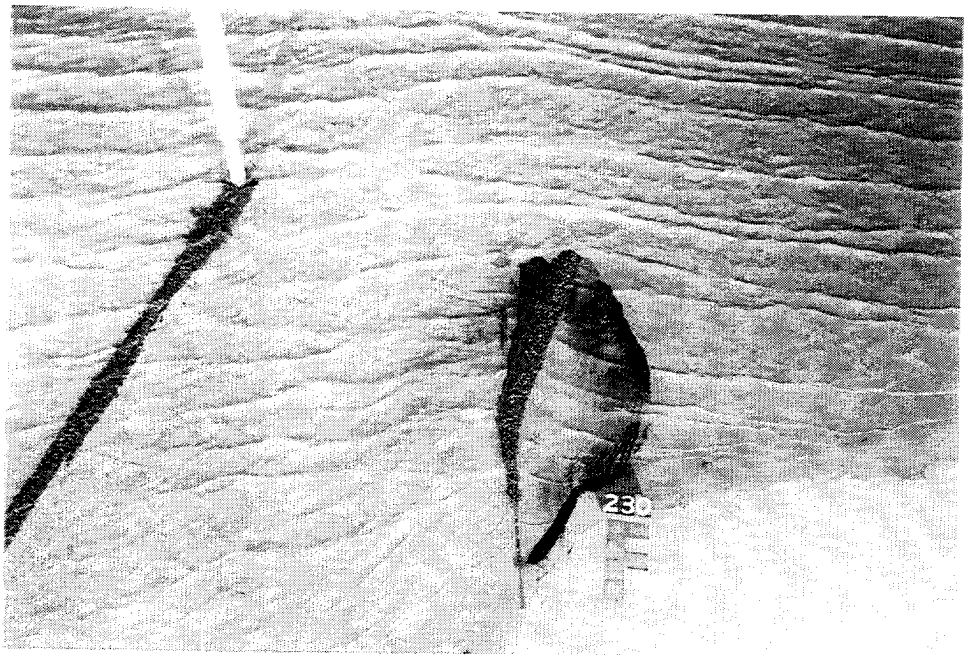

Figure D6. Tracer motion after 1 hr 15 min

Appendix E
North Jetty Photos

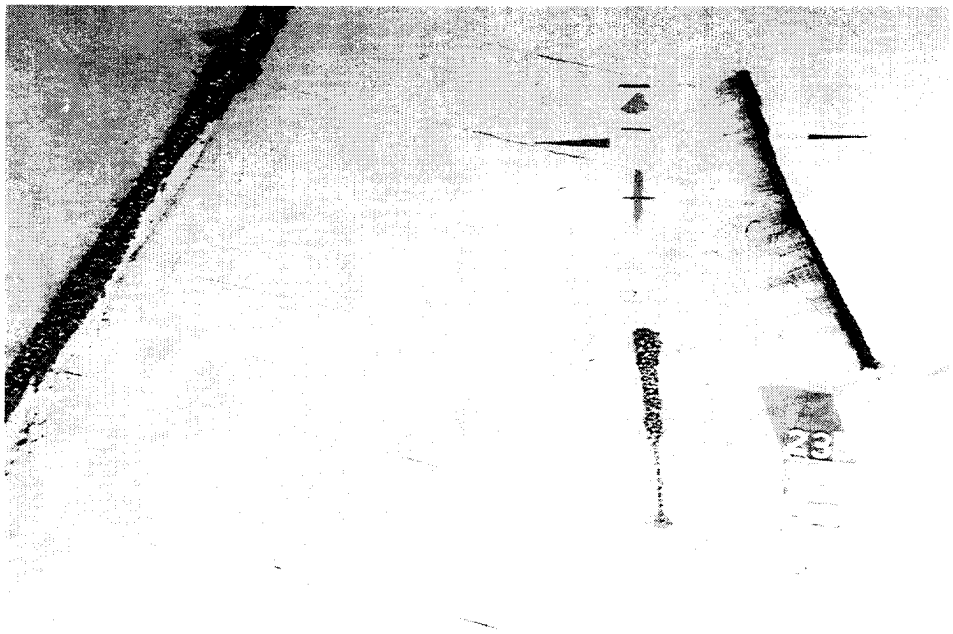

Figure D1 Initial placement of tracer material for the existing south jetty conditions

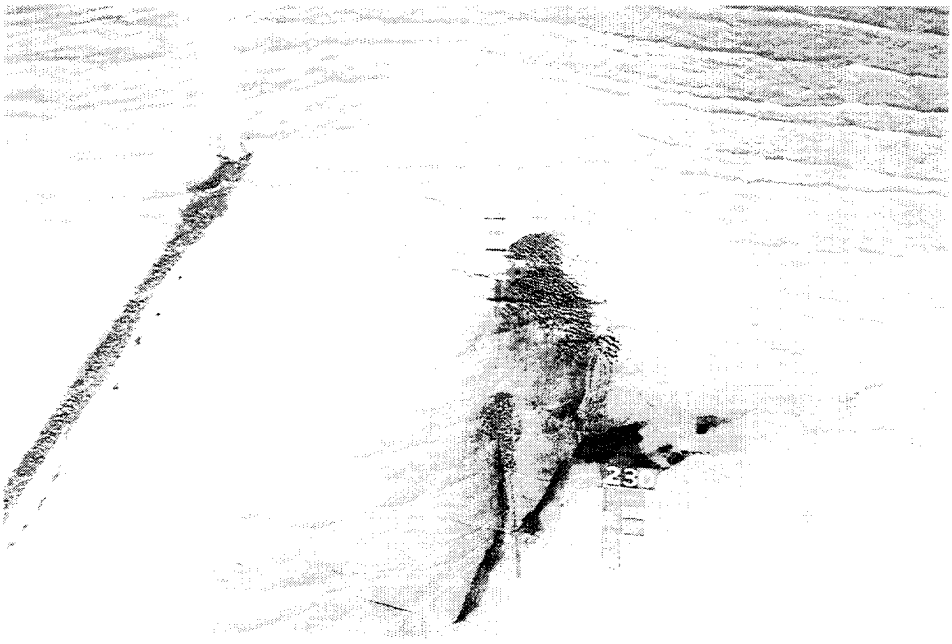

Figure D2 Tracer position after a prototype equivalent of 1 hr 15 min

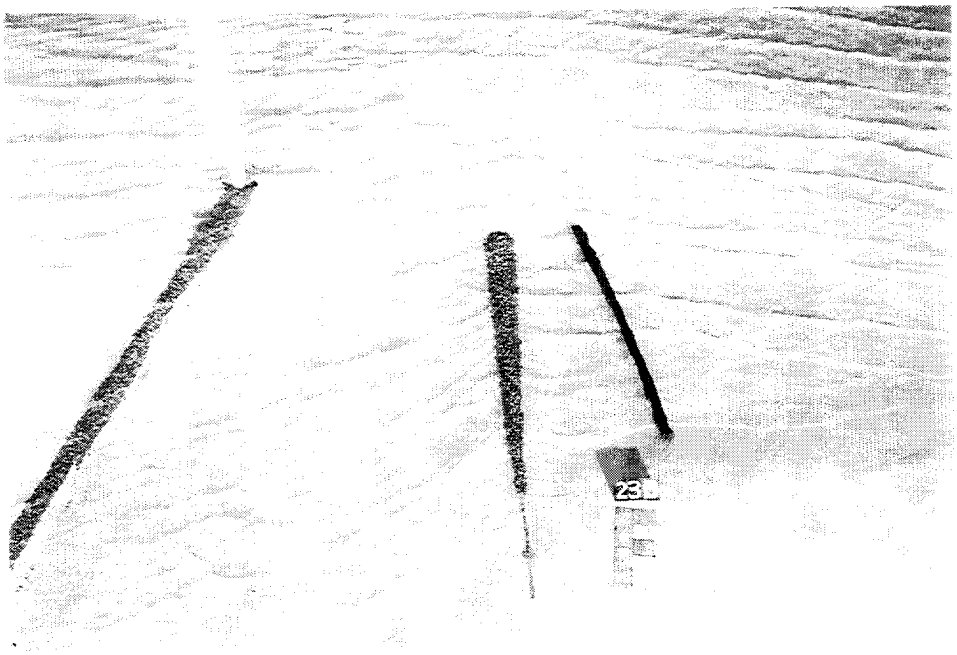

Figure D3. Initial placement of tracer material with 305-m (1,000-ft) south jetty straight extension

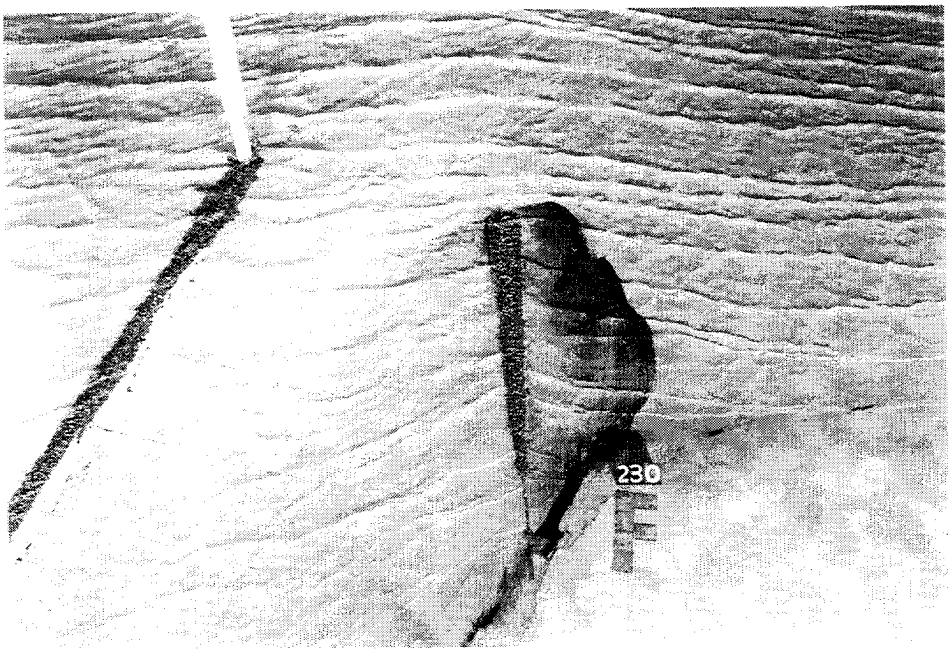

Figure D4. Tracer motion after 1 hr 15 min

Figure D5. Initial placement of tracer material with 305-m (1,000-ft) south jetty dogleg extension

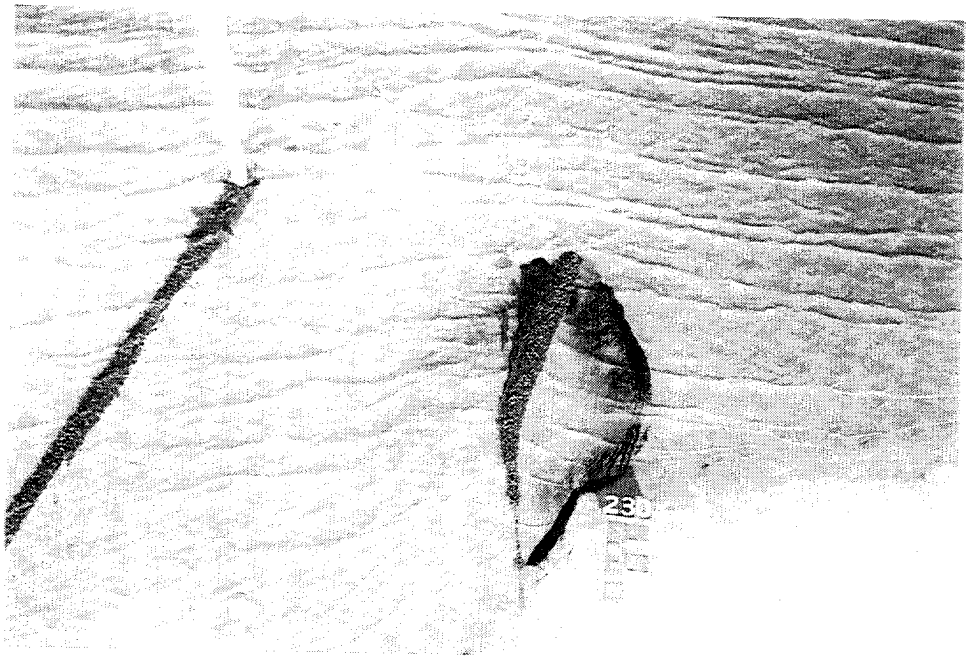

Figure D6. Tracer motion after 1 hr 15 min

Appendix E
North Jetty Photos

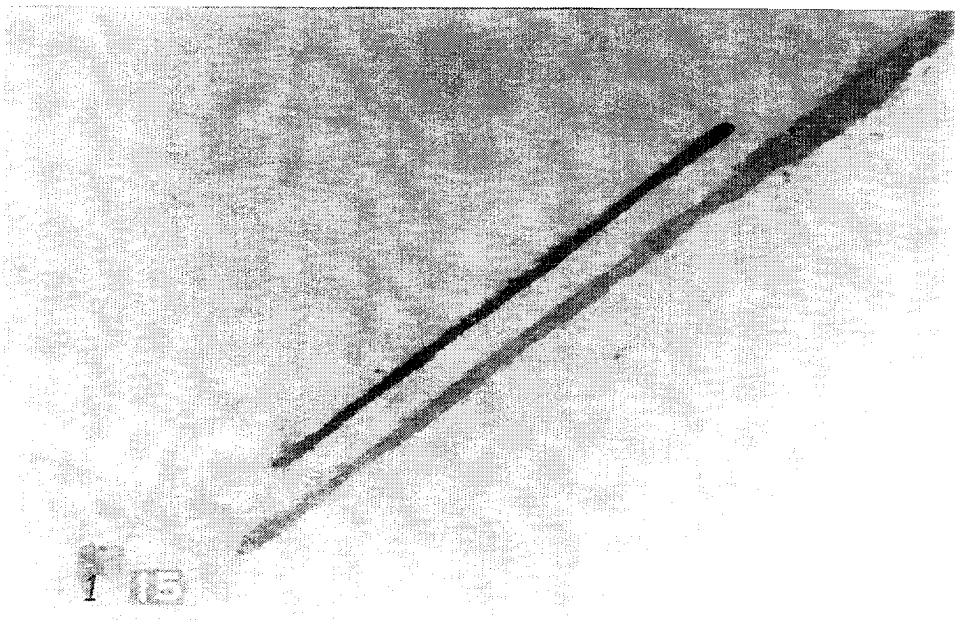

Figure E1 Initial location of tracer before each north jetty test

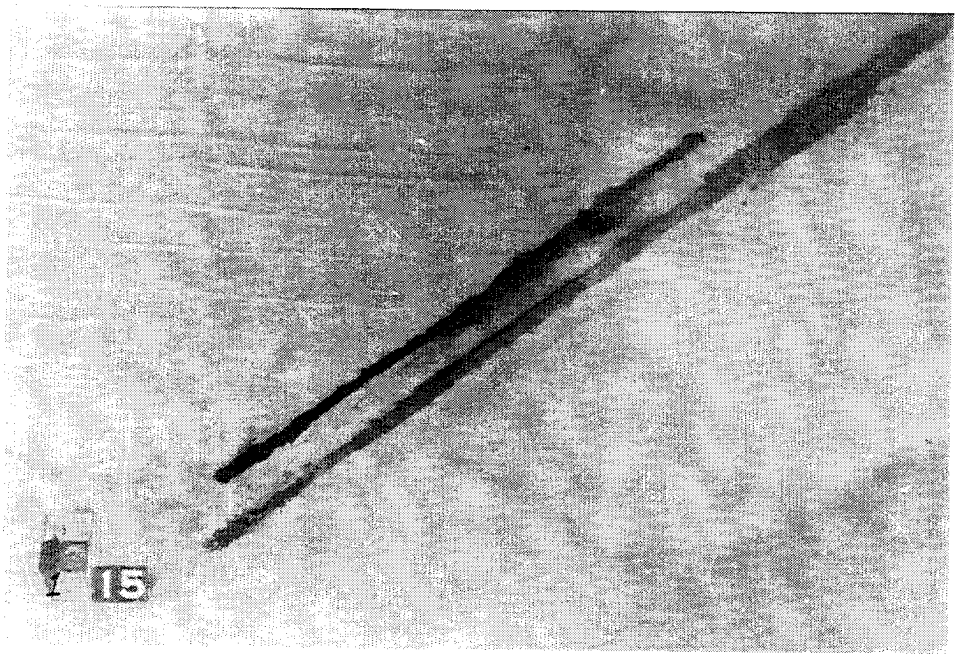

Figure E2. Tracer motion after a prototype equivalent of 1 hr 15 min under navigation wave N1 and spring peak ebb water level, no flow, full length weir opening

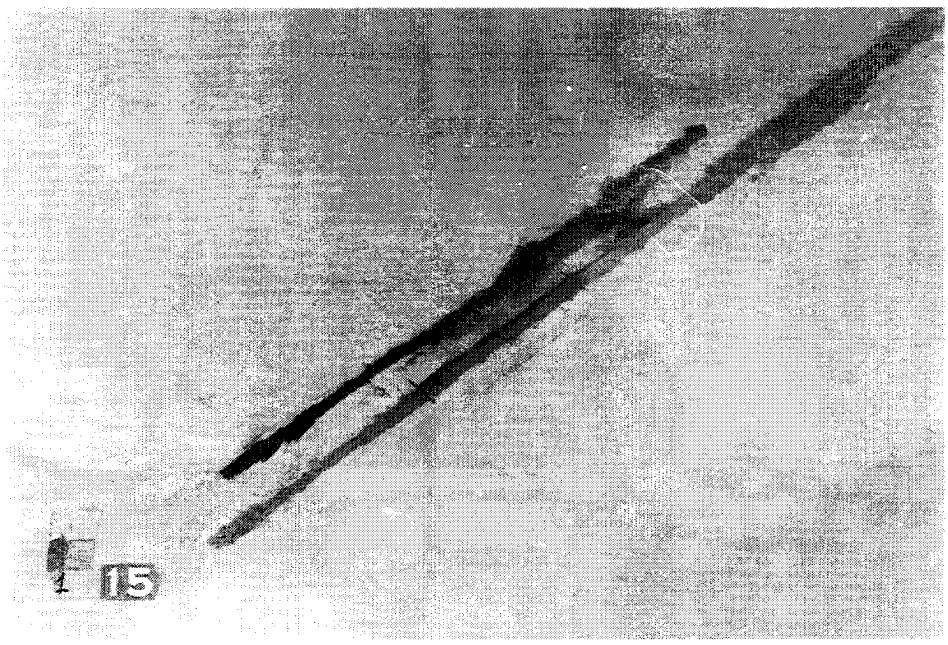

Figure E3. Tracer motion after a prototype equivalent of 2 hr 30 min under navigation wave N1 and spring peak ebb water level, no flow, full length weir opening

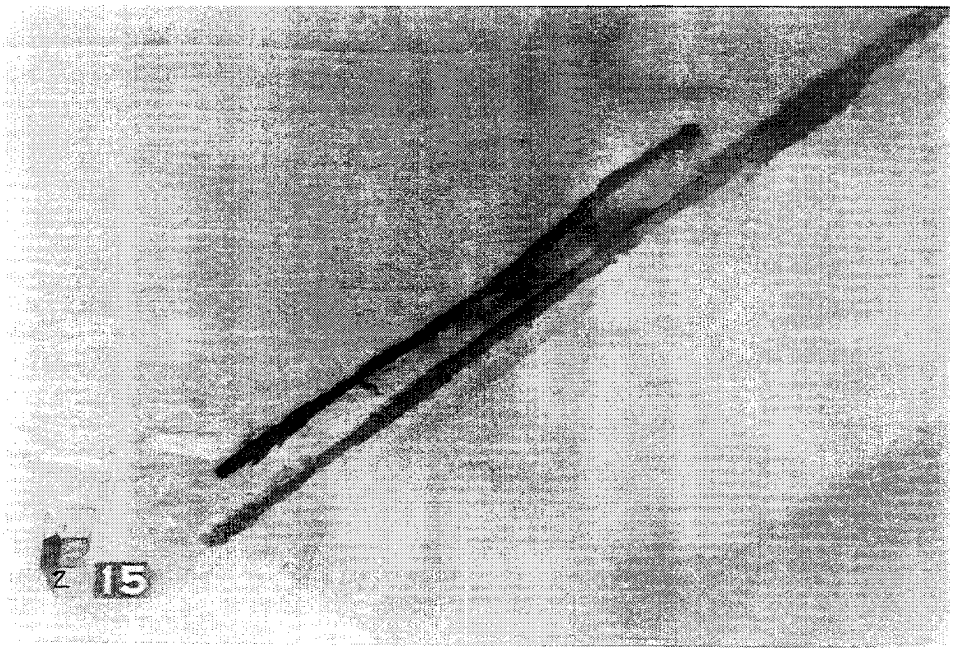

Figure E4. Tracer motion after a prototype equivalent of 1 hr 15 min under navigation wave N2 and spring peak ebb water level, no flow, full length weir opening

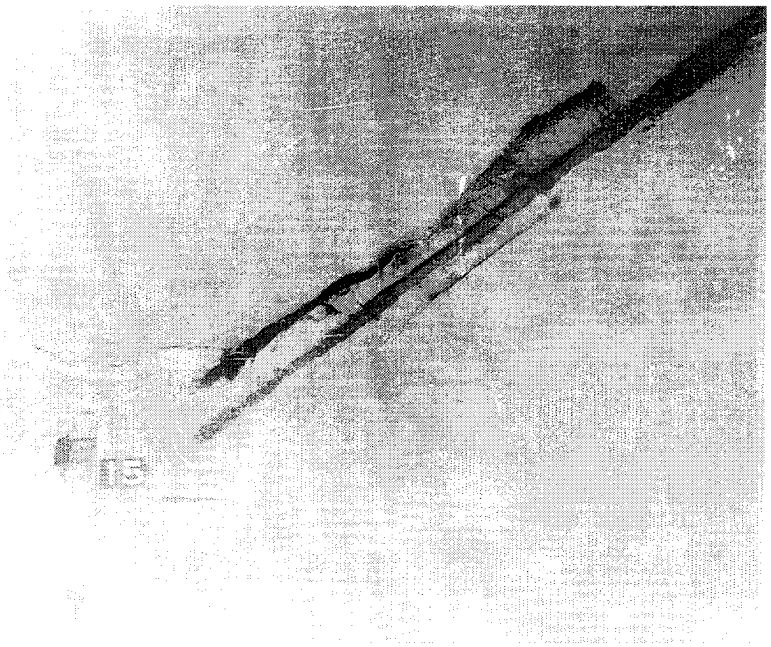

Figure E5. Tracer motion after a prototype equivalent of 2 hr 30 min under navigation wave N2 and spring peak ebb water level, no flow, full length weir opening

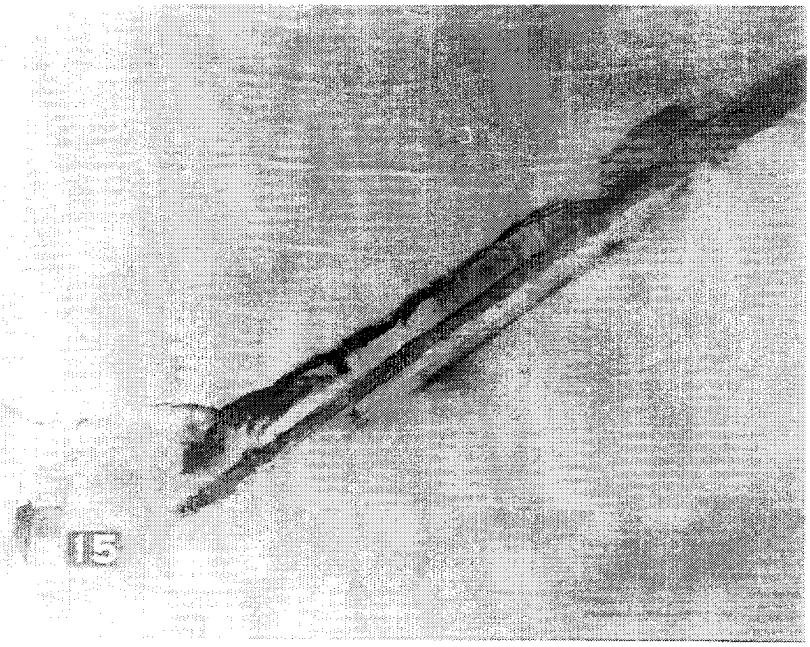

Figure E6. Tracer motion after a prototype equivalent of 1 hr 15 min under a 1-year storm event and spring peak ebb water level, no flow, full length weir opening

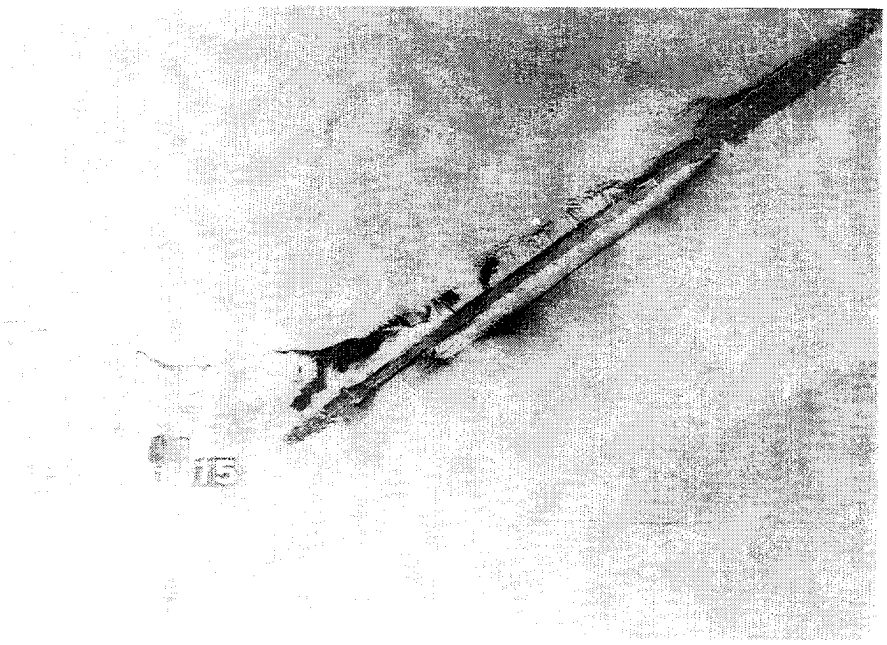

Figure E7. Tracer motion after a prototype equivalent of 2 hr 30 min under a 1-year storm event and spring peak ebb water level, no flow, full length weir opening

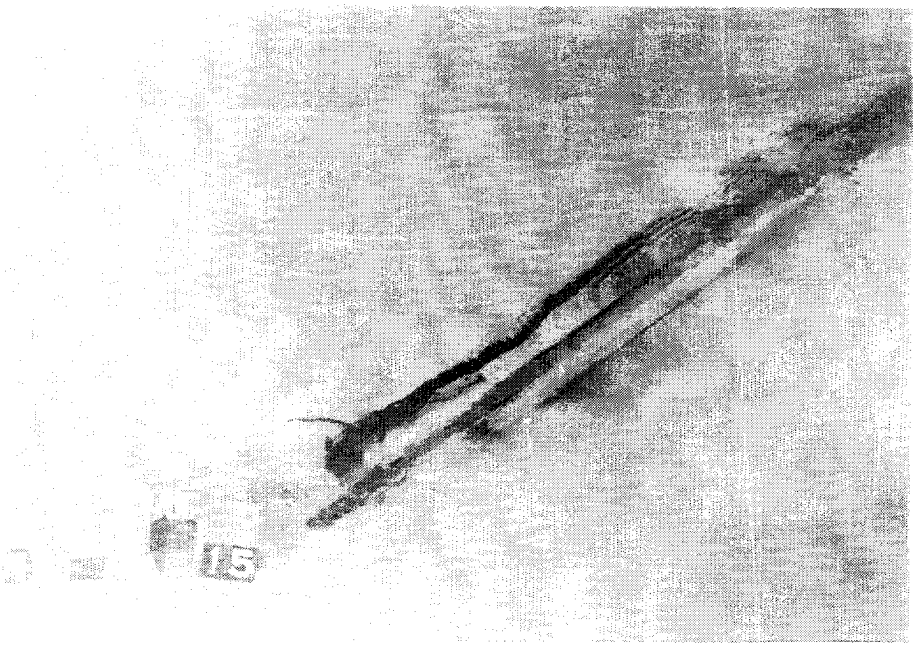

Figure E8. Tracer motion after a prototype equivalent of 1 hr 15 min under a 5-year storm event and spring peak ebb water level, no flow, full length weir opening

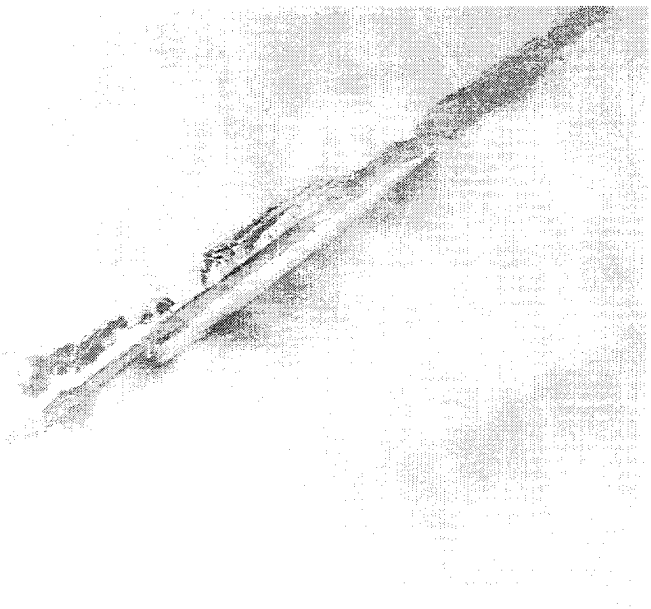

Figure E9. Tracer motion after a prototype equivalent of 2 hr 30 min under a 5-year storm event and spring peak ebb water level, no flow, full length weir opening

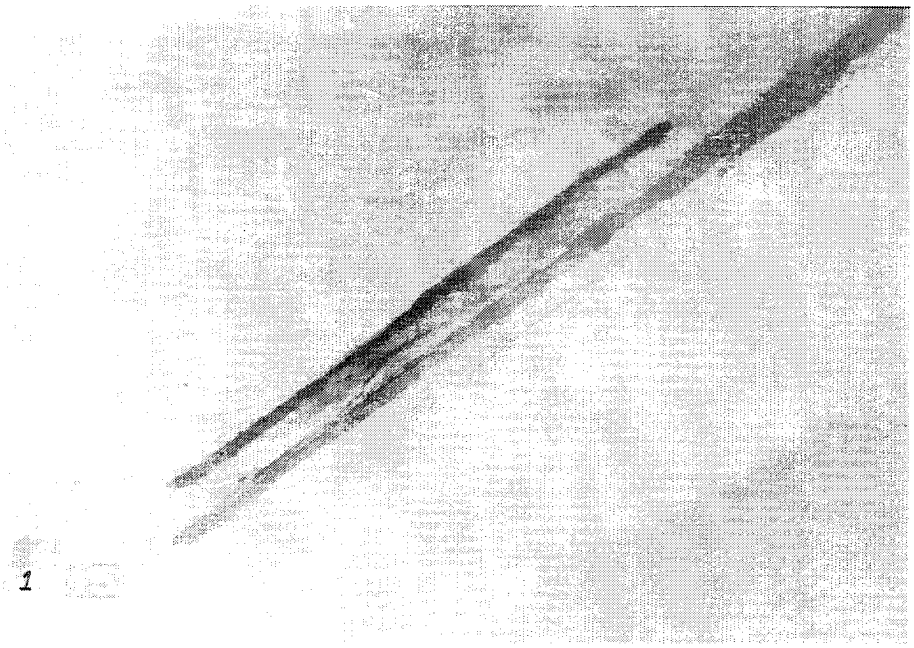

Figure E10 Tracer motion after a prototype equivalent of 1 hr 15 min under navigation wave N1 and spring peak flood water level, no flow, full length weir opening

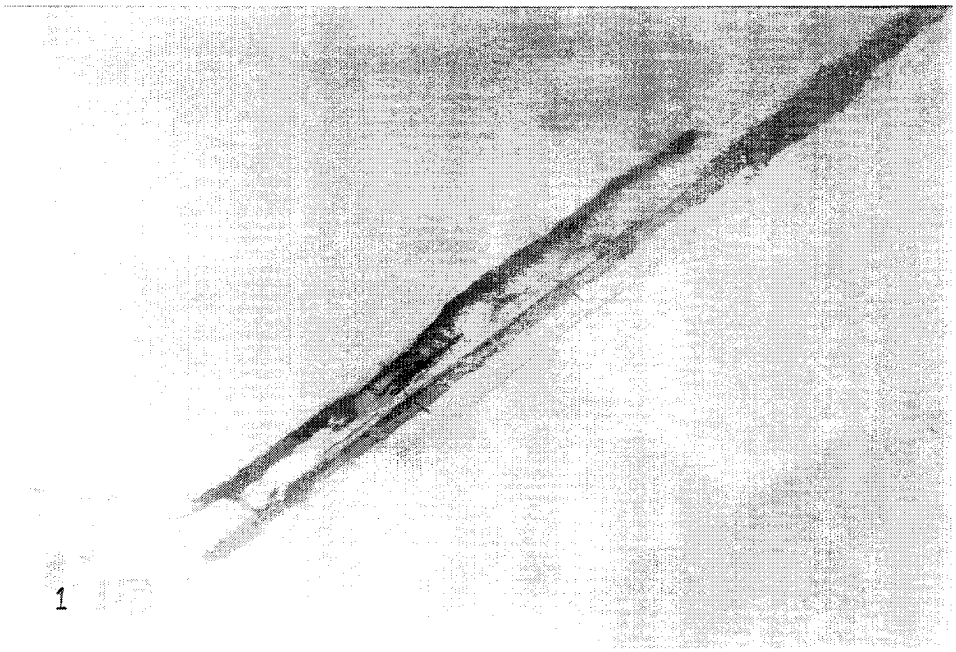

Figure E11. Tracer motion after a prototype equivalent of 2 hr 30 min under navigation wave N1 and spring peak flood water level, no flow, full length weir opening

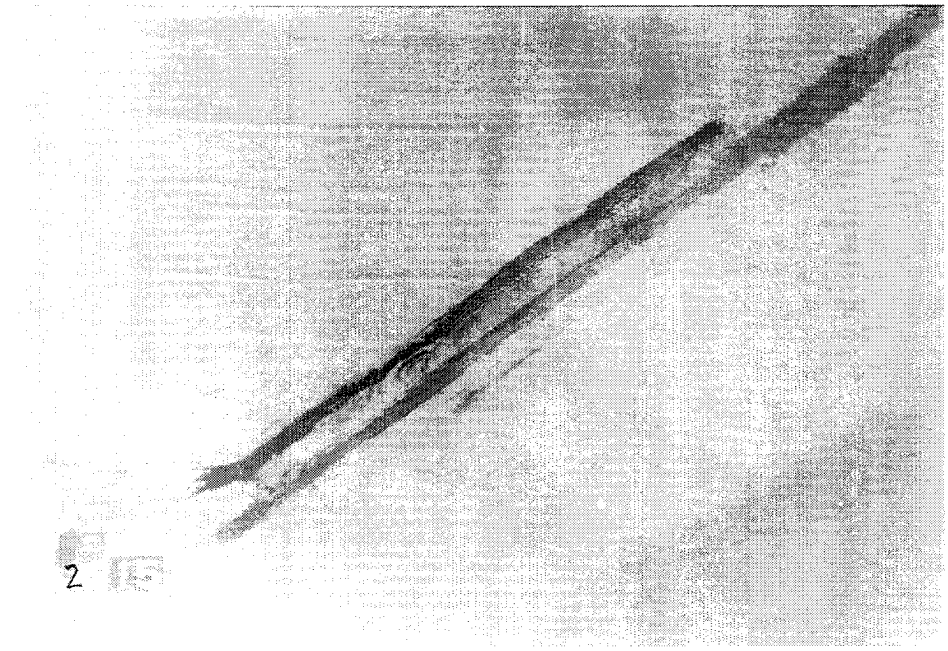

Figure E12. Tracer motion after a prototype equivalent of 1 hr 15 min under navigation wave N2 and spring peak flood water level, no flow, full length weir opening

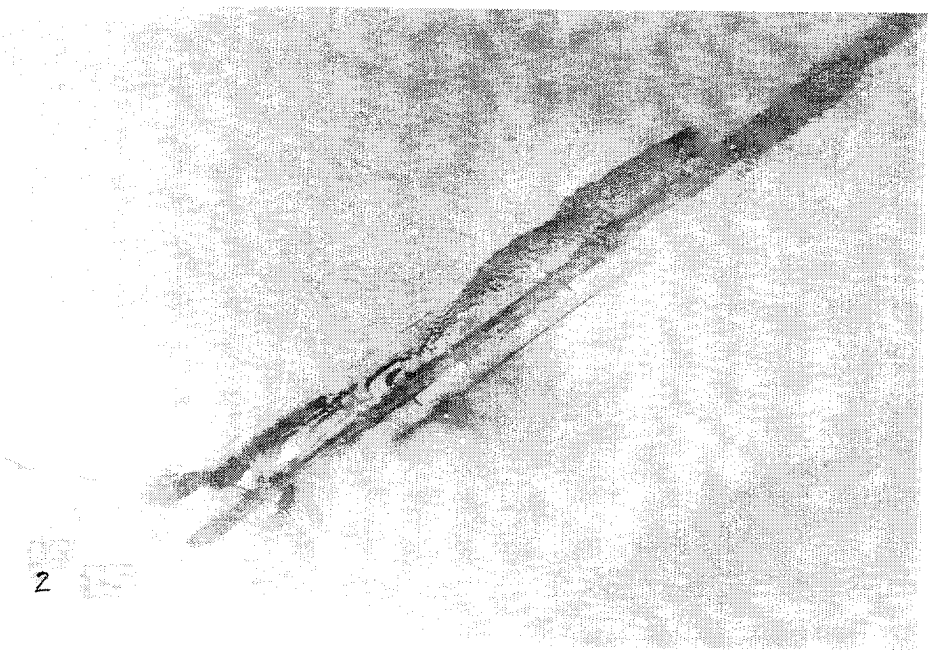

Figure E13. Tracer motion after a prototype equivalent of 2 hr 30 min under navigation wave N2 and spring peak flood water level, no flow, full length weir opening

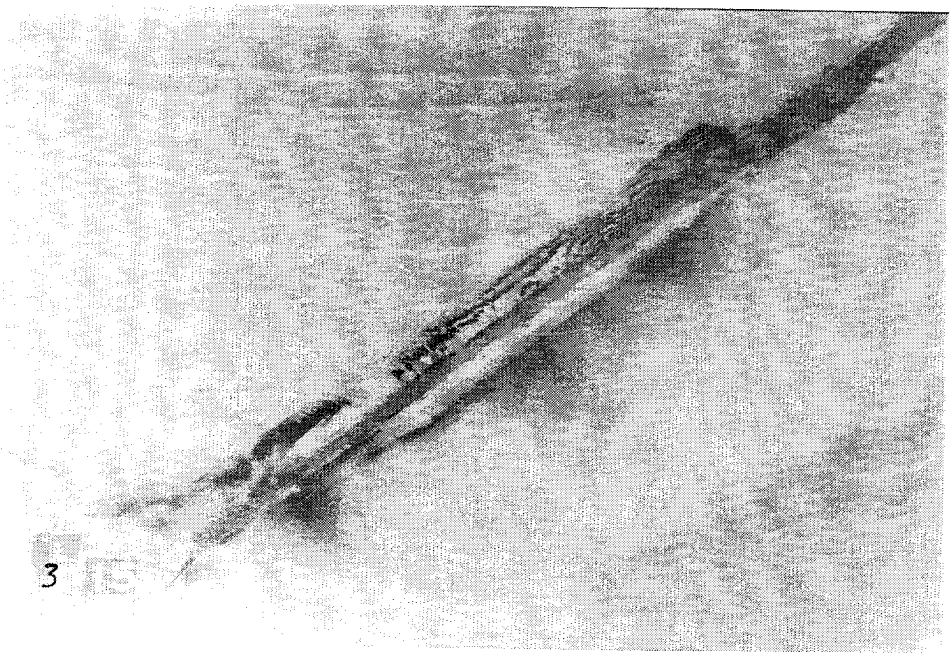

Figure E14. Tracer motion after a prototype equivalent of 1 hr 15 min under a 1-year storm event and spring peak flood water level, no flow, full length weir opening

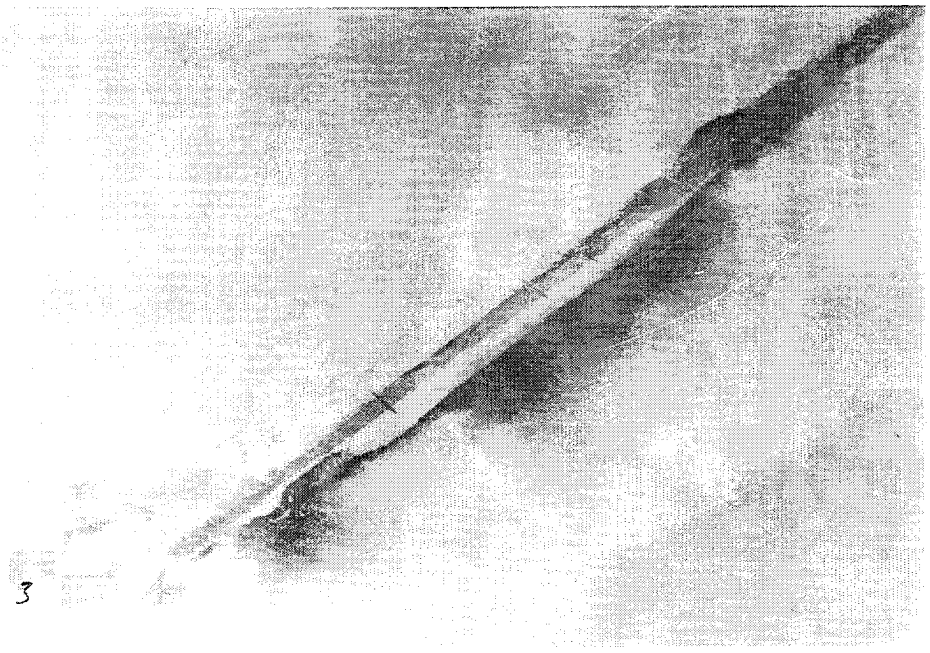

Figure E15. Tracer motion after a prototype equivalent of 2 hr 30 min under a 1-year storm event and spring peak flood water level, no flow, full length weir opening

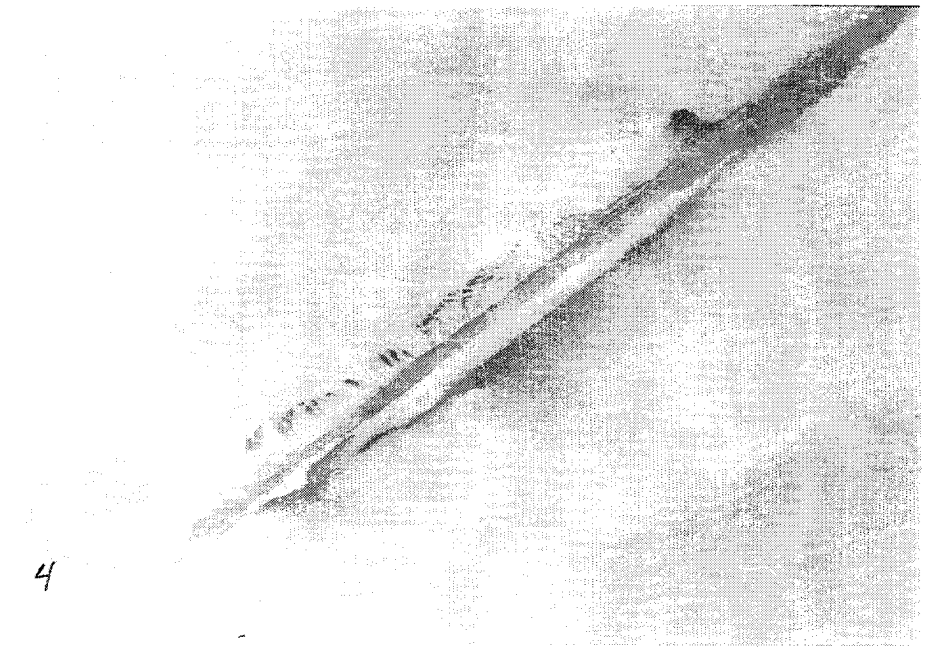

Figure E16. Tracer motion after a prototype equivalent of 1 hr 15 min under a 5-year event and spring peak flood water level, no flow, full length weir opening

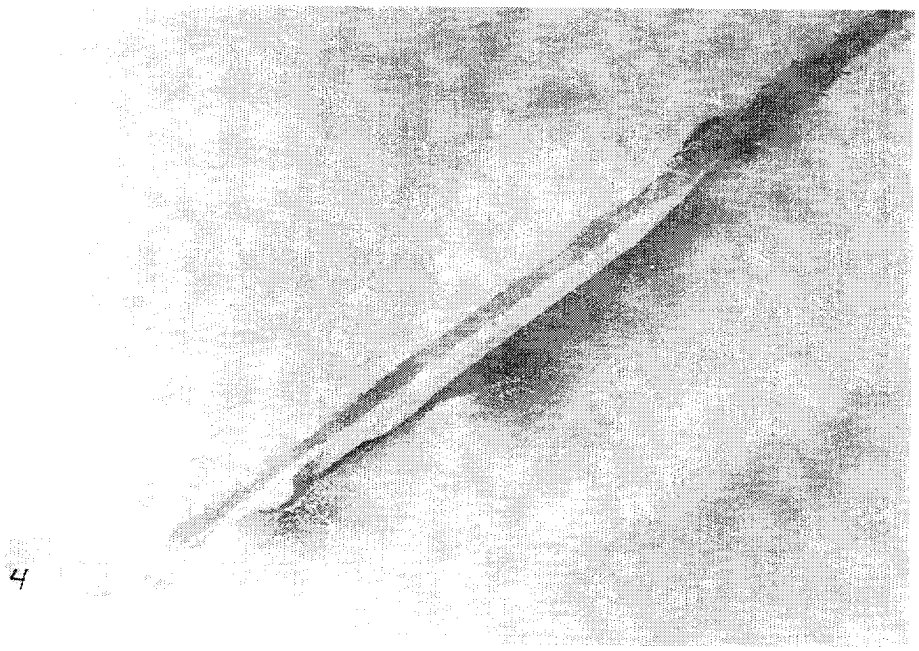

Figure E17 Tracer motion after a prototype equivalent of 2 hr 30 min under a 5-year storm event and spring peak flood water level, no flow, full length weir opening

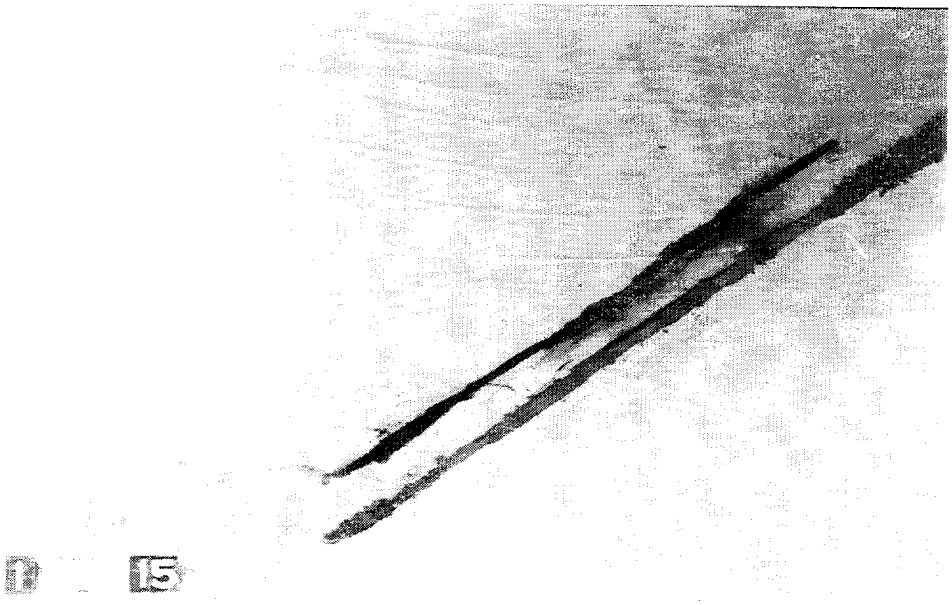

Figure E18. Tracer motion after a prototype equivalent of 1 hr 15 min under navigation wave N1 and spring peak ebb water level and flow, full length weir opening

Figure E19. Tracer motion after a prototype equivalent of 2 hr 30 min under navigation wave N1 and spring peak ebb water level and flow, full length weir opening

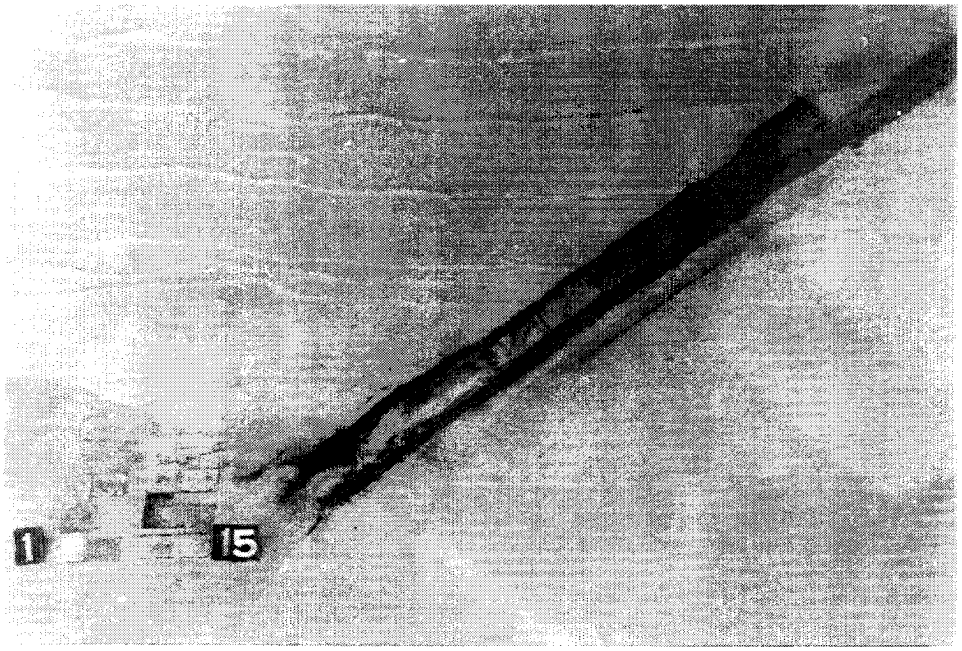

Figure E20. Tracer motion after a prototype equivalent of 1 hr 15 min under a 1-year storm event and spring peak ebb water level and flow, full length weir opening

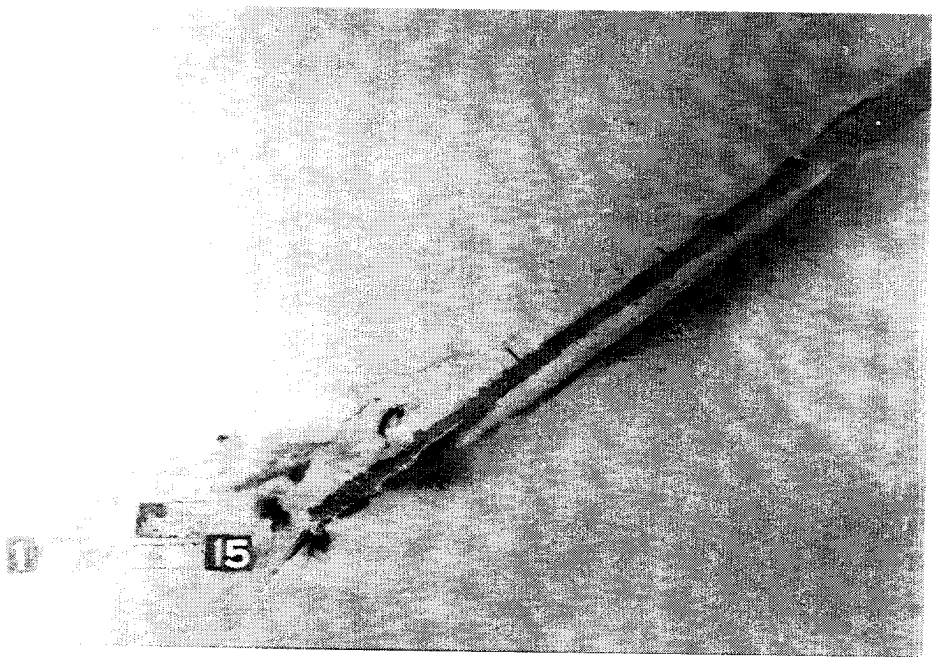

Figure E21. Tracer motion after a prototype equivalent of 2 hr 30 min under a 1-year storm event and spring peak ebb water level and flow, full length weir opening

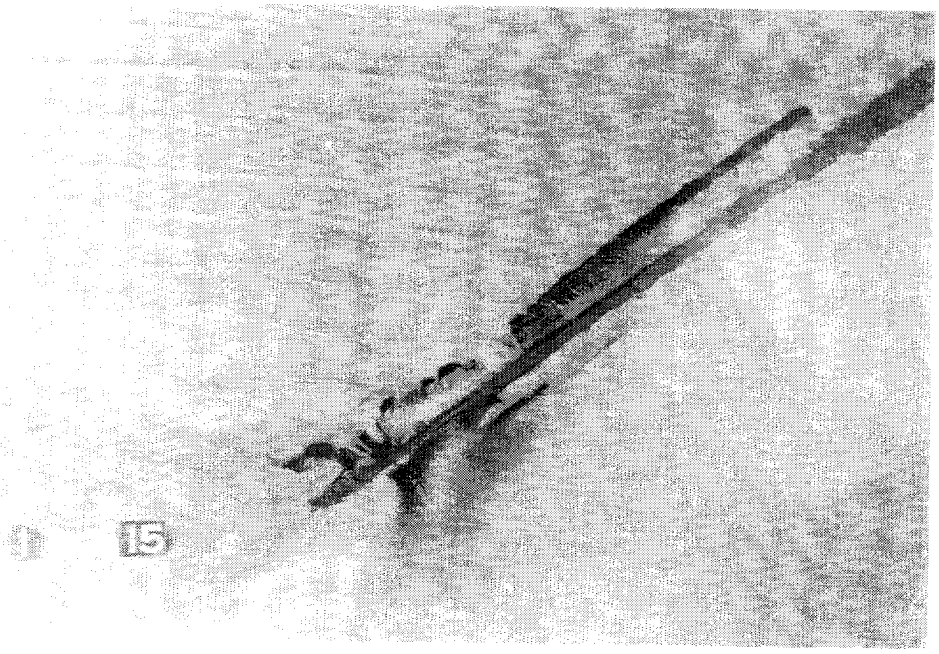

Figure E22. Tracer motion after a prototype equivalent of 2 hr 30 min under navigation wave N1 and spring peak flood water level and flow, full length weir opening

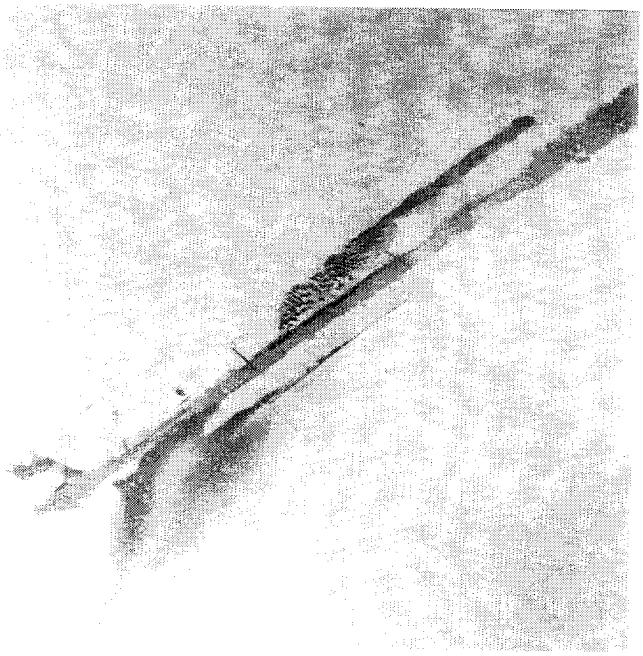

Figure E23. Tracer motion after a prototype equivalent of 2 hr 30 min under navigation wave N1 and spring peak flood water level and flow, full length weir opening

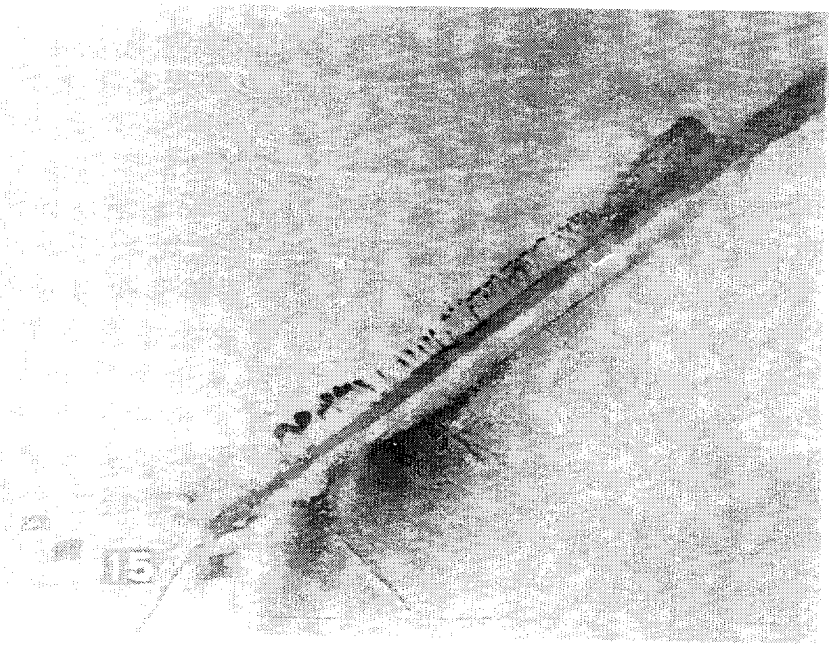

Figure E24. Tracer motion after a prototype equivalent of 1 hr 15 min under a 1-year storm event and spring peak flood water level and flow, full length weir opening

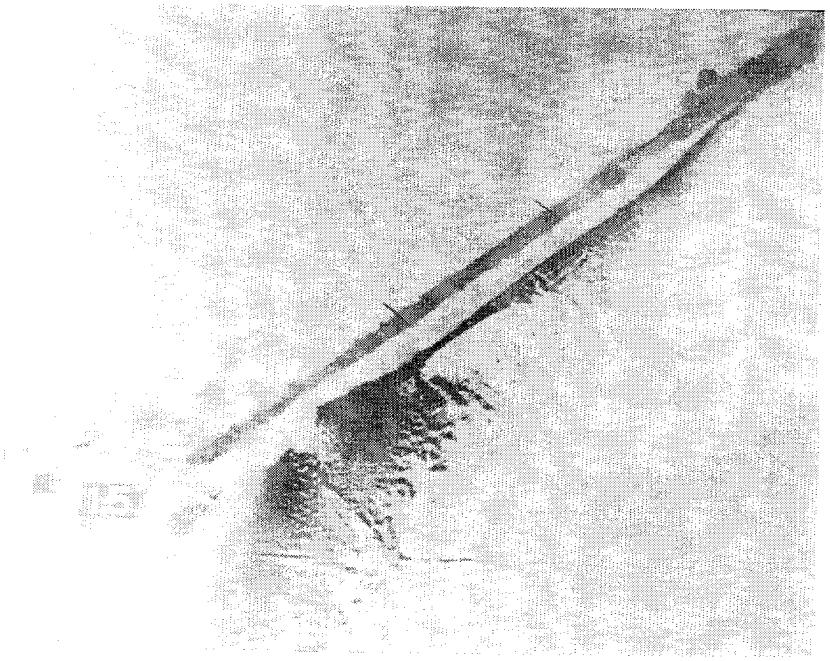

Figure E25. Tracer motion after a prototype equivalent of 2 hr 30 min under a 1-year storm event and spring peak flood water level and flow, full length weir opening

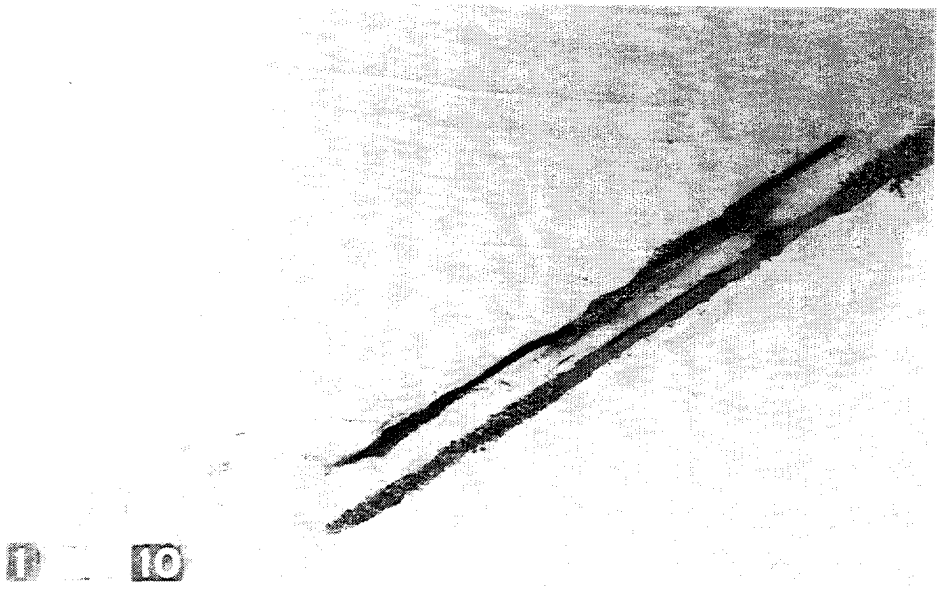

Figure E26. Tracer motion after a prototype equivalent of 1 hr 15 min under navigation wave N1 and spring peak ebb water level and flow, 305-m (1,000-ft) weir opening

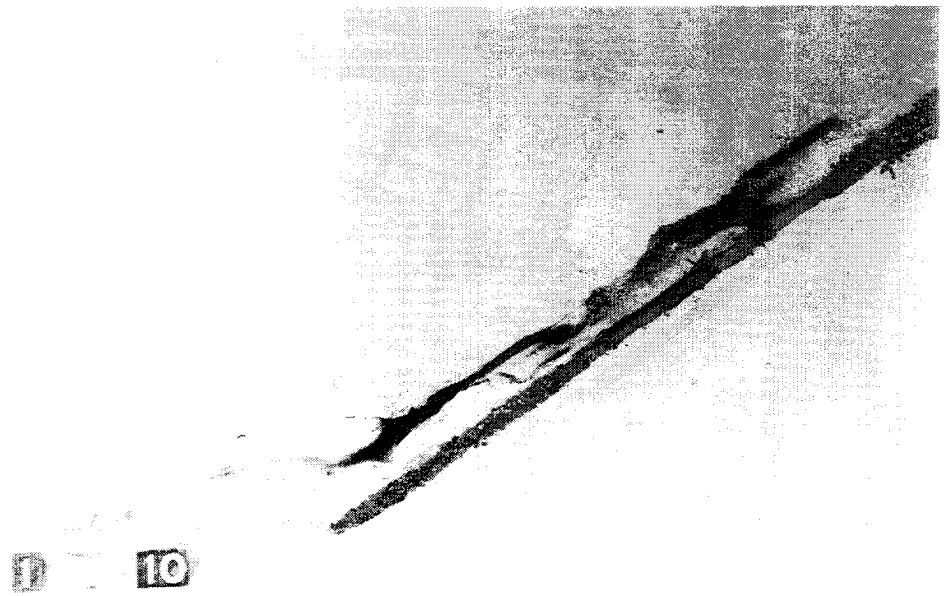

Figure E27. Tracer motion after a prototype equivalent of 2 hr 30 min under navigation wave N1 and spring peak ebb water level and flow, 305-m (1,000-ft) weir opening

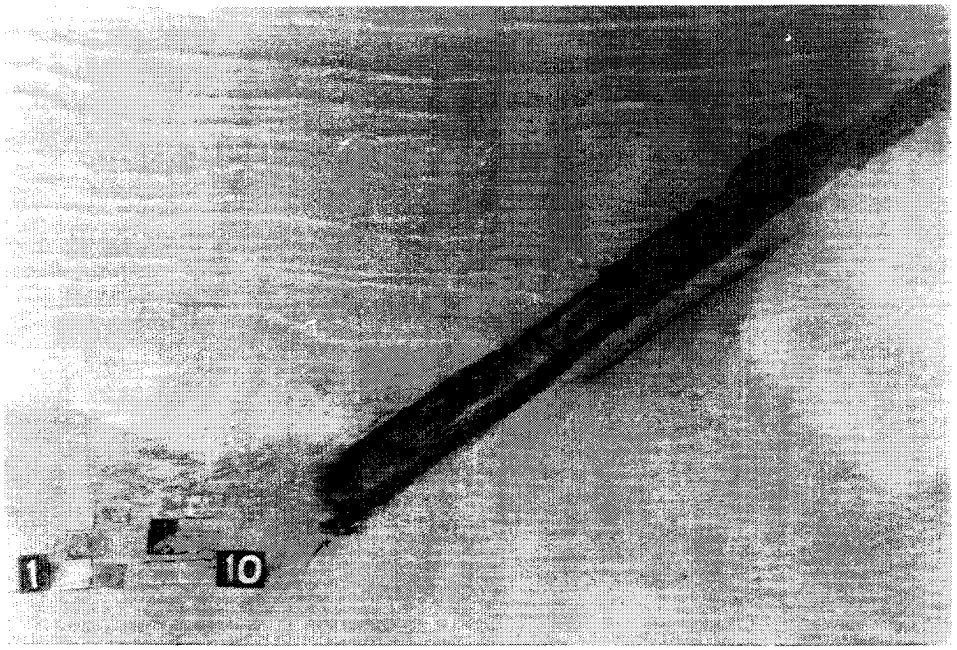

Figure E28. Tracer motion after a prototype equivalent of 1 hr 15 min under 1-year storm event and spring peak ebb storm water level and flow, 305-m (1,000-ft) weir opening

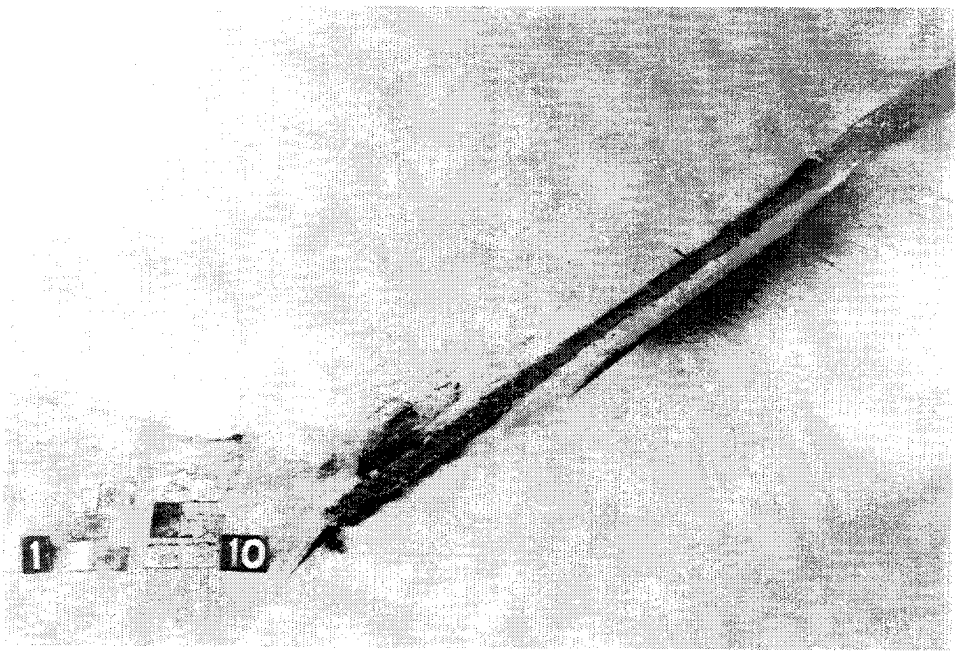

Figure E29. Tracer motion after a prototype equivalent of 2 hr 30 min under 1-year storm event and spring peak ebb storm water level and flow, 305-m (1,000-ft) weir opening

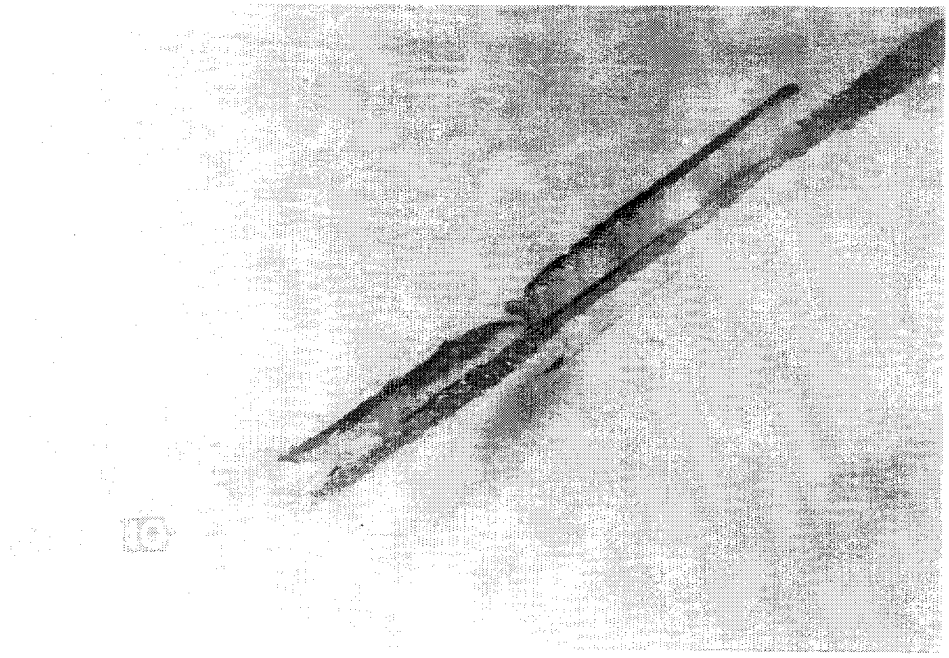

Figure E30. Tracer motion after a prototype equivalent of 1 hr 15 min under navigation wave N1 and spring peak flood water level and flow, 305-m (1,000-ft) weir opening

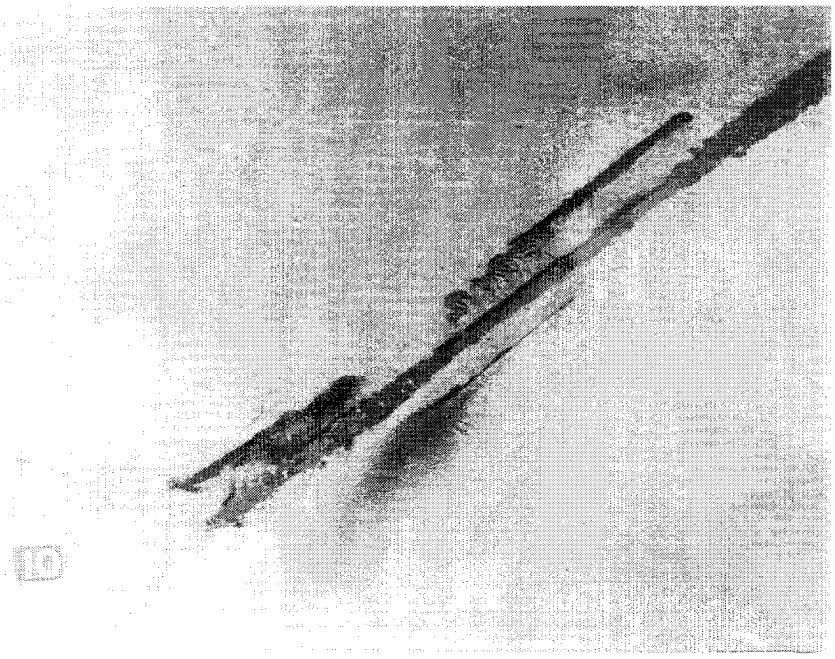

Figure E31. Tracer motion after a prototype equivalent of 2 hr 30 min under navigation wave N1 and spring peak flood water level and flow, 305-m (1,000-ft) weir opening

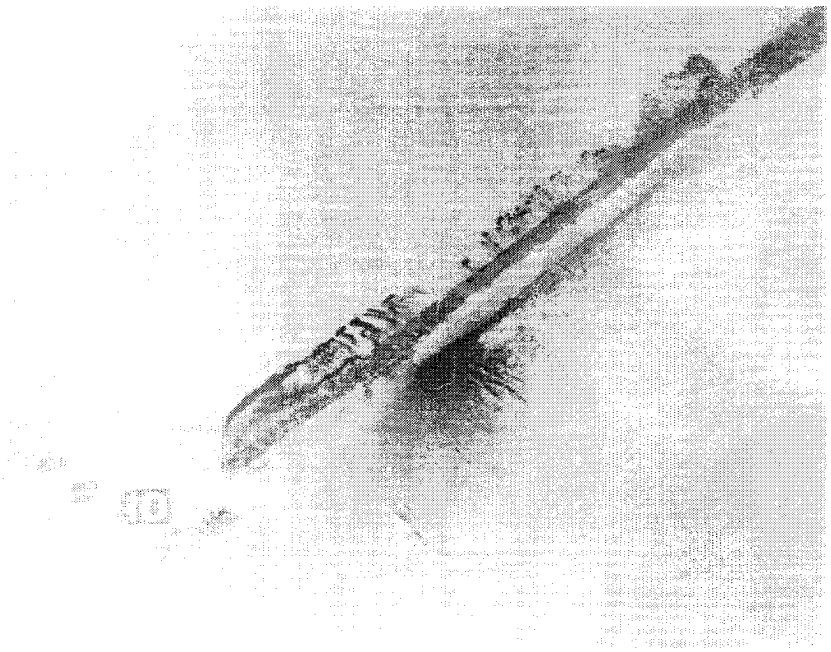

Figure E32. Tracer motion after a prototype equivalent of 1 hr 15 min under 1-year storm event and spring peak flood storm water level and flow, 305-m (1,000-ft) weir opening

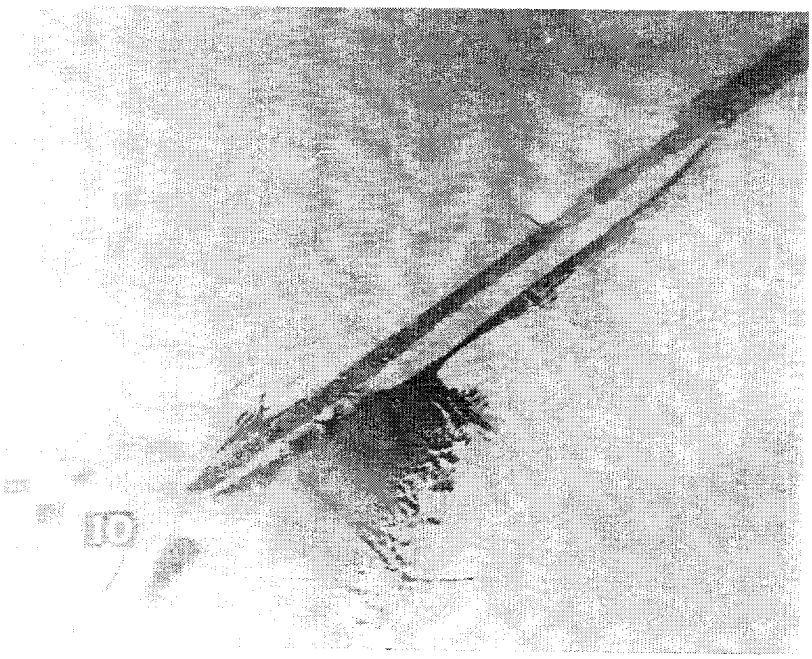

Figure E33. Tracer motion after a prototype equivalent of 2 hr 30 min under 1-year storm event and spring peak flood storm water level and flow. 305-m (1,000-ft) weir opening

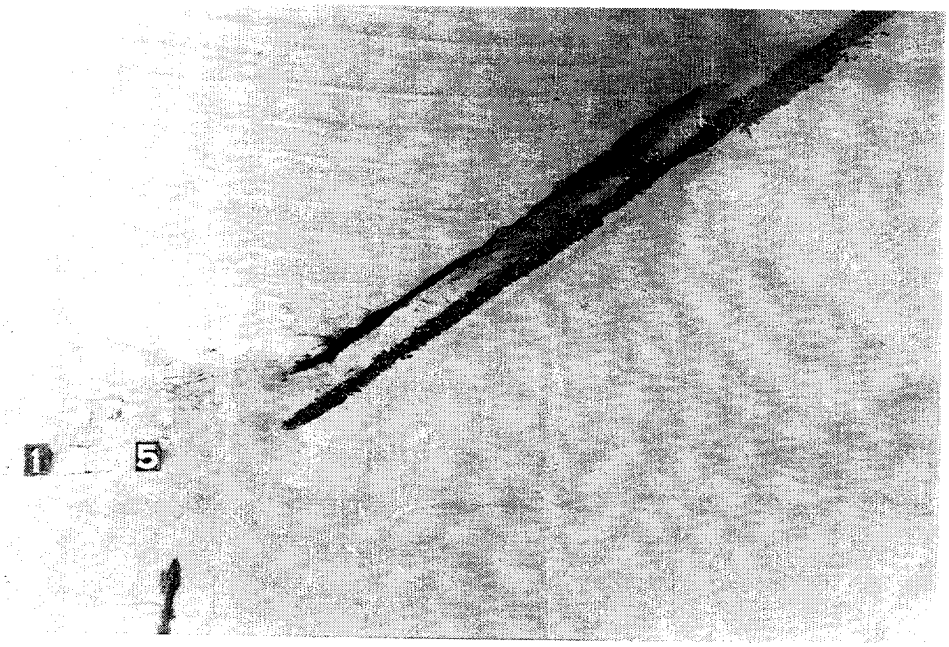

Figure E34. Tracer motion after a prototype equivalent of 1 hr 15 min under navigation wave N1 and spring peak ebb water level and flow, 152-m (500-ft) weir opening

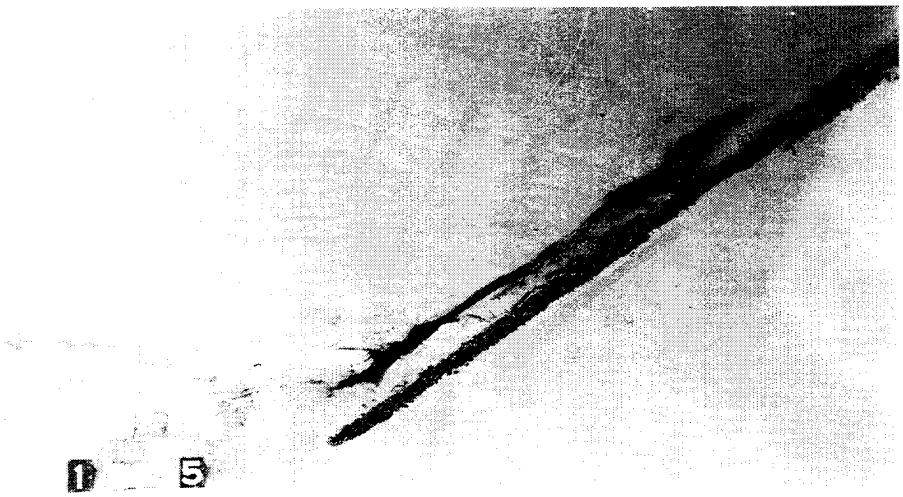

Figure E35. Tracer motion after a prototype equivalent of 2 hr 30 min under navigation wave N1 and spring peak ebb water level and flow, 152-m (500-ft) weir opening

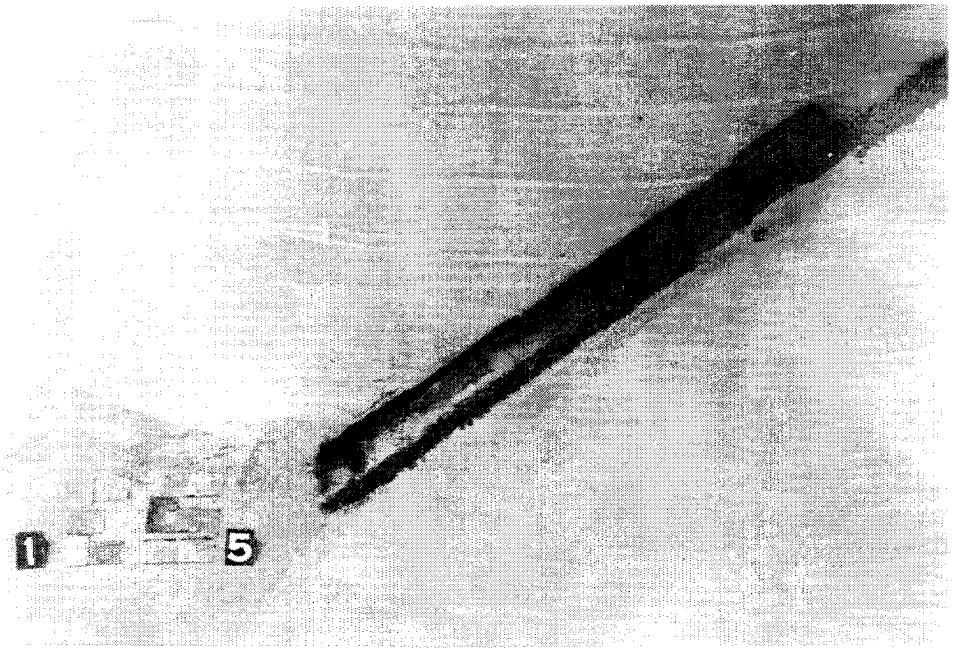

Figure E36. Tracer motion after a prototype equivalent of 1 hr 15 min under 1-year storm event and spring peak ebb storm water level and flow, 152-m (500-ft) weir opening

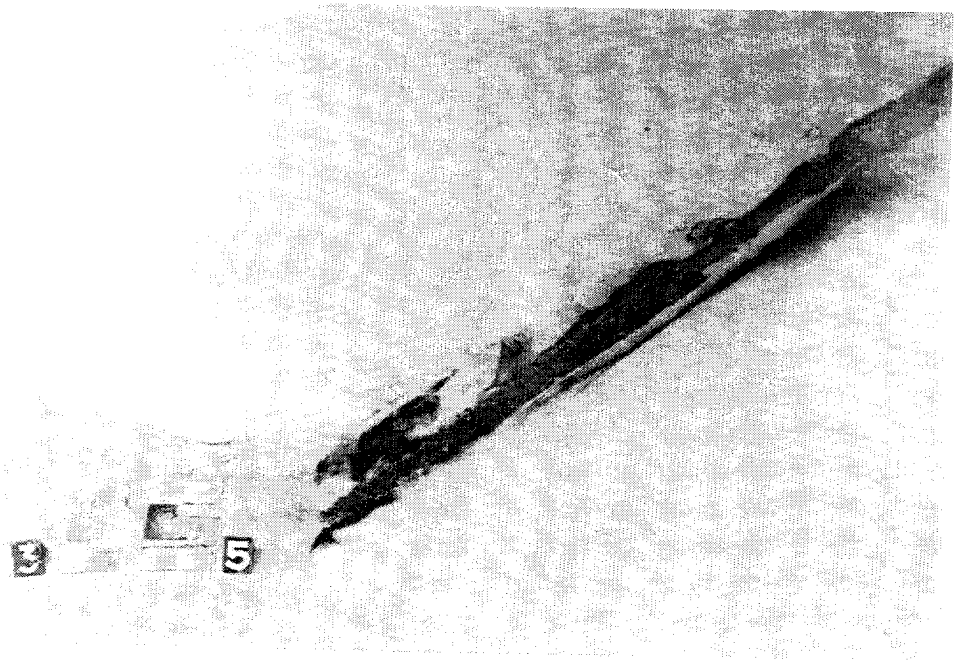

Figure E37. Tracer motion after a prototype equivalent of 2 hr 30 min under 1-year storm event and spring peak ebb storm water level and flow, 152-m (500-ft) weir opening

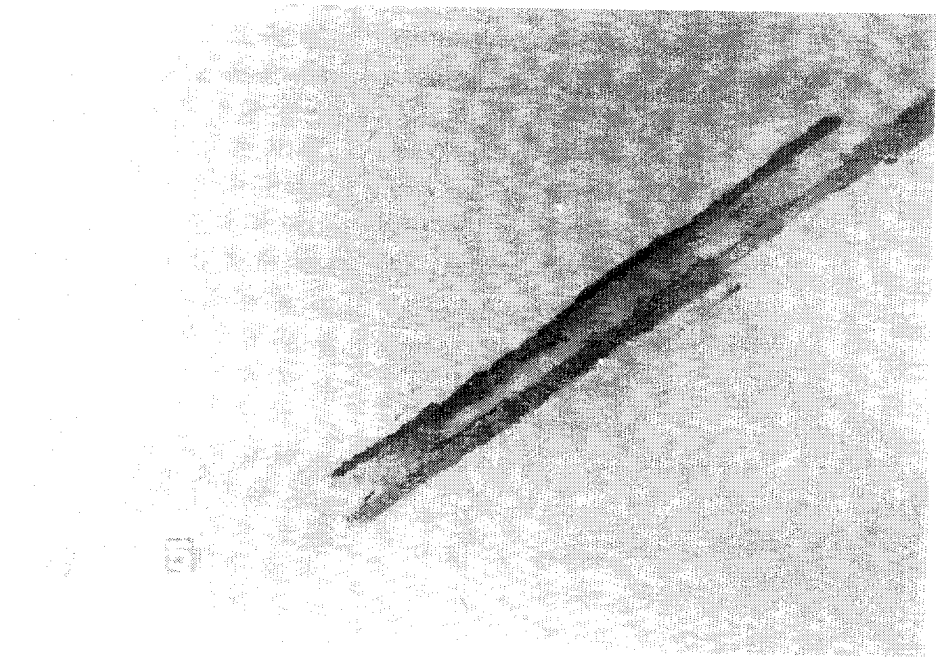

Figure E38. Tracer motion after a prototype equivalent of 1 hr 15 min under navigation wave N1 event and spring peak flood water level and flow, 152-m (500-ft) weir opening

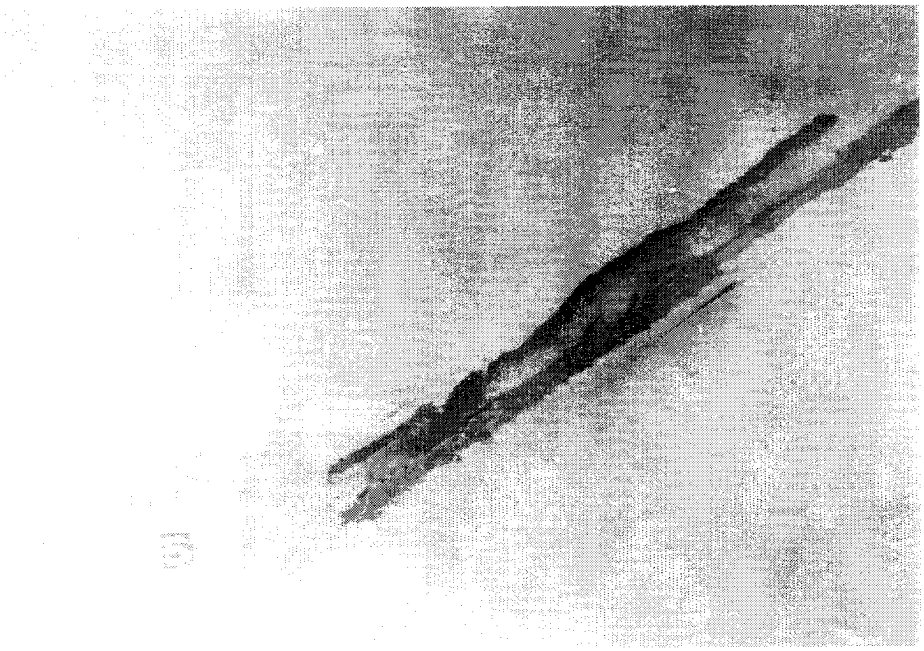

Figure E39. Tracer motion after a prototype equivalent of 2 hr 30 min under navigation wave N1 and spring peak flood water level and flow, 152-m (500-ft) weir opening

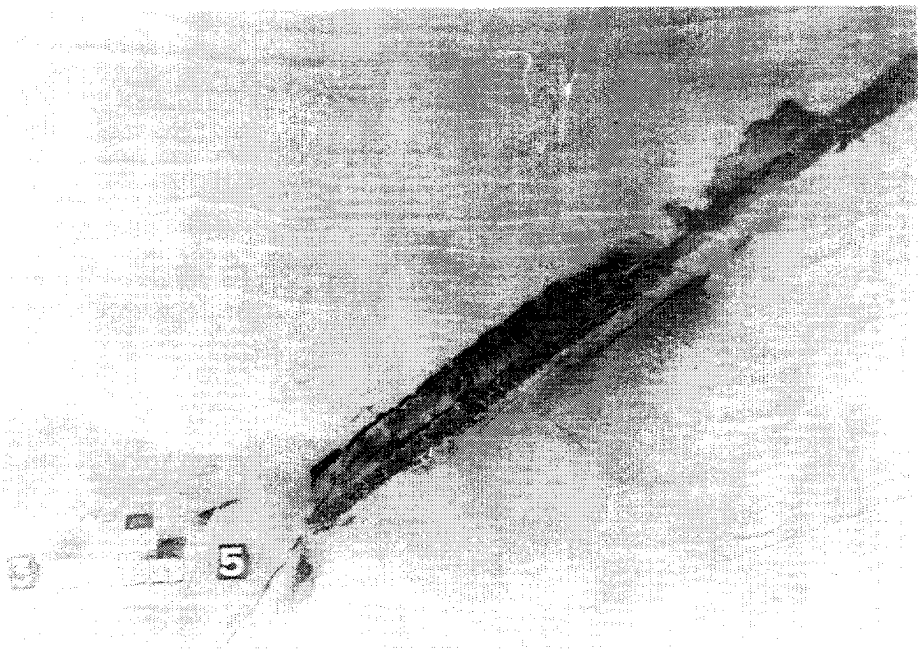

Figure E40. Tracer motion after a prototype equivalent of 1 hr 15 min under 1-year storm event and spring peak flood storm water level and flow. 152-m (500-ft) weir opening

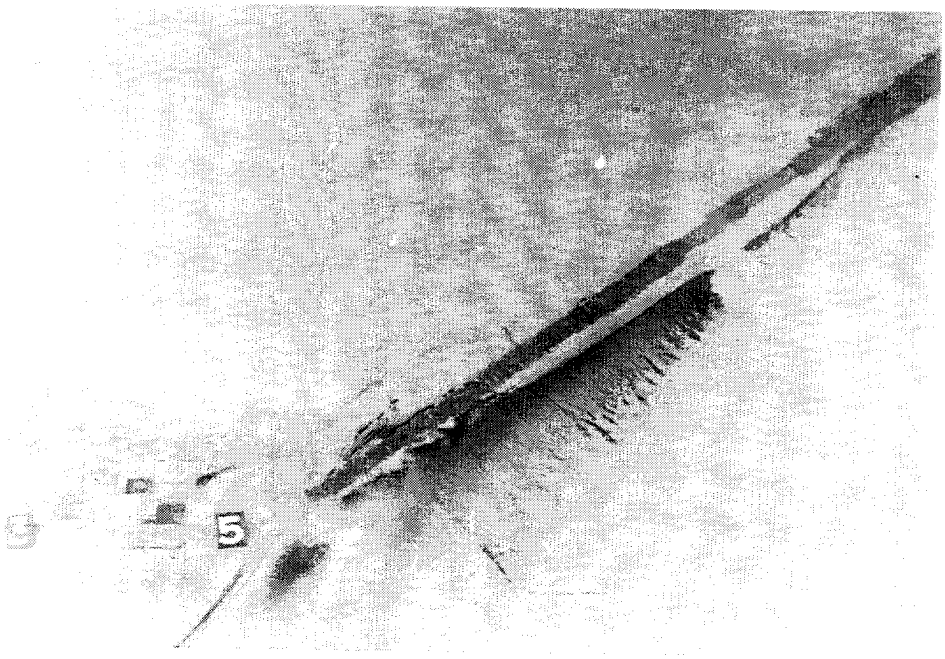

Figure E41. Tracer motion after a prototype equivalent of 2 hr 30 min under 1-year storm event and spring peak flood storm water level and flow. 152-m (500-ft) weir opening

Appendix F
Notation

A_r	Arch scale ratio between model and prototype
D_{50}	Mean grain size
G_r	Discharge
H_{m0}	Energy-based, or zero-moment, estimate of significant wave height, m (ft)
L	Length dimension
L_r	Length scale ratio between model and prototype
N_x	Horizontal scale
N_z	Vertical scale
N_D	Sediment size ratio
$N\rho$	Relative specific weight ratio
$(\rho\, solid)_{prototype}$	Density of prototype sand
$(\rho\, solid)_{model}$	Density of tracer material
$(\rho\, water)_{prototype}$	Density of seawater
$(\rho\, water)_{model}$	Density of fresh water
γ	Peakedness of the frequency spectrum
θ_p	Principal direction of wave propagation
T	Time dimension
T_p	Peak period
T_r	Time scale ratio between model and prototype
V_r	Velocity

REPORT DOCUMENTATION PAGE

Form Approved
OMB No. 0704-0188

1. AGENCY USE ONLY *(Leave blank)*	2. REPORT DATE	3. REPORT TYPE AND DATES COVERED
	September 1997	Final report

4. TITLE AND SUBTITLE

Physical Model Studies of Ponce DeLeon Inlet, Florida

5. FUNDING NUMBERS

6. AUTHOR(S)

Gordon S. Harkins, Paul Puckette, Cecil Dorrell

7. PERFORMING ORGANIZATION NAME(S) AND ADDRESS(ES)

U.S. Army Engineer Waterways Experiment Station
3909 Halls Ferry Road, Vicksburg, MS 39180-6199

8. PERFORMING ORGANIZATION REPORT NUMBER

Technical Report CHL-97-23

9. SPONSORING/MONITORING AGENCY NAME(S) AND ADDRESS(ES)

U.S. Army Engineer District, Jacksonville
Jacksonville, FL 32232-0019

10. SPONSORING/MONITORING AGENCY REPORT NUMBER

11. SUPPLEMENTARY NOTES

Available from National Technical Information Service, 5285 Port Royal Road, Springfield, VA 22161

12a. DISTRIBUTION/AVAILABILITY STATEMENT

Approved for public release; distribution is unlimited

12b. DISTRIBUTION CODE

13. ABSTRACT *(Maximum 200 words)*

Work completed by the U.S. Army Engineer Waterways Experiment Station's (WES) Coastal and Hydraulics Laboratory represents several elements of the larger study of Ponce DeLeon Inlet, Florida, aimed at improving navigation conditions within the inlet and preventing damage to the north jetty. Work performed at WES included field measurements and physical modeling of wave- and current-driven sediment transport and analysis of wave and current patterns for alternative inlet configurations. A steady-state three-dimensional physical model was designed and constructed to study spring peak ebb and flood velocity characteristics for various water level, flow, and wave conditions for the existing inlet and proposed inlet modifications. Objectives of the physical model study were to (a) assess proposed alternatives for improving navigation and inlet stabilization, and (b) investigate the impact of reopening the north jetty weir with present-day bathymetry. Field data were utilized to accurately develop, calibrate, and evaluate the accuracy of the physical and numerical models.

14. SUBJECT TERMS

Physical model study
Ponce DeLeon Inlet
Sediment transport
Wave and current patterns

15. NUMBER OF PAGES

230

16. PRICE CODE

17. SECURITY CLASSIFICATION OF REPORT	18. SECURITY CLASSIFICATION OF THIS PAGE	19. SECURITY CLASSIFICATION OF ABSTRACT	20. LIMITATION OF ABSTRACT
UNCLASSIFIED	UNCLASSIFIED		